

Assessment of Remote Data Capture Systems for the Characterisation of Rock Fracture Networks within Slopes


Xander P Gwynn

Camborne School of Mines
School of Geography Archaeology and Earth Resources
University of Exeter

Submitted by Xander Peter Gwynn to the University of Exeter as a thesis for the degree of Doctor of Philosophy in Earth Resources, September, 2008.

This thesis is available for Library use on the understanding that it is copyright material and that no quotation from the thesis may be published without proper acknowledgement.

I certify that all material in thesis which is not my own work has been identified and that no material has previously been submitted and approved for the award of a degree by this or any other University.


..... (signature)

ABSTRACT

The use of remote techniques to capture the geometrical characteristics of rock masses has seen increased use and development in recent years. Apart from the obvious improved Health and Safety aspects, remote techniques allow rapid collection of digital data that can be subsequently analysed to provide input parameters for a variety of geomechanical applications. Remote data capture is a new technique used to collect geotechnical data and little independent work has been done concerning the comparative limitations and benefits of photogrammetry and laser scanning. Photogrammetry and laser scanning produce three dimensional digital representations of a studied rock face which can then be mapped for geotechnical data using specialist software.

Research conducted at Camborne School of Mines, University of Exeter has focussed on developing robust and flexible methodologies for remote data capture techniques, namely photogrammetry and laser scanning. Geotechnical characterisation for photogrammetry was tested using the CSIRO Sirovision software and laser scanning was used with SplitFX from Split Engineering. A comparative method of assessing the error between orientation measurements was developed based on calculating the pole vector difference between remotely captured and traditionally hand-mapped data. This allowed for testing of the benefits of the remote data capture systems and limitations whilst comparing them with conventional hand-mapping. The thesis also describes the results of detailed comparisons between hand-mapping, photogrammetric and laser scanned data collection for discontinuity orientation, roughness, discontinuity trace lengths and potential end-use applications.

During fieldwork in Cornwall, Brighton Cliffs and northern France it was found that remote data capture techniques struggled to collect orientation data from intensely fractured rock masses where features are primarily represented as discontinuity traces.

It was found that both photogrammetry and laser scanning produce orientation data comparable to traditionally mapped data, with an average pole vector difference less than 12° from data mapped from the Tremough Campus road cutting to the University of Exeter's Cornwall Campus. Set analysis on 151 comparable data points yielded a maximum set pole vector difference of 9.8° , where the closest difference was 2.24° . Testing the accuracy of discontinuity trace orientations captured by photogrammetry

using the pole vector difference methods indicate that planar derived orientations are more accurate, with an average difference of 16.67° compared to 37.72° .

This thesis contains the reviews and analyses of photogrammetry and laser scanning for use in characterising natural and manmade rock slopes. Improved field and post-processing methodologies have been developed to aid the safe, efficient and suitable geotechnical characterisation of rock fracture networks. The continual development and use of remote mapping techniques, whilst supplementing their unique qualities with traditional mapping, have the capability to revolutionise rock mass mapping. Particular development needed is the implementation of ISRM guidelines to standardise photogrammetric and laser scanning fieldwork and post-processing data analysis.

CONTENTS

Abstract	2
Contents	4
List of Figures	8
List of Tables	18
Acknowledgements	21
1 Introduction	22
1.1 Aims of Project	24
1.2 Outline of Thesis	26
2 Remote Data Capture	28
2.1 Remote Sensing.....	28
2.2 Photogrammetry.....	29
2.2.1 History	29
2.2.2 Photogrammetric Systems.....	30
2.2.3 Photogrammetric Principles	30
2.3 Laser Scanning	32
2.3.1 History	32
2.3.2 Laser Scanning Systems	33
2.3.3 Laser Scanning Principle	33
2.4 Uses of Remote Data Capture.....	35
2.4.1 Geotechnical Aspects.....	35
2.4.2 Coastal Geotechnical Aspects	36
2.4.3 Non-Geotechnical.....	37
2.5 Review of Previous Work Undertaken	38
2.6 Summary.....	43
3 Data Capture Process Work-flow	44
3.1 Introduction	44
3.2 Workflow Sections Overview	46
3.2.1 Planning	46
3.2.2 On Site Assessment.....	46
3.2.3 Positioning.....	46
3.2.4 Data Capture	47
3.2.5 Data Capture / Data Compilation	47
3.2.6 Data Output / Analysis	48
3.2.7 End-Use Applications	48
3.3 Planning	48

3.3.1	Distance to Face and Study Area	48
3.3.2	Camera Separation / Baseline Ratio (Photogrammetry)	49
3.3.3	Orientation to Face	50
3.3.4	Geology of the Studied Rock Face	51
3.3.5	Equipment and Software Cost	56
3.4	On site Assessment	57
3.4.1	Camera Lens.....	57
3.4.2	Access.....	57
3.4.3	Atmospheric Conditions.....	57
3.4.4	Speed / Time	58
3.5	Positioning.....	58
3.5.1	Compass Clinometer and Tape Measure	58
3.5.2	Global Positioning System (GPS)	60
3.5.3	Differential GPS.....	61
3.5.4	Reflectorless Total Station.....	63
3.6	Data Capture.....	64
3.6.1	Photogrammetry	64
3.6.2	Laser Scanning	66
3.6.3	Traditional Hand-mapping Combined with Digital Photography	69
3.7	Photogrammetric 3D Image and Point Cloud Creation	72
3.7.1	Photogrammetric 3D image Creation.....	72
3.7.2	Laser Scanning Point Cloud Creation.....	76
3.8	Processing and Analysis of Remotely Captured Data.....	76
3.8.1	Data Import.....	76
3.8.2	Sirojoint and SplitFX Processing.....	77
3.9	End-Use Applications	82
3.10	Discussion and Conclusion	82
3.10.1	Fieldwork processes.....	82
3.10.2	Post-Processing/Data Analysis	84
4	Assessment of Fieldwork and Mapping Processes.....	86
4.1	Introduction	86
4.2	Pole Vector Difference.....	88
4.2.1	Pole Vector Difference Calculations	88
4.2.2	Pole Vector Difference of Hand-mapping.....	91
4.2.3	Interpretation of Pole Vector Difference Values	91
4.3	Area of Face Analysis	91
4.3.1	Photogrammetry.....	95

4.3.2	Laser Scanning	98
4.3.3	Orientation Data	99
4.3.4	Pole vector difference analysis	103
4.4	Rock Type/Structure Analysis.....	104
4.4.1	Gwithian and Gunwalloe Cliffs.....	105
4.4.2	Portreath Cliff	113
4.4.3	Porthgwarra, Carn Marth Quarry and Theatre Quarry.....	115
4.4.4	Portobello Cliffs	125
4.4.5	Assessment of Remote Data Capture to Collect Data from Varying Rock Types/Structures.....	126
4.5	Baseline to Face Ratio Analysis	127
4.6	Baseline Orientation to Face Analysis	131
4.7	Distance to Face Analysis	133
4.7.1	Imerys – Blackpool Pit.....	133
4.7.2	Delabole Quarry	136
4.7.3	Camborne School of Mines’ Test Mine	140
4.8	Equipment and Software Cost Analysis.....	143
4.9	Camera Lens Analysis.....	144
4.10	Access Analysis	144
4.10.1	Vegetation / Obstructions	144
4.10.2	Water Reflection.....	146
4.10.3	Rock Mesh	147
4.10.4	Blinding.....	149
4.11	Atmospheric Conditions.....	152
4.12	Field Speed / Time	154
4.13	Development of Positional Techniques.....	156
4.13.1	Compass Clinometer / Tape Measure.....	157
4.13.2	Global Positioning Systems / Differential Global Positioning Systems	157
4.13.3	Total Station	158
4.14	Development of Remote Data Capture /Data Compilation.....	158
4.14.1	Photogrammetry	158
4.14.2	Laser Scanning.....	160
4.14.3	Set Analysis.....	161
4.15	Summary.....	161
4.15.1	Pole Vector Difference.....	161
4.15.2	Scale	162
4.15.3	Impact of Lithology/GSI	162

4.15.4	Set-up Variations Affecting Data Capture	163
4.15.5	Distance	164
4.15.6	Costs	165
4.15.7	Access.....	165
4.15.8	Environmental and Timing Considerations.....	165
4.15.9	Image Processing.....	165
5	Data Output / Analysis Processes	167
5.1	Introduction	167
5.2	Tremough Campus Road Cutting Overview	169
5.2.1	Road Cutting Geographical Location and Geology	169
5.3	Orientation Comparison.....	176
5.3.1	Individual Feature	176
5.3.2	Set Comparison.....	177
5.4	Trace Analysis.....	180
5.4.1	Trace Orientation Analysis.....	180
5.4.2	Discontinuity Trace Length Analysis	181
5.5	Roughness Analysis.....	184
5.5.1	Conversion between Roughness Measurements.....	184
5.5.2	Using Profiles to Characterise Roughness	187
5.5.3	Scale of Roughness Affecting Orientation measurements	189
5.6	Tailoring Data for End-Use Applications	192
5.6.1	Geotechnical/Geological Data	193
5.6.2	RMR, Q System and GSI Ratings.....	202
5.6.3	Digital Elevation Model Data.....	203
5.6.4	Visual Data	209
6	Discussion.....	213
6.1	Introduction	213
6.1.1	Field and Mapping Processes.....	213
6.1.2	Data Output / Analysis Processes	216
6.2	Further Work	223
7	Conclusions	226
7.1	Key Findings	226
7.2	Summary.....	229
8	References	232

LIST OF FIGURES

Figure 2-1. Geometry for the determination of the position of a point in object space (from CSIRO, 2005).....	32
Figure 3-1. Process work-flow diagram with key underneath. The first stage requires that each parameter is considered before the site investigation starts, this can take place before or once the site is reached. The second stage uses an on site assessment to ascertain the conditions under which the remote data capture systems are to be used. The positioning technique is directly related to the data capture system used i.e. the tape measure and compass clinometer cannot be used to position the laser scanner. Once the data capture is completed the data is compiled using the programs specified. The dashed lines indicate that the photogrammetric/Sirovision process, once moved to data analysis, must be re-submitted into Sirovision to allow for the additional analysis facility to be used. The data analysis for all three techniques uses DIPS (Rocscience, 2006), however it is also used to compile the data for hand-mapping. Once the data is processed into spacing and roughness data, etc. it is available for use in the multiple end-uses.	45
Figure 3-2. Diagram showing scale effects upon overall rock mass strength. Capturing the rock mass characteristics at multiple scales is beneficial to geotechnical studies, as then instabilities of varying size can be factored into the analysis (from Wyllie & Mah, 2004).	49
Figure 3-3. Camera separation/ distance from face ratio. Cameras are orientated so that that the control point is in the centre of their view and spaced at a distance 1/6 of the baseline distance to the study face (modified from Siro3D manual, CSIRO, 2005).	50
Figure 3-4. Diagram showing potential distortion effects due to 'blinding'. Due to an unfavourable orientation/position of the camera or scanner, sections of the face are unseen. Photogrammetric 3D image creation will distort the final model to fit the data in view (blocked by the red section), where laser scan point clouds will have the red section missing (not to scale).....	51
Figure 3-5. Schematic from positional calculation sheet (eastings and northings). The schematic is used to visually assess the calculated locations for any gross errors, e.g. large camera separation or incorrect baseline to face orientation.	59
Figure 3-6. Magellan eXplorist handheld GPS. The GPS internal clock was synchronised with the clock of the camera/scanner, so to provide the most accurate positional data. The positional data can then be read off the screen or saved onto a GPS memory card (modified from www.magellangps.com).	60

Figure 3-7. Differential GPS Equipment – base station. The base station is setup over a known position that has previously been surveyed and begins to receive satellite signals. The location of the base station is input into the machine so it can then compare it with the positions that it calculates for itself using the satellite code, hence calculating the positional error for each moment in time. This error is then transmitted to the roving GPS unit so that it can calculate its position accurately.	61
Figure 3-8. Diagram showing the principle of Differential GPS.....	62
Figure 3-9. Roving GPS unit in backpack.....	62
Figure 3-10. TPS1200 reflectorless total station (from Leica, 2005).	64
Figure 3-11. Leica HDS3000 (from Leica, 2005). The laser is emitted through main window (pictured). A second window at the back of the scanner is used for capturing points at an angle of less than 40° from vertical.....	67
Figure 3-12. Photograph showing the Leica HDS4500 phase shift laser scanner. A mirror in the centre of the scanner spins reflecting the laser emitted vertically from the base of the scanner.	68
Figure 3-13. Schematic showing relative camera positions using Siro3D (CSIRO, 2006). Each camera position is labelled corresponding to the file name of the image on the computer. The blue rectangles show the extent of the photographs and how they relate to one another, along with the red cross indicating the control points and its location in the two images. This schematic allows for a visual assessment of the survey data.	74
Figure 3-14. Image showing result of poor matching of an underground rock face (~3 m wide) with multiple drill holes. The red box outlines the worst affected area of poor matching, however it is poor across the majority of the rock face. It is considered that this 3D image is poorly interpolated due the poor lighting and the multiple dark drill holes on the face which are incorrectly matched between the stereographic pair.	75
Figure 3-15. Post matching 3D mesh representing a full georeferenced rock face using Siro3D (CSIRO, 2005). Options are given for: manual editing of the 3D image, removing outliers automatically, cleaning up borders (by cropping), restoring original data (if one of the previous three options has already been applied), and to continue to save the 3D image.....	76
Figure 3-16. Full point cloud of example quarry (Carnsew) (red box, 6 m high, shows area required for analysis). The point clouds produced commonly contain points from areas that do not need to be analysed. They can be easily deleted from the point cloud file.....	79
Figure 4-1. Process work-flow diagram - indication of sections covered in Chapter 4.	87

Figure 4-2. Example stereonet shows differences in poles between hand (red), laser (green) and photogrammetric (blue) mapping. Each cluster of poles represents one discontinuity whilst each mapping technique has a slightly different orientation measurement.....	88
Figure 4-3. Diagram showing dip / dip direction conversion to Cartesian coordinates.	89
Figure 4-4. Map of Southern England, UK, showing location of Saltdean and Portobello coastal cliffs. © Crown Copyright/database right 2009. An Ordnance Survey/EDINA supplied service.	92
Figure 4-5. Geological map showing location of Portobello Cliffs (from Mortimore <i>et al.</i> , 2004).	92
Figure 4-6. Map showing photogrammetry study area and locations of laser scanner setup positions. © Crown Copyright/database right 2009. An Ordnance Survey/EDINA supplied service.	93
Figure 4-7. Image of cliff face at Portobello, UK, looking NE (30 m high).	94
Figure 4-8. Point cloud image (looking NW) showing area covered by two laser scans, 3 photogrammetric models (blue) and traditional hand-mapping (red) during morning visit (black line showing location of largest feature identified).....	94
Figure 4-9. Orthoimage (striking 085°) showing large scale structures (>1 m, blue) and small scale structures (<1 m, red).	97
Figure 4-10. Photograph showing small scale fractures found within the Portobello chalk (0.5 m high), looking north. The nodules within the chalk are flint and chert.	98
Figure 4-11. Point cloud showing large scale planes identified within SplitFX (red), Portobello Cliffs, Brighton, UK (30 m high), looking NE.....	99
Figure 4-12. Lower hemisphere representations showing contoured hand-mapped data taken from Portobello Cliffs, Brighton, UK (1 m - 30 m length), Lawrence (2007) (dip/dip direction of contour highs given in degrees). These large scale structures are predominantly steeply dipping and striking NE – SW, and NW – SE.....	100
Figure 4-13. Lower hemisphere stereonet showing contoured data from the SplitFX mapped point clouds, Portobello Cliffs, Brighton, UK (dip/dip direction of contour highs given in degrees). Similarly to hand-mapping, laser scanning only picks up the large scale features. The steeply dipping NE – SW, and NW – SE structure are identified, but a strong E – W striking set is also identified.	100
Figure 4-14. Lower hemisphere stereonet showing contoured orientation data from the large scale models, Portobello Cliffs, Brighton UK (dip/dip direction of contour highs given in degrees). The data is scattered but shows a similar NE – SW and NW – SE striking sets as hand-mapping.	101

Figure 4-15. Lower hemisphere stereonet showing contoured orientation data from the medium scale models, Portobello Cliffs, Brighton UK (dip/dip direction of contour highs given in degrees). The NW – SE striking set is clearly shown in the stereonet, although the NE – SW striking set is less apparent.	101
Figure 4-16. Lower hemisphere stereonet showing contoured orientation data from the small scale models, Portobello Cliffs, Brighton UK (dip/dip direction of contour highs given in degrees). The data is highly scattered and only weakly show the NE – SW and NW – SE striking sets identified from the large scale laser scanning and photogrammetric models.	101
Figure 4-17. Map of West Cornwall, UK, showing location of Gwithian and Gunwalloe cliffs. © Crown Copyright/database right 2009. An Ordnance Survey/EDINA supplied service.	105
Figure 4-18. Map showing photogrammetric study area at Gwithian cliffs. © Crown Copyright/database right 2009. An Ordnance Survey/EDINA supplied service.	106
Figure 4-19. Photograph of cliff face (~10 m high) at Gwithian, UK, looking east. The Variscan fold structures can be clearly seen within the face along with the complex jointing set orientations.	106
Figure 4-20. Lower hemisphere stereonet showing Gwithian orientation data.....	108
Figure 4-21. Equal area stereograms showing orientation data for: (a) Zones of distributed D3 shear, (b) D3 detachments, (c) D3 brittle listric extensional faults and (d) post D3 faults (from Alexander and Shail, 1995).....	108
Figure 4-22. Map showing location of photogrammetry study area at Blue Rocks, Gunwalloe. © Crown Copyright/database right 2009. An Ordnance Survey/EDINA supplied service.....	110
Figure 4-23. Photograph of cliff face at Blue Rocks, Gunwalloe, UK, looking north (cliff height from beach is 12 m). Folding is evident in the centre of the photograph, and wedge failures can be seen in the upper sections of the face.	110
Figure 4-24. Low angle detachments (faults) identified from the 'Big Wedge' model at Loe Bar, Gunwalloe (3 m high face, looking east). Using a visual assessment of separation and movement across discontinuity features, the faults were identified and mapped using the photogrammetric software.	111
Figure 4-25. Stereonet showing fault poles and associated slickenline data for the Loe Bar Lodge to Gunwalloe coastal section (from Shail & Wilkinson, 1994) (left) and the equivalent photogrammetrically mapped data (right).....	112
Figure 4-26. Map of West Cornwall, UK, showing location of Portreath. © Crown Copyright/database right 2009. An Ordnance Survey/EDINA supplied service.	113

Figure 4-27. Map showing location of laser scanning study area at Portreath. © Crown Copyright/database right 2009. An Ordnance Survey/EDINA supplied service. 114

Figure 4-28. Point cloud image showing identified large scale discontinuities (highlighted red) at Portreath beach cliff (15 m height) and failure material. The laser scan data also has the potential to be used to calculate the volume of the failed mass. 115

Figure 4-29. Map of West Cornwall, UK, showing location of Porthgwarra. © Crown Copyright/database right 2009. An Ordnance Survey/EDINA supplied service. 116

Figure 4-30. Map showing locations of photogrammetry study areas at Porthgwarra. © Crown Copyright/database right 2009. An Ordnance Survey/EDINA supplied service. 116

Figure 4-31. Photogrammetric orthoimage (striking E -W, 4 m high) showing discontinuity mapping at Porthgwarra Cliff, Cornwall, UK. Three roughly orthogonal discontinuity sets can be identified from the orthoimage. 117

Figure 4-32. Lower hemisphere stereonet from orientation data collected from Porthgwarra photogrammetric model. The three roughly orthogonal discontinuity sets identified from the orthoimage can be seen (delineated in red). The N - S striking set fluctuates cross the vertical, and can be separated into easterly and westerly dipping sub-sets. 118

Figure 4-33. Map of West Cornwall, UK, showing location of Carn Marth Quarry and Theatre Quarry. © Crown Copyright/database right 2009. An Ordnance Survey/EDINA supplied service. 120

Figure 4-34. Laser scan point cloud showing rock face at Carn Marth Quarry, Cornwall, UK, (5 m high, looking north) The blocky nature of the rock mass displays the discontinuities clearly. Sub horizontal features can also be identified. 121

Figure 4-35. 3D image screen capture of mapped rock face at Carn Marth Quarry with colours indicating similarly orientated discontinuities (scale shown in images, looking north). Similarly to the laser scanned point cloud, discontinuities are easily identified from the 3D model. 121

Figure 4-36. Map of Carn Marth and Theatre Quarries, stereonets representing each mapping type and location with set windows and major planes delineated in red. Photogrammetry = blue circles, laser scanning = green triangles and hand-mapping = red squares. © Crown Copyright/database right 2009. An Ordnance Survey/EDINA supplied service. 123

Figure 4-37. Map of West Cornwall, UK, showing location of Penlee Quarry. © Crown Copyright/database right 2009. An Ordnance Survey/EDINA supplied service. 127

Figure 4-38. Map showing locations of photogrammetry study area at Penlee Quarry with photographic overlay for detail. © Crown Copyright/database right 2009. An Ordnance Survey/EDINA supplied service. © 2009 Google, Map Data © 2009 Tele Atlas, © 2009 Getmapping plc.	128
Figure 4-39. Schematic diagram showing the set up method used to test baseline to face ratio setup variations.	129
Figure 4-40. Graph showing the average pole vector difference and standard deviation of each photogrammetric setup baseline ratio.....	130
Figure 4-41. Schematic diagram showing the set up method used to test baseline to face angle variations.	132
Figure 4-42. Graph showing the average pole vector difference and standard deviation of each photogrammetric setup with varying baseline to face angle (linear best fit line applied).....	133
Figure 4-43. Map of East Cornwall, UK, showing location of Blackpool Pit - Imerys. © Crown Copyright/database right 2009. An Ordnance Survey/EDINA supplied service.	134
Figure 4-44. Map showing locations of laser scanner setup positions at Blackpool Pit. © Crown Copyright/database right 2009. An Ordnance Survey/EDINA supplied service.	134
Figure 4-45. 3D model of one point cloud of Blackpool Pit, Imerys, St Austell, Cornwall, UK looking west. Each bench is ~15 m high. The reflectance intensity is represented as a green colour indicating a good reflectance, ranging to red for poor reflectance.	135
Figure 4-46. Map of East Cornwall, UK, showing location of Delabole Quarry. © Crown Copyright/database right 2009. An Ordnance Survey/EDINA supplied service.	136
Figure 4-47. Map showing locations of photogrammetry camera and control point setup positions at Delabole Quarry. © Crown Copyright/database right 2009. An Ordnance Survey/EDINA supplied service.....	137
Figure 4-48. 3D image showing the 1967 failure plane (highlighted red), Delabole Quarry, Cornwall, UK. It is considered that there has been little change in the slope profile since there has been no significant failure subsequently in this regularly monitored face. The camera positions had restricted views of the lower half of the pit slope, so only the upper part, which includes the failure surface, was modelled.	138
Figure 4-49. Comparison between the cross section of the 3D photogrammetric failure face (140 m and 190 m AOD) and the estimated original quarry profile (50 m – 200 m AOD), after Clover (1978).	139

Figure 4-50. Photograph of the 1967 failure face at Delabole Quarry viewed NNW, with the town of Delabole in the background. The slope is ~100 m high from the haul road.	140
Figure 4-51. Map of West Cornwall, UK, showing location of Camborne School of Mines - Test Mine. © Crown Copyright/database right 2009. An Ordnance Survey/EDINA supplied service.	141
Figure 4-52 . Point cloud of side wall within CSM Test Mine (2.5 m high). The footprint of scanner comes to the base of the rock face when ~1.5 m away from the face.....	142
Figure 4-53. An example of the multiple 3D images created of side walls and drives within CSM Test Mine. (2.5 m in height, and 3.5 m wide).....	143
Figure 4-54. Two images showing how the image of the obstruction (lamp post) is smoothed to the rock face. Some distortion has occurred between the yellow sign and the rock face, but it is minimal and does not affect the rest of the 3D model.	145
Figure 4-55. Point cloud image showing ghost points created by vehicles passing in front of laser scanner. The rock face is ~3 m high.....	146
Figure 4-56. Points within laser scanned cloud formed due to reflectance from puddle in the floor at CSM Test Mine (2.5 m tall drive, viewed east) (highlighted red).	147
Figure 4-57. Rock meshed face at excavation near Dielette, northern France (only discontinuity traces shown). The rock mesh has been bolted and closely follows to the rock face. Discontinuity orientations and discontinuity trace lengths from 68 features were successfully extracted from the ~3 m high, east - west striking model.....	148
Figure 4-58. Frequency graph showing line lengths collected from rock meshed face. The majority of the 1 m - 2 m discontinuities are sub vertical, while the longest are orientated at 35°.	148
Figure 4-59. Graph showing the percentage of features compared to those mapped in the 3D model at 90° baseline to face angle for models with decreasing baseline to face angles. At 90° - 60° to the face no discontinuity features were missed/blinded, although the number of planes that had to be mapped as discontinuity traces increased to 35%. At a 30° angle to the rock face, the number of blinded features increases to 8% at the expense of the planes (decreasing from 65% to 55%, with a 2% increase in discontinuity traces). At a 15° angle from the study face, 46% of features are blinded, where planes and discontinuity traces combined only make up 54%.	150
Figure 4-60. Evidence of dust particles picked up during laser scan at CSM Test Mine (highlighted red, 3 m high face).....	154
Figure 4-61. Field times comparison between photogrammetry, laser scanning and traditional mapping (100 fractures). Similar time is taken between the three mapping	

techniques for the preliminary stages, where the data capture/fracture measurement stage of remote mapping is ~8 times quicker than traditional mapping.	155
Figure 4-62. Geared camera head fitted with tribrach attachment (highlighted in red). The screw fitting for the geared head was modified so that it may be interchanged between normal photographic tripods and surveying tribrachs.....	159
Figure 5-1. Process work-flow diagram - indication of sections covered in Chapter 5 (red box).....	168
Figure 5-2. Map of West Cornwall, UK, showing location of Tremough Campus road cutting. © Crown Copyright/database right 2009. An Ordnance Survey/EDINA supplied service.....	169
Figure 5-3. Map showing layout of photogrammetric and laser scan setup positions, Tremough, Cornwall, UK. © Crown Copyright/database right 2009. An Ordnance Survey/EDINA supplied service.	170
Figure 5-4. Image showing blocky nature of the granite rock mass at the Tremough Campus road cutting (3 m wide, 2.5 m high rock face, looking south).....	171
Figure 5-5. Comparison between photogrammetric mesh (top) and point cloud (bottom) taken from Tremough Driveway (view orientated SE).	174
Figure 5-6. Lower hemisphere stereonet showing photogrammetrically captured orientation data.....	175
Figure 5-7. Lower hemisphere stereonet showing laser scanning captured orientation data.	175
Figure 5-8. Lower hemisphere stereonet showing hand-mapping captured orientation data.	175
Figure 5-9. Pole vector difference for remotely captured data compared with hand-mapped orientation as a function of area of the identified fracture plane (measured using photogrammetry). Plotted on log-log axes.	177
Figure 5-10. Stereonet showing set analysis on hand-mapped data.	179
Figure 5-11. Stereonet showing set analysis on photogrammetrically mapped data.	179
Figure 5-12. Stereonet showing set analysis on laser scanned mapped data.	179
Figure 5-13. Above: 2D orthoimage with discontinuity trace and plane highlighted red. Below: corresponding 3D image showing plane fitted to discontinuity trace.....	180
Figure 5-14. Tracelength identification using window mapping from a digital photograph, Tremough Road cutting, Penryn, Cornwall (3 m wide, 2.5 m high rock face, looking south). The discontinuity traces are coloured according to orientation to the rock face. Shaded areas indicate the planes from which the traces are delineated.	182

Figure 5-15. Photogrammetric discontinuity trace length identification, Tremough Road cutting, Penryn, Cornwall, UK (~3 m wide, 2.5 m high rock face, looking south).	183
Figure 5-16. Photogrammetric and traditionally mapped discontinuity trace length frequency distribution. Both are positively skewed normal or log normal distributions, although there is some variation in the larger ranges for both photogrammetric and traditional mapping techniques. On average the photogrammetric discontinuity trace lengths were shorter than the traditionally mapped features, 0.54 m and 0.61 m respectively.....	184
Figure 5-17. Hand-mapped JRC plotted against photogrammetrically mapped RMS showing a weak positive trend.	186
Figure 5-18. Hand-mapped JRC plotted against photogrammetrically mapped variance showing a weak negative trend.....	186
Figure 5-19. Hand-mapped JRC plotted against laser scanned roughness showing a weak negative trend.....	186
Figure 5-20. Measurement of joint roughness (from Wyllie & Mah, 2004, modified from Tse & Cruden, 1979).	188
Figure 5-21. Photogrammetric 3D image showing partition of large box (7.6 m ²) into smaller boxes, 4 x 1.9 m ² , 16 x 0.475 m ² and 64 x 0.119 m ² , Tremough Campus Road cutting, Penryn, Cornwall, UK, looking SSE.....	189
Figure 5-22. Stereonet and zoomed section showing photogrammetric poles (blue), laser scanned poles (yellow) and hand-mapped poles (red) (average shown in green).	190
Figure 5-23. Pole vector difference of photogrammetry at varying box areas from average orientation taken from total plane area. It shows that the range of the pole vector differences from the total plane orientation reduces as the size of the plane measured increase.	191
Figure 5-24. Pole vector difference of laser scanning at varying box areas from average orientation taken from total plane area. Mirroring photogrammetry; the graph shows that the range of the pole vector differences from the total plane orientation reduces as the size of the plane measured increase.	191
Figure 5-25. Process work-flow diagram for geotechnical end-uses.....	194
Figure 5-26. Map showing locations of laser scanner setup position at Saltdean. © Crown Copyright/database right 2009. An Ordnance Survey/EDINA supplied service.	196
Figure 5-27. Swedge back-analysis on fallen wedge, data collected from laser scanned point cloud at Saltdean, Brighton, UK. The ~18 m high cliff has been scaled	

for loose blocks and has had a buttress installed to increase stability and to act as a catchment for small rockfall (~1.5 m ³).	196
Figure 5-28. AutoCAD (Autodesk, 2008) 3D representation of blocks formed from virtual scanline spacing data (from Saliu, 2009).	197
Figure 5-29. Example circular window mapping from orthoimage of Carnsew Quarry (lower circles 6 m diameter, upper circles 10 m diameter). Using an orthoimage removes the perspective bias of using normal photographs. The circles were scaled using ImageJ (Rasband, 2007) and superimposed onto the orthoimage showing the discontinuity traces coloured according to orientation.	200
Figure 5-30. Process work-flow diagram for end-uses using digital elevation model data.	204
Figure 5-31. Point cloud image showing 2D profile section highlighted in red, Saltdean, Brighton, UK. The ~18 m high cliff has been scaled for loose blocks and has had a buttress installed to increase stability and to act as a catchment for small rockfall. ...	205
Figure 5-32. Simulated RocFall scenario showing rock fall paths from the cliff profile taken of Saltdean, Brighton, UK. The profile was constructed from a reduced number of points from the laser scanned point cloud as too many were imported for the RocFall program to compute without problems.	206
Figure 5-33. 3D mine map from laser scanned point cloud showing drives and collapsed stope (30 m wide approx). The grey indicates the interior surface of the mine, where the blue indicates the exterior.	208
Figure 5-34. Process work-flow diagram for end-uses using visual data.	210
Figure 5-35. Images showing colour recognition. The top image shows the four points from which the colour range is chosen. The bottom image shows the areas of the face that match the colour from selected range.	211
Figure 6-1. Diagram showing stereonet overlay indicating areas of precision for remote data capture systems (viewing along a horizontal plane and from one setup position). The highest precision is achieved for features that are near perpendicular to the viewing angle. As features become more oblique in both the horizontal and vertical planes then the precision decreases.	220
Figure 6-2. Ideal work-flow diagram (with key underneath). The process work-flow is more simplified whilst each mapping technique can assess multiple rock mass characteristics.	225
Figure 7-1. Venn diagram showing individual and shared advantages between hand and remote mapping techniques to capture rock mass characteristics.	231

LIST OF TABLES

Table 3-1. Field estimates of uniaxial compressive strength (from Hoek & Brown, 1997). Qualitative empirical descriptions of rock strength in the field can be used to roughly estimate the quantitative value.	52
Table 3-2. Weathering grades (from ISRM, 1981b). Using descriptions of the rock mass the grade of weathering can be estimated for use in subsequent analysis.	53
Table 3-3. Comparison of techniques used in measurement of joint surface roughness (from Unal, 2000). The table suggests that both digital photogrammetry and laser scanning are well suited for roughness measurements.....	55
Table 3-4. Example of spreadsheet calculating positional XYZ coordinates from particular data inputs. Inputs include the angles and distances to each camera and controls point. Triangulation calculations are used to estimate the unknown locations.	59
Table 3-5. Sirojoint reliability measure (CSIRO, 2005). Inaccuracies may be produced during matching, where points had to be interpolated from surrounding accurate matched points.	77
Table 4-1. Calculation of pole vector error between five hand-mapped discontinuities and the corresponding measurements made using remote mapping techniques. Arrows indicate direction of calculations.	90
Table 4-2. Locations of photogrammetry camera and control point setups at Portobello, Brighton, UK, indicating model scale and lens used.....	96
Table 4-3. Locations of laser scanner setup positions at Portobello, Brighton, UK, also indicating the scan density used.	99
Table 4-4. Orientations of contour highs found from the differing remotely mapped 3D models and from hand-mapping. Corresponding sets have been sorted next to one another for comparison.	102
Table 4-5. Orientations of contour highs compared using pole vector differences across the large scale data captured by photogrammetry, laser scanning and hand-mapping. Only comparable sets were used.	104
Table 4-6. Locations of photogrammetry camera and control point setups at Gwithian, Cornwall, UK, indicating model and lens used.	107
Table 4-7. Locations of photogrammetry camera and control point setups at Gunwalloe, Cornwall, UK, indicating model and lens used.....	111
Table 4-8. Locations of laser scanner setup positions at Portreath, Cornwall, UK, also indicating the scan density used.	113

Table 4-9. Locations of photogrammetry camera and control point setups at Porthgwarra, Cornwall, UK, indicating model and lens used.	117
Table 4-10. Locations of laser scanner setup positions, and photogrammetry camera and control point setups at Carn Marth Quarry and Theatre Quarry, Cornwall, UK, indicating model, lens and scan density used.	122
Table 4-11. Table showing the set analysis for each remote mapping model and hand-mapping. Six sets were identified across the two quarries. Set one from the Theatre Quarry was split into A and B (steeply and shallow dipping subdivisions).	124
Table 4-12. Pole vector difference analysis on data collected from northern section of Carn Marth Quarry.	125
Table 4-13. Assessment of remote data capture systems to collect data from varying rock structures (modified from Marinos & Hoek, 2000).	126
Table 4-14. Locations of photogrammetry camera and control point setups at Porthgwarra, Cornwall, UK, indicating camera separation, baseline ratio and lens used.	129
Table 4-15. Example table showing pole vector differences (PVD) between hand-mapping and photogrammetric mapping with varying baseline ratios.	130
Table 4-16. Locations of photogrammetry camera and control point setups at Porthgwarra, Cornwall, UK, indicating camera separation, baseline orientation to face and lens used.	131
Table 4-17. Locations of laser scanner setup positions at Blackpool Pit - Imerys, Cornwall, UK, also indicating the scan density used.	135
Table 4-18. Locations of photogrammetry camera and control point setups at Delabole Quarry, Cornwall, UK, also indicating lens used.	137
Table 4-19. Locations of laser scanner setup positions, and photogrammetry camera and control point setups for testing laser scanning blinding, indicating model, lens and scan density used.	151
Table 4-20. Results of blinding effects on laser scanning. The single laser scan only captured 86% of the features mapped using photogrammetry, had a pole vector difference of $\sim 18.83^\circ$ from hand-mapping and a standard deviation of 16.18° . The three combined laser scans were able to capture 13% more features than the single scan whilst obtaining a 11.96° pole vector difference from hand-mapping. The standard deviation was reduced by 40% to 9.6°	152
Table 4-21. Comparison of each positioning technique from experience during study (Additional data sourced: Leica, 2005; CG Surveying Ltd, 2007; RICS, 2007).	156
Table 5-1. Locations of photogrammetry camera and control point setups at the Tremough Campus road cutting, Cornwall, UK, indicating model and lens used.	172

Table 5-2. Locations of laser scanner setup positions at the Tremough Campus road cutting, Cornwall, UK, indicating the model and scan density used.....	173
Table 5-3. Number of planar features identified using each mapping technique.....	173
Table 5-4. A comparative table showing the average pole vector difference and standard deviation between each mapping technique. Data has been split into discontinuities dipping below and above 47°.....	176
Table 5-5. Set analysis for comparative data collected from Tremough Road Cutting. Each mapping technique is compared with one another. Fisher K and number of poles within each set are included in the set statistics.....	178
Table 5-6. Plane and discontinuity trace pole vector differences from hand-mapping.	181
Table 5-7. Photogrammetric and traditionally mapped discontinuity trace lengths frequency and frequency percentage.....	183
Table 5-8. Example roughness measurements taken from the Tremough road cutting.	185
Table 5-9. Correlation (R) and 95% confidence values of remotely mapped roughness measurements with hand-mapped JRC measurements.....	185
Table 5-10. Conversion of remotely mapped roughness measurements to JRC values developed from measurements taken from the Tremough Road Cutting.	187
Table 5-11. Table showing the pole vector difference between spot hand-mapped data taken from the study plane and the average plane orientation measured from the entire area by photogrammetry and laser scanning.	192
Table 5-12. By using the superimposed circles on the orthoimage, the discontinuity trace count for circular window mapping can be completed and split according to each set.	201
Table 5-13. Using the methodologies developed by Zhang & Einstein (1998); Zhang & Einstein (2000); La Pointe (2002); and Zhang <i>et al.</i> (2000) the mean fracture radius and standard deviation for each set and probabilistic distribution type can be calculated.	201
Table 5-14. Assessing the ability of photogrammetry and laser scanning to calculate parameters from RMR, Q system and GSI rating systems.....	203

ACKNOWLEDGEMENTS

I would like to thank my supervisors, Professor Robert Pine and Professor John Coggan for their continual help and guidance during the PhD project. Their wide knowledge, ideas, and logical way of thinking have been of great value to me during this project and will be with me throughout my future career.

My colleagues in the Camborne School of Mines PhD Room provided me with a friendly working environment and were always willing to help with many aspects of my project, specifically Muyideen Saliu and Dr Zara Flynn, who both assisted me with hand-mapping on certain field trips. I would also like to thank Dr Andrew Wetherelt who undertook the laser scanning fieldwork with me and taught me how to use the Leica hardware and software. Steve Pendray helped with the modifications to the equipment used during the project.

Also thanks to the rest of the CSM staff, all of whom helped me through my undergraduate degree at the old campus in Camborne during lectures and numerous field trips, they then continued to give helpful input and made constructive comments during my PhD study.

During the later stages of writing up my thesis SRK Consulting UK Ltd provided me with time and resources to help me finish my final corrections.

I would also like to thank my family; my brothers Tom and Leo, and my parents, Alec and Serena for their encouragement and support throughout my time at Camborne.

I would not have been able to complete the PhD without Emma. Thank you for your constant love, patience and understanding.

The location maps were accessed from the Digimap Ordnance Survey Collection (© Crown Copyright/database right 2009. An Ordnance Survey/EDINA supplied service) and via Google Earth (© 2009 Google, Map Data).

Financial support has been provided by the European Social Fund.

1 INTRODUCTION

Priest (1993) highlighted the need for effective rock mass characterisation prior to any excavation involving rock. This normally involves some form of field mapping that is conventionally undertaken by hand-mapping of representative scanlines or windows for the rock mass under investigation. Recent years have seen increased application and development of remote data capture techniques in order to reduce the exposure of personnel to potential hazards; where access may be a potential safety issue; to increase the speed of data collection and for automation of data capture and its subsequent processing. The adopted techniques make use of photogrammetry or laser scanning for acquiring raw data.

After post-processing these remote data capture techniques can produce spatially accurate, densely detailed 3D representations of the rock mass. Subsequent measurements of discontinuity features allow for collection of large quantities of data in a reasonably short space of time. In addition, where proposed mapping areas are inaccessible or restricted, remote data capture can record whole sections of a particular slope or exposed rock surface. For example, in open pits and quarries the techniques allow data to be collected rapidly (in minutes) from bench faces that may be too dangerous for manual data collection (Poropat, 2001). The increased data capture and subsequent analysis can also remove some of the subjectivity involved in interpretation (Coggan *et al.*, 2007).

A rock mass can be described as intact rock separated by discontinuities (Goodman, 1989; Brady & Brown, 1994). Characterising these discontinuities is imperative for calculating the mechanical behaviour of the rock mass (Bieniawski, 1989). One method of characterising the rock mass is to utilise three dimensional modelling, which requires large amounts of data to provide a reliable statistical basis from which to work. Currently the necessary data is collected using established traditional geological hand-mapping methods; these are routinely carried out so that consistent results can be obtained over a wide range of environments (Priest, 1993). However, hand-mapping can be time intensive due to a number of factors such as: excessive slope heights preventing total face mapping, restrictions imposed due safety considerations and adverse weather conditions. In addition, according to Poropat (2001) problems which arise from human errors whilst collecting large amounts of data are hard to prevent.

Because of the need for large amounts of statistically robust data, new, automated, non subjective data collection systems are being produced. Digital remote data capture technologies, photogrammetry and laser scanning, are currently in development which can quickly assess whole slopes and quarry benches, negating access and safety problems, whilst producing large amounts of discontinuity data. Laser scanning is also referred to as high definition surveying and LIDAR (Light Detection And Ranging) in the literature.

Unfortunately, as equipment for measuring rock mass features become more sophisticated, generally it also becomes more complicated to use. According to McCaffrey *et al.* (2005) this is the main reason for the reluctance to embrace these new technologies as some geoscientists believe that use of digital aids is complicated and will cause a weakening of standard geological skills. Other factors limiting the use of new technologies are the cost and time needed to train to use the new equipment, along with the accompanying software, therefore traditional techniques are still generally thought to be quicker and easier to use.

Current methods used to analyse data that is captured manually in the field have developed along with the advance of computers, e.g. DIPS (Rocscience, 2006). These speed up the analysis process and automate certain functions that are routinely practised, e.g. contouring. Conversely, standard geological data capture practices have not changed significantly from the use of compass clinometers and mapping boards.

As technology used for geological and geotechnical data capture advances, becoming more accessible to 'fieldwork' personnel, the methodologies that are employed to use them must also advance. Remote data capture systems are currently in use for geotechnical applications, although, robust and flexible methodologies must be developed so digital data collection systems can be fully understood, showing that they can enhance the basic understanding of geotechnical engineering. These systems must be thoroughly tested however, to demonstrate that the data captured using these systems is comparable to data collected using accepted traditional methods. As many different end applications exist, they must also be shown to have the ability to be customised and incorporated into these specific end-uses, such as numerical modelling, fracture network characterisation, and rock mass classification.

Any fieldwork requires safety to be considered above all other factors; hand measurement of a slope face has inherent dangers involved in the process. The remote data capture methods enable the user to be a safe distance away from the studied surface and so reduce exposure of personnel to potential hazards.

1.1 Aims of Project

The principal aims of this project are to develop and evaluate techniques of digital remote, non-contact, geotechnical data capture using photogrammetry and laser scanning for natural and manmade slopes, specifically coastal slopes and quarries. Methodologies that have been produced by the manufacturers of these systems will be adapted and refined so that the data collected can be used to better aid in the safe and efficient geotechnical characterisation of rock fracture networks. Assessments of the accuracies of the data capture systems will be made against one another and traditionally hand-mapped data collected as a part of the study.

These aims will be met through the following objectives:

- Create and develop robust and flexible field methodologies and post-processing work-flows for the respective data capture systems
- Critically review and compare remote data capture techniques with traditional hand-mapping techniques
- Identify the surveying systems that are best suited to each remote mapping technique
- Identify and assess limitations of each technique and provide critical boundaries for their use
- Determine the rock mass characteristic parameters that can be remotely mapped for robust geotechnical analysis
- Develop a new method for comparing orientation data: pole vector difference calculations
- Determine the accuracy and reliability of remote data capture systems to collect orientation data for individual discontinuities and discontinuity sets from both discontinuity planes and discontinuity traces
- Produce methods for calculating surface roughness values from remotely captured data and assess the effect of roughness on orientation measurement
- Assess which rock types are best suited for remote mapping
- Develop processing methodologies for the use of remotely captured data in multiple end-use applications

Remote data capture techniques require specialist equipment and individual field methodologies, all depending on the environment in which they are to be used. This project will compare the systems and their suitability for certain conditions, such as areas restricting equipment set up positions, and maximum/minimum distance ranges. As the methodologies and equipment used for remote mapping have not yet been standardised, it is considered that refinements and improvements can be made. Methodologies and work-flows for each practice will be developed and advanced, from task planning to analysis of the collected data.

Multiple characteristics must be collected from a rock mass for a robust geotechnical analysis (ISRM, 1981b). Currently the majority of these are collected by traditional hand-mapping, although additional lab testing and drilling can be used. Reviews of these hand-mapped characteristics were made along with assessing the suitability of the remote mapping systems used to collect them. However, some rock mass characteristics are required to be mapped from physical contact with a rock face. It is considered that not all features can be remotely mapped, but modification of methodologies and engineering experience can be used to estimate them remotely.

The data that can be remotely mapped will be assessed against traditionally mapped data so that it can be used as an acceptable substitute for use in geomechanical modelling. Comparisons will be made against each of the parameters output by geotechnical mapping, such as orientation and discontinuity trace length. The three dimensional representations of coastal geomorphology produced by photogrammetry and laser scanning have been compared previously, but they were used comparatively to measure coastal cliff erosion (Lim *et al.*, 2005) and glacier monitoring (Favey *et al.*, 2001). A new method of comparing orientation data using pole vector difference calculations (PVD) will be developed during this study and will be used to assess the accuracy of the discontinuity measurements by remote mapping techniques. It is hypothesised that the remote mapping systems should produce orientation data comparable to traditional hand-mapping as previous studies on their intrinsic accuracies showed that they were able to represent 'real-world' objects (covered in Section 2.5).

Roughness measurements are made by both remote mapping techniques, but they are not currently measured in a format that is used for geotechnical analysis. By comparing traditionally mapped joint roughness coefficients (JRC) with the remotely mapped roughness measurements, their reliability will be tested and conversion factors

developed. As previous studies have concentrated on the use of both very close range photogrammetry and laser scanning for characterising roughness (covered in Section 2.5) it is considered that measurements from the geotechnical analysis programmes of the two remote data capture systems should provide good roughness values to compare with JRC. The effect of large scale roughness on both traditional and remote mapping will also be analysed.

The differing systems provide distinct advantages over one another, as well as having unique limitations. They both share common boundaries for their use, such as maximum and minimum distances for practicable data capture and the restrictions of their use in poor environmental conditions. The manufacturers of the remote data capture systems have tested and published the limits of their systems using spatial accuracy assessments, but usually within ideal conditions. They have not been tested and compared for mapping geotechnical rock mass properties. Specific photogrammetric limitations will be tested, such as the affect of viewing angle and varying camera baseline to face distance ratio on the accuracy of discontinuity orientation measurements. Quantification of these boundaries will be completed using pole vector difference (PVD) calculations.

Case studies will be carried out on both natural coastal cliffs and manmade quarry slopes. These will be used to test the ability of each technique to capture data from the more amorphous coastal cliffs and the relatively angular slope faces of quarries, both containing a range of differing rock textures and vegetation cover. Several sites are identified that provide a range of rock types, different set-up problems, different target ranges and different scales of mapping in both natural and manmade environments. Additionally, the thesis will describe the results of a detailed comparison of hand-mapping, terrestrial photogrammetry and laser scanning of a blocky rock mass at one of the project locations. The captured data must undergo certain processing steps so that information can be relayed quickly and easily to the user. As many end-use applications for the remote data capture systems exist, then the resultant data must be tailored to fit that end-use. The implications of this adaptation of the remotely mapped data will be studied and assessed during this project.

1.2 Outline of Thesis

Chapter 2 gives a short outline of remote data capture and covers the theoretical principles of the emerging techniques used in the geotechnical industry:

photogrammetry and laser scanning. A brief overview is given of the current applications of these remote data capture systems.

Chapter 3 describes the processes that are undertaken to complete a geotechnical mapping project. The processes are represented by a flow chart depicting the individual parameters and how they interact with one another. The equipment used has been primarily assessed for speed and accuracy as well as suitability in differing field environments. The construction of the photogrammetric models and 3D point clouds use computer programs specifically developed for the task. The specific principles of each remote data capture technique means that each computer program, regardless of the manufacturer, must follow similar processes. These processes will be described for the systems used in this project.

To assess the accuracy and precision of the orientation data collected during the project a new method of comparing the data had to be devised. The beginning of Chapter 4 covers 'pole vector difference' calculations, which illustrates the method used to calculate the error between hand-mapped orientation and the remote data capture system derived orientations. Chapters 4 and 5 cover the development of field mapping and data output/ analysis processes respectively. The format of each chapter follows the flow chart described in Chapter 3. The remote mapping systems are tested against hand-mapped data wherever possible for each of the parameters along the process flow chart. The data outputs that correspond between all three mapping techniques, individual feature orientation, set orientation, and roughness are compared in Chapter 5. Trace length data collected using photogrammetry is compared with hand-mapped discontinuity trace lengths that were collected via window mapping. Example end-uses of the remotely captured data are also covered.

A discussion and consideration of contribution to knowledge of the work undertaken during this project are outlined in Chapter 6, along with suggestions of further work. Direct comparisons are determined and comments made between the data collected from traditional hand-mapping, photogrammetry and laser scanning.

Chapter 7 summarises the work undertaken and conclusions achieved. Additionally, a potential 'ideal' workflow is presented, formed from the knowledge gained during the project and potential software/ hardware advancements to the remote data capture technologies.

2 REMOTE DATA CAPTURE

Chapter 2 covers the history of remote sensing and describes how photogrammetry and laser scanning developed. Photogrammetric and laser scanning principles are also covered. Current applications of the techniques are described, both including geotechnical and non-geotechnical examples. A more detailed explanation of geotechnical applications is contained within Chapter 5. This chapter explains how photogrammetry and laser scanning have developed into systems that can now start to be confidently used for remote data capture.

2.1 Remote Sensing

The main two methods of remote data capture used for the characterisation of rock slope used in this project are terrestrial photogrammetry and laser scanning, both of which are forms of remote sensing. They rely on two differing approaches, photogrammetry using visible light, and laser scanning using infrared laser reflection. Mapping from standard 2D photographs is another remote sensing method that can be employed to calculate fracture discontinuity trace lengths for geomechanical modelling, usually coupled with traditional hand-mapping.

Remote sensing covers a large range of techniques and applications, and can be best described as the acquisition of physical data of an object without touch or contact (Lintz & Simonett, 1976). The techniques generally make use of the emitted or reflected electromagnetic radiation of a studied material within certain frequency ranges, such as visible light or infrared spectrums. Measuring the differing wavelengths and intensities of the radiation relays the orientation and condition of the object studied (Campbell, 2002). Other types of remote sensing include using reflected sound waves and measuring gravity and magnetic variations of an area.

Remote sensing began with the invention of photography in 1839; using cameras attached to weather balloons, the first remotely sourced maps were produced in 1858 (Campbell, 2002). Remote sensing continued to develop from there, accelerated by the World Wars. Cameras were routinely installed onto aeroplanes compelled by the need for reconnaissance of trench positions and troop movements. Aerial remote sensing from planes and satellites has been used for many years since; the 1960's and 1970's saw a great increase in research in the field Campbell (2002).

Satellites launched during the 1970's were able to take photographs of the surface of the Earth using multi-spectral electromagnetic radiation measurements. These are able to detect various characteristics, such as vegetation cover or chemical anomalies (Reeves, 1975). Remote sensing from satellites continues to be utilised today.

2.2 Photogrammetry

2.2.1 *History*

Photogrammetry is described as the science of obtaining reliable information from physical objects through processes of recording, measuring, and interpreting photographic images (Slama, 1980; McGlone, 2004).

Only ten years after the invention of the photograph in 1839, the first experiments on aerial photogrammetry began. The stability problems of weather balloons forced the main researcher, Colonel Aimé Laussedat, to concentrate on terrestrial photogrammetry. Another ten years followed and Laussedat presented his work to colleagues in France, giving him the title of 'Father of Photogrammetry' (Campbell, 2002).

As technology advanced, producing more stable balloons and subsequently aeroplanes, aerial photogrammetry was adopted for map making. The World Wars drove the technology on further, developing better cameras and more effective positioning equipment.

The phototheodolite was produced as one of the main methods of collecting photogrammetric photos, combining a camera with a theodolite mounted to the top, to accurately position the camera as well as the direction in which the camera was pointing.

With the introduction of affordable digital cameras in recent years, photogrammetry is now able to be undertaken using computers. Digital photographs are combined with surveying techniques to produce 3D images easily visualised and manipulated on computer screens.

2.2.2 *Photogrammetric Systems*

There are two types of photogrammetry: interpretive photogrammetry and metric photogrammetry. Interpretive photogrammetry includes 'mainstream' remote sensing, which has now become a discipline in its own right. This is the interpretation of a wide range of sensing instruments, including multispectral cameras, infrared, thermal and radar images, as well as traditional photographs (Wolf, 1983).

This project concentrates on systems based on metric photogrammetry, which is the practice of collecting precise measurements from images. Using relative point locations, images can be modified and orientated so that distances, angles, area, volumes, elevations, sizes and shapes of objects can be determined (Wolf, 1983).

The photogrammetric systems employed during this project are described as 'close range photogrammetry' by Slama (1980) and McGlone (2004), as the object studied is usually no more than 300 metres away from the camera, commonly less than 50 metres away. Two types of apparatus are used for capturing analogue photogrammetric images, single-metric and stereo-metric cameras. Single cameras are those that must be moved from their start positions to collect the second photograph for a stereopair, where stereo-metric cameras only need one setup position, as they are essentially two cameras mounted on either side of a bar. Metric cameras are those that are specifically designed for photogrammetric purposes, although professional and amateur standard cameras may also be used.

2.2.3 *Photogrammetric Principles*

A single orientated photograph can only relay the direction from which an object has originated. Combining two images, a stereopair, containing views of the same object, enables the calculation of distance and position of that object using triangulation techniques (Crone, 1963). Traditional metric photogrammetry must use images that are taken parallel with each other, and they must overlap so that common features can be seen. Generally only 60% of the original photographed area can be used due to the required overlap (Wolf, 1983).

Slama (1980) and McGlone (2004) explain that for analogue stereo-pairs to be converted into a useful form then a 'data reduction' system must be used, either being stereo-compactors or mono-compactors. The complex mathematical formulation used in the processing of photogrammetric data is described in the 'Manual of

Photogrammetry', edited by Slama (1980) and McGlone (2004) respectively. The systems used in this project, allowed by the availability of digitally captured photographs, applies the same mathematical principles using computer software, negating the need for analytical stereo-plotters.

Photographs captured with circular lenses must be corrected for distortion when viewed as a rectangular image. Another advantage of using digital photography is that radial lens distortion can be corrected by a computer program. The degree of the correction depends on the camera and lens used to capture the photograph.

The most recently developed photogrammetric systems can create a 3D image from photographs centred on a common 'control' point. This is advantageous, as a larger proportion (~95%) of the original images are used in the creation of the final 3D image, where only the overlap portion of traditional photogrammetry can be used.

Recently developed photogrammetric systems use the parallax phenomenon to estimate the distance to an object, which is analogous to the apparent displacement of an object when viewed with the left and then the right eye respectively. The parallax of a point is directly related to its distance from the camera and the relationship of the two camera positions (Figure 2-1). By knowing the parallax of a point, camera positions and orientation, along with their roll, pitch and yaw, the co-ordinate position of the point can be calculated in XYZ coordinates (CSIRO, 2005).

Multiple digital photogrammetric systems were studied during this project JointMetriX3D (3G Software and Measurement, Austria); 3DM Analyst (ADAM Technology, Perth, Australia) and Sirovision (CSIRO, Australia). The later software program, Sirovision, was used primarily during the project. The program suite is split into two modules, the first, Siro3D, creates the 3D images, Siro3D, the second, SiroJoint is the geotechnical module. The computer program, combining both modules, can represent the photogrammetric image in three dimensions and perform highly detailed examinations and collections of large amounts of data quickly and easily, without being 'in the field'.

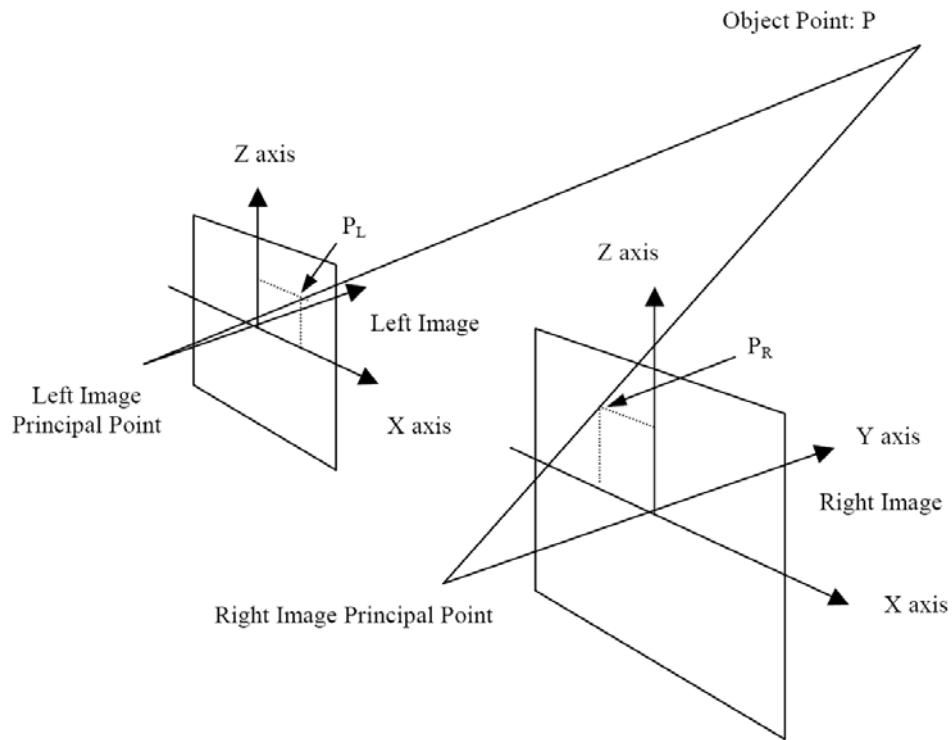


Figure 2-1. Geometry for the determination of the position of a point in object space (from CSIRO, 2005).

The other systems range from those that purely create photogrammetric 3D images to those that also have additional geotechnical analysis modules. The programs that could only create 3D images were imported into the Sirovision geotechnical module, SiroJoint for analysis.

2.3 Laser Scanning

2.3.1 History

Laser scanning was first developed from single beam laser range finders which were attached to surveying theodolites. These were able to pinpoint the position of a reflector station situated over the point of interest. As reflectorless laser technology developed, the need for the use of reflector stations was removed. The use of this new technology was applied to geotechnical applications by Feng *et al.* (2001). Feng *et al.* (2001) used non reflector total stations to find fracture orientations of planes on a rock face. Spatial XYZ co-ordinates of multiple points on the exposed fracture surface were captured. These points were then joined together to form a mesh representing the plane, through which a best-fit orientation was found. The best fit plane was used to measure the dip and dip direction of that fracture surface. This process was able to find spatial positions reasonably quickly compared to hand measurements, but was not automatic.

Automation was introduced by laser scanners that use rotating mirrors to project the laser, enabling quick scanning of large areas. These were developed and primarily used for surveying/ construction applications, and are currently produced by a range of companies, including: Leica Geosystems, I-Site Laser Scanning, Faro, Trimble, and Reigel. The earlier work of Feng *et al.* (2001) was continued by Feng & Roshoff (2004) whereby laser scanners were used to capture 3D points from rock faces to calculate their orientation, spacing, roughness, and persistence, although only for small study areas (± 3 m). As laser scanners became able to capture three dimensional data from larger areas, encompassing many discontinuity features, geotechnical research focused on mass extraction of orientation data (Kemeny & Donovan, 2005; Roncella & Forlani, 2005) using manual and automatic identification techniques. Kemeny & Donovan (2005) and Roncella & Forlani (2005) each use separate algorithms that allow the user to find 'flat' areas of the rock face (discontinuity planes) by setting certain cut-off criteria. The point cloud can be assessed as a whole, or selected areas of study can be used in a semi-automatic mode.

2.3.2 *Laser Scanning Systems*

Laser scanning uses one or more infrared lasers to collect spatial data from a scanned area. Two types of laser scanning are currently employed, Time-Of-Flight (TOF) and Phase Shift. The basic principle behind TOF and phase shift is that the position of a point in 3D space can be calculated by measuring its distance and orientation from a known point using reflected laser pulses.

2.3.3 *Laser Scanning Principle*

Both laser scanning systems start by emitting a laser beam towards the studied surface. The laser is reflected from an internal rotating mirror to a point on the face. A detector within the scanner is able to make a distance measurement based on the return signal reflected back from the surface. Each system generates these distance measurements from the returned signal. Time-of-flight scanners measure the time that a laser pulse takes to be sent from the scanner to the face and the return signal to be received. Knowing the speed of light a distance measurement can then be made (Leica, 2005). Phase-shift laser scanners use a continuous laser beam and works on the principle that the returning wave from the laser has the same frequency and amplitude of the sent wave; however they will be out of synchronisation. By comparing the phase difference between the sent signal and the returned signal, a distance measurement can be made (Faro, 2005). These distance measurements are

combined with the internal angle measurements of the rotating mirrors as they spin within the scanner. A scanner can then establish a relative three dimensional position in space for each point on a surface. This process is repeated thousands of times a second, collecting many points over the studied surface in just a few minutes. Based on the strength of the return laser signal, the intensity for each point within the cloud is also recorded.

Laser scanned point clouds can also be combined with digital photographs and this is completed in two ways. A digital image of the studied object is draped over the point cloud, providing a similar view to a photogrammetric 3D image. This process is primarily done manually, where points must be matched up with pixels from the digital image, although automatic algorithms have been developed (Ratcliffe & Myers, 2006). The second method uses the digital image to colour each point within the point cloud (Leica, 2006). If the point cloud is very dense then it should also be comparable to a photogrammetric 3D image, although in most cases, where there is space between the points there is no colour information. As the laser scanned 3D data is represented as point clouds, with photo overlays being difficult to implement, visualisation of lineament data (2D fractures) is problematic.

When viewed on a computer the collected points are represented as a 3D point cloud. Two laser scanning products were used during the project, the HDS3000, which is a time of flight laser scanner, and the HDS4500, a phase shift laser scanner, both produced by Leica Geosystems. The package includes core software to aid in data capture and point cloud management named Cyclone (Leica, 2006).

Geotechnical data processing was performed by SplitFX (Split Engineering, 2005), produced by Split Engineering, Arizona USA. SplitFX uses the raw point cloud data produced by laser scanners and meshing algorithms to create surfaces representing the scanned rock face. This 3D model can then be geotechnically mapped by delineating features using the computer mouse. The orientation, roughness and area of the delineated features are calculated automatically from the meshed surfaces of the rock face.

2.4 Uses of Remote Data Capture

2.4.1 *Geotechnical Aspects*

Engineering geology and geomechanics is the application of the science of geology to the understanding of the mechanics and physics of materials within the Earth to provide engineering solutions for geological hazards. Geotechnical studies are carried out during the planning, environmental impact analysis, civil engineering design, value engineering and construction stages of public and private work projects, and during post-construction evaluations. The principal aim is to prevent harm to people and property within all environments (Hudson & Harrison, 1997).

The main digital remote data capture techniques that are being developed by the geotechnical engineering industry for the use in rock face mapping are photogrammetry and laser scanning. Laser scanning is known to have many geotechnical applications (Kohoušek, 2006). Photogrammetry has long been thought of as a valuable tool for geomechanics as,

'photogrammetric methods offer considerable advantages and the authors believe that they will increasingly be used in rock engineering' (Hoek & Bray, 1977).

Since 1977 the technology behind remote data collection has developed considerably. Using specialised software, the systems produce spatially accurate, densely detailed 3D representations of the rock mass. Measurements from these 3D images allow the collection of large quantities of data in a reasonably short space of time. Using remote data capture systems for the characterisation of a rock mass is a relatively new procedure. Traditionally hand measurements of a face are recorded using a compass clinometer and notepad/ mapping board to map a rock face.

Use of remote data capture has become a necessity in the geomechanics and mining industries. The UK Quarries Regulations 1999 (Health and Safety Commission, 1999) came into force in 2000 and outlining detailed safety procedures to protect those working in the industry. These were implemented by restricting access to some areas which required data collection.

Quarries Regulations 1999; Regulation 30 states that:

'Tips and excavations have to be designed, constructed, operated and maintained to ensure the stability or movement which is likely to give rise to health and safety risks of any person is avoided'. (Health and Safety Commission, 1999).

Slopes must be appraised and monitored so that this regulation is met satisfactorily. If any slope in a quarry must be studied then, unavoidably, the person performing the examination is at risk when they get close to the face. Slope appraisal is usually a repetitive process, and each assessment is time consuming, as well as potentially dangerous for the conducting personnel. Remote mapping of quarry faces is now preferred to hand-mapping, as it has advantages concerning slope stability monitoring. It is used to capture data from potentially unstable slopes and results can be easily and non-subjectively compared over a predetermined time scale. Photogrammetry is commonly used to monitor rock and soil slope movements over large scale areas (Merel & Farres, 1998; Oka, 1998). Donnadieu *et al.* (2003) used aerial photogrammetry to represent volcano slope instability. Terrestrial photogrammetry is still continually being developed for use in the geotechnical engineering industry (Poropat, 2001).

2.4.2 Coastal Geotechnical Aspects

Natural coastal slopes/ cliffs make up approximately 75% of the worlds coastline (Bird, 2000). The instability of natural costal slopes, due to cliff retreat is a significant threat to coastal populations, especially with the potential of increased erosion due to sea level rise caused by global warming (Lim *et al.*, 2005). Hall *et al.* (2002) explain that the failure to understand the processes through which rock cliffs evolve means that many coastal protection schemes are poorly designed or inappropriate. Laser scanning and photogrammetry have been demonstrated to be a useful tool on monitoring coastal cliff erosion (Lim & Yang, 2004; Lim *et al.*, 2005; Rosser *et al.*, 2005). Multiple research projects and proof-of-concepts, such as Adams and Chandler (2002), Lim *et al.* (2005) and Barber & Mills (2007) showed that cliff monitoring by photogrammetry and laser scanning was achievable.

Rosser *et al.* (2007) conducted a quantitative rockfall hazard assessment using terrestrial laser scanning upon a coastal cliff section. By using comparative laser scanned point clouds taken across 15 months it was possible to assess the volume of individual rockfalls that took place over that time period. The minimum volume change

measured was 0.000001 m³ when the laser scanner was at 60 m from the toe of the slope. Even when this volume change is extrapolated to 0.001 m³, for when the scanner is used at its maximum range (700 m), it is far below the threshold used by conventional rockfall studies (Rosser *et al.*, 2007). Difficulty in comparing these results with conventionally captured data was highlighted; the inaccuracy of historically captured data was mainly due to the variability of human perception (Cleveland 1985, cited by Rosser *et al.*, 2007).

2.4.3 *Non-Geotechnical*

Remote data capture systems are used widely in many different working environments. This section gives an example of differing applications of photogrammetry and laser scanning.

Photogrammetric images are still predominantly captured aerially, as these cover large areas quickly and negate the problem of land access and safety. Because of these factors, photogrammetry is primarily used for topographic mapping, creating an orthophoto (a photo corrected for scale and distortion) of an area which is then converted to a map. The civil engineering industry uses photogrammetry extensively for planning and designing constructions, such as roads and bridges (Wolf, 1983). The topographical data captured photogrammetrically allows for detailed images to be created, which can then be used to plan accessible routes for new roads. Photogrammetry is also used for traditional surveying, where property boundaries are delineated accurately from aerial images.

Non-engineering applications for photogrammetry also involve map making for architecture, archaeology, hydrology, conservation, and mineralogy. Mining companies use these techniques, combining them with other remote sensing systems, to trace mineral lodes cheaply and quickly.

Terrestrial photogrammetry is still used for topographic mapping, restricted to use in deep ravines which cannot be easily seen from the air. Non-topographic applications for terrestrial photogrammetry are now widely used, ranging from archaeology to dentistry. It has become widely used for processing traffic accidents; whereby the scene is recorded using photogrammetry so that the debris can be collected, and the roads cleared quickly (Wolf, 1983). This is where the applications of photogrammetry and laser scanning overlap. Forensic investigations of traffic accidents or crime scenes need to have the positions of multiple objects measured very precisely. A detailed

laser scan or photogrammetric 3D image creation of a room takes minutes, rather than hours of procedural police sketches and hand measurements.

Laser scanning is extensively used for engineering surveying applications. Accurate measurements of engineering works can be captured by the laser scanner which can then be transferred in to computer-aided-design (CAD) software packages. At the moment, the construction industry is the major beneficiary of this new technology, making surveying of structural measurements very quick and reducing the 'down' time of projects, which is usually a problem when surveying is undertaken. Archaeology also benefits from both remote data capture techniques, where aerial photogrammetry can record ancient building layouts and laser scanning can be used to precisely record smaller artefacts held within them (Wolf, 1983).

2.5 Review of Previous Work Undertaken

Remote data capture systems are beginning to be implemented and compared in varying applications other than geotechnical engineering, upon which accuracy analysis has been undertaken by researchers, including: Bock *et al.* (1998), Heritage *et al.* (1998), Huising & Pereira (1998), Poterasu *et al.* (2001) and Adami *et al.* (2007). Accuracy of photogrammetry and laser scanning is shown to vary, with some tests resulting in more accurate measurements than others.

The intrinsic accuracy of terrestrial photogrammetry and laser scanning has been studied by numerous authors, including: Butler *et al.* (1998), Huising & Pereira (1998), Boehler *et al.* (2003), Kersten *et al.* (2004), Fraser *et al.* (2005) and Heikkinen (2005). Butler *et al.* (1998) used independent field surveys of gravel beds to check the accuracy to corresponding digital elevation models (DEMs) created from close range terrestrial photogrammetry. The study showed that digital photogrammetry can be used to produce high resolution DEMs of natural gravel surfaces. However, it was noted that whilst DEM creation parameters are important in increasing the 3D model creation 'success', it does not necessarily result in a more accurate DEM. The authors highlighted that errors that affect the accuracy of the models created include: instrument (survey measurement) errors, atmospheric interference and variable camera convergence angles.

Comparisons between photogrammetry and laser scanning have been undertaken previously to this study. They and other authors have proved that photogrammetry and

laser scanning can represent 'real world' objects accurately when within certain limits. The Sirovision manual states that 'Siro3D can produce spatial data with accuracies of the order of 10 to 20 mm at 100 metres when used with care with a calibrated camera and lenses'. The orientations of planes are measured in Sirojoint with 'accuracies of +/- 0.1 to 0.2 degrees at 100 metres for a 1 metre plane' (CSIRO, 2005). Accuracies of the other photogrammetric systems are similar and are thought to be comparable to the Sirovision system (Gaich, 2007). The Leica HDS3000 manual states that the laser scanner can achieve a positional accuracy of 6 mm and a distance accuracy of 4 mm when the scanner is between 1 m – 50 m of the study object (Leica, 2005). These accuracy tests, collected by the manufacturers of the systems, will have been undertaken in controlled scenarios and the results collected will be the best that can be achieved. When the remote data capture systems are tested under conditions that are not ideal the results obtained will be closer to the true accuracies that an end-user would regularly expect to achieve.

Research specifically upon automatic and semi-automatic discontinuity identification and related processes has been undertaken by numerous authors including: Slob, *et al.* (2004); Feng & Roschoff (2004); Donovan, *et al.* (2005); Slob, *et al.* (2005); Turner, *et al.* (2006); Slob, *et al.* (2007); Lato, *et al.* (2008) and Olariu, *et al.* (2008). They cover the 3D mesh creation process, whereby two algorithms are described by the various authors: polygonal and parametric. Additionally, multiple algorithms used to automatically identify discontinuities from these surfaces have been developed by these authors. They state that automatic/semi-automatic identification of discontinuities is capable of performing similarly to manual delineation but with increased speed. It is noted that the mesh density used to create the 3D model is important as its accuracy can be affected by natural roughness and laser scanning 'noise'. Shadowing and/or obstructions are also noted as being potential problems when using the data for geotechnical mapping as full coverage of the rock face is beneficial in capturing the maximum amount of accurate data.

Birch (2006) presents the 3DM Analyst (ADAM Technology) geotechnical mapping software suite, covering the features of the program in depth including the accuracies that can be achieved. An accuracy of 0.5 pixels, 0.7 mm, was achieved using 3DM analyst when locating circular targets. 3DM Analyst was tested during this study, although only for photogrammetric 3D model creation, as in the early stages of this project 3DM Analyst had not fully completed its geotechnical mapping module.

Gaich, *et al.* (2006) covers the use of the ShapeMetriX3D and JointMetriX3D (3G Software and Measurement) photogrammetric software for geotechnical mapping. Both software packages use the same general photogrammetric principals, but differ in that ShapeMetriX3D uses a standard calibrated DSLR camera where JointMetriX3D uses a 100 megapixel panoramic line-scan camera. Both systems produce 3D images that can be geotechnically mapped using JMX Analyst, also produced by 3G S&M. The ShapeMetriX3D White Paper (3G Software and Measurement, 2006) describes the accuracy of the system as being within the centimetre range. The geotechnical mapping module JMX Analyst was tested during early stages of this project on 3D models pre-produced by 3G S&M. The models created in the 2005 version of ShapeMetriX3D had to be created using a range pole that was placed in the field of view of both photographs.

Kemeny, *et al.* (2006) illustrate the use of SplitFX to manage and geotechnically map point clouds. It describes the accuracy of an individual point of a laser scanned point cloud as being dependent on the manufacturer, ranging between 5 mm – 8 mm at 100 m scan range. The affect of varying density of laser scanned points on a mapped discontinuity plane was studied; the orientation between a plane with 11 points existing on its surface was compared to the same plane with 91 points. Using Monte Carlo simulations it was found that the plane represented with 91 points had a dip/dip direction variation from the actual of $\pm 0.18^\circ$ and $\pm 0.1^\circ$ respectively. The same plane with 11 points resulted in variations of $\pm 0.5^\circ$ and $\pm 0.35^\circ$ respectively. This result suggests that laser scanning should produce good dip/dip direction data which can be used to compare against traditional hand-mapping.

Poropat (2006) describes the use of 3D images for the mapping of geotechnical characteristics and introduces the Sirovision software suite. The paper presents a table comparing compass/hand-mapped joints and the photogrammetric equivalent, which are all within 11° difference for both dip and dip direction. It warns that 'estimation or validation of the accuracy of the orientation measurement is fraught with difficulty', in that hand-mapped measurements are subject to human error.

Tonon & Kottenstette (2006) compare the datasets captured by 3G Software and Measurement against ADAM Technology taken from an outcrop near Morrison, Colorado. The comparison found that each system found joints sets the other could not visualise, but the orientations of those sets that both systems identified were very similar (within 5° for both dip and dip direction). Calculating joint set spacing had more

varied results, where the mean spacing differed by 60% and the standard deviation differed by 300%. The calculated tracelengths displayed much less variability, 10% for the mean and 20% for the standard deviation. Both systems also produced roughness profiles for one joint plane and were visually compared and assessed to be comparable, although no JRC value was calculated. The comparison made between the two systems was not made against traditionally hand-mapped data for any of the parameters measured, but they were shown to collect data that was similar between each of them. The setup positions of the cameras were not consistent between the two systems as the photographs were taken freehand, which may have been a factor in the slightly differing results.

Voyat, *et al.* (2006) used both photogrammetry and laser scanning as comparisons against traditionally surveyed orientation data, although at two differing locations. A software program, ESP, uses Ransac algorithms to automatically identify joint planes within a manually selected area of the study face. Comparison between photogrammetrically captured data and traditional survey data resulted in similar joint set orientations. However, the photogrammetric system failed to identify a sub horizontal fracture set as it was parallel to the views of the photographs used to make the 3D image, thus they were represented only as traces. Although, the remote mapping system did identify a joint set missed by the traditional survey as it was confused with another similarly orientated set. The laser scanned orientation data compared against traditionally mapped data from a separate site also found that joint set orientations were found to be similar between the two mapping techniques. However, alike to the photogrammetric system, it did not identify two joint sets because they were not within the field of view of the scanner.

Strouth & Eberhardt (2006) used SplitFX (Split Engineering, 2005) to geotechnically map a structurally controlled rockslide at Afternoon Creek, Washington, Unites States. Multiple laser scanned point clouds of the rock face were captured from varying positions and scales. Geotechnical properties such as joint orientation, persistence, and spacing were calculated and used successfully to create distinct element models for back analysis of a failure that occurred in November 2003.

Characterising fracture roughness using fractal parameters has been conducted by numerous authors including: Rahman, *et al.* (2006) and Baker, *et al.* (2008). The fractal dimension of a curve length is calculated by comparing the curve length when sampled at different scales (Barnsley, 1988, cited by Baker, *et al.*, 2008). Rahman, *et*

al. (2006) found that the density of the laser scan used to create the profile points was an important factor. A low density reduces the effectiveness of measuring small scale roughness and only larger scale asperities can be visualised. Baker, *et al.* (2008) used fractal measurements upon photogrammetrically derived surfaces, it was noted that the scale at which the roughness measurement was made, impacted on the results obtained. Currently there is no conversion factor between the fractal roughness measurement and joint roughness coefficient (JRC).

JRC measurements taken from profiles of the fracture surfaces have been researched by Haneberg (2007) and Poropat (2008). Profiles from 3D images are assessed using adapted methods by Tse & Cruden (1979) and Maerz (1990). Similarly to the fractal roughness measurements, the results are correlated with the scale of measurement. Conversely to the fractal studies, JRC values were obtained, although due to the nature of the adapted methodologies, values collected were occasionally outside the 0 – 20 JRC range.

Research into the use of topography maps to complete structural mapping has been adapted from larger scale projects. COLTOP 3D (Quanterra, Switzerland) is a software program that was originally developed to assess large scale digital elevation/terrain models (Derron, *et al.*, 2005; Metzger, *et al.*, 2008). Colours corresponding to dip/dip direction of each cell are displayed on a relief map giving a quick overview of the structural conditions of the study area (Jaboyedoff & Couture, 2003). This software, and related topography mapping techniques (Poropat, *et al.*, 2008) are now being used for assessing close range point clouds captured from rock faces (Jaboyedoff, *et al.*, 2007; Struzzenegger, *et al.*, 2007a). The accuracy of these techniques has not yet been fully assessed, but the orientations of measured structures is said to be 'in good agreement', but 'less steep than those measured in situ' (Jaboyedoff & Baillifard, 2004; Pedrazzini *et al.*, 2008).

Conclusions drawn from previous work are that remote data capture systems provide speed, safety and potential automation of the analysis for rock mass characterisation. They were used to successfully complete and compliment traditional mapped exercises that were then used for end-uses such as modelling and volume calculations. Each photogrammetric and laser scanning software system quoted their varying accuracies for the 3D models created. Comparisons between laser scanning and photogrammetry were primarily made in terms of discontinuity orientation. However, these comparisons did not directly dispute traditionally hand-mapped data from specific discontinuities

from the same study site. The comparisons between orientation measurements were taken from discontinuity sets; the difference in dip and dip direction respectively. It was also concluded that descriptions of roughness (JRC), wall strength (JCS), weathering, seepage and discontinuity infill could not be fully completed using remote data capture systems.

2.6 Summary

Photogrammetry and laser scanning are subdivisions of remote sensing. Photogrammetry has been used for many applications for many years, where laser scanning is a relatively new technique of remote data collection, both of which have been updated and incorporated into the digital medium and computer visualisation. The remote data capture systems used during this project are known as terrestrial photogrammetry and terrestrial laser scanning.

The remote data capture techniques differ in their basic principles; laser scanning actively applies illumination (via laser) to the study face so that information can be collected by the scanner. Photogrammetry is a passive system, relying on external sources of radiation, e.g. the sun, to enable the capture of data from the rock face.

Remote data capture systems are beginning to be used for geotechnical analysis of quarries and coastal slopes. These methods are being adopted as increasing health and safety legislations are restricting the access to unsafe areas which still need mapping. Aerial photogrammetry and laser scanning have been used to assess possible instabilities over large areas, such as hills and volcanoes. Remote data capture has many non-geotechnical applications, ranging from map making, to crime investigation.

Photogrammetry and laser scanning have been tested for intrinsic accuracy, proving that they are capable of representing the 3D morphology of study objects. However, differing studies conclude with results of varying accuracy for photogrammetry and laser scanning using differing geotechnical parameters. The remote data capture systems are yet to be comprehensively compared against traditionally hand-mapped geotechnical data; are they sufficient for the use in geotechnical mapping?

3 DATA CAPTURE PROCESS WORK-FLOW

3.1 Introduction

During the project a process work-flow was developed (Figure 3-1). This chapter describes each individual section of the work-flow diagram and its subdivisions. Each section must be completed and considered before moving onto the next stage of the data capture process. This chapter also shows how each process interrelates between each mapping technique and establishes how they can be assessed and compared in later chapters.

The first stages of the data capture process were based on the Sirovision user manual which described parts of the planning and on site assessment stages (CSIRO, 2006). These were modified to also include the preliminary stages needed for laser scanning and traditional hand-mapping. The next stage is positioning, where the mapping equipment is positioned to a local or worldwide grid. Some surveying techniques are unsuitable for particular mapping techniques, indicated in Figure 3-1. Once the equipment is setup and positioned, the raw data capture can then be undertaken, completing the fieldwork process. The post-processing section starts with model creation and data compilation, from which discontinuity features are mapped. The second processing stage involves the data analysis, including identifying sets and output of geotechnical data. The resulting data, e.g. orientation and discontinuity trace length values, can then be brought forward for the use in multiple end-uses: such as kinematic analysis, geotechnical modelling and RMR/Q ratings.

The examples given are taken from Carnsew Quarry, Mabe, Cornwall (Latitude: 50°10'6.34"N, Longitude: 5° 8'20.81"W)

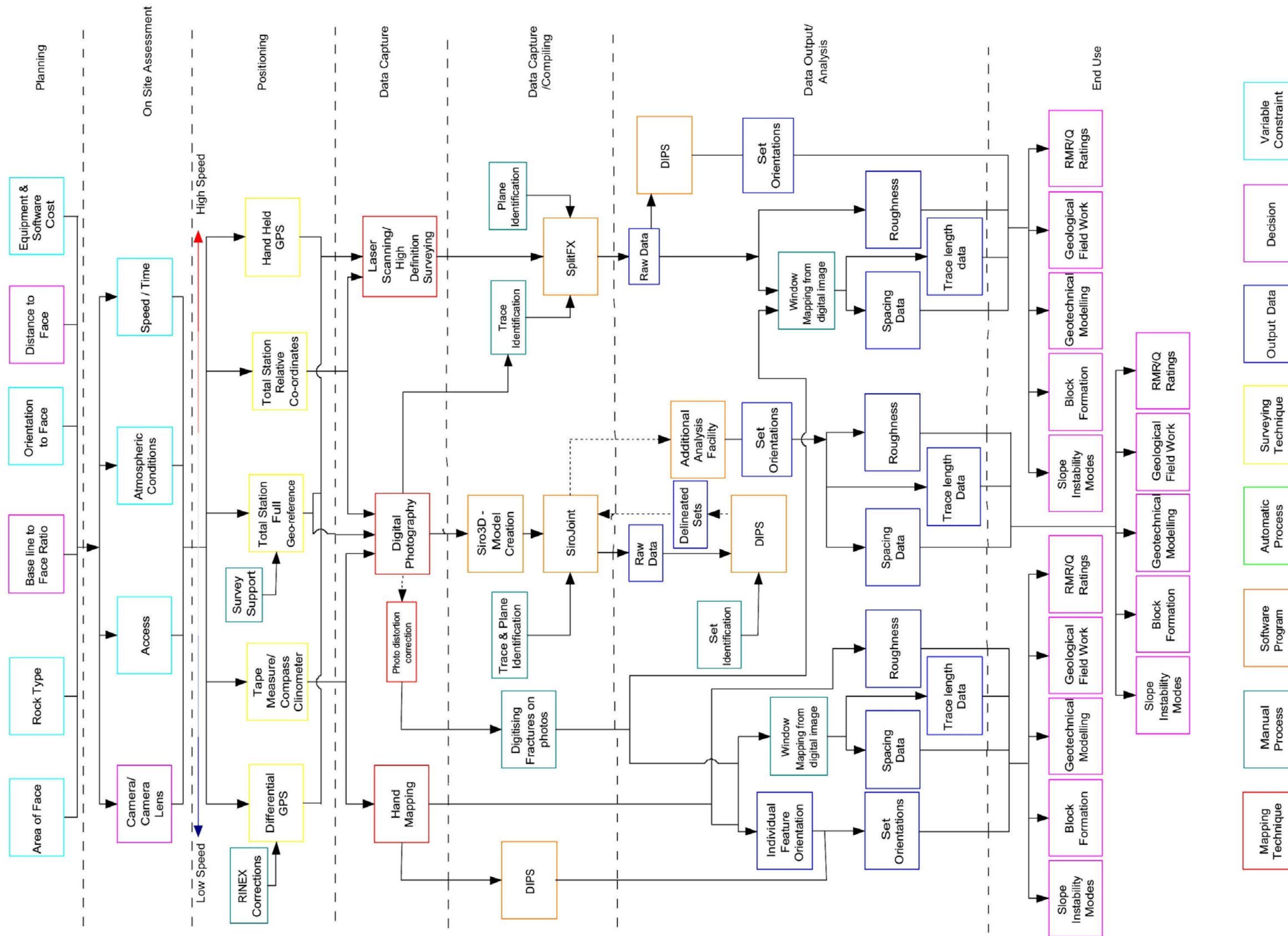


Figure 3-1. Process work-flow diagram with key underneath. The first stage requires that each parameter is considered before the site investigation starts, this can take place before or once the site is reached. The second stage uses an on site assessment to ascertain the conditions under which the remote data capture systems are to be used. The positioning technique is directly related to the data capture system used i.e. the tape measure and compass clinometer cannot be used to position the laser scanner. Once the data capture is completed the data is compiled using the programs specified. The dashed lines indicate that the photogrammetric/Sirovision process, once moved to data analysis, must be re-submitted into Sirovision to allow for the additional analysis facility to be used. The data analysis for all three techniques uses DIPS (Rocscience, 2006), however it is also used to compile the data for hand-mapping. Once the data is processed into spacing and roughness data, etc. it is available for use in the multiple end-uses.

3.2 Workflow Sections Overview

3.2.1 *Planning*

This section describes the field parameters that have to be considered before fieldwork should take place. Completing these will save time in the field and should increase the effectiveness of the chosen mapping system. Some parameters are applicable to all the mapping systems, where others, such as camera baseline ratio, are specific to photogrammetry. Each of the parameters described in the following sections have been assessed during the project. Where limits have been found, recommendations are made in later chapters.

3.2.2 *On Site Assessment*

On site assessment is conducted once in the field and is usually affected by factors that are highly variable. These factors include access to the face, weather/ environmental/ atmospheric conditions at the site and the speed/ time that it will take to complete the remote and/ or hand-mapping fieldwork. Each of these factors affects the fieldwork process that will be undertaken and each has been assessed during the project. The conditions that are considered during the on site assessment may affect the parameters decided upon during the planning stage which results a modification.

3.2.3 *Positioning*

Positional data is taken using the eastings, northings, and elevation (XYZ) coordinate system, either within a relative or full geo-referenced system. Varying positioning techniques have been tested for their suitability to the project, each with their own advantages and disadvantages. The photogrammetric module Siro3D requires that the camera positions and controls points are surveyed to centimetre accuracy to provide an accurate 3D image. The laser scanning systems also require centimetre accuracy, but as the data is captured from a single position the input of an accurate directional orientation into the machine is the essential measurement for precise 3D point cloud creation. The positioning techniques tested during the project are:

- Compass bearings and tape measure - relative coordinates
- Handheld global positioning systems (GPS) – full geo-reference
- Differential global positioning systems (DGPS) – full geo-reference
- Reflectorless total station – full geo-reference

- Reflectorless total station – relative coordinates

Full Georeference versus Relative Coordinates

Using full geo-referencing, the 3D images created are represented in accurate 3D space relative to the surface of the Earth, i.e. geographically correct. This method is useful if multiple 3D images were to be combined to make a large image, as no repositioning would be required during the data compiling stage. Relative coordination for photogrammetric 3D images is taken relative to north, providing exactly the same accurately orientated data points as full-georeferenced 3D images, but without actual Earth coordinates. By inputting the direction of north into the laser scanner controlling computer the point cloud created is relatively coordinated to north, this can be done before or after scanning. To create a large combined 3D image/point cloud, using relatively coordinated 3D images/point clouds, requires the repositioning of those original images/point clouds by visual matching. This can be performed in both Siro3D and Cyclone for photogrammetry and high definition surveying respectively.

3.2.4 Data Capture

The data capture process includes hand-mapping, laser scanning and digital photography, which then goes on to be used for photogrammetry and is also used as an aide for the other two mapping techniques. Field methodologies for each technique were tested and refined so that the time spent was minimised whilst collecting suitable 3D data.

3.2.5 Data Capture / Data Compilation

The raw 3D data collected by the remote mapping systems is converted for use with geotechnical analysis programs. The photogrammetric 3D model and point cloud are created during this process. The point cloud is easily exported from the scanner as an XYZ file, containing the coordinates for each point. The digital photographs go through a lengthier process to be converted to a three dimensional photogrammetric image. This converted 3D data is subsequently analysed using the specially designed software packages, SiroJoint and Split FX, where discontinuity traces and planes are identified. Photographs of the face are also used by laser scanning systems to help recognise discontinuity features seen in the rock. Using traditional hand-mapping, the rock face data is collected during the field mapping process, such as discontinuity orientation and roughness. Additional features are digitised on photographs once corrected for lens distortion.

3.2.6 *Data Output / Analysis*

The data analysis differs between each of the mapping techniques, primarily due to the differing software programs and the resultant formats used to describe the characteristics of the rock mass. Each process is used with a stereographic analysis program, DIPS, produced by Rocscience (2006). The photogrammetric program SiroJoint exports orientation data which is delineated into sets using DIPS. This is subsequently fed back into the original program which then exports orientations, spacing, roughness, and discontinuity trace lengths organised into separate fracture sets. Hand-mapping also uses DIPS to analyse the field collected data and to delineate fracture sets. The features that were digitised on the photographs during data compilation are then window mapped to find discontinuity trace lengths and spacing. Laser scanning data can also be used with DIPS, in conjunction with the SplitFX program, to delineate set orientations. Roughness of planes can be exported along with discontinuity orientation, although spacing and discontinuity trace length data is recorded from window mapping similarly to hand-mapping from photographs.

3.2.7 *End-Use Applications*

The output data and methodologies described are generic so that they can suit most geotechnical end-uses/ applications; these are covered in more detail in Section 5.6. The data obtained by hand-mapping, photogrammetry and laser scanning can be customized to suit other purposes, such as monitoring, 3D geotechnical modelling, or blast planning.

3.3 Planning

3.3.1 *Distance to Face and Study Area*

The distance to the studied object is directly proportional to the obtainable study area for both photogrammetry and laser scanning. Before any photogrammetric fieldwork is undertaken the equipment configuration must be decided. The 3D image creation module, Siro3D, provides imaging creation planning, which allows the user to estimate extent (m^2) of the 3D image, depending on certain input parameters, such as distance from face or lens type. The program uses distortion calibrations of the lens, and the known resolution loss at distance to calculate the spatial precision. The distance from a face predominantly dictates the resolution of the 3D image that will be created and the size that can be acquired. The Siro3D manual uses an example of 90 m to create a good 3D image (CSIRO, 2005).

The maximum distance range for high definition laser surveying is restricted by the power of the laser used by the scanner. The maximum distance for the HDS3000, a time of flight laser scanner, is around 300 m (Leica, 2005). The spot size of a long range scan will be large; this may affect the reliability of the scan. The distance to the face also affects the density of the resultant scan; whilst a dense scan from a great distance can be achieved, the time to complete the scan would be excessive and the problem of the increased spot size would also need to be accounted for.

It is important to decide on the scale that the remote data capture systems are to be employed, and whether it is suitable for the application (Figure 3-2). Capturing the rock mass characteristics at multiple scales is beneficial, as then instabilities of varying size can be factored into the analysis.

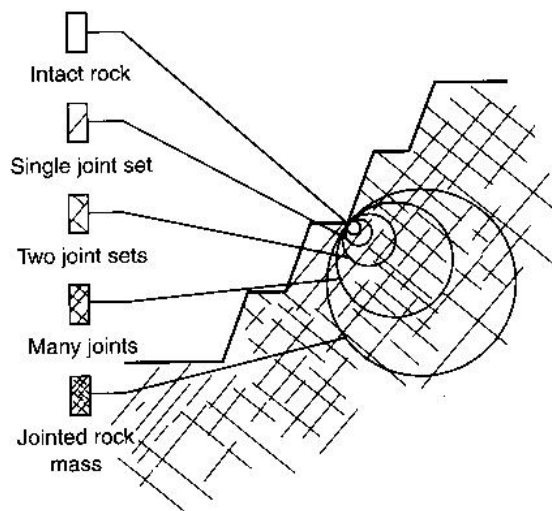


Figure 3-2. Diagram showing scale effects upon overall rock mass strength. Capturing the rock mass characteristics at multiple scales is beneficial to geotechnical studies, as then instabilities of varying size can be factored into the analysis (from Wyllie & Mah, 2004).

3.3.2 Camera Separation / Baseline Ratio (Photogrammetry)

The distance from the face also dictates the spacing between the two camera setups (Figure 3-3). The camera separation is recommended to be between $\frac{1}{6}$ and $\frac{1}{8}$ of the distance to the face (CSIRO, 2005). This ratio is determined to create a sufficient parallax for the subsequent 3D photogrammetric image to be made.

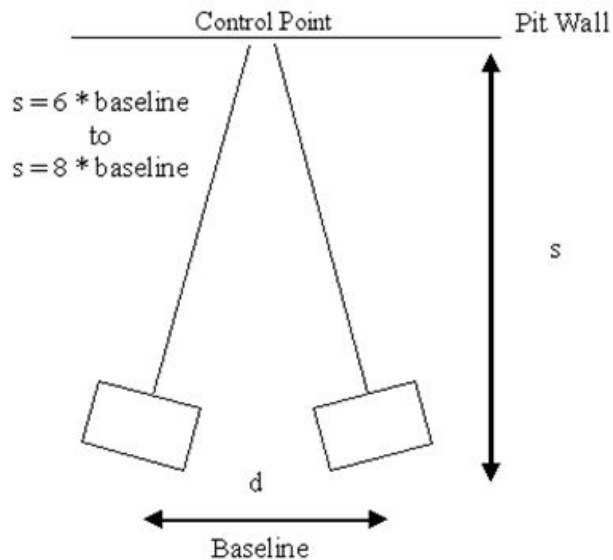


Figure 3-3. Camera separation/ distance from face ratio. Cameras are orientated so that the control point is in the centre of their view and spaced at a distance 1/6 of the baseline distance to the study face (modified from Siro3D manual, CSIRO, 2005).

The position of the control point for a photogrammetric image is recommended to be at the centre of the two images to achieve the greatest accuracy. If that is not possible the control point can be placed anywhere in the field of view of both cameras. It may be demarcated previously, i.e. a reflective marker, or it may be a recognisable feature on the face, such as the intersection of two discontinuity traces.

3.3.3 Orientation to Face

Preferably the cameras should be near perpendicular (in both horizontal and vertical planar fields) to the face being photogrammetrically measured. This is so the parallax can be calculated more easily by the computer algorithms. Cameras may have an oblique angle to the face, i.e. less than 90°, the maximum range of which was tested during the project. Moving obliquely to the rock face will result in inaccuracies of the resultant 3D image, as the photographs will have an uneven distortion, one side being closer to the face than the other, which is hard to correct. An indirect view of the rock face will also increase the likelihood that blinding will occur (Figure 3-4).

An oblique orientation to the face also causes blinding for laser scanned point clouds; as a laser scan is completed from one position the probability of blinding is even greater with high definition surveying.

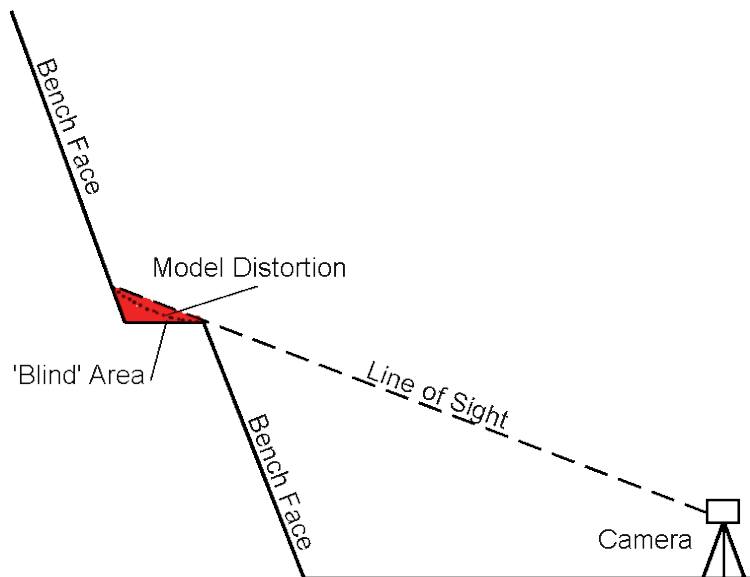


Figure 3-4. Diagram showing potential distortion effects due to 'blinding'. Due to an unfavourable orientation/position of the camera or scanner, sections of the face are unseen. Photogrammetric 3D image creation will distort the final model to fit the data in view (blocked by the red section), where laser scan point clouds will have the red section missing (not to scale).

3.3.4 Geology of the Studied Rock Face

Standardised methods of characterisation and measurement of the rock discontinuity properties are given by ISRM guidelines (ISRM, 2007). They vary depending on the purpose of the engineering work. The main characteristics of each of these properties are recorded and then reassessed according to the objective undertaken (Hudson & Harrison, 1997). The scales of the features affect the ability of remote data capture systems to record them. Many rock mass characteristics must be recorded by physical or close proximity inspection of the studied rock face. Digital photography can be used as the remote data capture system for most rock features, where photogrammetry or laser scanning must be used when more accurate or larger data sets are required. As digital image capturing advances, the resolution of the remotely acquired images can negate the need to be in contact with the face.

Rock Type and Rock Strength

The internal structure of rock, e.g. mineralogy, and porosity, influences the strength of the rock mass regardless of the presence discontinuities. Knowing the rock type gives a general indication of its strength (Table 3-1). The rock strength indicates the shear strength and deformability of the entire rock mass, across non infilled closed boundaries (Wyllie & Mah, 2004).

Table 3-1. Field estimates of uniaxial compressive strength (from Hoek & Brown, 1997). Qualitative empirical descriptions of rock strength in the field can be used to roughly estimate the quantitative value.

Example Rock Types	Term	Uniaxial Compressive Strength (MPa)	Point Load Index (MPa)	Field Estimate of strength
Fresh basalt, chert, diabase, gneiss, granite, quartzite	Extremely Strong	>250	>10	Specimen can only be chipped with a geological hammer
Amphibolite, sandstone, basalt, gabbro, gneiss, granodiorite, limestone, marble, rhyolite, tuff	Very Strong	100 - 250	4 - 10	Specimen requires many blows of geological hammer to fracture it
Limestone, marble, phyllite, sandstone, schist, shale	Strong	50 - 100	2 - 4	Specimen requires more than one blow of a geological hammer to fracture it
Claystone, coal, concrete, schist, shale, siltstone	Medium Strong	25 - 50	1 - 2	Cannot be scraped or peeled with a strong pocket knife, specimen can be fractured with a single blow from a geological hammer
Chalk, rocksalt, potash	Weak	5 - 25	-	Can be peeled with a pocket knife with difficulty, shallow indentation made by firm blow with point of geological hammer
Highly weathered or altered rock	Very Weak	1 - 5	-	Crumbs under firm blows with point of a geological hammer, can be peeled by pocket knife
Stiff fault gouge	Extremely Weak	0.25 - 1	-	Indented by thumbnail
Point load tests on rocks with a uniaxial compressive strength of below 25 MPa are likely to yield highly ambiguous results				

Remote data capture systems provide information on the rock type by visual examination. Rock strength can be inferred visually, but lab testing is required to achieve accurate estimations. Most rock types can be broadly identified from just viewing them, although more detailed information, such as grain size, can only be found whilst being in close proximity/ contact with the rock. The UCS and point load index can be generally attributed to the rock type, but once again, contact with the rock is needed for accurate measurement.

Weathering

Weathering results in the deterioration of rock strength, resulting in the weakening of the rock mass as a whole. A range of weathering grades is described in Table 3-2.

Assessment of weathering grades is performed by studying the rock mass as a whole, usually across multiple exposures or benches. Therefore close proximity to the face is not required, so weathering grades can be estimated remotely.

Table 3-2. Weathering grades (from ISRM, 1981b). Using descriptions of the rock mass the grade of weathering can be estimated for use in subsequent analysis.

Term	Description	Grade
Fresh	No visible sign of rock material weathering; perhaps slight discolouration on major discontinuity surfaces	I
Slightly Weathered	Discolouration indicates weathering of rock material and discontinuity surfaces. All the rock material may be discoloured by weathering and may be somewhat weaker externally than its fresh condition	II
Moderately Weathered	Less than half of the rock material is decomposed and/or disintegrated to a soil. Fresh or discoloured rock is present either as a continuous framework or as corestones.	III
Highly Weathered	More than half of the rock material is decomposed and/or disintegrated to a soil. Fresh or discoloured rock is present either as a continuous framework or as corestones.	IV
Complete Weathered	All rock material is decomposed and/or disintegrated to soil. The original mass structure is largely intact.	V
Residual Soil	All rock material is converted to soil. The mass structure and material fabric are destroyed. There is a large change in volume, by the soil has not been significantly transported	VI

Discontinuity Types

Discontinuities are described as a break in the rock continuum, which have little or no effective tensile strength (ISRM, 1981b; McClay, 1992). Shear strength along the discontinuity plane can vary depending on its properties, such as its roughness, or infill.

Discontinuities are subdivided according to their geometry, planar, curvilinear and linear so that they may be characterised and further subdivided (Van der Pluijm & Marshak, 2004). The identification of the discontinuity formation mode, e.g. tensile opening or shearing, is important for rock mechanics, as it may relate to its current geomechanical properties (Price & Cosgrove, 1990).

Joints are discontinuities formed as a result of the effects of tensile stress within the rock; they exhibit a partition in the rock without any significant movement across them. Tectonic tensile joints can also occur within compressive environments. When compression acts in a certain direction, a perpendicular tensile force is created. The tensional stresses must overcome the compressive forces in that direction, and exceed the tensile strength of the rock for it to fracture, forming a joint.

Bed jointing (bedding) can occur as a non-tectonic structure formed by sedimentary processes. Bedding itself does not automatically form a structure that controls the engineering properties of the rock mass; bedding surfaces may not form discontinuities that affect the rock mass at all. Beds form discontinuities when they undergo parting, which is a splitting of the rock parallel to bedding, e.g. along parallel lying clay particles.

Faults are discontinuities that have undergone appreciable movement across them (Dennis, 1967), usually accepted to be a metre or more. Shears are classed as discontinuities that have undergone a smaller amount of movement, i.e. less than 150 mm. Shears are also described as deformation within brittle–ductile and ductile rocks, where the rock deforms, ranging from more brittle rheologies causing brittle failure along with brecciation, to plastic conditions causing deformation through dislocation creep, mineral fracturing and sub-grain boundary growth (Van der Pluijm & Marshak, 2004). Faults and shears are important to engineering geology as they are usually large and highly persistent, ranging from less than a metre, to thousands of metres (Hudson & Harrison, 1997).

Reactivations of previous fault/ shears create fault zones, where the aperture across the opposing surfaces has opened so that rock material can intrude. The inner material then undergoes brecciation forming fine particles, which act as a matrix between larger rock fragments. These zones are important to the engineering properties of the rock mass because of the loss of cohesive strength across the discontinuity.

Discontinuities can be visualised using 3D images produced by photogrammetry and laser scanned point clouds. Multiple parameters of these features can be measured remotely once represented within the geotechnical analysis programs. Dip and dip direction is recorded when each feature is delineated on the computer. Trace length is also calculated, as well as area if the feature is exposed as a plane. Once identified, these features can then be classified through visual inspection and engineering judgement, as well as recording their termination edges. These data can then be used to determine the particular sets within the studied rock mass.

Roughness

Even though discontinuities are assumed to be planar for the purpose of orientation measurement, they actually possess a three dimensional roughness. Roughness directly influences the shear strength of a discontinuity. For example, when a fracture is rough and interlocked it is less likely to have shear movement across it, than if it were smooth. Roughness is traditionally measured using 2D profiles taken along the dip line of a face, but in reality, discontinuity surface profiles are three dimensional features. Research has suggested that fractals can be used to describe fracture roughness surface (Belem *et al.*, 1997; Bagde *et al.*, 2002; Kulatilake *et al.*, 2006). Measuring the 3D roughness of fracture planes has been undertaken using

profilometers (Yang & Di, 2001; Kulatilake *et al.*, 2006), where samples had to be prepared and placed within the equipment for scanning. Fardin *et al.* (2004) has used a high resolution scan of a fracture located within a quarry to profile the roughness of that fracture, subsequently analysing it back in the laboratory. Unal *et al.* (2000) compared the differing techniques of roughness measurement (Table 3-3) for numerous parameters, such as ease of use and qualitative sensitivity.

Table 3-3. Comparison of techniques used in measurement of joint surface roughness (from Unal, 2000). The table suggests that both digital photogrammetry and laser scanning are well suited for roughness measurements.

<i>Roughness measurement techniques</i>	<i>Simplicity usage</i>	<i>Sensitivity of measurement</i>	<i>Scanning dimension</i>	<i>Flexibility of usage area</i>	<i>Measurement span</i>	<i>Usability of system for other purposes</i>	<i>Cost</i>	<i>Evaluation</i>
Profilometry	Usage is simple but it takes many times	Poor, used technology is also poor,	2-D	Good (Lab.) Poor (Field)	Short-Long, depends on the purpose of study .	Unavailable	Low-Fair	Suitable for 2-D measurements. But it is not functional adequately
Scanner (Type of profilometry)	Good, usage of it depends on the its technology	Fair-Good, depends on the sensitivity of mechanical and electronic system and change depends on the used technology	2-D 3-D	Good (Lab.) Poor (Field)	Medium-Short, depends on the used technology.	Unavailable, its accessory equipment can be used.	Fair-High	Suitable methods for roughness measurements.
Stringline	Simple, but it takes many times and needs hard studying	Poor, used in the field for rough measurements.	2-D	Poor (Lab.) Fair (Field)	Short – Long depends on the experience	There is no specific equipment	Low	It is not suitable method for sensitive measurements
Photogrammetry	Fair, needs experience and expertise.	Fair-good, change depends on the experience and expertise	2-D 3-D	Fair- Good (Field) Poor-Fair (Lab.)	Medium, depends on the experience and expertise	Main function is mapping.	High	It is not suitable method for sensitive measurements
Photograph	Fair-good, drawing and image software provides easiness.	Poor-Fair, change depends on the used technology.	2-D	Fair- Good (Lab.) Fair- Good (Field)	Medium, can be short ,depends on the technological background	There is no specific equipment, all used apparatus can be used other purposes.	Fair-High	Suitable for 2-D measurements
Digital photogrammetry	Fair-good, depends on the sensitivity of used software	Good	2-D 3-D	Good (Lab.) Good (Field)	Good, depends on the software	It can be used in different purposes.	Fair-High	Suitable for roughness measurements. Especially for field study
Laser	Good	Very good	2-D 3-D	Very Good (Lab.) ----- (Field)	Good	It can be used effectively for different purposes	Very high	Very suitable for all type of studies

The ability for the roughness of a feature to be recorded remotely depends on the scale at which it is viewed. Roughness is more easily determined with close proximity as a better view of the surface and/or higher density of pixels/points is possible. As this is not always possible, and to test scenarios representative of standard remote mapping conditions, quantitative assessment of remote roughness measurements has been conducted using standard ranged 3D models with traditional joint roughness coefficient (JRC) measurements.

Wall Strength

The strength of the rocks forming the walls of discontinuities will influence the shear strength of rough surfaces (Wyllie & Mah, 2004). Stronger walls lessen the tendency of discontinuities to smooth out, as asperities will not shear off as easily, thus increasing the strength of the rock mass. Weathering can greatly affect the wall strength of a discontinuity. Physical contact with the rock is needed to record the wall strength as remote systems are only able to estimate this from visual inspection.

Aperture and Infill

'Aperture is the perpendicular distance separating the adjacent rock walls of an open discontinuity, in which the intervening space is air or water filled' (Wyllie & Mah, 2004) and is very important to the overall rock mass behaviour (Bieniawski, 1973). The aperture of a discontinuity dictates its hydraulic conductivity and cohesion. Infill describes the material that fills the space between open discontinuities. The material may be weak, such as clay, or relatively strong such as quartz. Their individual characteristics: grain size, mineralogy, water content all have a bearing on the engineering behaviour of the discontinuity (Wyllie & Mah, 2004). If the aperture of the feature can be viewed by remote systems, again depending on the scale, then it can be recorded. Infill is more difficult to estimate remotely as, by its nature, it is formed between discontinuities and hard to visualise using remote data capture methods.

Persistence and Spacing

Spacing is the perpendicular distance between parallel discontinuities, and persistence is the distance a fracture pervades into the rock mass. When these two parameters combine they dictate the size and shape of blocks that may slide out of a face. A large spacing of the discontinuities within the rock mass could result in large block sizes; if the persistence of these fractures is large enough, so that they all intersect one another, then the block is formed.

Estimating persistence is a complex task, traditionally window mapping collecting discontinuity trace length data and subsequent mathematical algorithms are used (Zhang & Einstein, 1998; Zhang & Einstein, 2000; Zhang *et al.*, 2000). Remote data capture systems are unable to calculate persistence, but are useful for collecting large amounts of data to be used to estimate discontinuity persistence.

3.3.5 Equipment and Software Cost

The cost of the remote data capture equipment and accompanying software will dictate which system is more suitable to the needs of the user. Prices of the systems vary with time due to advances in technology and cheaper manufacturing costs. Differing manufacturers charge differing rates depending on the advantageous aspects their technologies or services provided have over the competition.

3.4 On site Assessment

3.4.1 Camera Lens

The choice of camera lens for photogrammetry is governed by the variable factors mentioned above. The varying focal length of lenses will provide options for different viewing distances from the face. If access means that proximity to the face is limited a lens with a larger focal length can be used, in effect, zooming into the face.

The cameras primarily used for photogrammetry are high-end pieces of equipment that come with a choice of fixed focal length lenses. Almost any camera (and lens) can be used for creating photogrammetric images as long as the distortion correction calibration is known. Some photogrammetric systems allow the use of zoom lenses, which are harder to correct for distortion, as the focal length of each photograph taken must be recorded.

3.4.2 Access

Access problems are variables that usually cannot be planned for, especially when fieldwork is being undertaken in industrial environments, such as mines and quarries. Inherently, remote data capture systems are conducted away from a face, which are usually unsafe for traditional mapping. Machinery and vehicles are always a danger in quarries, and the remote data capture setup positions required to avoid these dangers may result in positions that are not favourable for satisfactory photogrammetric or high definition surveying model creation. This is caused by distances to the face being larger than planned, or more oblique to the face, possibly resulting in blinding problems. Hand-mapping is always restricted to the accessible areas of the face, usually the lower 2 m - 3 m section.

3.4.3 Atmospheric Conditions

The weather most conducive to remote data capture is 'overcast', with no precipitation and little wind. Adverse weather affects the ability of the equipment to capture 'good' data but usually does not prevent it from operating totally. Fieldwork has been undertaken in most weather conditions that occur in the study areas. Once in the field considerations have to be made on brightness, protecting electronic equipment from precipitation, and overall visibility. In particular situations, such as working quarries and underground spaces, dust and artificial lighting must also be assessed.

3.4.4 *Speed / Time*

The time it takes to complete the fieldwork for a photogrammetric model or to complete a laser scan is dependent on many factors. The main consideration must be made to the overall size and resolution of the resultant model, whether or not multiple models or scans are needed, as this adds the most time. The amount of data collected remotely in a certain time period is important to compare with the amount of data collected in the same time period by hand.

3.5 Positioning

3.5.1 *Compass Clinometer and Tape Measure*

This is the most basic of the positioning techniques tested. The start orientation of laser scanner equipment is measured by compass and input into the system computer. From there the point cloud is orientated to north. The technique used for photogrammetry uses the angles and distances measured between the cameras and control point to calculate their relative positions using triangulation. The inclination between cameras and control point are also measured to calculate the relative change in height. The distances are measured to the nearest half centimetre and the angles to the nearest half degree.

The first camera setup would use base coordinates of, e.g. 1000, 1000, 100 (eastings X, northings Y, and elevation Z) and the other camera position and control point would be calculated relative to that point. Usually this would be done manually, but as the process is relatively repetitive, an Excel spreadsheet has been developed to provide coordinates automatically (Table 3-4 and Figure 3-5). Using distance and angle measurements taken in the field, applying trigonometry and Pythagoras theorem, the positions of each camera and control point are calculated.

Table 3-4. Example of spreadsheet calculating positional XYZ coordinates from particular data inputs. Inputs include the angles and distances to each camera and controls point. Triangulation calculations are used to estimate the unknown locations.

Data Output	Eastings(m)	Northings(m)	Elevation(m)	Total Height(m)
Cam 1	1000.0000	1000.0000	100.0000	101.5600
Cam 2	999.2641	998.7506	100.0453	101.5853
CP	994.6612	1003.6011	100.6549	100.6549
Data Input				
Cam 1-Cam 2 (°)	1.45			
N-Cam 1-CP (°)	304			
N-Cam 1-Cam 2 (°)	210.5			
Cam 1 Height (m)	1.56			
Cam 2 Height (m)	1.54			
Hori-C1-CP (inclination) (°)	-8			
Hori-C1-C2 (inclination) (°)	1			
N-Cam 2-Cam 1 (°)	30.5			
N-Cam 2-CP (°)	316.5			
Calculations				
C1-C2-CP (°)	74			
Northing (m)	-1.249362	q		
Easting (m)	-0.735931	p		
Easting (m)	-5.338842	m		
Northing (m)	3.601095	n		

Schematic

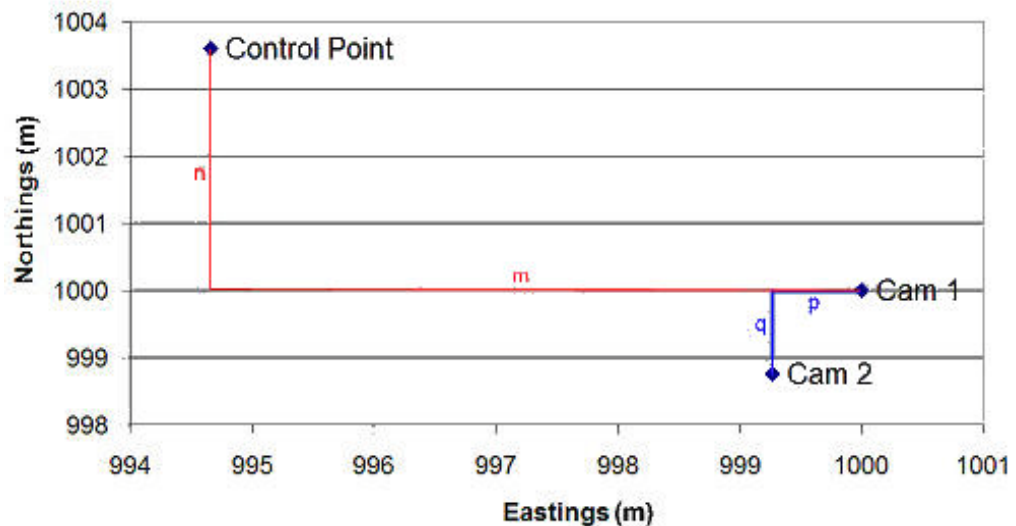


Figure 3-5. Schematic from positional calculation sheet (eastings and northings). The schematic is used to visually assess the calculated locations for any gross errors, e.g. large camera separation or incorrect baseline to face orientation.

3.5.2 Global Positioning System (GPS)

The basic principle of GPS is trilateration from 3 satellites to find a position in 3D space. The distance between the satellites and the GPS receiver is measured using the travel time of radio signals. A pseudo random code is transmitted from the satellite at the same time as the receiver. When the satellite code reaches the receiver it will have been delayed by the distance travelled. This delay is calculated by shifting the codes back into synchronisation. The time difference between the two codes multiplied by the speed of code will give the distance between the satellite and GPS receiver (Ordnance Survey, 2005). Due to problems in distance calculations conventional GPS is accurate to 1 - 2 metres at best and is usually around 6 m when within an open pit, due to restricted line-of-sight to satellites. The speed of the pseudo random code changes depending on the atmospheric systems through which it travels, e.g. it would travel faster on a clear day opposed to an overcast one. The GPS receiver also has problems when multipath errors occur when the signal is reflected from large objects, such as buildings or cliff faces. The receiver cannot distinguish between the original signal and the reflected ones, affecting its distance calculations (Beutler *et al.*, 1999). A Magellan eXplorist handheld GPS receiver was tested during the project (Figure 3-6).



Figure 3-6. Magellan eXplorist handheld GPS. The GPS internal clock was synchronised with the clock of the camera/scanner, so to provide the most accurate positional data. The positional data can then be read off the screen or saved onto a GPS memory card (modified from www.magellangps.com).

3.5.3 Differential GPS

Differential GPS (DGPS) (Figure 3-7, Figure 3-8 and Figure 3-9) (Leica, 2005) was developed to negate the atmospheric and multipath errors involved with conventional GPS systems. It requires a static base station and roving GPS units which communicate via radio. DGPS uses the principle that the multipath and atmospheric errors will be relatively the same for GPS units that are close (< 10 km) to one another.



Figure 3-7. Differential GPS Equipment – base station. The base station is setup over a known position that has previously been surveyed and begins to receive satellite signals. The location of the base station is input into the machine so it can then compare it with the positions that it calculates for itself using the satellite code, hence calculating the positional error for each moment in time. This error is then transmitted to the roving GPS unit so that it can calculate its position accurately.

The roving unit is placed upon the tripod from which data is captured. The DGPS is accurate to mm scale, and capable of communicating with several roving units at one time (Trimble, 2005).

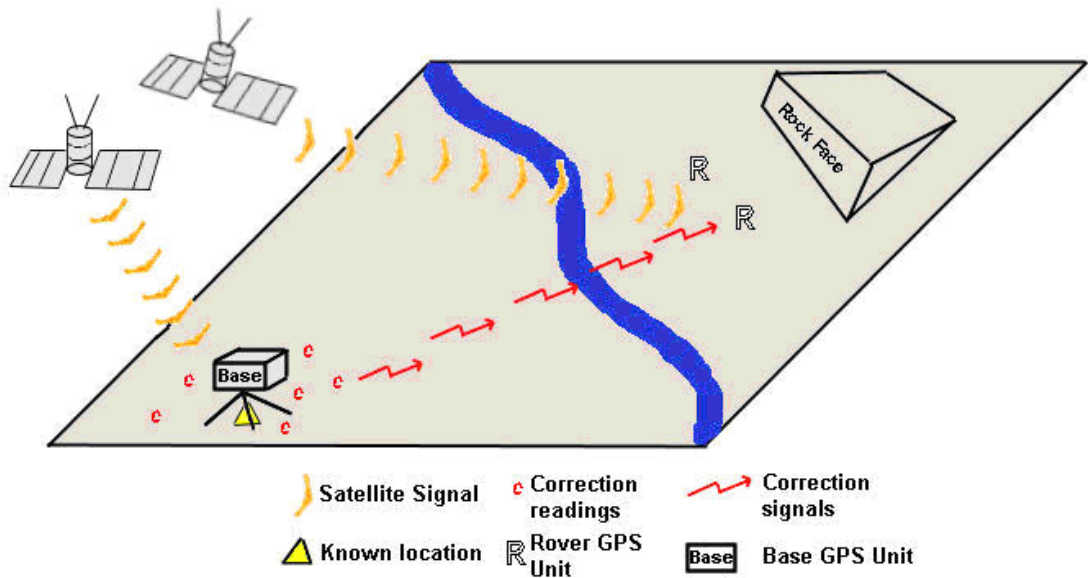


Figure 3-8. Diagram showing the principle of Differential GPS.

The Leica GPS 1200 system, used during this project, can also use RINEX (Receiver INdependent EXchange Format) post-processing, where the base station may be setup at an unknown position and all the positional readings and the corresponding times are recorded onto a memory card. These can then be downloaded, once out of the field, and compared with the published RINEX data for that area (published on the internet) which then applies the error calculations producing corrected, accurate positioned data (Ordnance Survey, 2005).



Figure 3-9. Roving GPS unit in backpack.

3.5.4 *Reflectorless Total Station*

The Leica TPS 1200 Total Station (Figure 3-10) used during this project can perform both relative and full geo-referencing to provide positional data for the camera setups. It is a powerful surveying tool and is used to execute many different surveying tasks. It incorporates a highly accurate laser range finder, theodolite and computer for surveying calculations and data recording (to memory card). To fully georeference a position the total station must perform a resection calculation from two known (previously surveyed) points. The positions of the known points must be input into the machine as well as the instrument height. The total station is then aimed at each point measuring the angles and distances, allowing for the resection calculation for its full geo-referenced position using the internal computer. For another position to be calculated, i.e. the second camera position, the total station is aimed at a point on the ground over which the second camera would be setup, and its position is calculated. The total station is then swapped for the laser scanner or digital camera, and the data capture can then be undertaken. For the second camera setup, a surveying tripod and tribrach would be used to accurately setup over the position measured for the second camera. The XYZ coordinate data for each point is saved onto the internal computer of the total station which can be downloaded once out of the field.

Relative coordinates can be measured by the total station if photogrammetry is the remote data capture method used. Rather than performing a resection to calculate the position of the total station, a start position of 1000, 1000, 100 is input into the machine. The other setup positions can be measured relatively from that point, in the same way as full-georeferencing.



Figure 3-10. TPS1200 reflectorless total station (from Leica, 2005).

3.6 Data Capture

3.6.1 *Photogrammetry*

Photogrammetric Equipment

Precision equipment is required for the capture of photogrammetric images during this project. The original equipment was recommended by the developer of Sirovision, George Poropat (Poropat, 2005) as they would most suit the Sirovision photogrammetric system.

- Professional Digital Camera
- Geared Head
- Tripod

Certain digital cameras from a range of manufacturers are supported by Siro3D, as well as the various lens sizes that fit them. The radial distortion and decentring of each supported camera and lens has been pre-installed into the Siro3D program to correct images. A Nikon D100, 8 Mega pixel camera was used to capture photographs, whilst using two differing lenses. The first was a 50 mm AF Nikkor f/ 1.4 D Nikon lens; the second was a 20 mm AF Nikkor f/ 2.8 D Nikon lens, which is primarily used to capture wider angled photographs, e.g. underground/ close to face. Certain setup parameters of the digital camera must also be configured before any photographs should be taken (CSIRO, 2005).

- Sensitivity – Automatic
- Aperture – F8
- Image Quality – RGB Tiff
- White Balance – Automatic

The Siro3D software can only process photographs that are in the tagged image format (TIF). Cameras are able to capture the images in smaller RAW format, enabling more photographs to be recorded to a memory card. The files can then be converted to TIFs once downloaded to a computer, taking a few minutes for each photo. The geared head and the tripod provide pinpoint positioning and levelling for the digital camera. It can hold camera setups that weigh up to 7.5 kg, whilst also allowing movement through 360° pan and +90° -30° frontal and lateral tilt. A Manfrotto Triman tripod was purchased with the digital camera. It has a geared centre column so that the camera can be raised and lowered according to preference. It also has a twin shank leg design so that height can be adjusted further.

Field Methodology for Photogrammetry

Once the camera separation and distance to the measured face is determined the camera setups can be positioned, as described in Section 3.5.

Field parameters to be measured using positioning techniques

- X, y, z (m) of 1st camera
- X, y, z (m) of 2nd camera
- X, y, z (m) of a point that both cameras can see (control point)
- Height (m) of 1st camera
- Height (m) of 2nd camera

When the setup positions have been determined the surveying equipment can be swapped for the camera and geared head. The photograph can then be taken ensuring that the control point must be within view of the camera, and the picture focused. Ensuring that all the details of the photograph have been recorded on to the field data sheet, i.e. number of photographs taken for that setup, the file name saved onto the camera, and which control point is to be used, the camera can then be moved to the next setup position, where the process is repeated. The photographs are saved to the cameras internal memory card. They can then be downloaded to a computer once out of the field.

3.6.2 *Laser Scanning*

Laser Scanning Equipment

Laser scanning during the project was primarily performed by the Leica HDS3000 (Figure 3-11), which uses the 'time of flight' laser distance calculations. Placement of the scanner is straightforward, as long as the face to be scanned is approximately perpendicular and within distance range. The laser scanning system only needs a compass clinometer to be surveyed to produce a relatively coordinated point cloud, although surveying equipment needs to be used for full geo-referencing.

The equipment list for standard laser scanning includes:

- Laser scanner - Leica HDS3000 or Leica HDS4500
- Separate battery
- Laptop computer
- Surveying tripod
- Optional positioning equipment for full georeferencing

Differing HDS systems have a range of specifications and abilities, although the specific characteristics of the Leica hardware are described. The Leica HDS3000 is able to spin through 360° when scanning, as well as having the ability to scan 270° vertically through two separate viewing windows. It has been published (Leica, 2005) that the laser scanner has a less than 6 mm spot size, and 6 mm positional accuracy at 50 m from face. This spot size increases with distance from the face, 6 mm/50 m therefore if the scanner density is set to 10 mm, and the laser spot size is equal or greater then noise/inaccuracies can be introduced into the model. It collects a maximum of 1800 points/ second using a green 3R class laser, with an optimum effective range of 1 m – 100 m. The range is dependent on the reflectance of the

material being studied (Lichti and Harvey, 2002); coal will reflect less than chalk. When viewing, the reflectance strength can be super-imposed upon the individual points, this allows for a quick visual assessment of the point cloud. Laser scanners are also able to take digital photographs using a camera (1 Megapixel for the Leica HDS3000), which is used to add colour to individual points to aid viewing.



Figure 3-11. Leica HDS3000 (from Leica, 2005). The laser is emitted through main window (pictured). A second window at the back of the scanner is used for capturing points at an angle of less than 40° from vertical.

The apparatus allows for the setup over known surveyed points, using a vertical laser beam, for full georeferencing (Leica, 2005). Through testing it was found that the Leica HDS3000 took 25 minutes to scan a 25 m x 50 m face, at 20 mm point cloud resolution, from 20 m away.

The Leica HDS4500 phase shift laser scanner (Figure 3-12) is available with two distance modules: a 25 m and 53 m ambiguity range. The 25 m range module was used during this project. It has the same horizontal field of view as the HDS3000, but increases the vertical angle to 310°. At 10 m distance from the study face the scanner has 6 mm positional accuracy. It collects up to 500,000 points per second using a red

class 3R laser with a 5 mm spot size at 10 m (Leica, 2006). This increase in speed is beneficial to time-sensitive applications whilst sacrificing maximum distance ranges.



Figure 3-12. Photograph showing the Leica HDS4500 phase shift laser scanner. A mirror in the centre of the scanner spins reflecting the laser emitted vertically from the base of the scanner.

Field Methodology for Laser Scanning

The laser scanning undertaken during this project was primarily conducted with the supervision of Dr. A. Wetherelt, from the Camborne School of Mines. The field methodologies are described for Leica hardware, although are analogous to most other laser scanner systems. A position for the apparatus is selected so that it has an unobstructed view of the rock face. The tripod can then be erected and levelled, after which the position can be surveyed using the positioning equipment. The laser scanner is then placed onto the tripod, where it is connected to its battery and the laptop computer. The computer can then be booted up and is used to control the laser scanner through the Cyclone software (Leica, 2006). A quick scan of the area displays onto the laptop, from which an area can be selected for the more detailed scan. The resolution is then input onto the laptop and the scan can be started. The points are

displayed as they are measured as well as the estimated remaining time of the scan. Once the scan is completed the point cloud is saved, ready for export to data analysis software.

3.6.3 *Traditional Hand-mapping Combined with Digital Photography*

The convention for analysing structural geology is to identify the planar structures which influence the rock mass strength properties. This is traditionally performed by measuring them by hand. Features that are inaccessible to hand-mapping are captured with photographs. The traditional hand-mapping methodologies described can be perceived as basic and straightforward, but are required to indicate the distinction in accuracy and sophistication between remote data capture and hand-mapping techniques.

- Standard engineering geological equipment include,
- Waterproof field notebook
- Compass clinometer
- Hand Lens
- Mapping board
- Tape measure
- Schmidt Hammer
- Digital Camera

Digital Photography

Photography has long been used as a tool for aiding geological hand-mapping. Photography is used to capture details of the rock structure that cannot be accessed by hand, e.g. discontinuity trace length data (Pine *et al.*, 2006). A scale must be seen in each of the photographs so to help aid measurements of rock fractures. The angle at which the camera is orientated to the studied rock face has a bearing on the measurements being made. Due to distortions caused by the camera not being perfectly perpendicular to the face, length data proportions can be different from one area of the photograph to the other.

Plane Orientations

The inclination of a discontinuity in engineering geology is traditionally measured using a compass clinometer, by dip and dip-direction, where the dip is the highest magnitude of the inclination on the surface. The bearing in which the maximum dip occurs is

measured as the dip-direction. The dip direction is absolute and measured in degrees. Alternatively, strike and dip can be used. The strike of a rock is its line of intersection with a horizontal plane, and the dip is the magnitude of the inclination at right angles to that.

The roughness and size of the surface to be measured dictates the methodology of the data collection. If the surface is reasonably smooth then the measurement is straight forward in that the compass clinometer can be used normally.

If the plane is large and shallow dipping, Barnes (1990) suggests that to *'estimate a strike line a metre or more long (if necessary mark it with a couple of pebbles), then stand over it with your compass opened out and held parallel to it at waist height'*. He also explains how to calculate an unexposed dip angle by measuring the trace of the structure, ensuring that the line of sight is horizontal, and in the strike of the measured plane.

For large, uneven, irregular planes Barnes advises to kneel so that eye level is as close to the measured plane level as possible, then sighting a horizontal strike line. The dip is measured using a similar method to the previous, whereby moving to a position where most of the plane can be seen, then taking an 'end on' reading of the dip.

Discontinuity Traces - Line and Window Mapping

Line and window (circular and rectangular) mapping can be performed to systematically study a section of a rock face so that the general discontinuity properties can be measured. Line mapping involves placing a measuring tape along the face usually at waist height, and the measurement of every feature that cuts the tape, whilst recording its position. The tape can then be surveyed and the features geo-referenced. Window mapping involves similar mapping processes but features are measured that fall within the selected areas of the face. This is aided by using digital photography so that measuring discontinuity trace lengths can be done on the computer. Window mapping was conducted upon a rock face at the Tremough road cutting and is shown in Figure 5-13 and described further in Section 5.4.1. Techniques currently used to map discontinuity trace lengths from digital images include using computer programs to scale the digital image and subsequently measuring lengths by digitising them. There are many varying programs that are available, such as the freeware application called ImageJ (Rasband, 2007). A photograph is scaled using a known distance within the image. The discontinuity traces are then digitised from which a length is output by the

computer program. This data is then exported to a spreadsheet program for processing.

Roughness

The ISRM (2007) has defined a standard for roughness that is described by the use of a two dimensional surface profile. It is first expressed in large scale (metre) as either, stepped, undulating or planar, then smaller scale as, rough, smooth or slickensided. This measurement is not quantitative. It is suggested to take several 2D profile measurements at varying directions upon the surface of the feature.

Quantitative field measurements of roughness were classified by Barton (1973) using the Joint Roughness Coefficient (JRC). Visual evaluation of the roughness of a discontinuity surface would be performed and compared with charts proposed by Barton, which take into account surface irregularities at centimetre scale and waviness at a metre scale, ranging from zero for a smooth flat surface to 20 for a very rough surface. The 'i°' value is also used to characterise roughness, where it is the average measurement of the inclination of irregularities (or asperities) on the joint surface (Wyllie & Mah, 2004). 'i°' can be calculated from JRC by:

$$i = JRC \log_{10} \left(\frac{JCS}{\sigma'} \right)$$

Where JCS is the joint compressive strength, JRC is the Joint Roughness Coefficient (Barton, 1973) and σ' is the effective normal stress acting on the surface.

Spacing

Discontinuity spacing is measured by counting the number of discontinuities within a set that cross a traverse line of a known length. The mean fracture spacing and range is then calculated, usually in metres. Calculations of spacing should preferably be made along three mutually perpendicular axes to counteract the sampling bias of measuring along a single line. Bias occurs due to the relative angle that discontinuities intersect with the measured face. Discontinuities perpendicular to the mapped face will give the correct spacing, where sub parallel discontinuities will form apparently wider spacing than is actually present. Parallel features will not show up on the mapped face at all and could be completely missed out. Terzaghi (1965) fixed the bias by applying the following:

$$S = S_{app} \sin \theta$$

Where S is the true set spacing; S_{app} is the apparent measured spacing and θ is the angle between the scanned face and the strike of the discontinuities.

The number of discontinuities measured across a scan line is also biased due to the relative orientations of itself and the discontinuities. The true number of discontinuities is calculated as follows, Terzaghi (1965):

$$N = \frac{N_{app}}{\sin \theta}$$

Where N is the actual number of discontinuities measured if the scan line were perpendicular; N_{app} is the apparent measured number and θ is as above.

3.7 Photogrammetric 3D Image and Point Cloud Creation

Both remote data capture systems produce dense three dimensional digital elevation models, described as 3D images/ models for photogrammetry and 3D point clouds for laser scanning. Photogrammetry must be subjected to more processing than laser scanning, as positional data must be collected from the integration of two photographs. Laser scanning produces its digital elevation model as a point cloud whilst scanning is conducted with little processing needed before analysis.

3.7.1 *Photogrammetric 3D image Creation*

This process describes the 3D image creation using the Sirovision Siro3D software program based on the user manual (CSIRO, 2006). The main methods used during processing are described, although the program is capable of performing many other functions, which can be explored further in the Sirovision manual. As new versions of the Sirovision software were released the 3D image creation process developed, becoming more streamlined and efficient. Other photogrammetry processing software is available, but all contain the same basic principles as the 3D image creation of Sirovision.

Image Correction

The first step when using the Siro3D module of the Sirovision software is to correct the images for distortion. When rectangular photographs are taken with circular lenses they are affected by radial distortion, where straight lines at the edge of the photograph become curved and points are moved in a radial direction from their correct position. There are two main types of radial distortion: negative displacement, where points are moved from their correct position towards the centre of the image, and positive displacement, where points are displaced further away from the image centre. Negative distortion is usually associated with wide angle lenses and positive distortion for more narrow lenses (Slama, 1980; McGlone, 2004; Wolf, 1983). The radial distortion of a particular camera and lens is measured by the manufacturers using calibration apparatus; these are usually pieces of equipment with points of known locations placed upon them. Photographs of the apparatus are taken and the difference between the points in the photograph and their real locations gives their distortion. Using these radial distortion values, a radial shift for each pixel can be calculated according to its distance away from the image centre. This shift can be corrected for every pixel in the image (Atkinson, 1996). This process usually takes a few minutes using the Siro3D software and can be performed in a batch mode, where all the photographs taken during fieldwork can be corrected at the same time.

The brightness, sharpness, colour balance, contrast and size of the corrected photograph can then be manipulated if required. The most useful is the brightness adjustment, which is particularly effective when used for photographs taken under poor lighting conditions, e.g. underground.

Image Orientation

The 3D image is formed from the information contained by two photographs, making up a stereopair, as described in Section 2.2.3. The two photographs must then be orientated using the positioning data collected in the field. Siro3D imports the data from a text file containing each setup and control point, along with their individual positional data. Once the data is loaded, the control point on each photograph is identified, and three matching points are selected on both the left photo and the right photo, helping to identify the parallax of the stereo-pair. Each photo is assigned to the surveyed camera position and a schematic is displayed showing their relative positions provided in Figure 3-13.

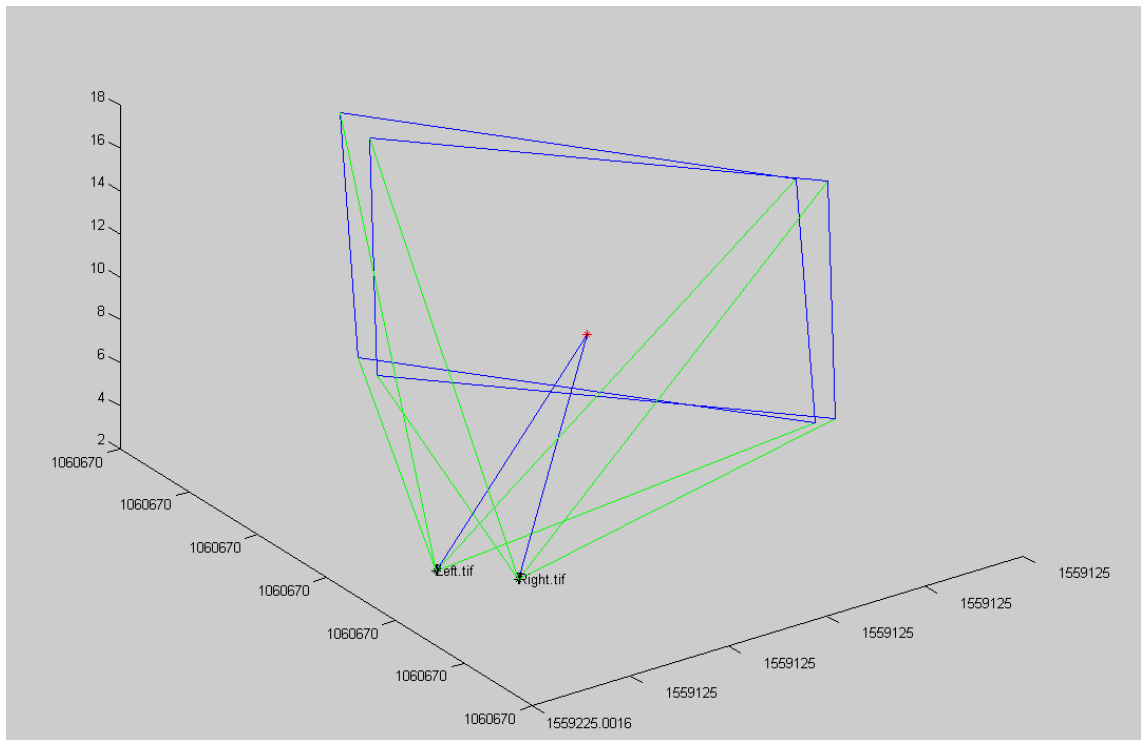


Figure 3-13. Schematic showing relative camera positions using Siro3D (CSIRO, 2006). Each camera position is labelled corresponding to the file name of the image on the computer. The blue rectangles show the extent of the photographs and how they relate to one another, along with the red cross indicating the control points and its location in the two images. This schematic allows for a visual assessment of the survey data.

3D Image Task Setup

The positioned photographs can then be set up as a 3D image ‘task’, which can then be modified and run at a later date by Siro3D if required. The task is set up by selecting the matching four corners in each photo that are to be used for the 3D image. This allows for problem areas to be ‘cut out’ of the image, such as sky or excess vegetation. The 3D task is then saved as a text file.

3D Image Matching

The 3D image can then be created by assigning Siro3D to ‘run’ the task using block matching. This process can take up to 10 minutes depending on the size of the 3D image. The matching technique employed by Sirovision uses the grey values of groups of pixels to match the corresponding groups in a second image. The red, green and blue values for each pixel are converted to grey value (intensity), hue and saturation. A template size is selected as a first step, which is the number of pixels that are grouped together to ascertain their collective grey value. The template size is square and made up of an odd number of pixels so that the centre pixel is used for the template position during matching. The template moves within the area defined in the ‘3D image task setup’ stage matching pixel groups from both images (Schenk, 1999).

If pixel groups are not matched, their positions are interpolated from accurately positioned groups. Poor matching is usually the result of areas that cannot be easily identified by the program. Shadows or particularly dark areas are hard to match, as well as features that are oblique to the view of the camera. Vegetation is another problem encountered when matching, as firstly it obscures the view of the face, and it can easily move position between each photo capture if conditions are windy.

Once the 3D image is created the matching success is confirmed, where >90% creates a good image, and the option for further matching is given. A 3D image with a low matching success can still be useful as long as the unmatched points can be interpolated correctly. If unmatched points are interspaced between correctly matched points then the interpolation will be accurate, if there is a dense area of unmatched points then interpolation will fail, as shown in Figure 3-14.

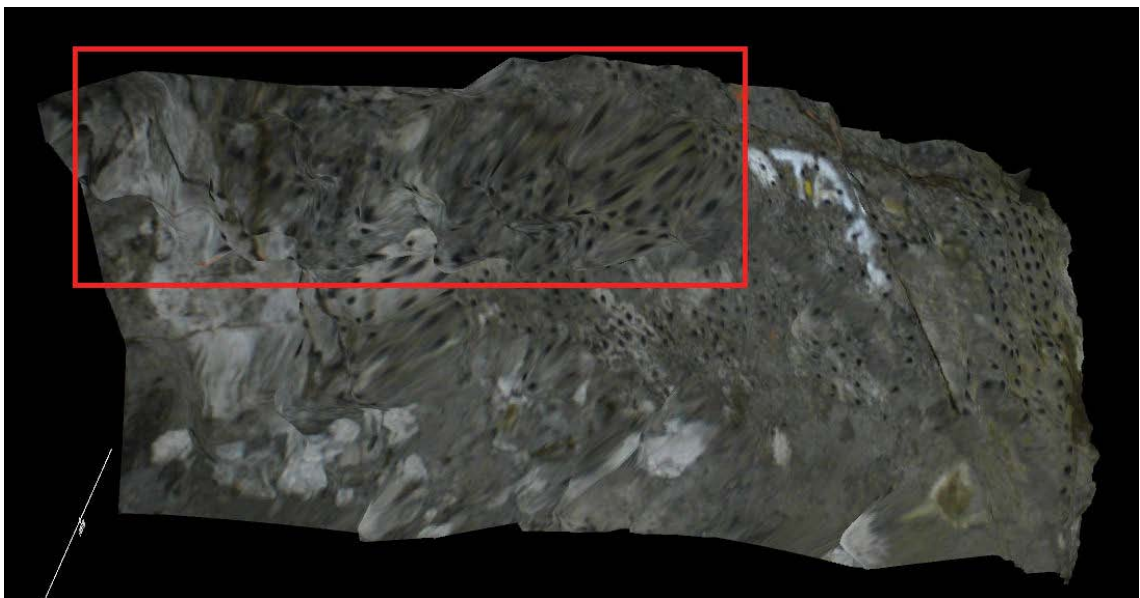


Figure 3-14. Image showing result of poor matching of an underground rock face (~3 m wide) with multiple drill holes. The red box outlines the worst affected area of poor matching, however it is poor across the majority of the rock face. It is considered that this 3D image is poorly interpolated due the poor lighting and the multiple dark drill holes on the face which are incorrectly matched between the stereographic pair.

The 3D image is then displayed as a 3D mesh/ digital elevation model (Figure 3-15). The 3D image is made up of thousands of interconnected triangles, whose points are the centre of each matched pixel group. The image can then be saved onto the hard disk for later processing/ analysis within Siro3D or for geotechnical analysis by Sirojoint.

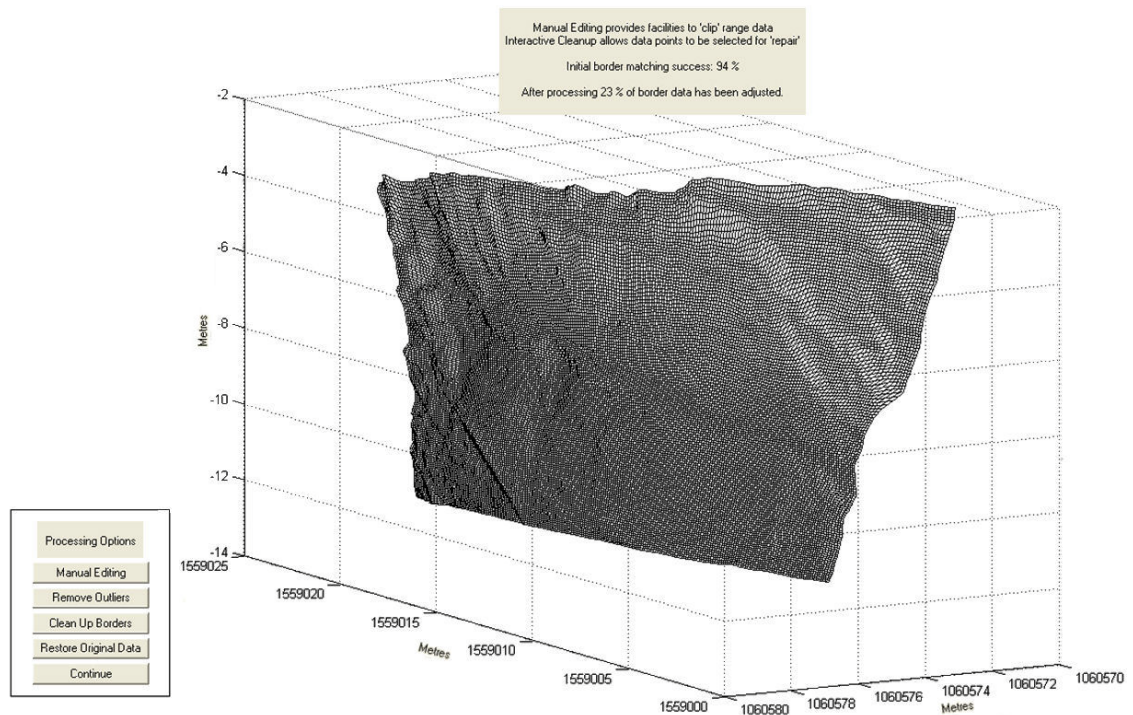


Figure 3-15. Post matching 3D mesh representing a full georeferenced rock face using Siro3D (CSIRO, 2005). Options are given for: manual editing of the 3D image, removing outliers automatically, cleaning up borders (by cropping), restoring original data (if one of the previous three options has already been applied), and to continue to save the 3D image.

3.7.2 Laser Scanning Point Cloud Creation

The point cloud creation process for laser scanning takes little time as, intrinsically, it is the raw data that is collected by the laser scanner. The point cloud file is viewed using Leica Cyclone, to check for potential errors. It is then exported as an XYZ text file, which can then be imported into the SplitFX geotechnical analysis program.

3.8 Processing and Analysis of Remotely Captured Data

3.8.1 Data Import

Data processing and analysis is performed on photogrammetric 3D images by the SiroJoint program (CSIRO, 2005). The photogrammetric 3D image is imported into the program from Siro3D and is displayed as a 2D orthoimage. The image can also be viewed in 3D within the program, which allows the image to be spun, magnified, and panned so that individual features may be more closely examined. The 3D position of any point on the rock mass can be identified by placing the mouse cursor at the corresponding position on the 2D orthoimage.

The core Leica laser scanning laser software, Cyclone, does not provide any geotechnical analysis but it is able to export the point cloud produced by the scanner

as a number of differing text files: tab, space or comma separated. Point cloud analysis is performed using SplitFX (Split Engineering, 2005), which is a program specifically designed for point clouds produced by laser scanning systems. Similarly to SiroJoint, discontinuities can be delineated from the 3D displays and represented on stereonet.

3.8.2 Sirojoint and SplitFX Processing

Plane Identification

The data points, planes and discontinuity traces, can be delineated manually in the primary Sirojoint program using the mouse. Planes are delineated using the mouse to select a polygon shape close to the extremities of the discontinuity. The Sirojoint program then identifies the triangle points found within the plane and calculates the dip and dip direction of the ‘best fit plane’ running through the points. The program then calculates the area of the plane from the number of delineated triangles. Automatic plane recognition can also be applied to the 3D image, where plane characteristic ranges, such as orientation tolerance angle, minimum area and number of dominant discontinuity sets are predetermined. Planes are formed according to these parameters and are displayed on the 3D image after processing is completed. Accuracy of a plane is gauged by Sirojoint using a reliability measure, ranging from 0 to 5 (Table 3-5).

Table 3-5. Sirojoint reliability measure (CSIRO, 2005). Inaccuracies may be produced during matching, where points had to be interpolated from surrounding accurate matched points.

Reliability Measure	No. of Triangles with 3 reliable vertices
1	< 60%
2	60% to 70%
3	70% to 80%
4	80% to 90%
5	> 90%

Point clouds exported from the Leica laser scanning program, Cyclone, are imported into SplitFX where they must be meshed to form a 3D surface before mapping can take place. A mesh is created from the point cloud, where each point is connected to the ones adjacent, creating a network of non-overlapping triangles. Before generating the mesh a grid, perpendicular to the scanner’s line of sight, is imposed over the point cloud. The centres of each grid cell are then used to create the points of each

triangular element (Split Engineering, 2005). The SplitFX manual notes that this particular technique of meshing/triangulation generates an accurate surface model, but makes the mesh sensitive to extraneous points. These extraneous or 'ghost' points, created from the reflection from dust particles or other objects moving in front of the laser during scanning are deleted manually.

Once the point cloud is reduced to the area required (Figure 3-16), edited for ghost points and meshed, planes can be delineated either manually or automatically. Similarly to Sirojoint, orientations are taken from the triangles situated within the delineated plane. Automatic plane recognition, described as 'patch' recognition by the SplitFX software, uses parameters defined by the user. The minimum patch size (m^2) and maximum neighbour angle ($^\circ$) parameters define the size of accepted patches and the tolerance used to form them. The minimum patch size refers to the size of the group of triangles forming one patch, where the maximum neighbour angle is the maximum angle that a triangle could be orientated from its neighbour. The orientation of each triangle is calculated and compared to the surrounding triangle. If the difference is less than maximum neighbour angle, the triangles are grouped together. However, if this group of triangles is less than the minimum patch size (m^2), it is ignored (Split Engineering, 2005). Two other parameters, 'point filter', and 'exclusion of noisy patches' can be adjusted by using scales ranging from 'low' to 'high' and 'exclude none' to 'exclude all' respectively. These two parameters are not explained in the SplitFX user manual (Split Engineering, 2005) but through continual use of the software it was found that the 'point filter' removed points that created triangles that were excluded by the 'maximum neighbour angle', essentially 'smoothing out' some planes to fit the criteria. The 'exclusion of noisy patches' blocked the delineation of patches if the number of points (allowed by the 'point filter') were too high, thus rejecting planes that were too rough/irregular (either due to natural roughness or due to too much noise). During testing of the software the values for these two parameters that produced results most comparable to manual delineation of discontinuities were determined to be the default values of 'medium' and 'exclude some' respectively.

Once the parameters are selected then automatic plane/ patch recognition can begin. Manual plane selection can also be performed within SplitFX using the mouse, delineating the outline of planes, similar to Sirojoint.

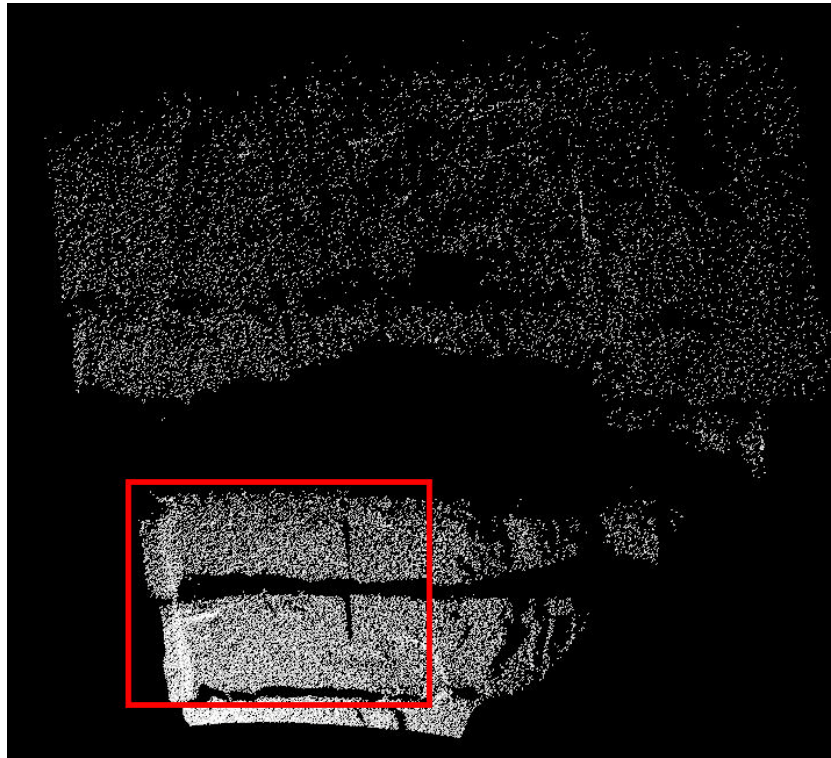


Figure 3-16. Full point cloud of example quarry (Carnsew) (red box, 6 m high, shows area required for analysis). The point clouds produced commonly contain points from areas that do not need to be analysed. They can be easily deleted from the point cloud file.

Trace Identification

Using Sirojoint, discontinuity traces can be identified on the face by using automatic trace identification or by manually selecting points along the line of the linear features. The program uses the 3D spatial data of the selected points to calculate the orientation of the plane that runs through those points. The program also uses the combined distance between the individual points to calculate the length of the discontinuity trace as it forms to the 3D morphology of the rock face. The program also measures the distance between the first and last selected points, outputting is as an end-to-end discontinuity trace length, which is more analogous to the traditionally measured discontinuity trace length, taken with a tape measure.

Accuracy of discontinuity traces is dependent on the ability of the software to fit a plane to the discontinuity trace. If the trace is delineated and is close to a straight line then an infinite number of planes can be fitted to it. The Sirovision User Manual (CSIRO, 2005) indicated that using traces for orientation data must be taken with care for this reason. Traces that vary from a straight line will provide the more accurate orientations. The orientations from selected discontinuity traces are given a variability value reflecting the straightness of the traces and the numerical quality of the positional data (CSIRO, 2006).

Traces cannot be mapped to the point cloud using SplitFX; this is due to the absence of a photographic overlay. Traces are manually or automatically (using an algorithm similar to Sirojoint) delineated upon scaled and orientated photographs within SplitFX. As the photographs contain no three dimensional data, dip and dip directions cannot be calculated from the identified discontinuity traces. Alternatively, the rake angles are calculated, measured clockwise from horizontal. Trace lengths can be calculated from scaled images within SplitFX, using the same technique as ImageJ (Rasband, 2007).

Individual planes and discontinuity traces can be classified into bedding, joints, etc, using the 'plane attributes' menu of Sirojoint, accessed by right-clicking over the object. Termination characteristics can also be input within that menu (in rock, against trace, outside of image, etc). The object information can also be viewed through this menu, such as orientation, area, 3D position, and accuracy. SplitFX currently does not have a facility to label the classification of discontinuities.

Roughness

The programs used to process the remotely mapped data during this project to capture the roughness profiles are analogous to those of Fardin *et al.* (2004), covered in Section 0.0.0. Although, whilst recording the 3D nature of the fracture surface, unlike Fardin *et al.* (2004) the remote data capture systems do not use fractals to describe the roughness of the plane. The photogrammetric program, Sirovision, and laser scanning program, SplitFX, use their own terminology to describe the roughness of the measured discontinuity feature.

The Sirovision program uses roughness to describe the '*measure of the overall deviation of the actual rock surface from the plane that is fitted to the measured data on the surface*' (CSIRO, 2005).

When an orientation measurement is made using a remote mapping system the resulting orientation is an average of the general orientation of the feature. If that feature was very rough then the discrepancy between the remotely mapped orientation and hand-mapped orientation may be large. The Sirovision program quantifies this by using RMS:

'The 'RMS' deviation from the plane is a measure of the 'roughness' of the plane expressed as the square root of the sum of the distance of all the points in the plane from the mathematically derived plane that is the best fit, in the least mean square

sense, to all the points in the selected plane. This is a three dimensional analogue of the errors observed when fitting a straight line to data in regression analysis. If the selected plane is perfectly flat with no roughness and no measurement error on any points the RMS deviation will be 0.' (CSIRO, 2005).

The RMS is affected by the accuracy of the spatial data. Poor image creation can cause false roughness on features that are flat in reality. The Sirovision manual explains that RMS may increase with viewing distance to the plane. Sirovision also uses 'variance' to quantify roughness in terms of orientation, where:

'Variance is a numerical measure of the statistical deviation of the orientation of the fitted plane from a perfect (flat) plane. Essentially it is another measure of roughness. This measure is a mathematical estimate of the roughness or curvature of a surface expressed as an angle, i.e. expressed in terms of the variance of the estimated orientation of the plane.' (CSIRO, 2005).

Variance is calculated each time the properties of a selected feature are requested/ called up on screen, so it may slightly vary each time. When exporting and analysing this data it must be acknowledged that the variance values may not be constant.

SplitFX described its roughness parameter as: *'a measure of the goodness of fit for the points that make the patch (/plane)'* (Handy, 2007). The roughness measurement ranges from 0 – 1, where 0 is the roughest; if all the points were perfectly co-planar the roughness would be 1.

Spacing

Remote data capture systems record the spatial position of identified discontinuities, therefore the combination of their known orientations and spatial positions allow for the calculation of their true spacing. Using the photogrammetric analysis program Sirojoint, discontinuities within the same set are manually selected. The program, knowing the coordinates of the discontinuities in 3D space, averages their orientations and measures the perpendicular distances between them, resulting in the spacing. SplitFX is unable to measure the spacing like Sirojoint. Using the same scaled photographs used for discontinuity trace length identification apparent spacing can be calculated between discontinuities held within the same set.

Set Analysis

Each of the remote data capture systems have their own stereographic interpretation facilities, although they differ in the data export options and ease of use.

Sirojoint uses its 'additional analysis program' which is able to accept orientation data from Sirojoint itself and from any other source (imported as a text file). The program has a clustering program allowing for automatic set delineation. The algorithm requires manual input of the number of sets present and then is able to cluster the data accordingly.

The orientation data compiled in SplitFX is automatically exported to its stereographic program, allowing for the data to be manually delineated into sets. The set statistics, such as the Fisher K value (scatter about the mean orientation) can then be viewed. It also has a function where the poles can be sized as a function of the areas of the features or roughnesses, which is a useful visual tool.

Data Export

Both remote data capture geotechnical analysis programs allow for the export of the data as text files. Each program has options for exporting a selection of data, i.e. orientation and roughness as well as a total data export. Exporting as a text file allows for simple conversion to a spreadsheet program for data compilation and storage.

3.9 End-Use Applications

As there are multiple end-uses/ applications that the remotely mapped data can be used with, tailoring of that data must be undertaken. Data other than the geotechnical measurements can be used, such as the digital elevation model data, the three dimensional morphology of the slope can be used. Photogrammetric systems can make use of the visual/ colour data that they collect. The various end-uses are covered in more depth in Section 5.6.

3.10 Discussion and Conclusion

3.10.1 Fieldwork processes

It has been shown that many factors must be considered before starting any fieldwork, either for remote data capture, or traditional mapping. Knowing the limits for these factors, such as camera baseline ratio, is important, as it will allow for more efficient

planning stages for when a large remote data capture project is undertaken. Identifying which geological parameters cannot be mapped remotely can be ascertained at this early stage. Aperture, infill, rock strength and wall strength need close contact to be measured accurately so are not studied during this project. Weathering and rock type can be assessed visually and so do not need to be visualised in three dimensions. Discontinuity orientations can be assessed using remote data capture methods, although the identification between each feature type, e.g. a joint and a fault are not undertaken during the project as they can usually be assessed visually. Visualising the rock mass in 3D allows for the calculation of a roughness value of a discontinuity as well as discontinuity trace length, which can subsequently be used to aid calculation of persistence and spacing.

Once on the site, decisions can change during the course of the visit because of varying weather and constantly moving machinery or tides. Because of this each factor is dynamic and is usually affected by a change in one another. Decisions must be made considering the resources available. During the project only two lenses were available for the use with the digital camera, restricting the ability of testing this parameter. Access problems vary during fieldwork, e.g. plant movement and tides, so a range of scenarios caused by restricted access are tested during the project. Few studies have been made on the effects that poor environmental conditions have on photogrammetric and laser scanning systems. To a regular user of these systems it is known that adverse atmospheric situations, such as precipitation, cause data capture problems and can sometimes damage the equipment.

It has been shown that each positioning technique has its advantages and disadvantages compared with the others. Some are more accurate, whilst taking the longest time in the field, and vice-versa. The most suitable positioning method for this project had to be decided (covered in Section 4.13), whilst balancing between these two factors: satisfying the accuracy requirements of the remote data capture systems (e.g. centimetre accuracy for photogrammetry), as well as speed and portability in the field.

Photogrammetric field methodologies require the assembly and positioning of two equipment setups compared to only one when setting up laser scanning. The position of the photogrammetric control point on the rock face must then be surveyed. This process is repeated along the length of the rock face to capture subsequent photogrammetric images. The laser scan area and density are selected using the

connected laptop computer controlling the scanner, once started, displays points in real-time as they are captured. These processes were made more efficient during the project and thus decreased the time and the equipment required in the field. The fieldwork of traditional mapping involved no collection of the 3D morphology of the rock face, directly identifying and recording geotechnical data. Assessing the affect of scan density and laser beam spot size on geotechnical data capture is covered in Section 4.7.

3.10.2 Post-Processing/Data Analysis

Photogrammetric 3D image creation is a long process when compared to laser scanning, first involving image distortion correction and then image orientation. Image matching is then performed, triangulating positional data from matching pixels between the two photographs. Poor matching can result in distortion if interpolations between successful matches are unsuccessful. In contrast, point clouds are created automatically from laser scanning and require little processing. Streamlining the photogrammetric 3D image processing will enable a quicker route into geotechnical analysis.

Photogrammetry and laser scanning geotechnical analysis share the ability of capturing plane orientation data. Comparing this data type can be problematic as it contains two parameters: an inclination (dip) and a direction/azimuth (dip direction). A new method of comparing orientation data is outlined in the beginning of Chapter 4. SplitFX is currently unable to calculate discontinuity trace lengths and orientations from the 3D point cloud. It has a module within its program that is able to map standard photographs using the same methods as traditional window mapping. Even though photogrammetry is able to calculate orientations from discontinuity traces, it is recommended in the Sirovision user manual that the measurements are to be used with care. Testing discontinuity trace orientations with their corresponding planar features will assess the effectiveness of using traces for orientation data. Both remote mapping systems can calculate roughness from identified planar features, although each have differing descriptions. Assessing the exchangeability between these photogrammetric and laser scanning terms, as well as the effect that roughness has on the orientation of measured features must be explored. Currently SplitFX cannot automatically calculate set spacing, although distance measurement tools within the program could be used to overcome the problem.

Assessing the various end-uses and the processes that need to be completed so that the remotely capture data can be used with them must be undertaken. Assessment of the advantages of using remotely mapped data, and whether or not it is suitable will be made in Chapter 4.

This chapter has illustrated and described the fieldwork and post-processing analysis using each mapping technique. It shows that the data collected by the remote data capture systems is interrelated and comparable, so that they may be further compared and analysed in the subsequent chapters.

4 ASSESSMENT OF FIELDWORK AND MAPPING PROCESSES

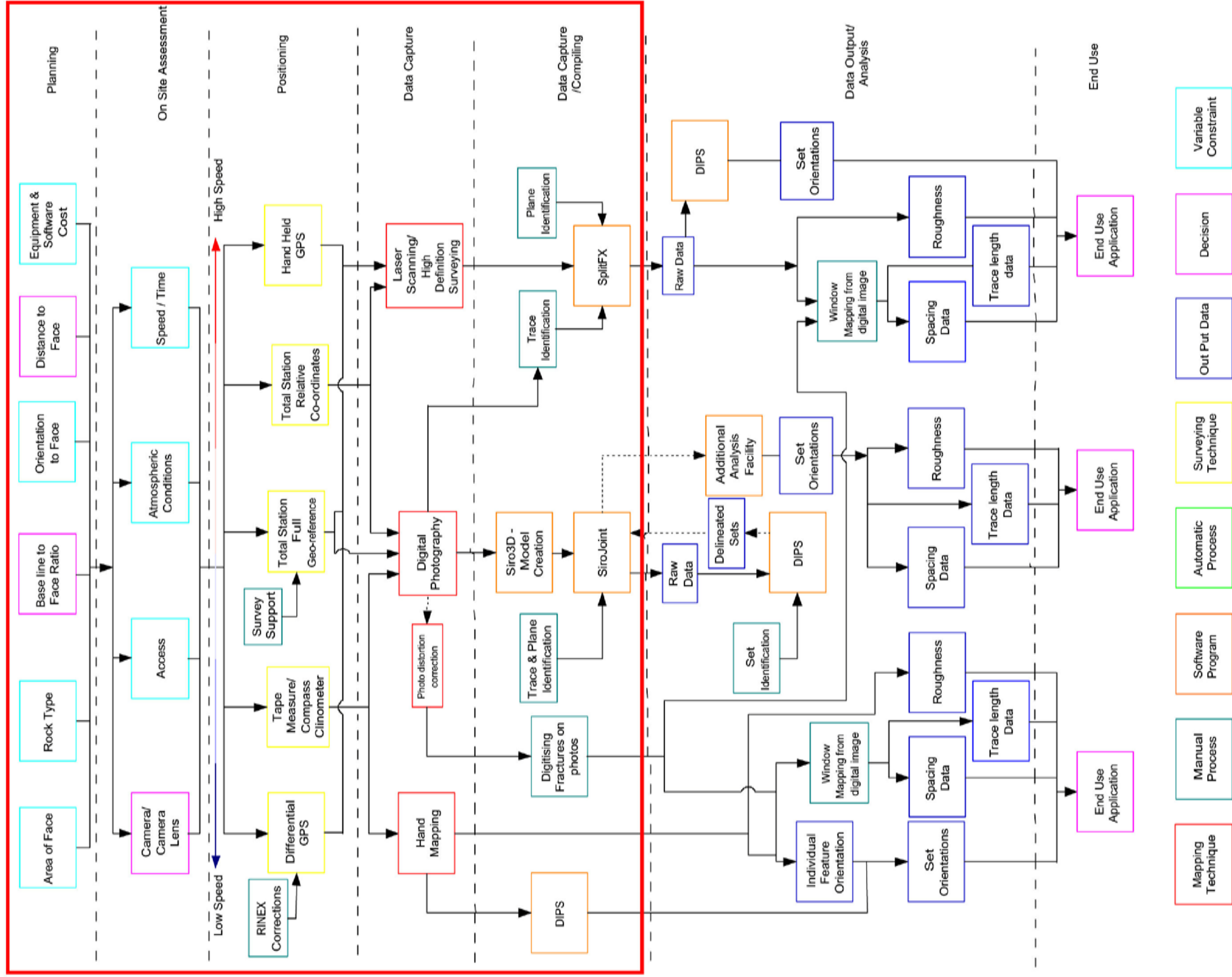
4.1 Introduction

The beginning of this chapter covers the development of the pole vector difference calculations which is used to quantify the error between mapped orientation data. This is the primary method used to assess accuracy between remotely mapped and hand-mapped techniques within this and subsequent chapters. The different aspects affecting the remote mapping field processes described in Chapter 3 are investigated in Chapter 4, starting with planning and moving to the raw data capture itself (Figure 4-1). The development of positional and data capture techniques resulted from information gathered and testing during the project as a whole, allowing for continual improvements.

A large portion of the analysis was conducted at cliffs near Brighton, UK as previous studies, ROCC (Risk of Cliff Collapse) had identified that chalk cliffs contained multi-scaled fractures which directly influence stability (Genter *et al.*, 2004). The chalk cliffs also have differing rock mass characteristics to the other lithologies studied during the project in Cornwall, UK. The locations around Cornwall were chosen due to suitability for testing specific aspects of the data capture processes, such as maximum distance ranges and rock type.

The effect of varying the remote data capture field setup parameters on discontinuity trace lengths and spacings have not been explored greatly in this study. As long as the distortion/blinding of the models produced are not too great, it is considered that the effects would be minimal. The assessment of the ability of remote data capture systems to collect discontinuity trace data is covered in Chapter 5.

Completing the field mapping processes, shown in the work-flow diagram (Figure 4-1) will allow the production of geotechnical data. The subsequent analysis of the captured data is conducted in Chapter 5.



4.2 Pole Vector Difference

4.2.1 Pole Vector Difference Calculations

Hand-mapping is the traditionally accepted form of measuring the orientation of rock features. The mapping data collected by hand during this project is used as the reference measurement from which the errors of remote data capture measurements are made as it is a traditional technique for geotechnical mapping (Figure 4-2). To compare an orientation measurement it is traditionally completed by comparing the difference in dip and then in dip direction separately. This can make comparison confusing, especially when dip directions are 180° different for steeply dipping (90°) discontinuity sets. A new methodology was formulated to calculate the error between the remotely mapped orientation and hand-mapped data with input from Professor R.J. Pine of the Camborne School of Mines.

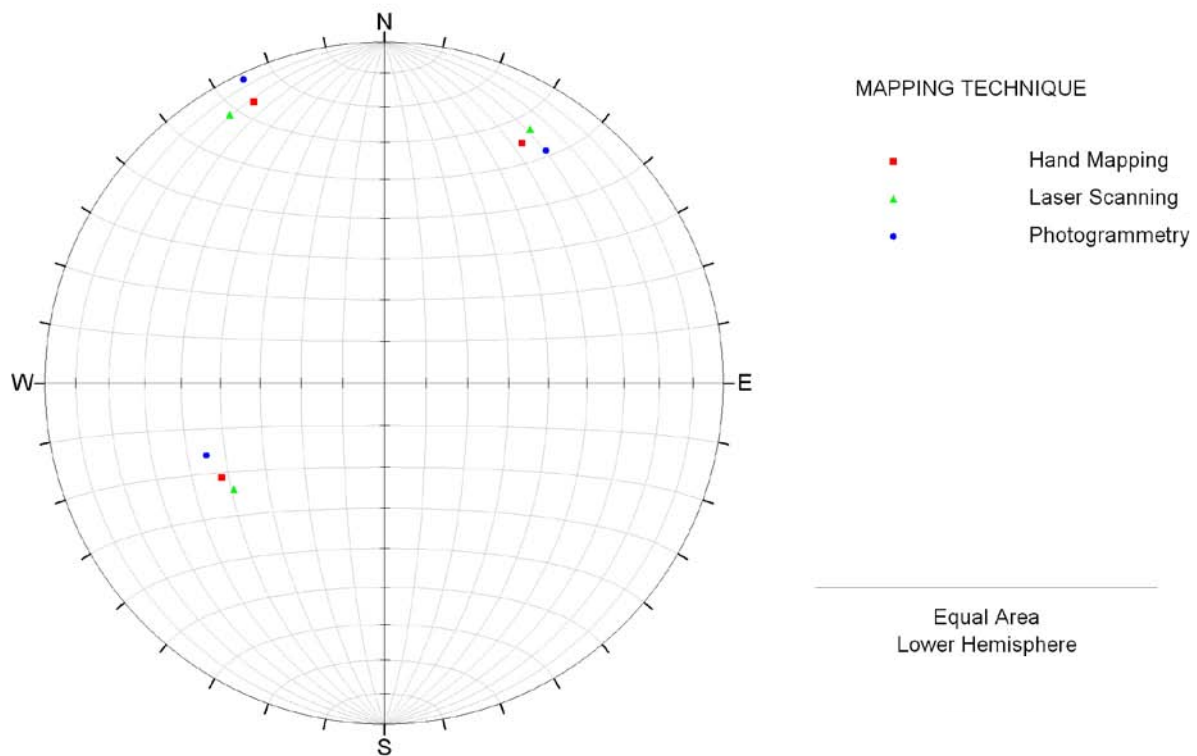


Figure 4-2. Example stereonet shows differences in poles between hand (red), laser (green) and photogrammetric (blue) mapping. Each cluster of poles represents one discontinuity whilst each mapping technique has a slightly different orientation measurement.

Orientation data is hard to compare as it has two components to each measurement, conventionally collected as dip and dip direction readings. By converting the data to pole vectors, this can be used to calculate the difference between them more easily. Dip and dip direction

measurements are first converted to represent their poles by subtracting the dip from 90°, and adding/ subtracting 180° from the dip direction (whether or not it was originally greater than 180°). This data is then converted to Cartesian coordinates (Figure 4-3).

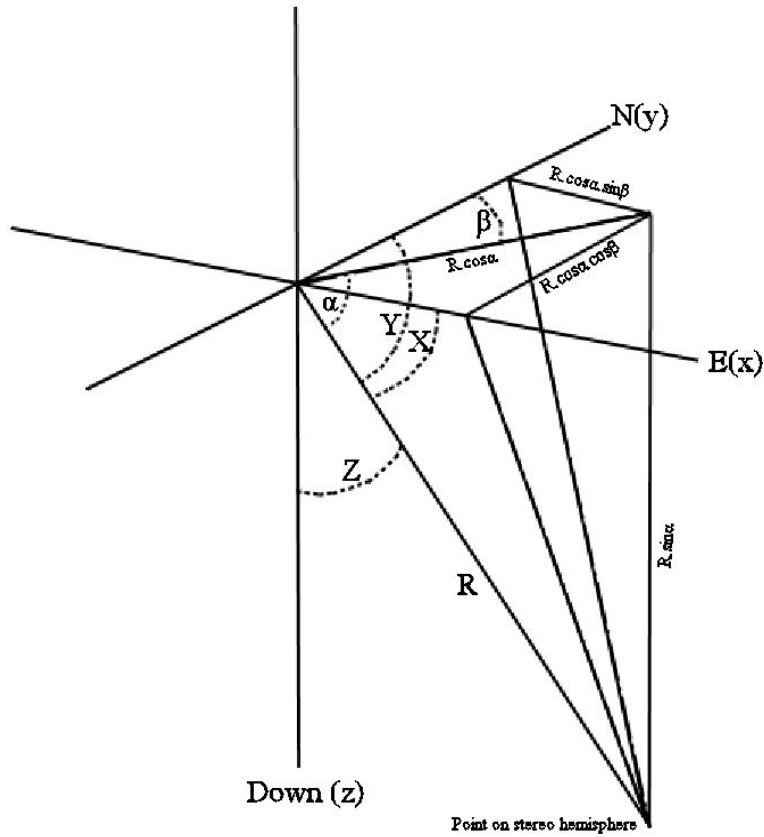


Figure 4-3. Diagram showing dip / dip direction conversion to Cartesian coordinates.

α = pole measured from y/x plane

β = polar direction measured from y axis

R = pole vector distance

X = angle between x axis and pole vector

Y = angle between y axis and pole vector

Z = angle between z axis and pole vector

N(y) = north

E(x) = east

The pole vector distance R can be represented as a direction cosine relative to the X, Y, and Z axes of $\cos X$, $\cos Y$ and $\cos Z$, where:

$$\cos X = \frac{R \cdot \cos \alpha \cdot \sin \beta}{R} = \cos \alpha \cdot \sin \beta$$

$$\cos Y = \frac{R \cdot \cos \alpha \cdot \cos \beta}{R} = \cos \alpha \cdot \cos \beta$$

$$\cos Z = \frac{R \cdot \sin \alpha}{R} = \sin \alpha$$

To determine the difference between two pole vectors, i.e. the 'error', the cosine of their 'dot' product can be used, where:

$$\cos(\text{error}) = R_1 \cdot R_2$$

$$\text{error} = \cos^{-1}(R_1 \cdot R_2)$$

To avoid problems with the calculations arising when poles are either side of the stereonet the absolute value of the dot products must be taken. For example, the correct error between 89°/ 002° and 89°/ 186° is 4.47°, where without taking the absolute value, an error reading of 175.53° (180° minus the correct error) would occur.

In full, to calculate the pole vector difference:

$$\text{error} = \cos^{-1} \sqrt{(\cos \alpha_1 \cdot \sin \beta_1 \cdot \cos \alpha_2 \cdot \sin \beta_2 + \cos \alpha_1 \cdot \sin \beta_1 \cdot \cos \alpha_2 \cdot \sin \beta_2 + \sin \alpha_1 \cdot \sin \alpha_2)^2}$$

Example pole vector differences/ errors are shown in Table 4-1 (Full Microsoft Excel file on appendix DVD).

Table 4-1. Calculation of pole vector error between five hand-mapped discontinuities and the corresponding measurements made using remote mapping techniques. Arrows indicate direction of calculations.

Hand Mapped Dip	Hand Mapped Dip Direction	X	Y	Z
02	140	-0.022	0.027	0.999
02	011	-0.007	-0.034	0.999
89	002	-0.035	-0.999	0.017
23	049	-0.295	-0.256	0.921
00	004	-4.27E-18	-6.11E-17	1

Remotely Mapped Dip	Remotely Mapped Dip Direction	X	Y	Z
08	142	-0.086	0.110	0.990
17	004	-0.020	-0.292	0.956
89	186	0.105	0.994	0.017
29	048	-0.360	-0.324	0.875
05	003	-0.005	-0.087	0.996

X product	Y Product	Z Product	R1.R2	Pole Vector Difference/ Error
0.002	0.003	0.990	0.995	6.00
0.0001	0.010	0.956	0.966	15.02
-0.004	-0.994	0.0003	0.997	4.47
0.106	0.083	0.805	0.994	6.02
1.95E-20	5.32E-18	0.996	0.996	5.00

4.2.2 Pole Vector Difference of Hand-mapping

A comparison between two hand-mapping studies of the same rock face was conducted for this project at Penlee Quarry, Cornwall, UK. Hand-mapping was undertaken upon discontinuities that were then numbered on the rock face using chalk (by Dr Zara Flynn, Camborne School of Mines). Five weeks later the same numbered discontinuities were mapped for a second time. The pole vector difference was calculated between each mapped feature (50 in total). It was found that the average individual feature pole vector difference between the two hand-mapping data sets was 13.75° with a standard deviation of 17.38° .

4.2.3 Interpretation of Pole Vector Difference Values

The results collected from the hand-mapping comparison undertaken at Penlee Quarry provides a useful base to interpret the errors that will result from the comparison between hand-mapping and remote data capture. The results from Penlee have to be used with caution as they only come from one specific rock mass and only 50 discontinuity features. Using the average pole vector difference from the hand-mapping study at Penlee Quarry of 13.75° minus a half standard deviation would mean that a 'low' PVD value should be $\sim 5^\circ$, however an allowance for noise within the 3D models must also be applied. It is suggested that a 10° allowance for noise can be made. An acceptable, 'low' error between hand-mapping and remote data capture systems should be below 15° , where an error between laser scanning and photogrammetry should only result due to noise and should be less than 10° . A 'medium' PVD value is calculated to be up to 32° using the Penlee hand-mapping error average of 13.75° , plus half standard deviation and the allowance for noise, where a greater value is deemed to be 'high'. As the error trends to 90° it indicates that the compared features have been misidentified or that a severe distortion in a part of the 3D model has occurred.

4.3 Area of Face Analysis

The ability of the remote data capture systems to collect data from rock faces with varying scales of fractures was tested at a coastal cliff location at Portobello near Brighton, UK (Figure 4-4). The Portobello chalk is within the Newhaven Chalk Formation spanning the late Santonian and early Campanian (~ 80 Ma) (Mortimore *et al.*, 2004) (Figure 4-5). Both laser scanning and photogrammetry was conducted upon the cliffs (Figure 4-6). Hand-mapping data was collected

by Dr. J. Lawrence, Brighton University. Abseiling from the top of the cliff was the only method available to map the large scale structures.



Figure 4-4. Map of Southern England, UK, showing location of Saltdean and Portobello coastal cliffs. © Crown Copyright/database right 2009. An Ordnance Survey/EDINA supplied service.

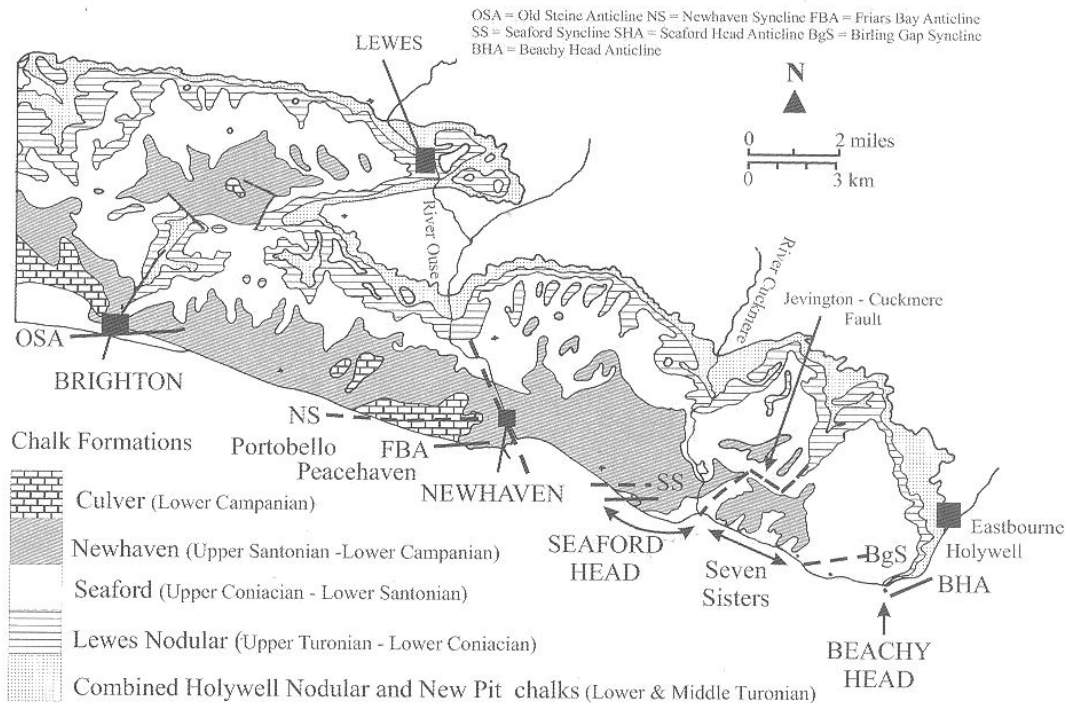


Figure 4-5. Geological map showing location of Portobello Cliffs (from Mortimore *et al.*, 2004).

The cliffs at Portobello are approximately 30 m in height with an average slope angle of 70° (Figure 4-7 and Figure 4-8). The rock mass had an average RQD of 70%. Bedding features, which run sub horizontally along the length of the cliff, were treated separately to joints and faults during the remote mapping study, but were recognised as geotechnically important as they could act as release surfaces for potentially forming wedges. It was postulated that the orientation of the small and medium scale structures within the rock mass would also be identified at the large scale.

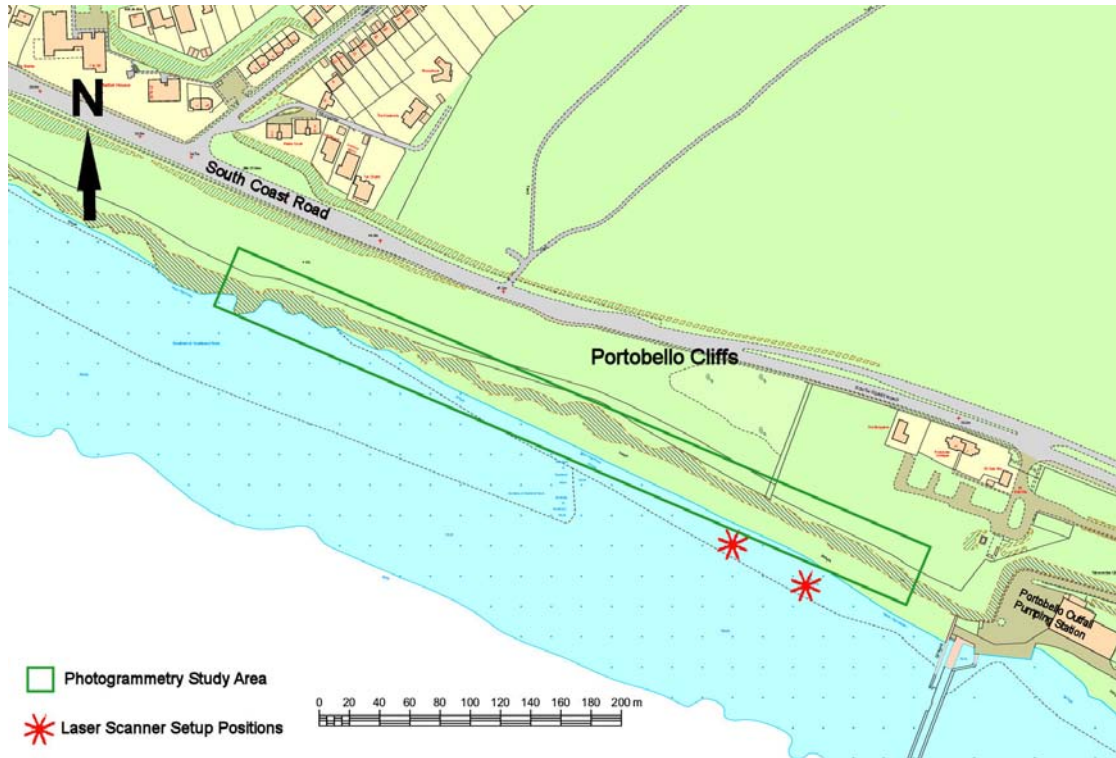


Figure 4-6. Map showing photogrammetry study area and locations of laser scanner setup positions. © Crown Copyright/database right 2009. An Ordnance Survey/EDINA supplied service.



Figure 4-7. Image of cliff face at Portobello, UK, looking NE (30 m high).

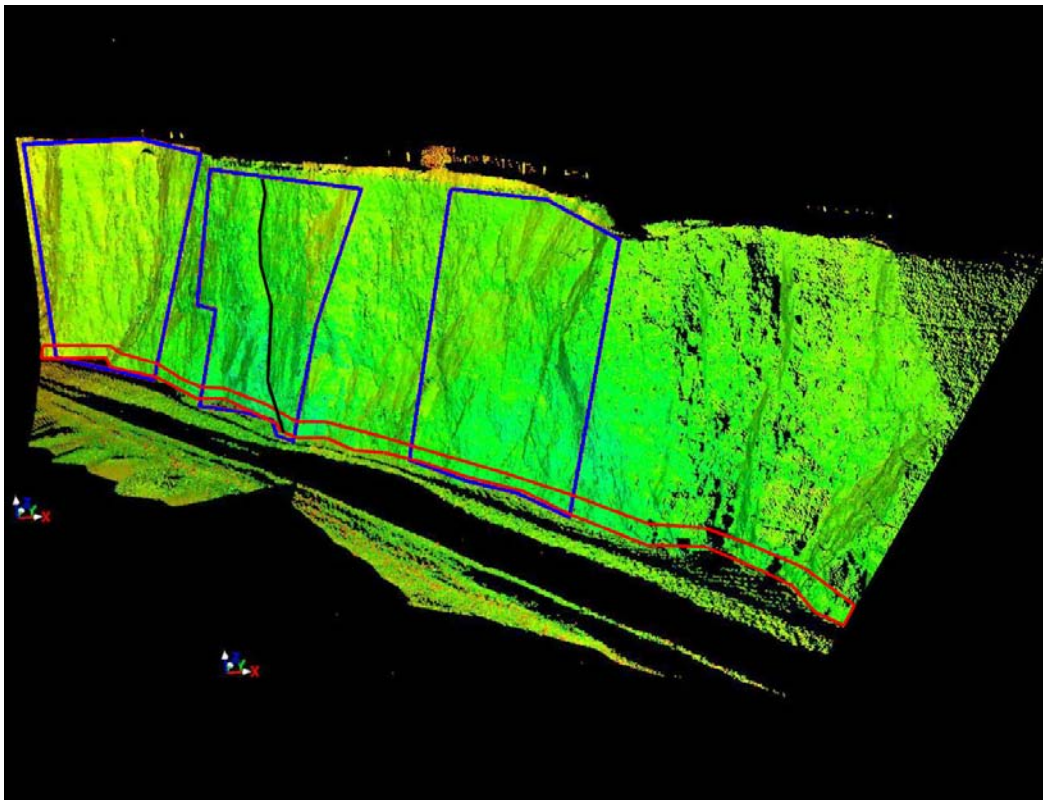


Figure 4-8. Point cloud image (looking NW) showing area covered by two laser scans, 3 photogrammetric models (blue) and traditional hand-mapping (red) during morning visit (black line showing location of largest feature identified).

4.3.1 *Photogrammetry*

In order to assess the effects of representative scale on mapped discontinuity orientations, different models were made of the chalk cliff (Table 4-2). In total there were sixteen models made, from which approximately 2000 fractures were recorded (appendix DVD). The first eight models were made during a first visit in June 2006, each measuring $\sim 15 \text{ m}^2$ covering half the cliff height. Subsequently, in March 2007, another eight models were completed during a second visit. Three large scale models were made encompassing the entire height of the cliff ($\sim 30 \text{ m}^2$). The overall height of the cliff face limited the maximum length of fracture that could be identified. Two small scale models viewing single bedding structures, 0.75 m - 1 m in height were captured to study the centimetre scale fractures. Three medium scale models, one of which is shown in Figure 4-9, were then made of multiple bedding planes to visualise discontinuities that crossed between them.

Table 4-2. Locations of photogrammetry camera and control point setups at Portobello, Brighton, UK, indicating model scale and lens used.

GB National Grid (m)			Camera / Control Point	Model	Lens	Scale
Eastings	Northings	Elevation				
539084	101470	1	Camera 1	Model 1	50mm	Medium Scale
539078.9	101473.1	1.005	Camera 2			
539090	101513.6	25.563	Control Point A			
539082	101473	2	Camera 3	Model 2	50mm	Medium Scale
539076.9	101476.1	2.005	Camera 4			
539098.2	101509.7	26.167	Control Point B			
539125	101451	2	Camera 5	Model 3	50mm	Medium Scale
539119.9	101454.1	2.005	Camera 6			
539126.8	101494.9	12.771	Control Point C			
539020	101507	3	Camera 7	Model 4	50mm	Medium Scale
539014.9	101510.1	3.005	Camera 8			
539038.3	101538.5	12.929	Control Point D			
538568	101514	1	Camera 9	Model 5	50mm	Medium Scale
538563.9	101517.3	0.967	Camera 10			
538577.6	101552.7	21.404	Control Point E			
539034	101497	2	Camera 11	Model 6	50mm	Medium Scale
539029.9	101500.3	1.967	Camera 12			
539054.6	101528	22.719	Control Point F			
539094	101468	1	Camera 13	Model 7	50mm	Medium Scale
539089.9	101471.3	0.967	Camera 14			
539105.3	101504.7	13.832	Control Point G			
539098	101475	3	Camera 15	Model 8	50mm	Medium Scale
539093.9	101478.3	2.967	Camera 16			
539116.9	101504.5	12.977	Control Point H			
538526	101599.2	4	Camera 17	Model 9	50mm	Medium Scale
538525.1	101600.1	4.102	Camera 18			
538528.7	101607	4.768	Control Point I			
538929	101568	2	Camera 19	Model 10	50mm	Medium Scale
538927.5	101568.7	2.025	Camera 20			
538932.9	101579.1	4.603	Control Point J			
538790	101623	4	Camera 21	Model 11	50mm	Medium Scale
538788.3	101623.8	3.998	Camera 22			
538792.3	101634.4	5.953	Control Point K			
538860	101601	4	Camera 23	Model 12	20mm	Small Scale
538860.6	101600.5	4.094	Camera 24			
538861.6	101602.6	5.04	Control Point L			
538909	101588	6	Camera 25	Model 13	20mm	Small Scale
538909.3	101587.4	5.959	Camera 26			
538912.8	101589.3	6.057	Control Point M			
539206	101424	1	Camera 27	Model 14	20mm	Large Scale
539202.3	101425.8	1.295	Camera 28			
539211.6	101453.8	15.101	Control Point N			
539215	101417	0	Camera 29	Model 15	20mm	Large Scale
539210.6	101419	0.045	Camera 30			
539219.3	101448.7	13.401	Control Point O			
539119	101468	0	Camera 31	Model 16	20mm	Large Scale
539114.7	101470.1	0.054	Camera 32			
539126.9	101496.6	14.661	Control Point P			



Figure 4-9. Orthoimage (striking 085°) showing large scale structures (>1 m, blue) and small scale structures (<1 m, red).

The largest non-bedding feature identified was a sub vertical undulating fracture measuring 27.9 m in length, which extended the height of the cliff. The smallest feature identified was 0.05 m in length. This minimum size was controlled by the mesh used to generate the photogrammetric image; smaller features are present but were too small to resolve even at the closest proximity. These small scale features, depicted in Figure 4-10, were found to cause some unstable sections. They form 'sugar cube' like blocks, ~0.25 m in size, which fall out of the cliff easily, and as they are so numerous are hard to mitigate.



Figure 4-10. Photograph showing small scale fractures found within the Portobello chalk (0.5 m high), looking north. The nodules within the chalk are flint and chert.

4.3.2 Laser Scanning

Figure 4-11 shows another view of the two combined laser scanned point clouds captured using the Leica HDS3000. These point clouds were subsequently geotechnically mapped using SplitFX (appendix DVD). The laser scanning was conducted at two sites along the Portobello cliffs during the first visit to the site; they covered a 180 m section in total (Table 4-3). Each laser scan was set at a density of 15 mm at 50 m distance from the face. This resolution was chosen to cover the area required and to complete the scans within a reasonable time available before the tide came in. The laser scanner was not available for the second site visit so a higher density scan was not possible. Little orientation data was taken from the point clouds when compared to photogrammetry, as most of the fractures seen within the rock were linear discontinuity traces. Similar sized large and medium scale features were identified as photogrammetric mapping, but due to the relatively low density of the laser scan and the fact that these features were predominantly represented as discontinuity traces the smallest scaled structures were not captured.

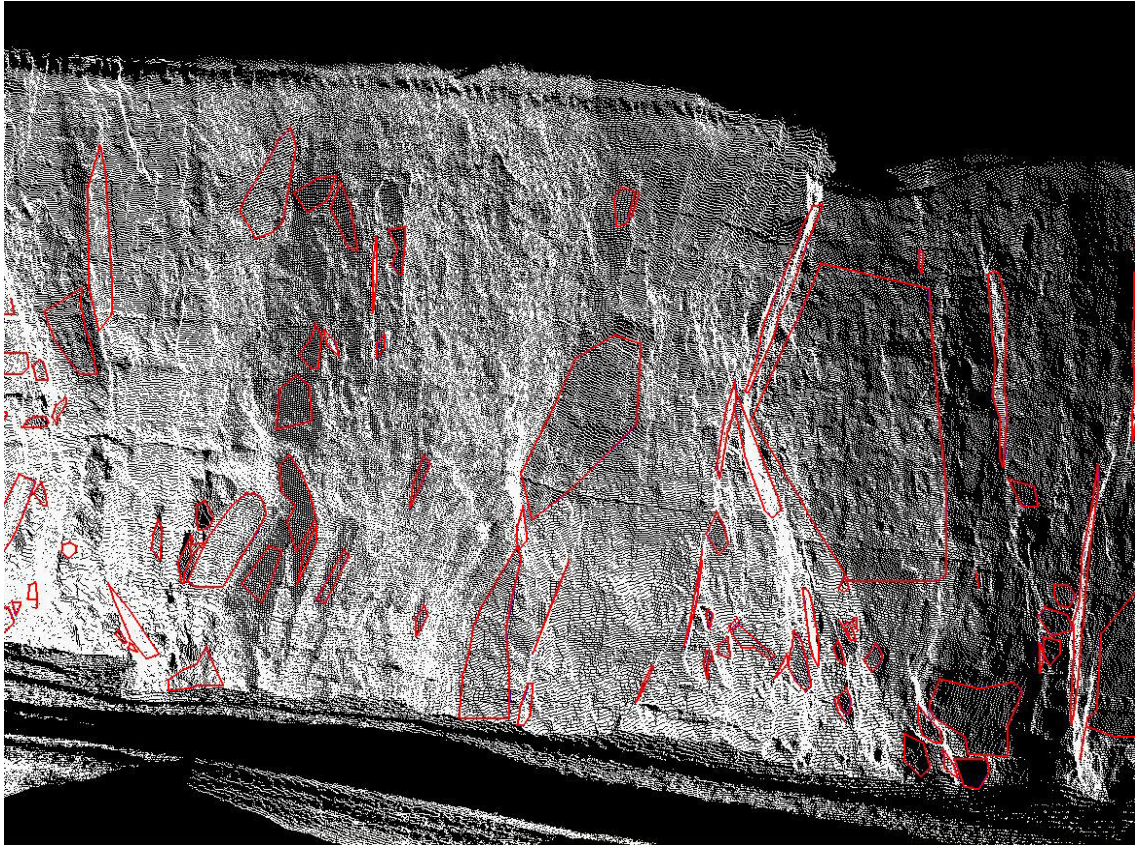


Figure 4-11. Point cloud showing large scale planes identified within SplitFX (red), Portobello Cliffs, Brighton, UK (30 m high), looking NE.

Table 4-3. Locations of laser scanner setup positions at Portobello, Brighton, UK, also indicating the scan density used.

GB National Grid (m)			Laser Scanner Type	Model	Density
Eastings	Northings	Elevation			
539171	101434	0	Leica HDS3000	Laser 1	15 mm at 50 m distance
539141	101445	1		Laser 2	15 mm at 50 m distance

4.3.3 Orientation Data

Orientation data collected from laser scanning is compared to the hand-mapped data between Figure 4-12 and Figure 4-13. Hand-mapped data collected by J. Lawrence (Lawrence, 2007) was also used as a comparison against orientation data captured from large scale structures through photogrammetry (Figure 4-12 - repeated for comparison, Figure 4-14, Figure 4-15, and Figure 4-16). These stereonet were created using the data from each of the captured photogrammetric scales: large, medium, and small.

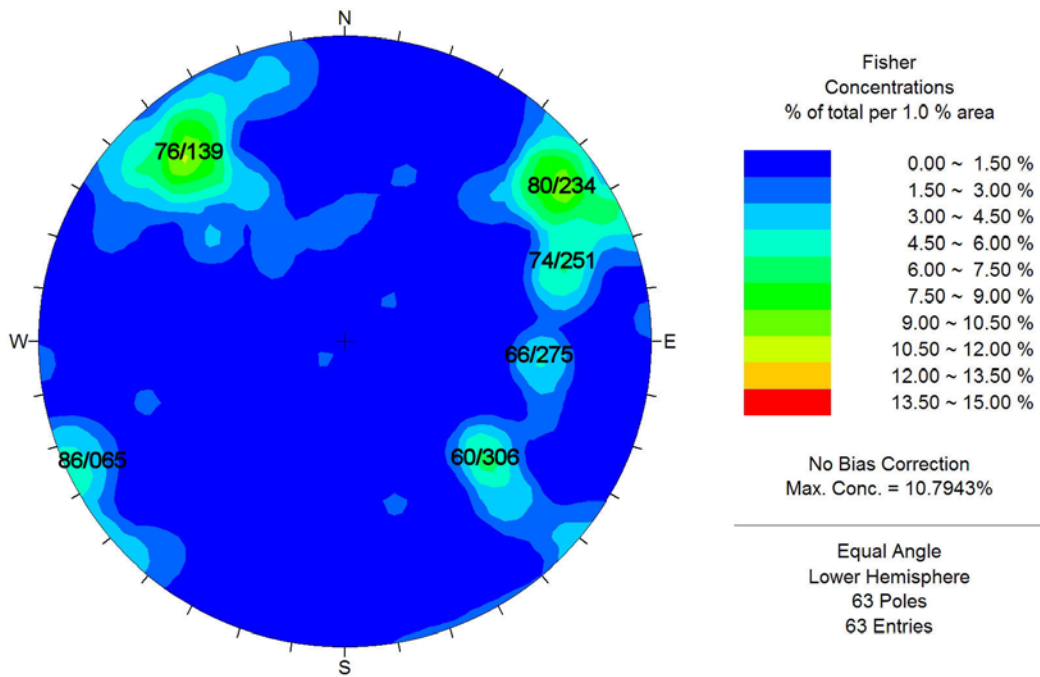


Figure 4-12. Lower hemisphere representations showing contoured hand-mapped data taken from Portobello Cliffs, Brighton, UK (1 m - 30 m length), Lawrence (2007) (dip/dip direction of contour highs given in degrees). These large scale structures are predominantly steeply dipping and striking NE – SW, and NW – SE.

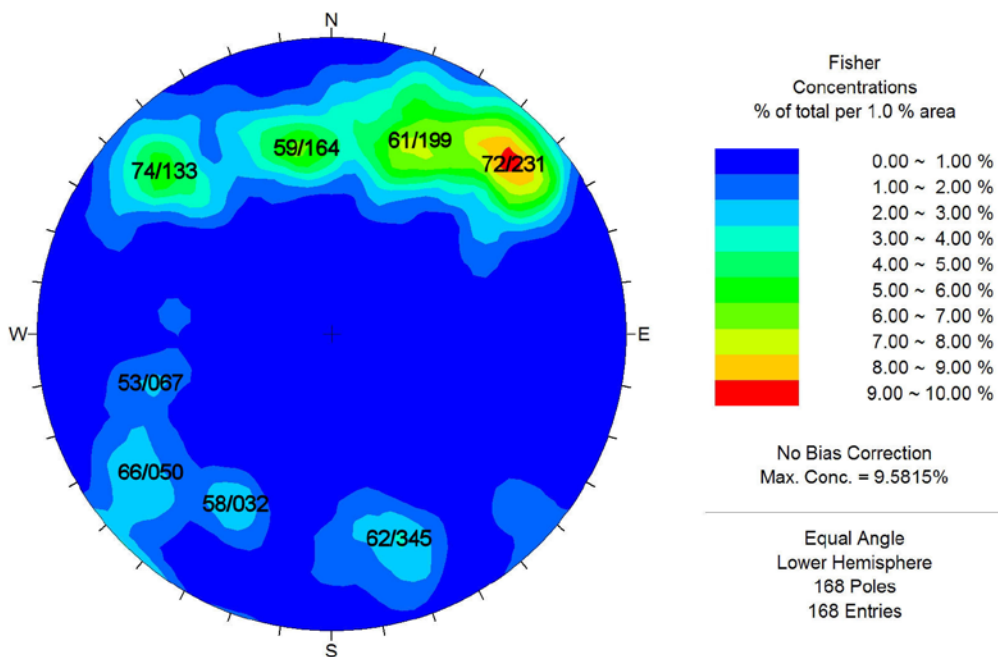


Figure 4-13. Lower hemisphere stereonet showing contoured data from the SplitFX mapped point clouds, Portobello Cliffs, Brighton, UK (dip/dip direction of contour highs given in degrees). Similarly to hand-mapping, laser scanning only picks up the large scale features. The steeply dipping NE – SW, and NW – SE structure are identified, but a strong E – W striking set is also identified.

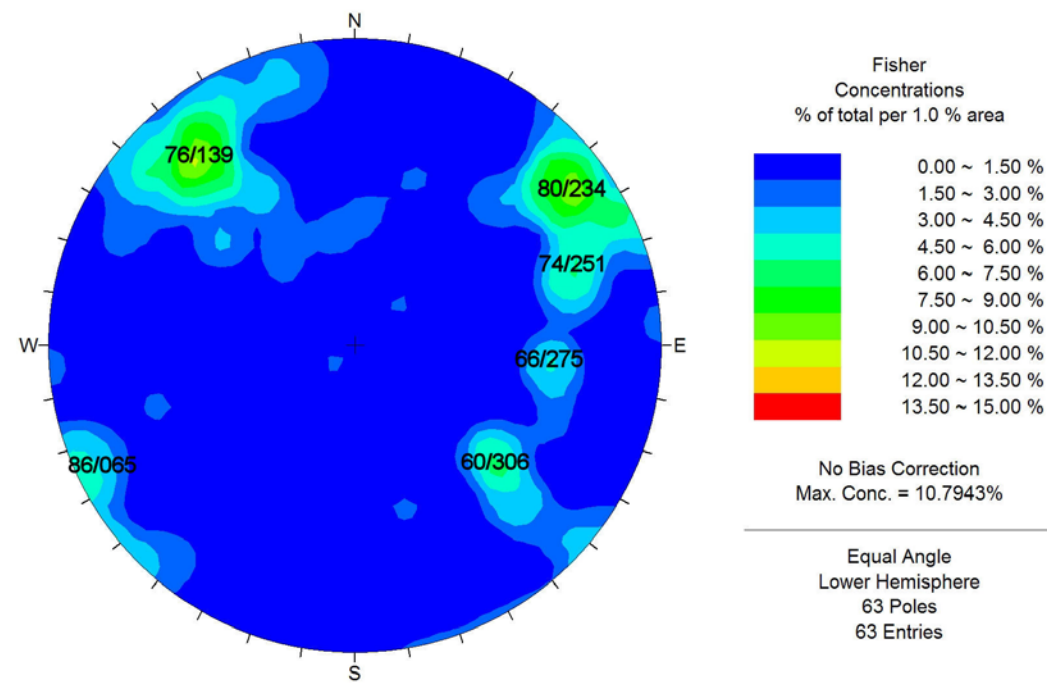


Figure 4-12 (repeated for comparison). Lower hemisphere representations showing contoured hand-mapped data taken from Portobello Cliffs, Brighton, UK (1 m - 30 m length), Lawrence (2007) (dip/dip direction of contour highs given in degrees). These large scale structures are predominantly steeply dipping and striking NE – SW, and NW – SE.

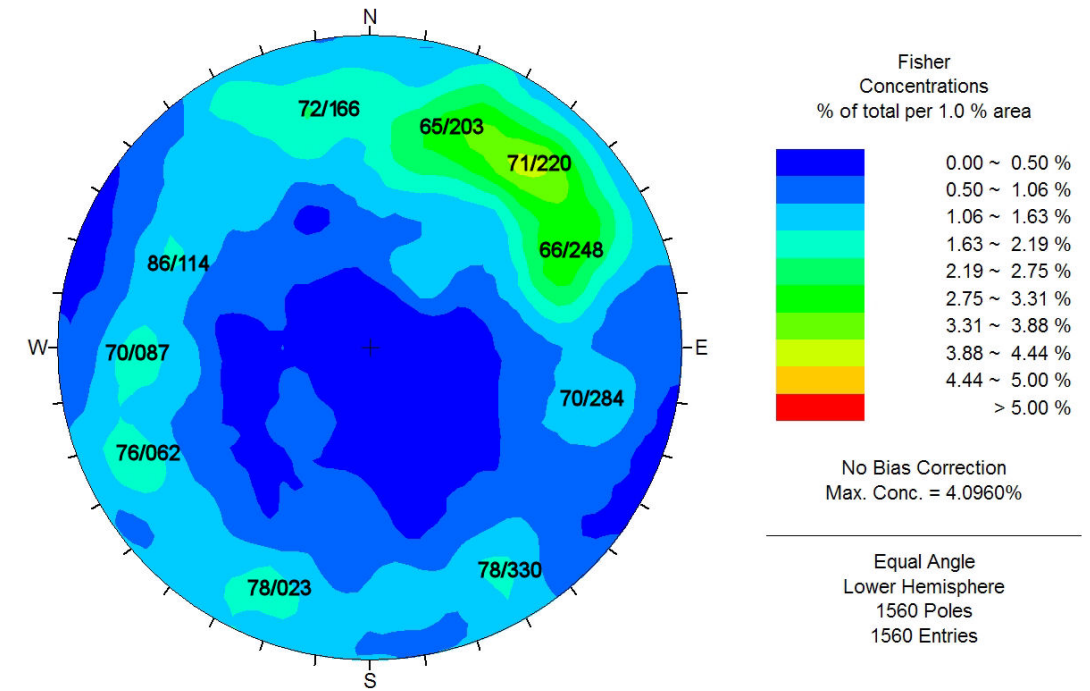


Figure 4-15. Lower hemisphere stereonet showing contoured orientation data from the medium scale models, Portobello Cliffs, Brighton UK (dip/dip direction of contour highs given in degrees). The NW – SE striking set is clearly shown in the stereonet, although the NE – SW striking set is less apparent.

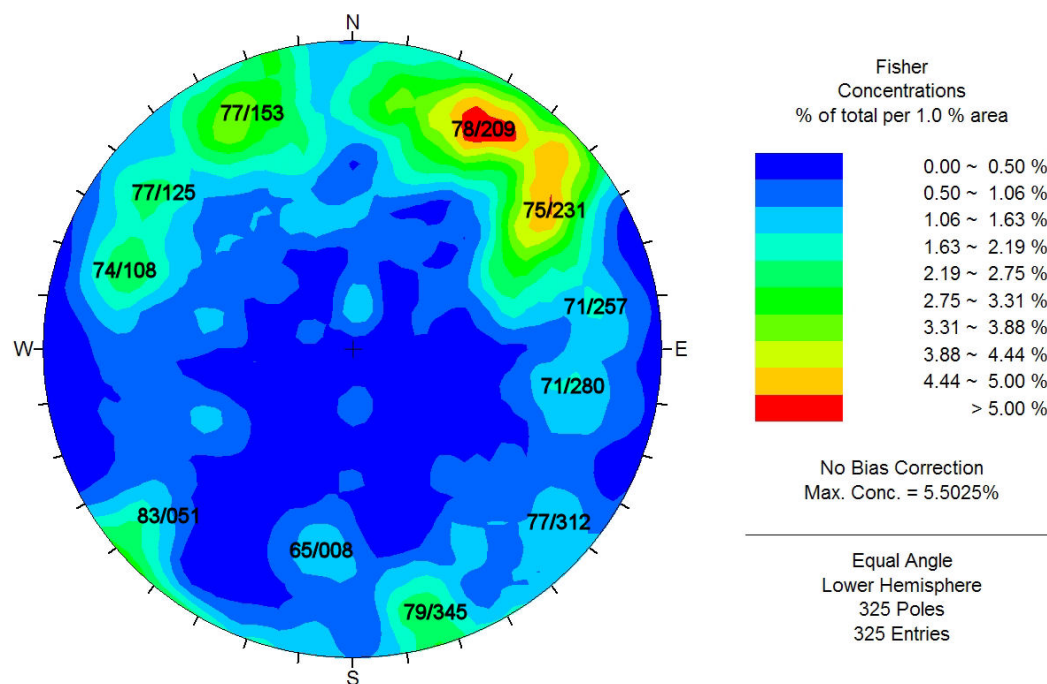


Figure 4-14. Lower hemisphere stereonet showing contoured orientation data from the large scale models, Portobello Cliffs, Brighton UK (dip/dip direction of contour highs given in degrees). The data is scattered but shows a similar NE – SW and NW – SE striking sets as hand-mapping.

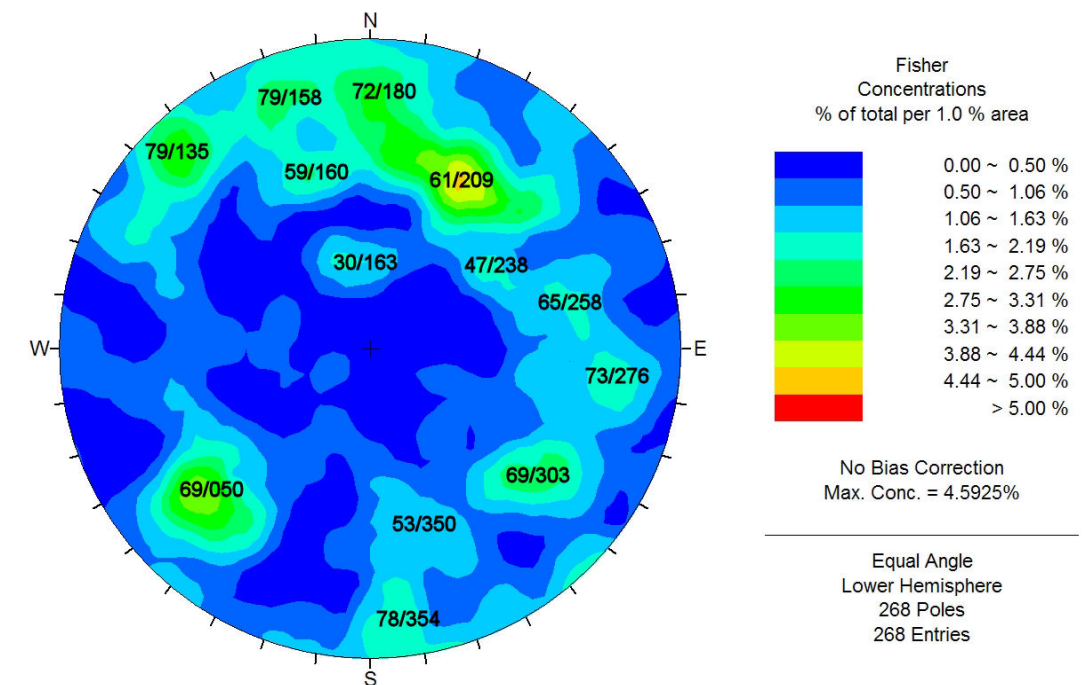


Figure 4-16. Lower hemisphere stereonet showing contoured orientation data from the small scale models, Portobello Cliffs, Brighton UK (dip/dip direction of contour highs given in degrees). The data is highly scattered and only weakly show the NE – SW and NW – SE striking sets identified from the large scale laser scanning and photogrammetric models.

Table 4-4. Orientations of contour highs found from the differing remotely mapped 3D models and from hand-mapping. Corresponding sets have been sorted next to one another for comparison.

Set	Discontinuity Set Data				
	Photogrammetry			Laser Scanning	Hand-Mapping
	Small Scale	Medium Scale	Large Scale		
1	72°/180°	-	-	-	-
2	30°/163°	-	-	-	-
3	61°/209°	65°/203°	78°/209°	61°/199°	-
4	47°/238°	71°/220°	75°/231°	72°/231°	80°/234°
5	65°/258°	66°/248°	71°/257°	-	74°/251°
6	73°/276°	70°/284°	71°/280°	-	66°/275°
7	69°/303°	-	-	-	-
8	-	-	77°/312°	-	60°/306°
9	53°/350°	78°/330°	79°/345°	62°/345°	-
10	-	78°/023°	65°/008°	58°/032°	-
11	78°/354°	-	-	-	-
12	69°/050°	76°/052°	83°/051°	66°/050°	86°/065°
13	-	70°/087°	-	53°/067°	-
14	-	-	74°/108°	-	-
15	79°/135°	86°/114°	77°/125°	73°/133°	76°/139°
16	79°/158°	-	-	-	-
17	59°/160°	72°/166°	77°/153°	59°/164°	-

Three set orientations are comparable across all three photogrammetric scales, laser scanning data and hand-mapped data, set 4, set 12, and set 15 (Table 4-4). Large planar features and their orientations identified using SplitFX are comparable to the large scale features mapped from the photogrammetric models using Sirovision. There are fewer features and therefore fewer contour highs mapped using the point cloud as the photogrammetric 3D models include additional orientation data taken from discontinuity traces. Although laser scanning could not collect orientation data from discontinuity traces, the data collected showed two more large scale sets than hand-mapping. The lower hemisphere stereonet showing orientation data captured from the laser scanned point cloud and hand-mapping had less contour variation than the equivalent large scale photogrammetric model. This may be due to the larger amounts of data collected increasing data scatter, or the accuracy variability of the discontinuity trace orientations, as discussed in Section 0.0.0. The stereonet of the large scale hand-mapped, photogrammetrically mapped and laser scanned data all show the major conjugate sets, striking NE – SW and NW – SE. As shown in the lower hemisphere stereonet plots, each scale is characterised by similar contouring, indicating that similarly orientated fractures exist throughout the rock mass, with slight rotation of the contour highs. Although the conjugate sets can be identified at each scale, the NE – SW striking set is not as apparent in the medium scale models. Blocks that form from the interconnection between these fracture sets can be easily seen in the cliff at the

larger scale. The laser scanned data shows a distinct E-W striking set, which follows the general strike of the cliff face. These orientations are also represented in the photogrammetric data stereonet within the lower concentrated contours between the NE – SW and NW – SE striking sets. However the hand-mapping has not identified the E – W striking orientations. The hand-mapping may not have identified these features as a set, as being so close to the face during mapping they could be mistaken for the general orientation of the cliff face.

It was postulated that the sub bedding sized and the medium scale discontinuities would reflect the same fracture orientations seen within the larger scaled models/ point cloud, although at differing intensities. The remote mapping data capture systems were able to collect data from varying scales. The stereonet showing the small scale fractures indicate a larger scatter of data than seen in the other scales even though comparatively fewer features were mapped. This may be due to the natural fracturing of the rock mass, or it may indicate the inability of the 3D model to properly visualise the discontinuities at that scale. The small scale model identified the most discontinuity highs (13); only six of these were also identified in the medium photogrammetric model and large scale models (photogrammetry and laser scanning). Two sets identified in the large scale models, 8 and 14, were not identified in the small scale models. These results suggest that even though the majority of the large scale orientations are reflected in the small scale, there are multiple other sets that could affect overall strength of the rock mass at varying scales.

4.3.4 Pole vector difference analysis

Table 4-5 shows the results of the pole vector differences across the mapping techniques. As mentioned in the previous section, sets 4, 12 and 15 are the only sets that are comparable across all three mapping techniques. These sets are also seen in all of the photogrammetric model scales. Set 4 has the lowest average PVD value, 5.77°, where set 12 has a medium average PVD of 18.65°. With a high PVD it is possible that the mapping techniques picked up different, but close, set orientations. Set 15 has an average pole vector difference of 9.62°.

Table 4-5. Orientations of contour highs compared using pole vector differences across the large scale data captured by photogrammetry, laser scanning and hand-mapping. Only comparable sets were used.

Set	Photogrammetry		Laser Scanning		PVD
3	78°	209°	61°	199°	19.39°
4	75°	231°	72°	231°	3.00°
9	79°	345°	62°	345°	17.00°
10	65°	8°	58°	32°	22.17°
12	83°	51°	66°	50°	17.03°
15	77°	125°	73°	133°	8.70°
17	77°	153°	59°	164°	20.66°

Set	Laser Scanning		Hand-Mapping		PVD
4	72°	231°	80°	234°	8.51°
12	66°	50°	86°	65°	24.68°
15	73°	133°	76°	139°	6.51°

Set	Photogrammetry		Hand-Mapping		PVD
4	75°	231°	80°	234°	5.79°
5	71°	257°	74°	251°	6.46°
6	71°	280°	66°	275°	6.83°
8	77°	312°	60°	306°	17.88°
12	83°	51°	86°	65°	14.25°
15	77°	125°	76°	139°	13.65°

The comparison between photogrammetrically captured orientations and hand-mapping produced the lowest average pole vector difference across all six comparative sets, 10.81°; it also produced the lowest standard deviation of 5.1°. Laser scanning and hand-mapping were only comparable across three sets and produced a low average PVD of 13.24° and standard deviation of 10°. Photogrammetry and laser scanning matched the most sets from the large scale models, (seven) although with the highest average PVD of 15.42°, along with a standard deviation of 7°. The standard deviation of each of the comparisons was lower than the Penlee Quarry hand-mapping vs. hand-mapping value of 17.4° (Section 4.2.2). As the majority of the PVD values are low (<15°) the comparison between the mapping techniques provide comparable measurements of the rock mass at Portobello, Brighton, UK.

4.4 Rock Type/Structure Analysis

To assess the suitability of the remote data capture systems to collect data from differing rock types/structures with differing fracture intensities, laser scans and photogrammetric images were made of igneous, metamorphic and sedimentary lithologies. The sedimentary lithologies studied are the chalk cliffs at Portobello, Brighton, UK, which have been covered in Section 4.3. It was considered that the rock

types with blockier discontinuity patterns would produce more accurate orientation data (when compared to hand-mapping) than the complexly fractured rocks. The larger planes (and discontinuity traces) exhibited by the blockier rock masses would contain more 3D positional data from which to obtain accurate measurements.

4.4.1 *Gwithian and Gunwalloe Cliffs*

The cliffs at Gwithian, Cornwall, UK (Figure 4-17) are composed of Devonian aged metamorphosed sand and mudstones of the Porthtowan Formation of the Gramscatho Basin (Figure 4-18 and Figure 4-19). The rocks at Gunwalloe, Cornwall, UK are also mud and sandstones of Devonian age but have a higher percentage of sandstone. A section of the Gunwalloe Cliffs are named ‘Blue Rocks’ as they have a high organic content giving them a distinct colour. These localities were chosen to assess the ability of photogrammetry to capture data and subsequently geotechnically map highly complex rock masses.

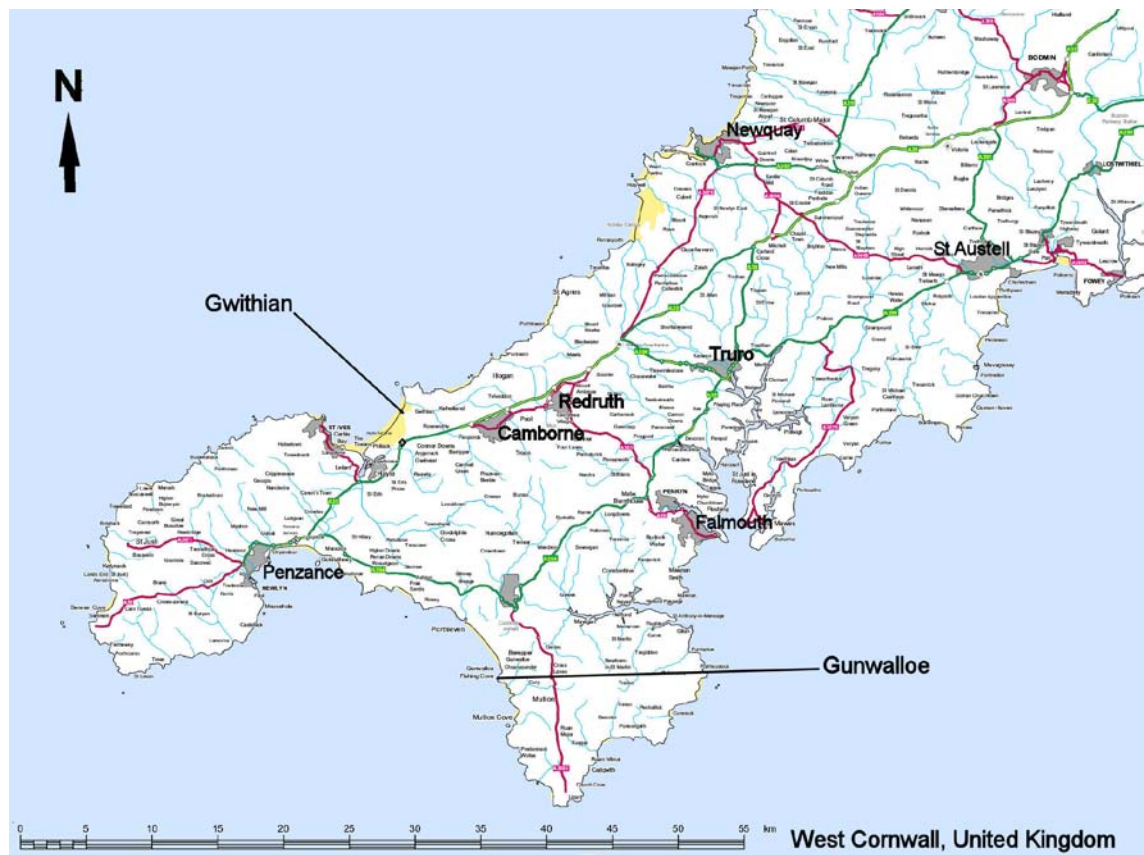


Figure 4-17. Map of West Cornwall, UK, showing location of Gwithian and Gunwalloe cliffs. © Crown Copyright/database right 2009. An Ordnance Survey/EDINA supplied service.

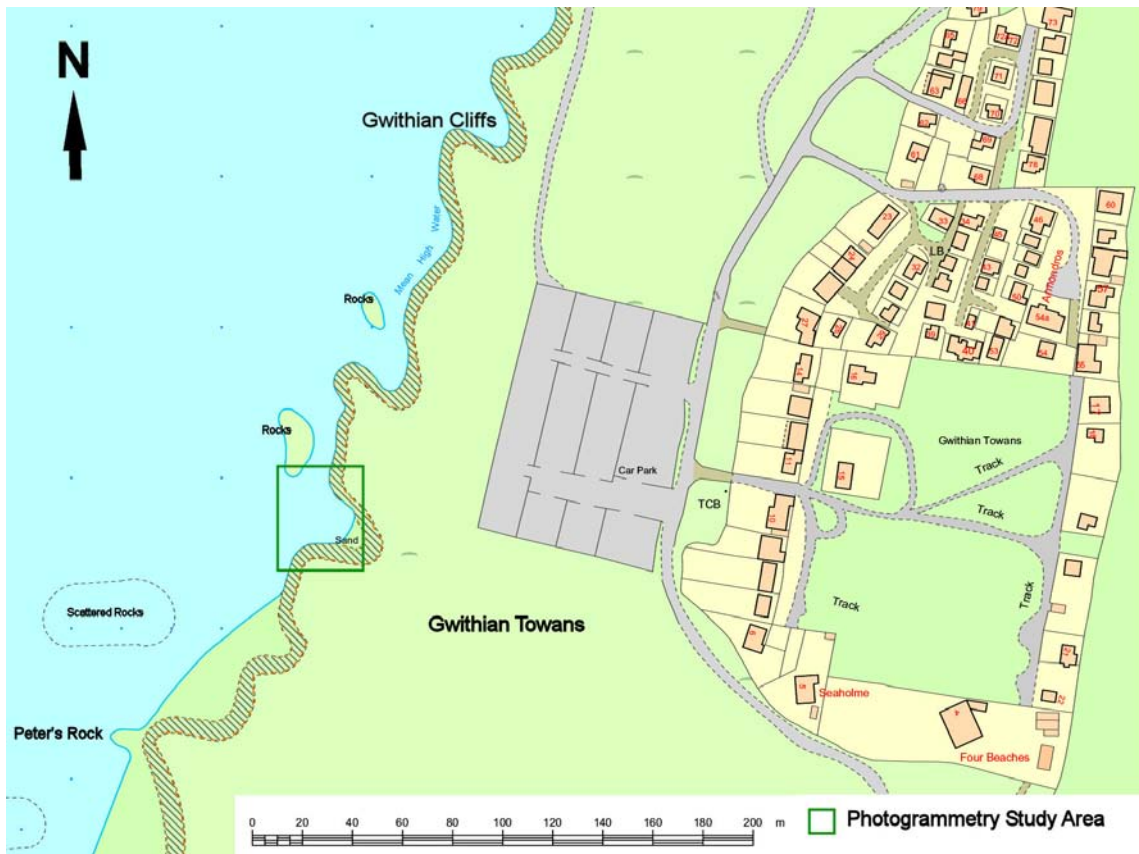


Figure 4-18. Map showing photogrammetric study area at Gwithian cliffs. © Crown Copyright/database right 2009. An Ordnance Survey/EDINA supplied service.

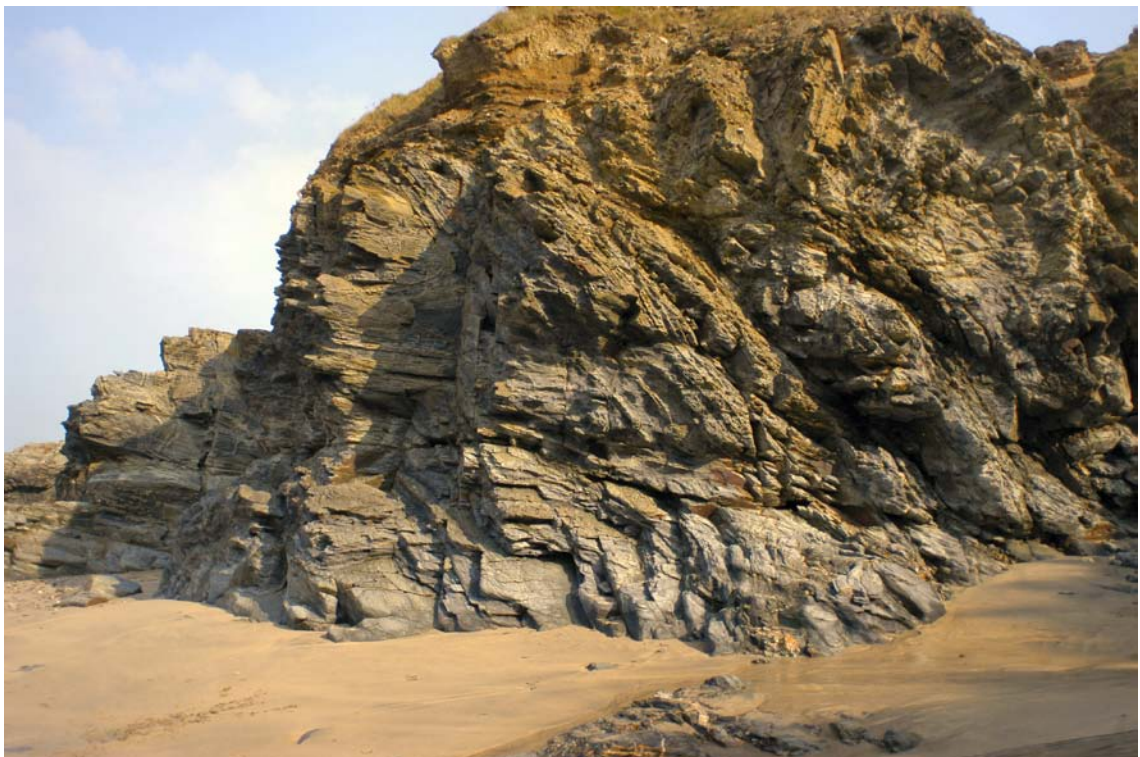


Figure 4-19. Photograph of cliff face (~10 m high) at Gwithian, UK, looking east. The Variscan fold structures can be clearly seen within the face along with the complex jointing set orientations.

Each of the localities have been folded and faulted during the Variscan orogeny whilst experiencing multiple episodic deformation events. After the Variscan the crust experienced NNW – SSE extension controlled by the reactivation of thrust faults, as well as ENE – WSW extensional faults. The sediments were subsequently baked and in parts mineralised when the Cornubian Batholith intruded into the country rock around 280 Ma (Selwood *et al.*, 1998). Triassic rifting caused basinal fluids to be expelled from depth, which intruded into the Cornish rocks forming NW – SE to N – S striking quartz veins, which are present throughout SW England. The repeated attempts to open the north Atlantic began during the Cretaceous, causing E – W extension across the region (Shail & Alexander, 1997).

The 8 m high rock face seen at Gwithian is highly fractured, displaying evidence of the deformation episodes previously described, which run throughout the rock mass. Quartz veining is evident which may have sutured some of the potentially unstable features. Evidence of wedge and toppling failures can be seen within the cliff. The locality had an average RQD rating of 30%.

Five photogrammetric models were created at the site from three setup positions, each viewing the cliff from differing angles to capture a three dimensional view of the rock mass (Table 4-6 and appendix DVD). Two sites had two models made from the same set up position, one using a 50 mm lens and the other using a 20 mm lens to capture orientations from a range of fracture sizes. From the photogrammetric images 355 features were identified, 33 of which were identified as planes, and 322 were discontinuity traces (Figure 4-20). Due to the high intensity of fracturing within the rock mass, most discontinuities were identified as traces as they had too small an area to be delineated as planes within the geotechnical analysis module. Data from hand-mapping conducted by Alexander & Shail (1995) is shown in Figure 4-21.

Table 4-6. Locations of photogrammetry camera and control point setups at Gwithian, Cornwall, UK, indicating model and lens used.

GB National Grid (m)			Camera / Control Point	Model	Lens
Eastings	Northings	Elevation			
157769	41255	1	Camera 1	Model 1 & 2	20 mm & 50 mm
157768.3	41253.92	1.143	Camera 2		
157773.4	41251.19	1.54	Control Point A		
157777	41287	0	Camera 3	Model 3 & 4	20 mm & 50 mm
157776.4	41285.24	0.089	Camera 4		
157784.7	41282.24	1.333	Control Point B		
157786	41265	1	Camera 5	Model 5	20 mm
157787.6	41265.03	1.23	Camera 6		
157786.8	41274.79	2.21	Control Point C		

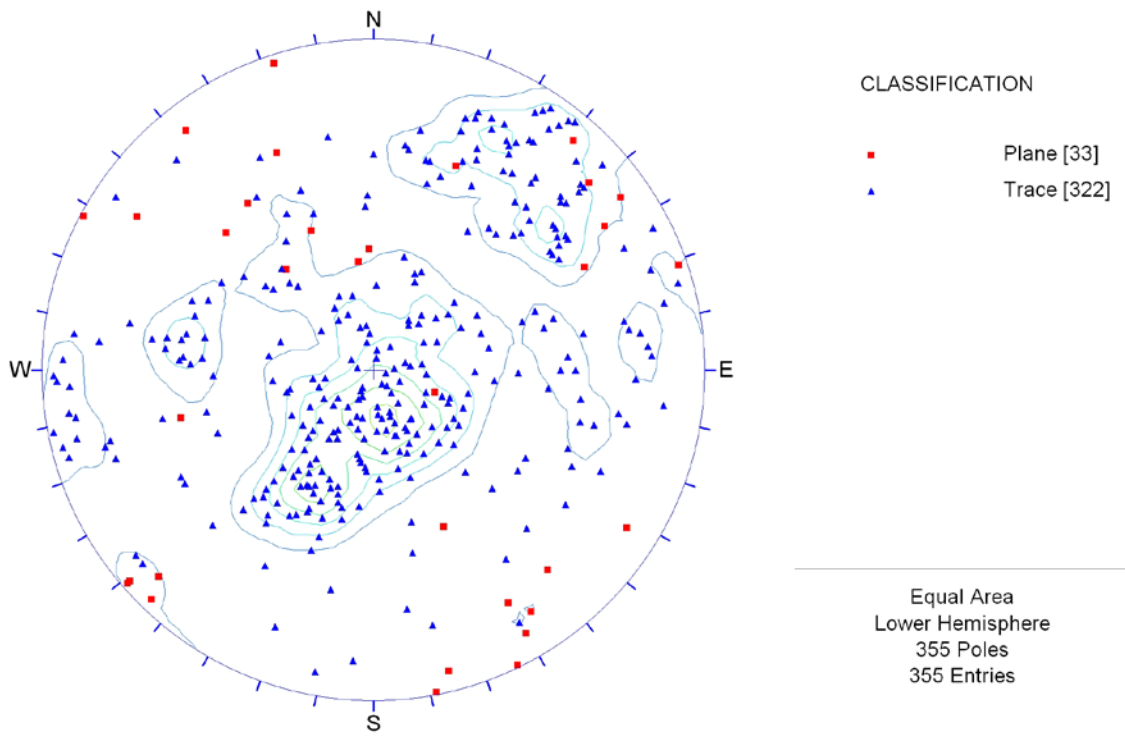


Figure 4-20. Lower hemisphere stereonet showing Gwithian orientation data.

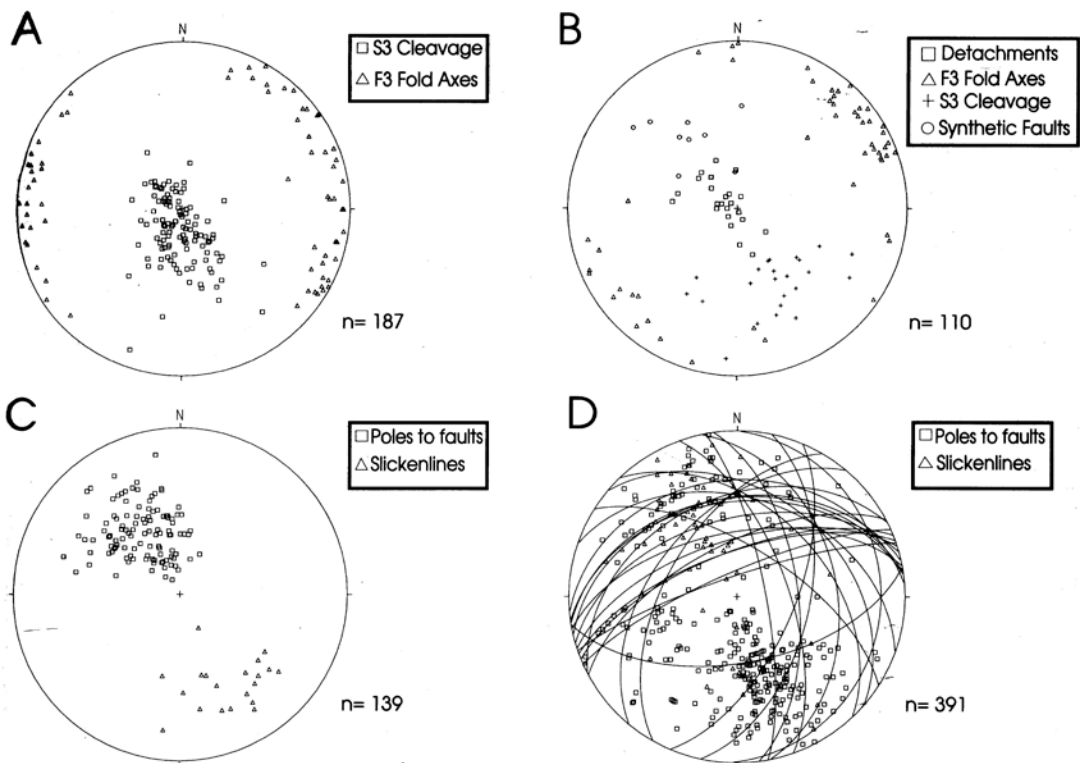


Figure 4-21. Equal area stereograms showing orientation data for: (a) Zones of distributed D3 shear, (b) D3 detachments, (c) D3 brittle listric extensional faults and (d) post D3 faults (from Alexander and Shail, 1995).

The hand-mapped data from Alexander & Shail (1995) is subdivided according to the deformation events. These features have been picked up using photogrammetry (S3 cleavage and detachments are strongly shown), but the resolution of the model is insufficient to distinguish between features. This highlights a fundamental disadvantage of using remote mapping techniques. Without physical contact with the rock face it cannot be certain that a bedding feature is a discontinuity. Engineering judgement must be used to assess whether or not certain bedding planes are joints across which failure can occur.

Assuming the remotely captured sub horizontal features were S3 cleavage, pole vector differences were used to compare the average orientations. As the original data was not available, the S3 cleavage average dip/dip direction was estimated to be 06°/029° from part A of the stereonet sets produced by Alexander & Shail (1995). The remotely captured data produced an orientation of 10°/351°, resulting in a low pole vector difference of 6.43°. This value was close to the hand-mapped data, but it was not sure that the remotely captured data represented the same deformation features.

The rocks seen at Gunwalloe (Figure 4-22) are of the same fracture intensity as the lithology seen at Gwithian. The studied cliff face is larger than the face at Gwithian, being 15 m in height. The same failure types are seen, with wedge failures being the most dominant. To the east of the first photograph in Figure 4-23, a large wedge failure is situated encompassing the entire height of the cliff. The locality had an RQD rating of 35%.

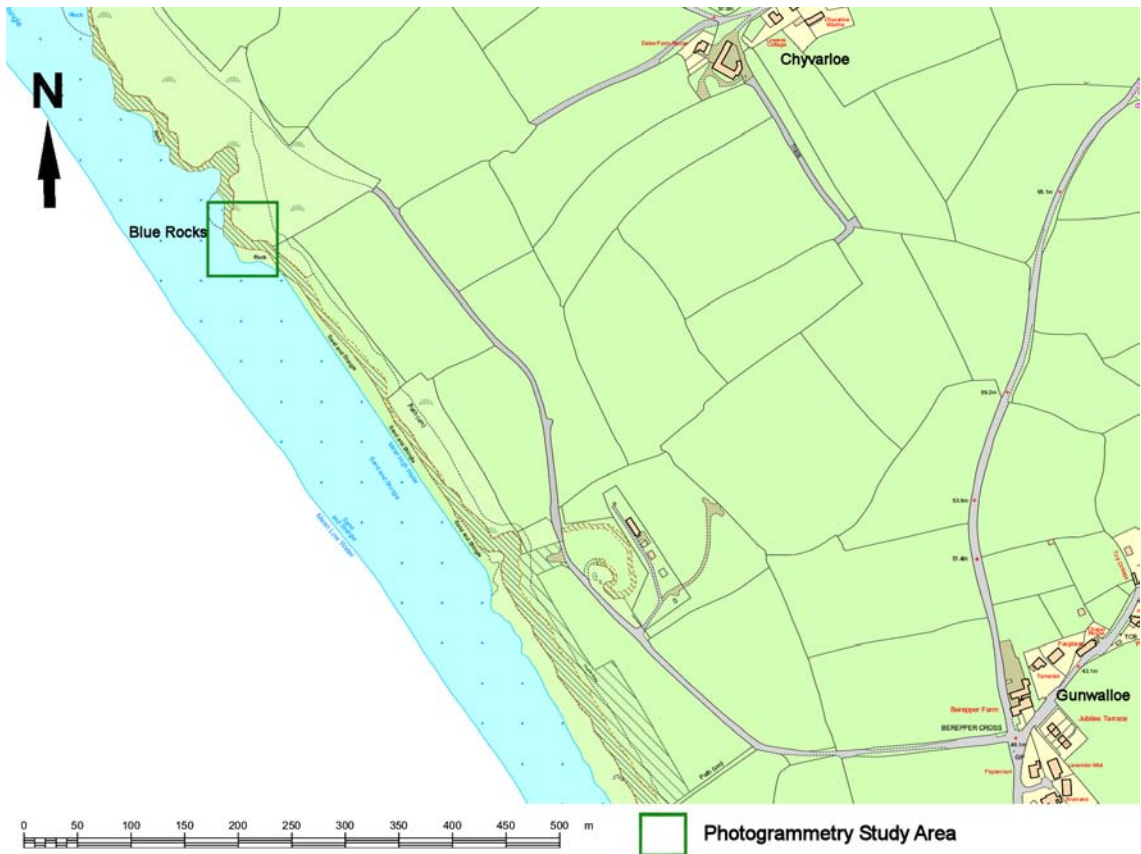


Figure 4-22. Map showing location of photogrammetry study area at Blue Rocks, Gunwalloe. © Crown Copyright/database right 2009. An Ordnance Survey/EDINA supplied service.



Figure 4-23. Photograph of cliff face at Blue Rocks, Gunwalloe, UK, looking north (cliff height from beach is 12 m). Folding is evident in the centre of the photograph, and wedge failures can be seen in the upper sections of the face.

Three photogrammetric images were made of the rocks at Gunwalloe (Table 4-7 and appendix DVD). The first gives a view of the medium to large scale fractures seen within the rock mass. The second was taken of the western side of the large wedge seen in the cliff. It is shown in Figure 4-24 as an orthoimage with mapped structures. Both sides of the wedge could not be captured as the tide restricted the maximum viewing distance. The third image was taken close up to the face to record small scale fractures.

Table 4-7. Locations of photogrammetry camera and control point setups at Gunwalloe, Cornwall, UK, indicating model and lens used.

GB National Grid (m)			Camera / Control Point	Model	Lens
Eastings	Northings	Elevation			
164937	23220	2	Camera 1	big wedge	20 mm
164939.9	23222.85	2	Camera 2		
164925	23223.8	7.75	Control Point A		
164864	23283	2	Camera 3	blue rocks	50 mm
164862.2	23280.24	1.755	Camera 4		
164875.8	23284.45	5.646	Control Point B		
164923	23221	2	Camera 5	close up	20 mm
164923.2	23220.67	1.98	Camera 6		
164927.1	23223.99	3.231	Control Point C		

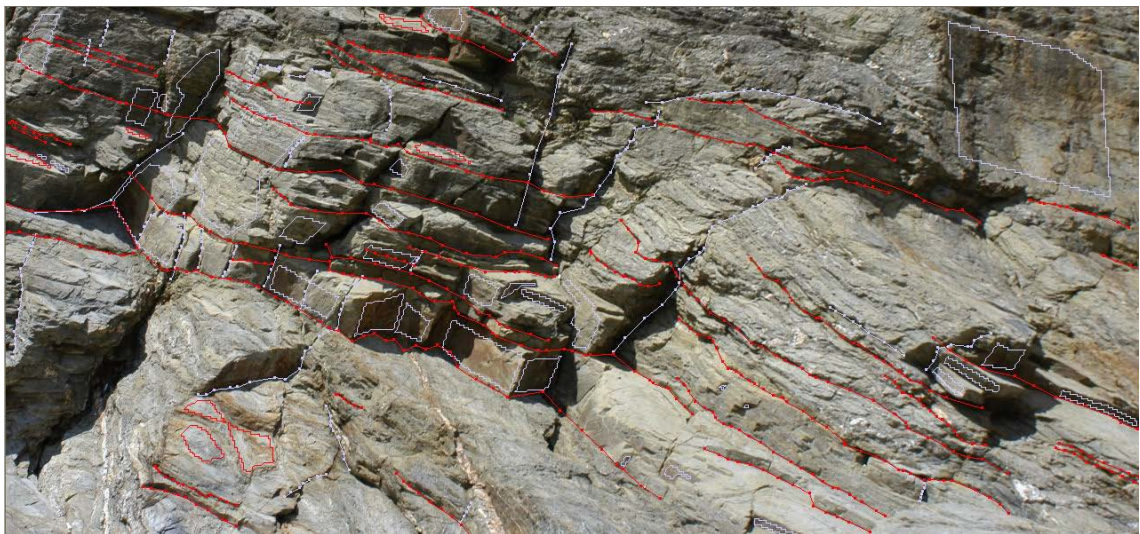


Figure 4-24. Low angle detachments (faults) identified from the 'Big Wedge' model at Loe Bar, Gunwalloe (3 m high face, looking east). Using a visual assessment of separation and movement across discontinuity features, the faults were identified and mapped using the photogrammetric software.

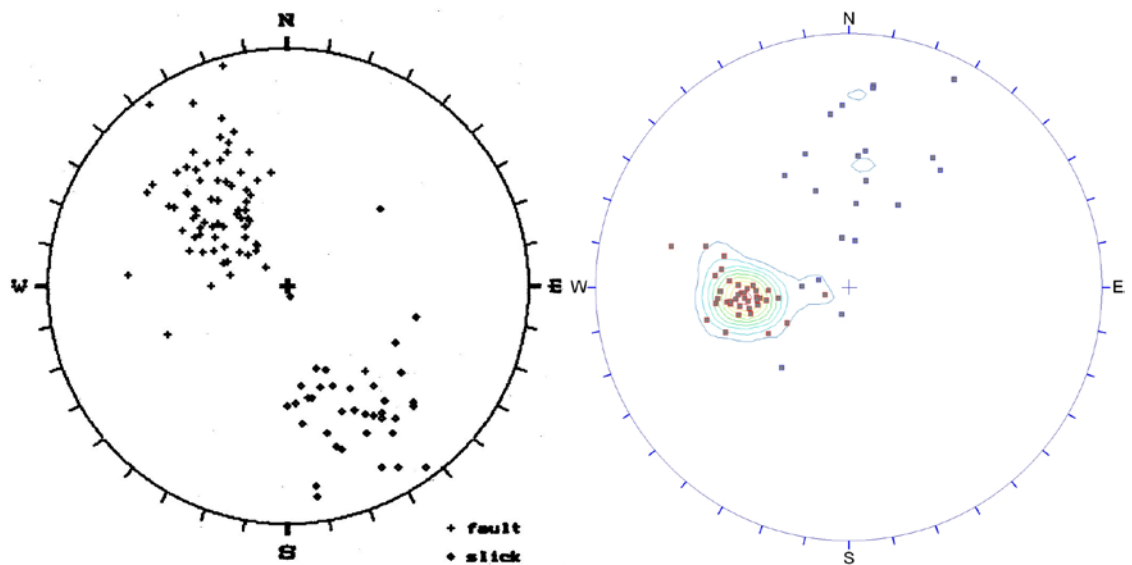


Figure 4-25. Stereonet showing fault poles and associated slickenline data for the Loe Bar Lodge to Gunwalloe coastal section (from Shail & Wilkinson, 1994) (left) and the equivalent photogrammetrically mapped data (right).

Hand-mapping of the location was undertaken by Shail & Wilkinson (1994) who produced a stereonet showing the faults they identified (Figure 4-25). It should be noted that the mapping exercises were undertaken 12 years apart. The majority of the features mapped remotely were bedding planes; to ascertain whether or not they had experienced movement across them was problematic unless closer, physical contact was possible. Additionally, it cannot be sure that the exact same features were mapped across both mapping exercises.

An estimation of the average fault dip/dip direction of the faults mapped by Shail & Wilkinson (1994) was made to be $46^{\circ}/140^{\circ}$. This produced a high pole vector difference of 36.12° from the remotely mapped orientation of $32^{\circ}/085^{\circ}$. The photogrammetrically derived orientation data shows that it can capture similar features as hand-mapping, although they do not match well. In comparison with the Gwithian analysis, where all the discontinuity data is assessed, only faults were identified and exported from the Gunwalloe photogrammetric models. The stereonets may indicate that faults were not present within the rock mass at that location (the hand-mapped data is taken from a larger stretch of coast). However, it does indicate the difficulty to distinguish between discontinuity types using photogrammetry. As noted in previous paragraphs, physical contact with the cliff would be advantageous as it would allow for the confirmation of the type of features mapped. The possible misidentification of geological features may be a reason for the large pole vector difference between the data sets.

4.4.2 Portreath Cliff

The geology at Portreath is similar to the geology seen at Gwithian as it is only seven miles NE along the coast, still situated within the Porthtowan Formation. Laser scanned point cloud data taken from the cliff at Portreath, Cornwall, UK (Figure 4-26, Figure 4-27 and Table 4-8) was used to assess the ability of laser scanning to capture geotechnical data from metamorphosed complexly fractured rock. A section of the cliff had been identified showing a potentially hazardous rock slope. Explosive charges were used to bring the most unstable section down leaving behind fresh competent rock from which geotechnical data could be mapped (Figure 4-28 and appendix DVD).

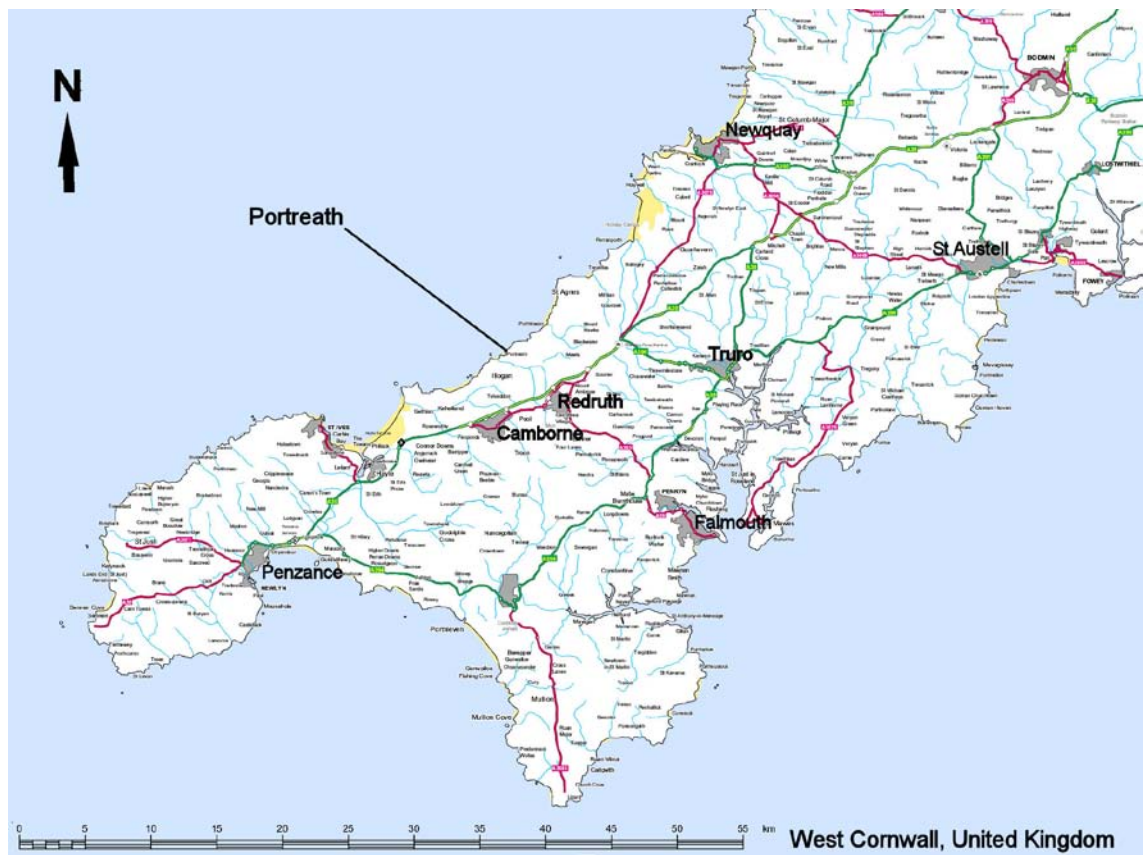


Figure 4-26. Map of West Cornwall, UK, showing location of Portreath. © Crown Copyright/database right 2009. An Ordnance Survey/EDINA supplied service.

Table 4-8. Locations of laser scanner setup positions at Portreath, Cornwall, UK, also indicating the scan density used.

GB National Grid (m)			Scanner	Model	Density
Eastings	Northings	Elevation			
165660	45653	1	Leica HDS3000	Laser 1	15 mm at 30 m distance

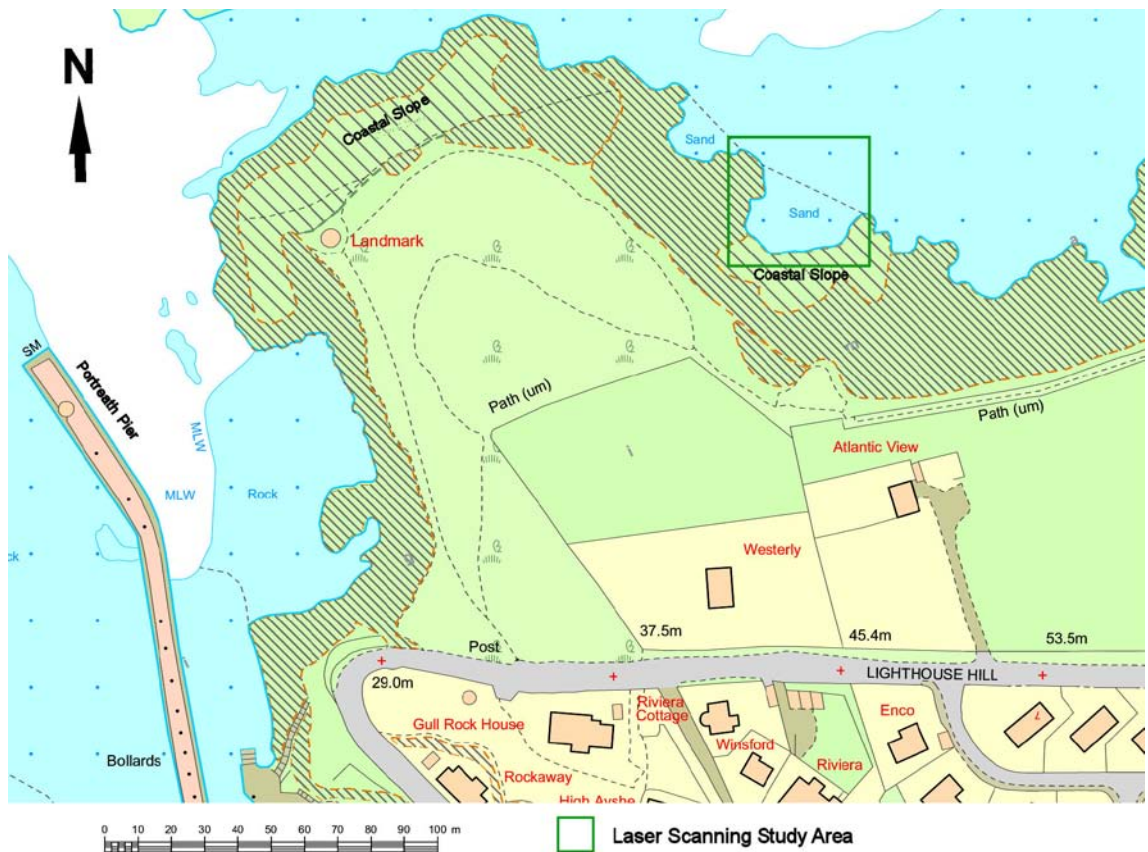


Figure 4-27. Map showing location of laser scanning study area at Portreath. © Crown Copyright/database right 2009. An Ordnance Survey/EDINA supplied service.

When the point cloud data was mapped within the SplitFX software program it was found that the scan density was not high enough to visualise most fracture planes sufficiently. Only the larger fracture planes were mapped, not providing adequate data to perform stereographic analysis of the failed mass. To complete a scan at a suitable density to visualise the smaller scaled fractures would have taken an excessive amount of time. Similar to photogrammetry, laser scanning struggles to resolve the small scale structures and should be used in conjunction with hand-mapping to sufficiently assess the rock mass characteristics of complex/highly fractured rocks. This result shows that the scan density must be high so to visualise the small features held within a highly fractured rock mass.

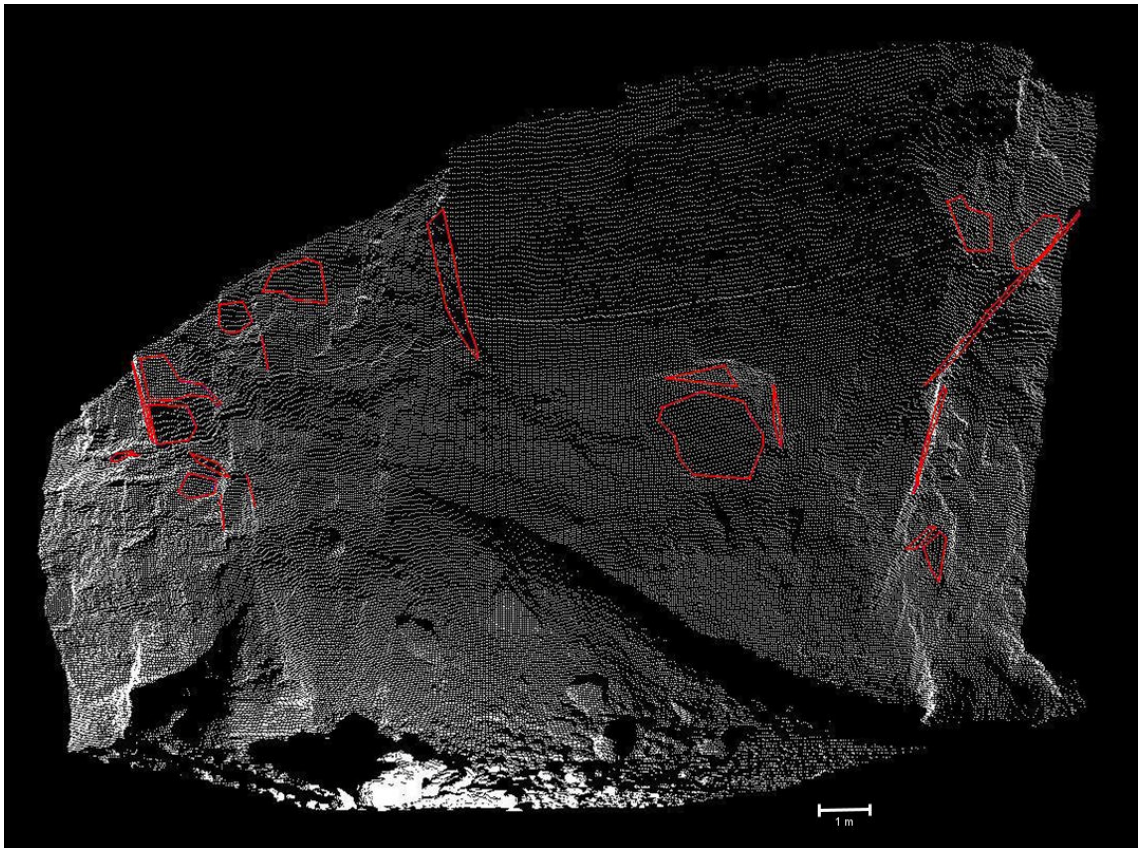


Figure 4-28. Point cloud image showing identified large scale discontinuities (highlighted red) at Portreath beach cliff (15 m height) and failure material. The laser scan data also has the potential to be used to calculate the volume of the failed mass.

4.4.3 Porthgwarra, Carn Marth Quarry and Theatre Quarry

Porthgwarra

The coastal cliffs at Porthgwarra cove, Cornwall, UK (Figure 4-29) are made up of Land's End Granite of approximately 272 Ma age (Selwood *et al.*, 1998). The rock is described as coarse grained, megacrystic granite, containing feldspar up to 80 mm in length. These localities were chosen to test the remote data capture systems in very blocky rock masses. The rocks contain highly persistent widely spaced planar discontinuities, and have an RQD of 100% (Figure 4-31). LeBoutillier (2003) cites Booth (1966) who identified three major joint sets existing throughout the Land's End Granite: NNW-SSE (330°) striking, ENE-WSW (070°) striking vertical sets, and a sub horizontal set.

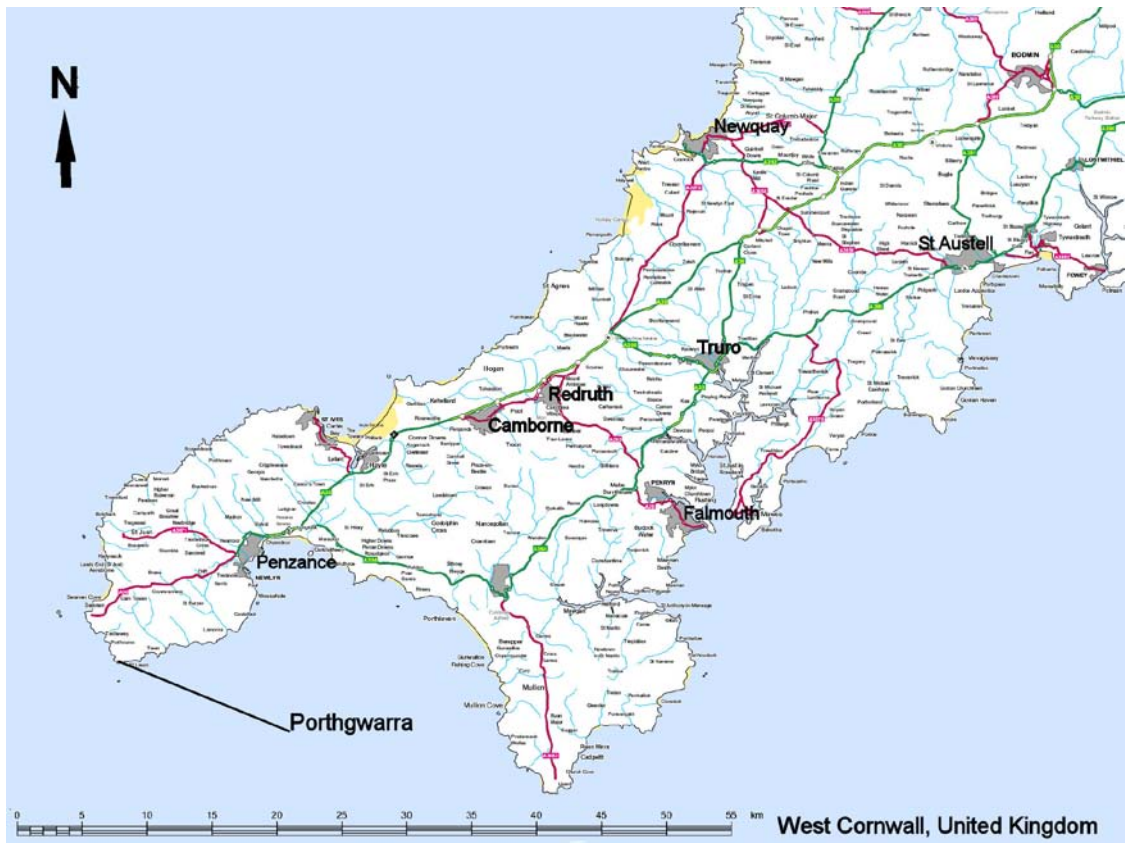


Figure 4-29. Map of West Cornwall, UK, showing location of Porthgwarra. © Crown Copyright/database right 2009. An Ordnance Survey/EDINA supplied service.

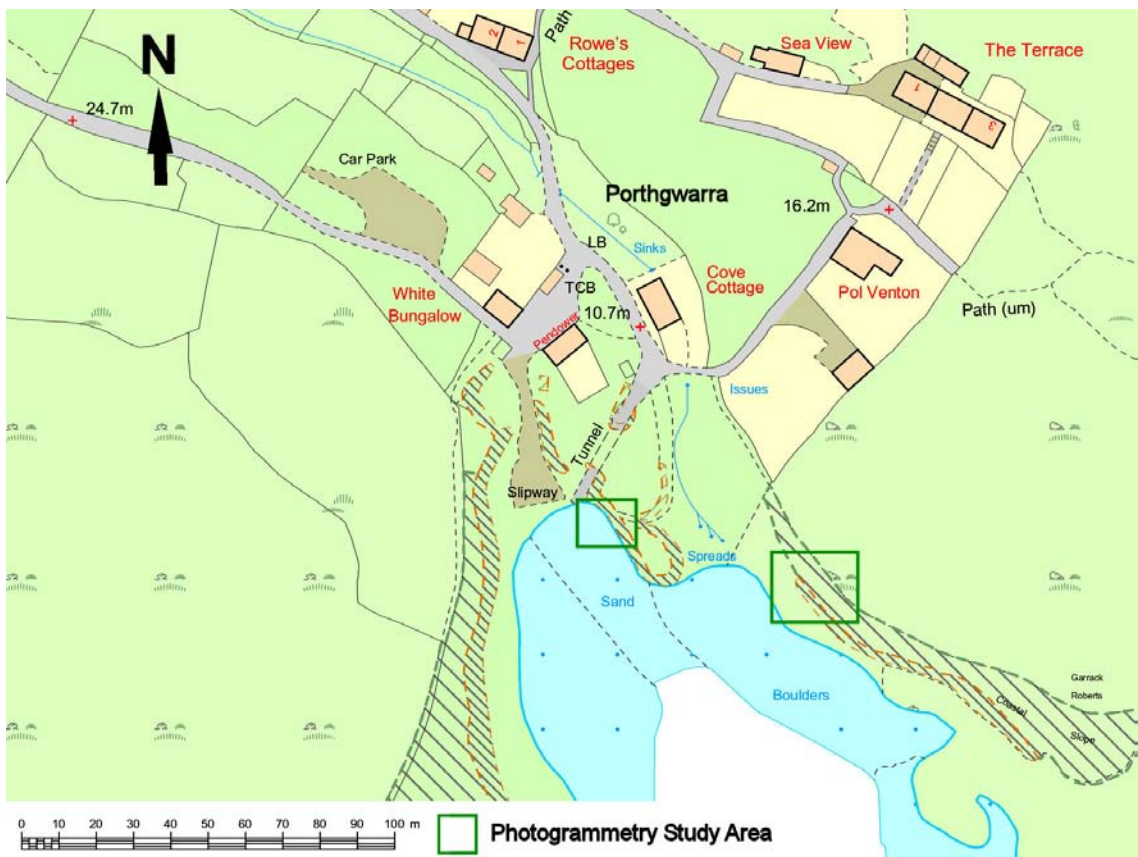


Figure 4-30. Map showing locations of photogrammetry study areas at Porthgwarra. © Crown Copyright/database right 2009. An Ordnance Survey/EDINA supplied service.

Table 4-9. Locations of photogrammetry camera and control point setups at Porthgwarra, Cornwall, UK, indicating model and lens used.

GB National Grid (m)			Camera / Control Point	Model	Lens
Eastings	Northings	Elevation			
137130	21699	2	Camera 1	Model 1 & 2	20 mm
137131.8	21695.17	1.756	Camera 2		
137156.6	21700.08	2.658	Control Point A		
137158.1	21689.77	3.967	Control Point B		
137178	21677	4	Camera 3	Model 3	50 mm
137178.8	21683.93	5.075	Camera 4		
137211.9	21683.42	5.901	Control Point C		

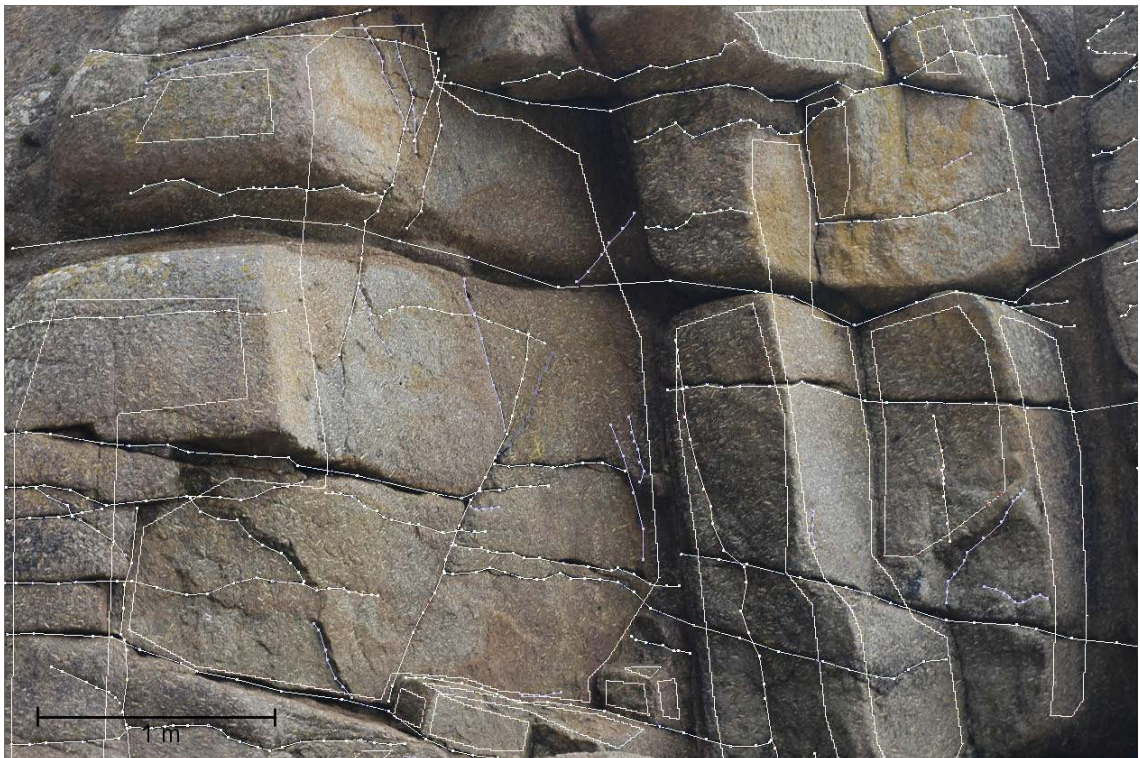


Figure 4-31. Photogrammetric orthoimage (striking E -W, 4 m high) showing discontinuity mapping at Porthgwarra Cliff, Cornwall, UK. Three roughly orthogonal discontinuity sets can be identified from the orthoimage.

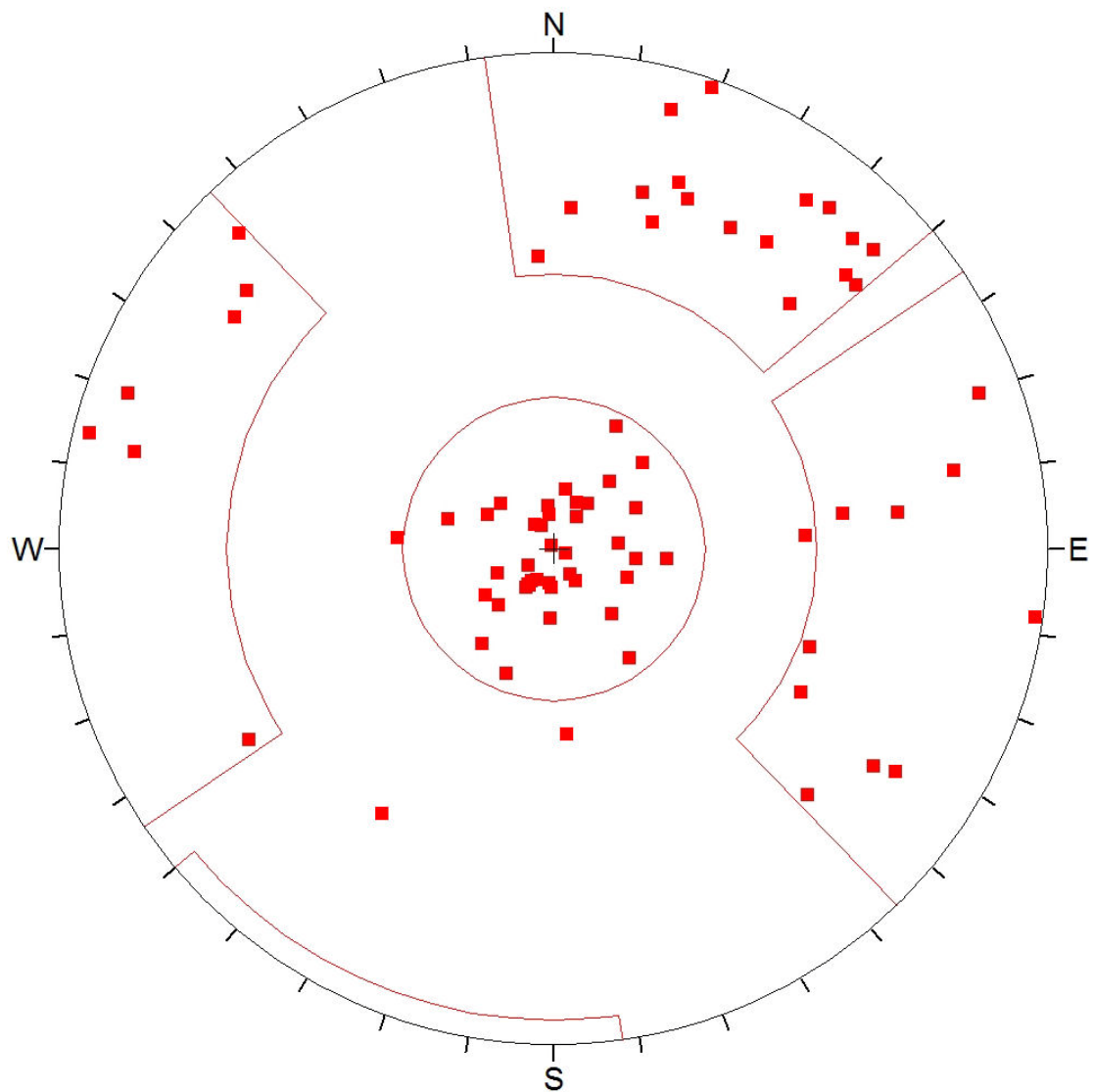


Figure 4-32. Lower hemisphere stereonet from orientation data collected from Porthgwarra photogrammetric model. The three roughly orthogonal discontinuity sets identified from the orthoimage can be seen (delineated in red). The N - S striking set fluctuates cross the vertical, and can be separated into easterly and westerly dipping sub-sets.

The cliffs at Land's End can be as high as 50 m indicating the stability of the constituent rock. Far fewer fractures were recorded within the granite than at Gwithian, Gunwalloe and the chalk at Brighton, when factoring in the respective areas covered by the remote mapping techniques. Three photogrammetric 3D images were made of the Porthgwarra cliffs (Figure 4-30, Table 4-9, and appendix DVD). The stereographic data from Figure 4-31 is shown in Figure 4-32. The stereonet shows that similarly orientated joint sets are recorded using photogrammetry as Booth (1966), although each set is rotated to the West $\sim 15^\circ$. The sub-horizontal set described by Booth (1966) is clearly identified by the remote mapping technique. Due to the blocky formation, fractures were primarily identified as planes, although the sub- horizontal features were recorded as discontinuity traces. The fracture intensity and orientation causes most of

the identified instabilities to be toppling failures at this location, with predominantly large block formation ($>1 \text{ m}^3$).

The blocky nature of the rock mass at Porthgwarra allowed for easy visual assessment of the discontinuity types and orientations. The large, planar represented features were easy to map and produced data comparable to the published data. The slight westerly rotation of the steeply dipping sets could be a result of the data being collected from one location and compared with a regional structural interpretation.

Carn Marth Quarry and Theatre Quarry

Carn Marth Quarry and Theatre Quarry (Figure 4-33) are situated within the Carmenellis Granite, which is older than the Land's End Granite at Porthgwarra at an age of $\sim 290 \text{ Ma}$ (Selwood *et al.*, 1998). The granite is medium grained with smaller phenocrysts ($\sim 5 \text{ mm}$) of feldspar than the rocks seen at Porthgwarra. The fracture intensity is slightly higher in the Carmenellis quarries, although the RQD still measured at 100%. It is a blocky rock mass, and the highly persistent, planar fractures form large blocks ($>1 \text{ m}^3$), which were exploited while the quarries were in production. Both laser scanned and photogrammetric 3D images were made at each quarry at varying locations (Table 4-10, Figure 4-34, Figure 4-35 and appendix DVD). Due to the blocky nature of the lithology, and the large areas of the subsequent features, mapping the laser scanned point cloud was more successful than mapping at Portreath, allowing for geotechnical analysis.

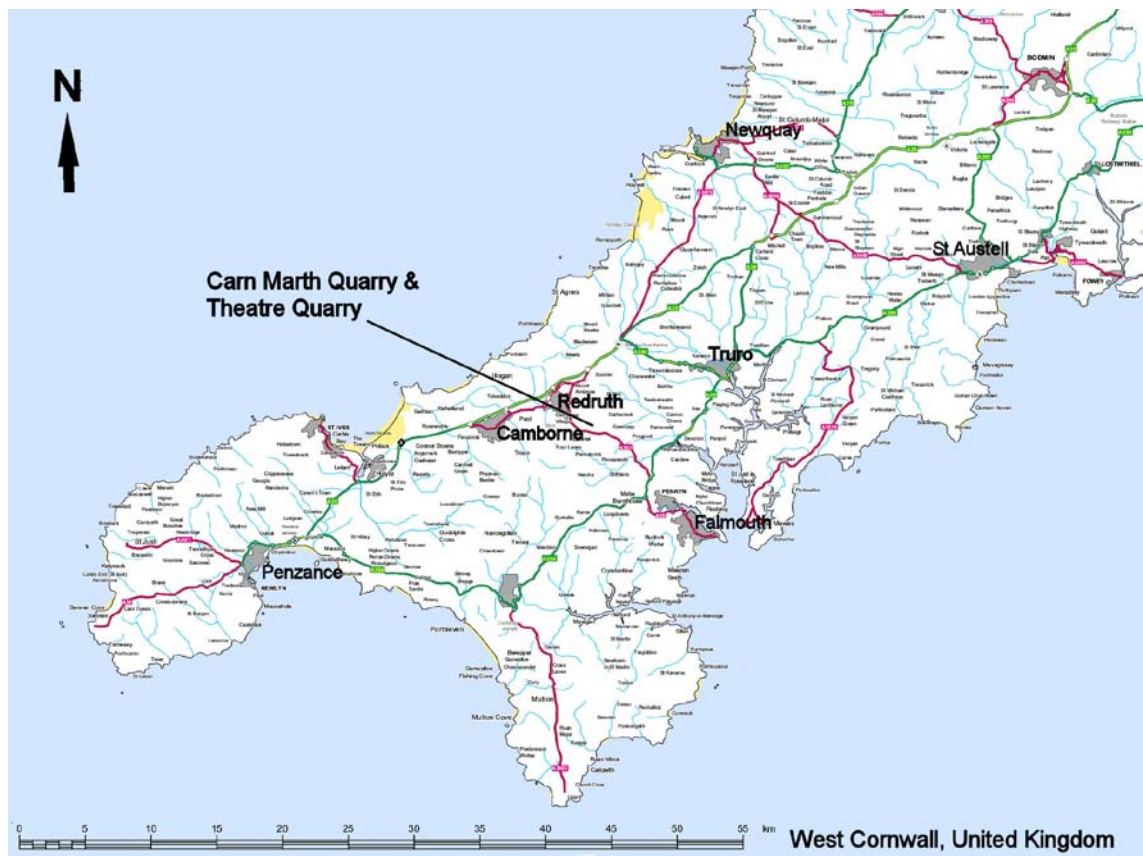


Figure 4-33. Map of West Cornwall, UK, showing location of Carn Marth Quarry and Theatre Quarry. © Crown Copyright/database right 2009. An Ordnance Survey/EDINA supplied service.

The same section was captured by a photogrammetric 3D image, whilst additional models and scans were also made at other locations. Hand-mapping was conducted in the areas of the quarries that were accessible. The results of the mapping are represented in Figure 4-36 which also shows the location of each of the mapped faces.

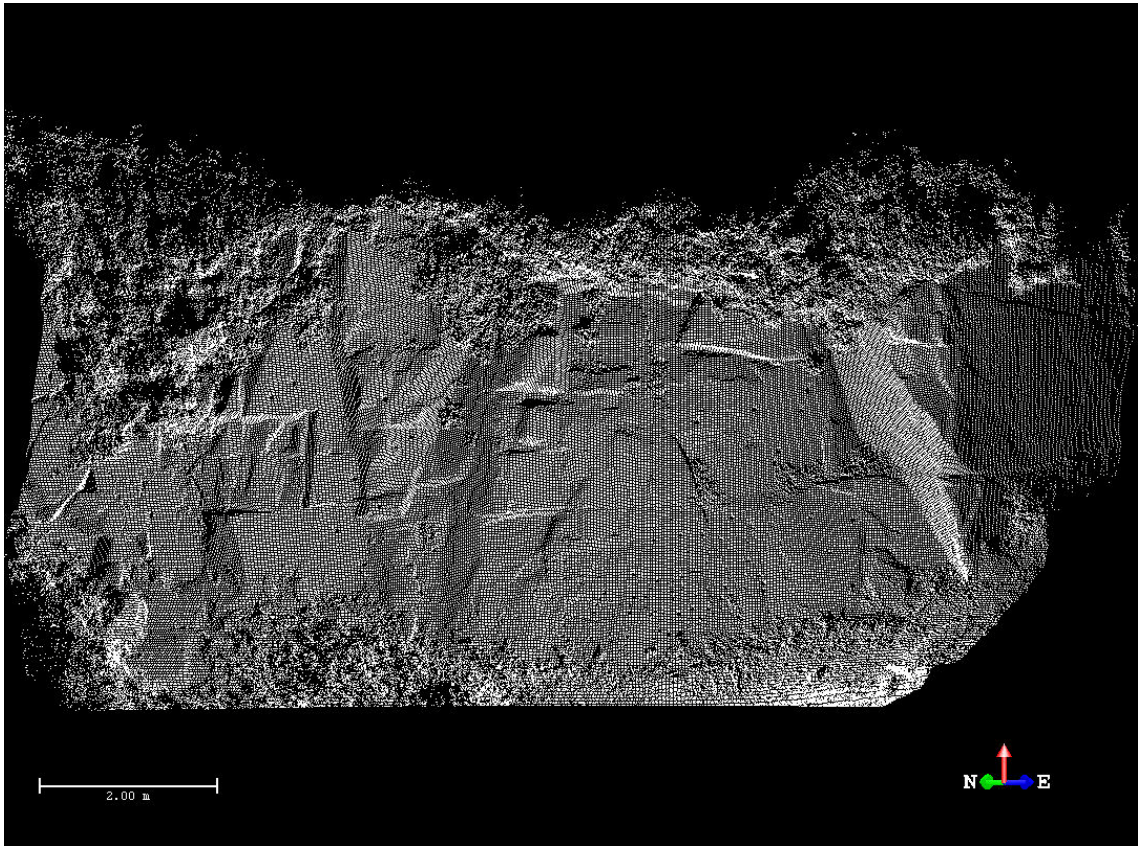


Figure 4-34. Laser scan point cloud showing rock face at Carn Marth Quarry, Cornwall, UK, (5 m high, looking north) The blocky nature of the rock mass displays the discontinuities clearly. Sub horizontal features can also be identified.

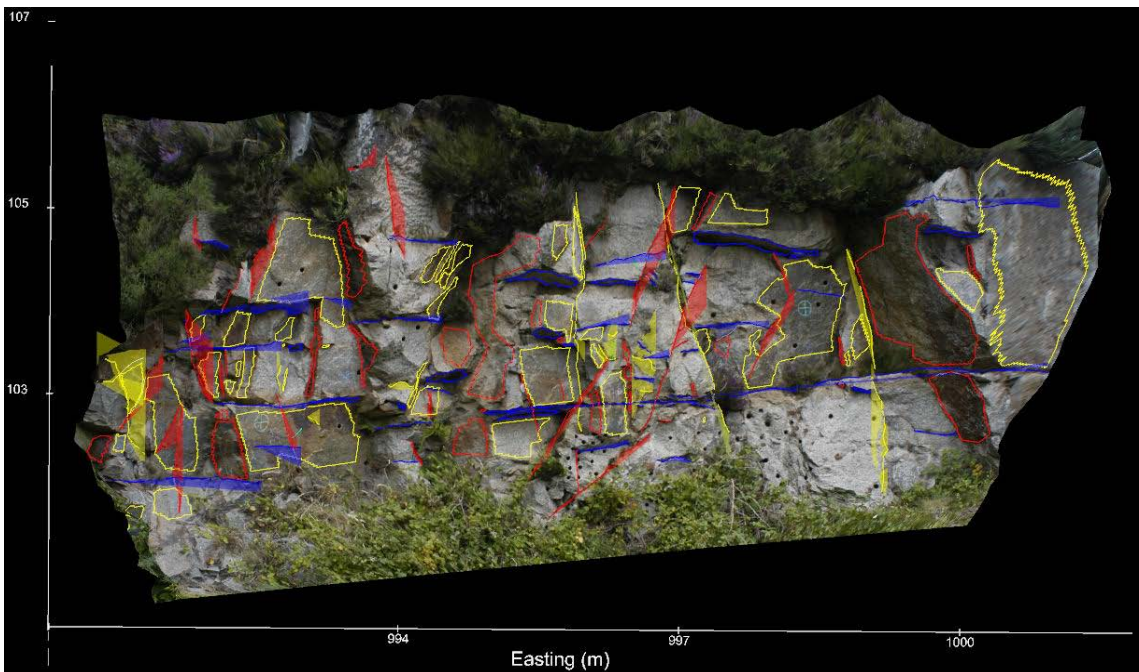


Figure 4-35. 3D image screen capture of mapped rock face at Carn Marth Quarry with colours indicating similarly orientated discontinuities (scale shown in images, looking north). Similarly to the laser scanned point cloud, discontinuities are easily identified from the 3D model.

Table 4-10. Locations of laser scanner setup positions, and photogrammetry camera and control point setups at Carn Marth Quarry and Theatre Quarry, Cornwall, UK, indicating model, lens and scan density used.

GB National Grid (m)			Camera / Control Point	Model	Lens
Eastings	Northings	Elevation			
171485	40942	205	Camera 1	Carn Marth - east facing	20 mm
171483.6	40937.05	205.087	Camera 2		
171506.2	40933.1	210.122	Control Point A		
171484	40951	207	Camera 3	Carn Marth - SE facing	50 mm
171481.3	40946.63	207.077	Camera 4		
171506.3	40933.92	214.56	Control Point B		
171484	40891	203	Camera 5	Carn Marth - south facing	50 mm
171480.1	40888.58	202.787	Camera 6		
171484.8	40865.06	212.507	Control Point C		
171445	40950	203	Camera 7	Carn Marth - north facing	20 mm
171442.5	40948.97	203.147	Camera 8		
171441.5	40958.86	205.538	Control Point D		
171470	40713	183	Camera 9	Theatre Quarry	50 mm
171471.9	40711.68	183.055	Camera 10		
171472.8	40728.8	186.517	Control Point E		

GB National Grid (m)			Laser Scanner Type	Model	Density
Eastings	Northings	Elevation			
171445	40950	203	Leica HDS3000	Carn Marth - north facing	10 mm at 15 m distance
171470	40713	183		Theatre Quarry	10 mm at 15 m distance

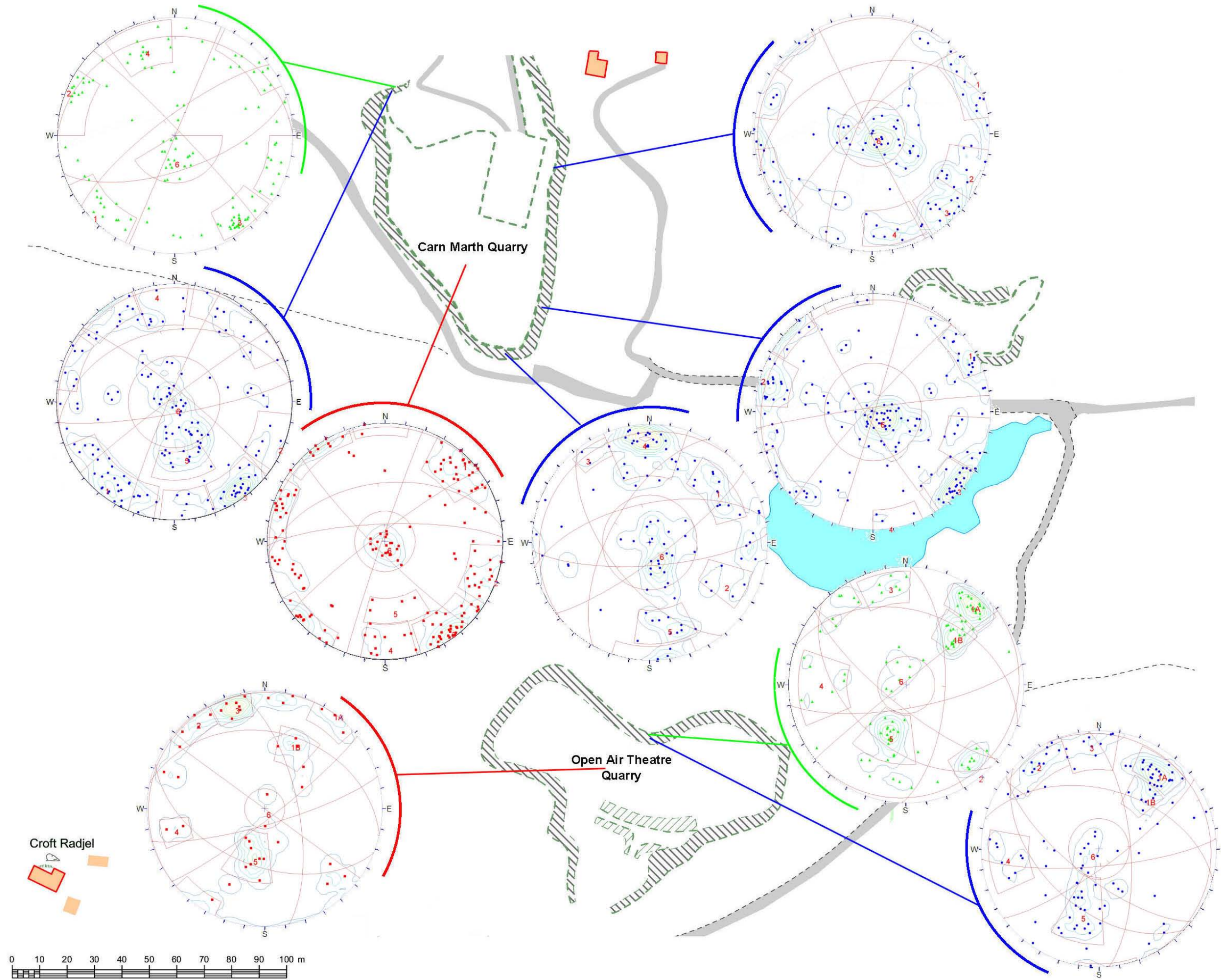


Figure 4-36. Map of Carn Marth and Theatre Quarries, stereonets representing each mapping type and location with set windows and major planes delineated in red. Photogrammetry = blue circles, laser scanning = green triangles and hand-mapping = red squares. © Crown Copyright/database right 2009. An Ordnance Survey/EDINA supplied service.

Table 4-11. Table showing the set analysis for each remote mapping model and hand-mapping. Six sets were identified across the two quarries. Set one from the Theatre Quarry was split into A and B (steeply and shallow dipping subdivisions).

Carn Marth Quarry												
Set	Laser Scanning		Hand-Mapping		Photogrammetry north facing		Photogrammetry SE facing		Photogrammetry east facing		Photogrammetry south facing	
	Dip	Dip Direction	Dip	Dip Direction	Dip	Dip Direction	Dip	Dip Direction	Dip	Dip Direction	Dip	Dip Direction
1	86°	046°	83°	225°	82°	039°	85°	238°	89°	243°	61°	232°
2	90°	113°	88°	289°	86°	293°	89°	107°	79°	293°	62°	299°
3	77°	323°	84°	323°	87°	323°	86°	312°	78°	316°	79°	143°
4	66°	161°	78°	358°	82°	170°	87°	352°	73°	348°	74°	176°
5	-	-	49°	353°	39°	349°	-	-	-	-	63°	348°
6	17°	360°	04°	333°	04°	339°	08°	318°	04°	307°	10°	316°

Theatre Quarry						
Set	Laser Scanning		Hand-Mapping		Photogrammetry	
	Dip	Dip Direction	Dip	Dip Direction	Dip	Dip Direction
1A	76°	219°	90°	216°	70°	218°
1B	48°	224°	50°	202°	49°	223°
2	88°	321°	83°	142°	78°	144°
3	74°	170°	79°	164°	78°	175°
4	63°	92°	67°	78°	68°	085°
5	37°	19°	35°	13°	48°	015°
6	07°	136°	02°	315°	06°	064°

Allowed by the blocky nature of the rock mass, the majority of the discontinuities were captured as planar features, which suited both remote data capture geotechnical analyses. The resulting stereonet comparisons and set analysis (Table 4-11) show similar orientations were collected by each mapping system. Set 5, striking WNW – ESE, was identified in the Theatre Quarry by all three mapping techniques, but it was not seen clearly in the data from Carn Marth Quarry. The eastern and SE photogrammetric models and laser scanning did not identify set 5. This could be due to the orientation of the rock faces causing them not to express that particular set, or that they were not present at all. Laser scanning of the northern facing slope at Carn Marth Quarry did not pick up set 5 that was seen when using hand-mapping and photogrammetry at the same location, this was due to the discontinuities representing themselves on the face as traces.

The laser scanned and photogrammetrically derived data from the northern side of Carn Marth Quarry has been analysed using pole vector difference calculations as the data was collected from the same location making it the most comparable (Figure 4-36). The sets identified from the laser scanning data had a low average pole vector difference of 14.54° from the hand-mapped data, with a standard deviation of 14.1°. Set 4 had the highest PVD (39.65°). Although both mapping techniques identified an ENE – WSW striking set, laser scanning showed it dipping to the south, where hand-mapping indicated it was dipping to the north, producing the high PVD. Set 4 also produced the greatest PVD between photogrammetry and hand-mapping for the same reason, 21.52°. The pole vector difference between photogrammetrically identified sets

and hand-mapping produced the lowest average, 9.32°, mainly due to very low error (0.42°) for sub-horizontal set 6, whilst the standard deviation was 8.2°. The average set PVD between photogrammetry and laser scanning was 10.71°, but with the lowest standard deviation, 5.4°.

Table 4-12. Pole vector difference analysis on data collected from northern section of Carn Marth Quarry.

SET	Laser Scanning		Hand-Mapping		PVD
	Dip	Dip Direction	Dip	Dip Direction	
1	86	46	83	225	11.05
2	90	113	88	289	4.47
3	77	323	84	323	7.00
4	66	161	78	358	39.65
5	-	-	49	353	-
6	17	360	4	333	13.55

SET	Laser Scanning		Photogrammetry		PVD
	Dip	Dip Direction	Dip	Dip Direction	
1	86	46	82	39	8.03
2	90	113	86	293	4.00
3	77	323	87	323	10.00
4	66	161	82	170	18.17
5	-	-	39	349	-
6	17	360	4	339	13.34

SET	Photogrammetry		Hand-Mapping		PVD
	Dip	Dip Direction	Dip	Dip Direction	
1	82	39	83	225	16.15
2	86	293	88	289	4.47
3	87	323	84	323	3.00
4	82	170	78	358	21.52
5	39	349	49	353	10.37
6	4	339	4	333	0.42

Reasonably low set analysis pole vector differences and standard deviations from these study locations (when compared to the hand-mapping vs. hand-mapping at Penlee Quarry) have shown that remote data capture systems can effectively collect data from blocky rock masses. However, a single remote data capture model or scan did not identify all the discontinuity sets present within the two quarries. This highlights the need for multiple remote data capture setup positions to collect data from various views of the rock mass.

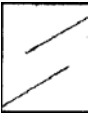
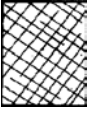




4.4.4 Portobello Cliffs

The geology and fracture intensity of the chalk cliffs at Portobello have been covered in Section 4.3. This locality was chosen to assess the remote mapping systems capacity for collecting data from a range of fracture intensities, small, medium and large scale. Photogrammetric image creation and subsequent geotechnical mapping was successful, capturing hundreds of data points. Laser scanning was less successful as most discontinuities were represented within the rock mass as discontinuity traces which are hard to visualise using 3D point clouds (covered in Section 0.0.0). Larger, planar features were easily mapped using the SplitFX software.

4.4.5 Assessment of Remote Data Capture to Collect Data from Varying Rock Types/Structures

The previous sections have tested the ability of laser scanning and photogrammetry to collect data from varying rock type and fracture intensities. Table 4-13 uses the descriptions of the Geological Strength Index rock structure (Marinos & Hoek, 2000) to provide a basis for summary comments on the ability of each mapping technique to capture suitable data within normal field conditions and post-processing times.

Table 4-13. Assessment of remote data capture systems to collect data from varying rock structures (modified from Marinos & Hoek, 2000).

Structure	Laser Scanning	Photogrammetry	Test Site(s)
 <p>Intact or Massive - intact rock specimens or massive <i>in situ</i> rock with few widely spaced discontinuities</p>	Collection of orientation, roughness, and spacing data possible	Collection of orientation (from planes), roughness, trace length and spacing data possible	Porthgwarra, Cornwall, UK
 <p>Blocky - well interlocked undisturbed rock mass consisting of cubical blocks formed by three intersection discontinuity sets</p>	Collection of orientation, roughness, and spacing data possible	Collection of orientation (from planes), roughness, trace length and spacing data possible	Carn Marth Quarry & Tremough Driveway, Cornwall, UK
 <p>Very Blocky - interlocked, partially disturbed mass with multi-faceted angular blocks formed by 4 or more joint sets</p>	Collection of orientation, roughness, and spacing data possible	Collection of orientation (from planes), roughness, trace length and spacing data possible	Penlee Quarry, Cornwall, & Portobello, Brighton, UK
 <p>Blocky/Disturbed/Seamy - Folded with angular blocks formed by many intersecting discontinuity sets. Persistence or bedding planes or schistosity</p>	Collection of planar data difficult. Increased scan density required	Collection of data from planar structures difficult (orientation & roughness). Orientation data can be collected from traces	Godrevy & Gunwalloe, Cornwall, UK & Dielette, northern France.
 <p>Disintegrated - poorly interlocked, heavily broken rock mass with mixture of angular and rounded rock pieces</p>	Little geotechnical data collection possible. Increased scan density required. Can be used for volume measurement	Collection of data from planar structures difficult (orientation & roughness). Higher focal length must be used. Trace length collection possible	Blackpool Pit Imerys, Cornwall, UK
 <p>Laminated/Sheared - lack of blockiness due to close spacing or weak schistosity or shear planes</p>	No geotechnical data collection possible. Increased scan density required. Can be used for volume measurement	No data collection from planar structures. Higher focal length must be used. Trace length collection difficult but possible	-

Decreasing interlocking of rock pieces

4.5 Baseline to Face Ratio Analysis

Testing the relationship between accuracy and baseline ratio was conducted at Penlee Quarry, Newlyn, Cornwall, UK (Figure 4-37 and Figure 4-38). The lithology is composed of a metadiorite, contact metamorphosed by the intruded Cornubian Batholith (Parker, 2004). Some sections have a high fracture frequency and contain many fracture sets; Parker (2004) identified five sets, although there is evidence that an additional 2 – 3 fracture sets exist in differing areas of the quarry. Due to the complexity and intensity of the fracturing many features could be assessed over a small area. This reduced the time taken to complete hand-mapping, also allowing for the analysis of discontinuities with varying orientations. Hand-mapping was conducted on 50 accessible discontinuity features, recording their dip and dip directions.

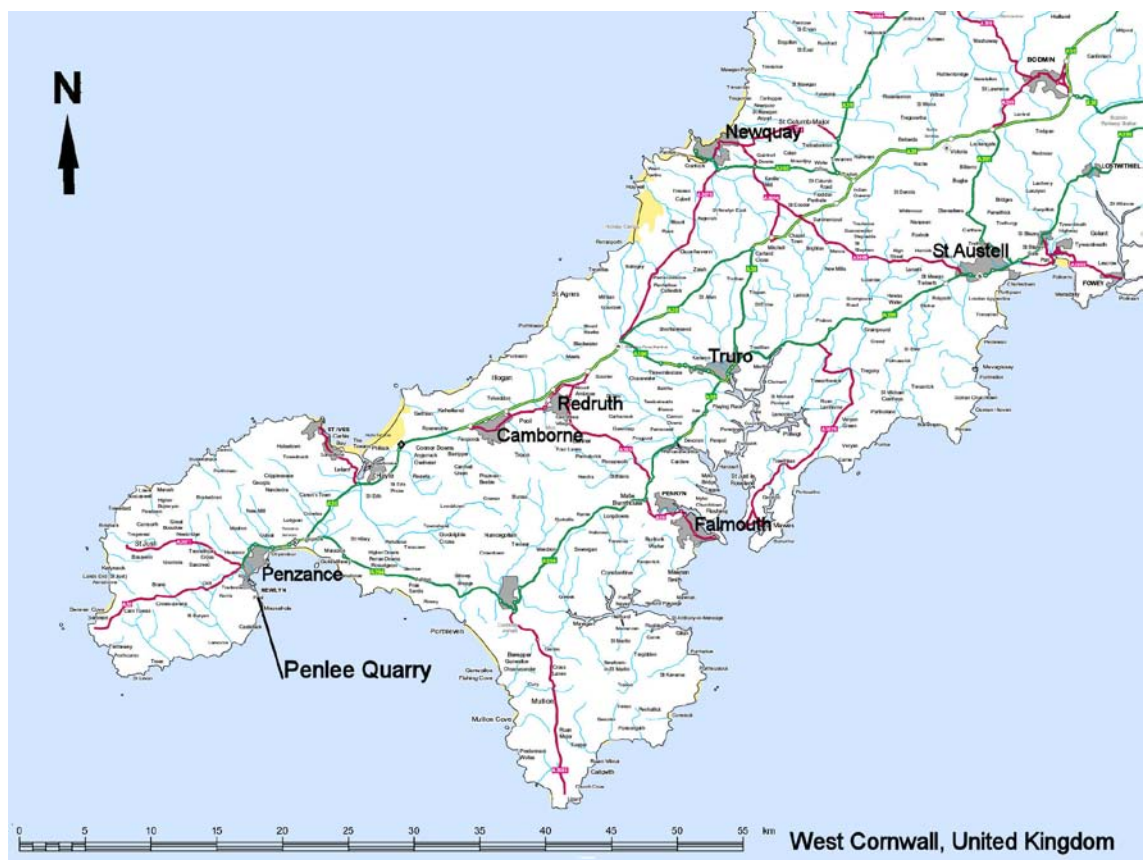


Figure 4-37. Map of West Cornwall, UK, showing location of Penlee Quarry. © Crown Copyright/database right 2009. An Ordnance Survey/EDINA supplied service.

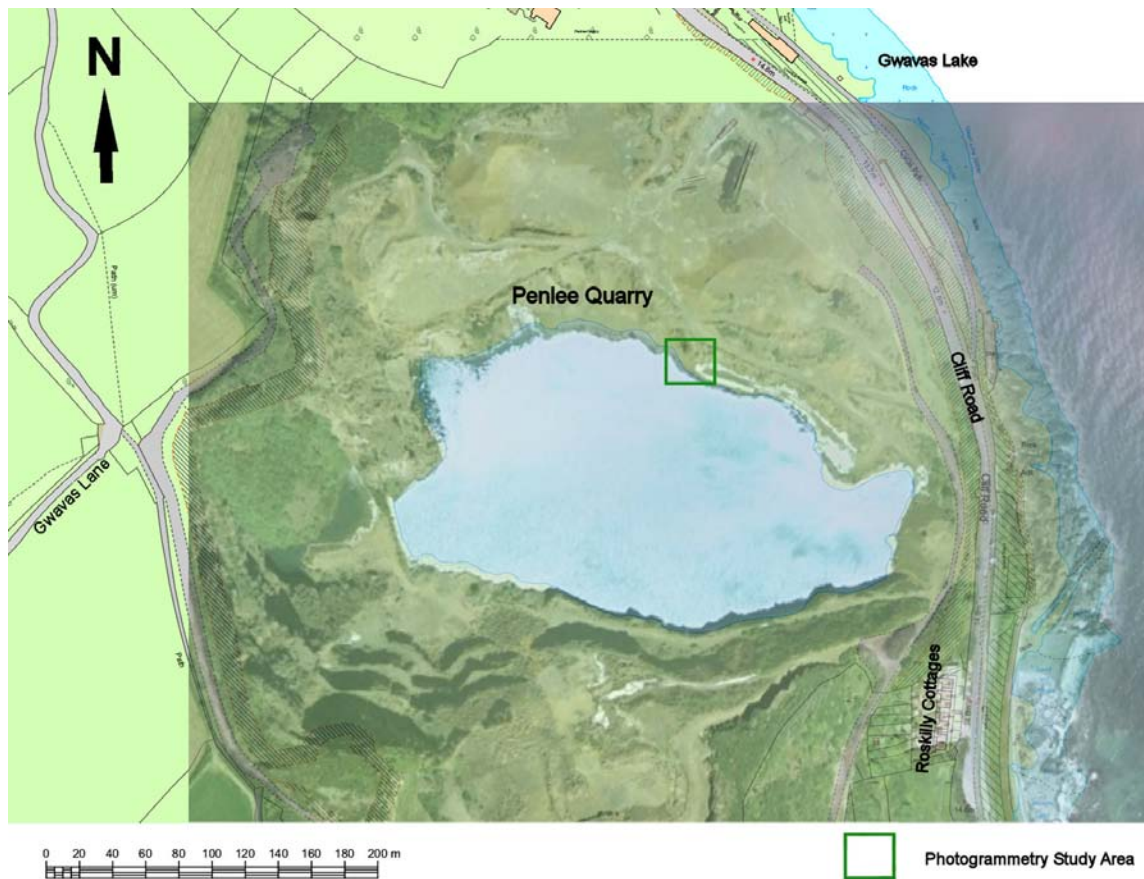


Figure 4-38. Map showing locations of photogrammetry study area at Penlee Quarry with photographic overlay for detail. © Crown Copyright/database right 2009. An Ordnance Survey/EDINA supplied service. © 2009 Google, Map Data © 2009 Tele Atlas, © 2009 Getmapping plc.

The Sirovision manual recommends that the separation between the two cameras should be between $\frac{1}{6}$ and $\frac{1}{8}$ of the distance between the camera baseline and the face. The photogrammetric equipment was setup 8.5 m away and perpendicular to the hand-mapped rock face (Figure 4-39). The first camera baseline ratio used was $\frac{1}{6}$ of the distance to the face, making the camera separation 1.41 m apart. A 20 mm lens was used to capture the data from the same area that was hand-mapped. Subsequent photogrammetric equipment setups were tested and are represented in Figure 4-39 and Table 4-14.

Table 4-14. Locations of photogrammetry camera and control point setups at Porthgwarra, Cornwall, UK, indicating camera separation, baseline ratio and lens used.

GB National Grid (m)			Camera / Control Point	Camera Separation (m)	Ratio	Lens
Eastings	Northings	Elevation				
146748	27881	3.5	Control Point	-		20 mm
146741.6	27874.99	3.754	Camera 1	4	1/2.125	
146744.9	27872.67	3.475	Camera 2			
146742	27874.66	3.455	Camera 3	3	1/2.8	
146744.5	27872.98	3.434	Camera 4			
146742.4	27874.37	3.433	Camera 5	2	1/4.25	
146744.1	27873.27	3.442	Camera 6			
146742.6	27874.23	3.417	Camera 7	1.4	1/6	
146743.8	27873.41	3.421	Camera 8			
146742.9	27874.07	3.444	Camera 9	0.94	1/9	
146743.7	27873.55	3.456	Camera 10			

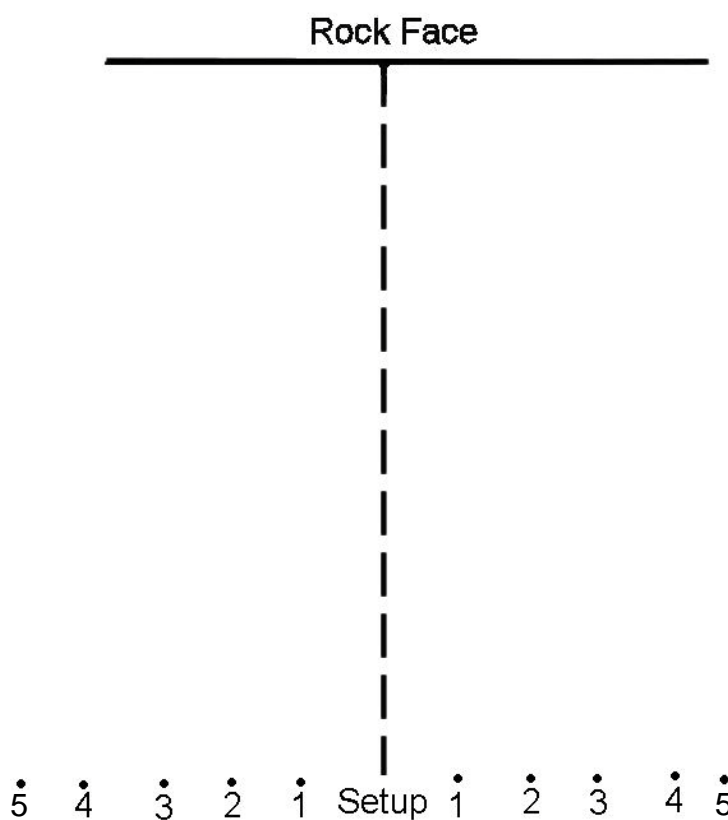


Figure 4-39. Schematic diagram showing the set up method used to test baseline to face ratio setup variations.

Photogrammetric 3D images were made from each of the setup locations (appendix DVD). The same features mapped by hand were delineated within the geotechnical module of the Sirovision software, as either discontinuity traces or planes, depending on the available view. Some of the 3D images were unable to map all the fractures identified by hand-mapping as they existed outside the view of the images. The dip and dip direction from hand-mapping and from each of the setups of the remote mapping systems were compared resulting in a pole vector difference for each feature (Table 4-15).

Table 4-15. Example table showing pole vector differences (PVD) between hand-mapping and photogrammetric mapping with varying baseline ratios.

Classification of Discontinuity	PVD at Differing Baseline Ratios				
	1/2.125	1/2.8	1/4.25	1/6	1/9
Trace	36.96	4.24	2.52	3.54	4.80
Plane	25.32	28.88	22.14	14.41	14.88
Trace	76.84	13.91	18.52	8.69	8.84
Plane	72.24	15.94	12.41	14.28	17.24
Plane	12.23	13.20	6.37	4.90	6.76
Plane	10.30	10.40	8.32	9.74	9.83

An average pole vector difference was taken for each setup with differing base line to face ratios and plotted (as a graph along with the standard deviation error bars) shown in Figure 4-40. The graph shows that the camera baseline to face ratio affects the accuracy of the captured data. The standard deviation follows the same trend, but seems to be more affected by the baseline to face ratio than the accuracy. When the ratio increases above 0.36 then the PVD increases to above the 13.75° PVD value found between hand-mapping at Penlee Quarry. To ensure the PVD remains below 10° and to increase the precision the camera baseline to face ratio should be between 0.166 and 0.25. The graph shows that any ratio below 0.111 will have a high likelihood of a medium/high PVD. As the camera separation becomes smaller the cameras begin to see a very similar view of the face as one another, thus causing problems in the ability for the computer algorithm to reproduce an image in three dimensions. A similar problem arises when the cameras become too separated as the photogrammetric algorithm is unable to efficiently match the pixels between the photographs because the photographs are too dissimilar. This results in the collection of erroneous orientation data.

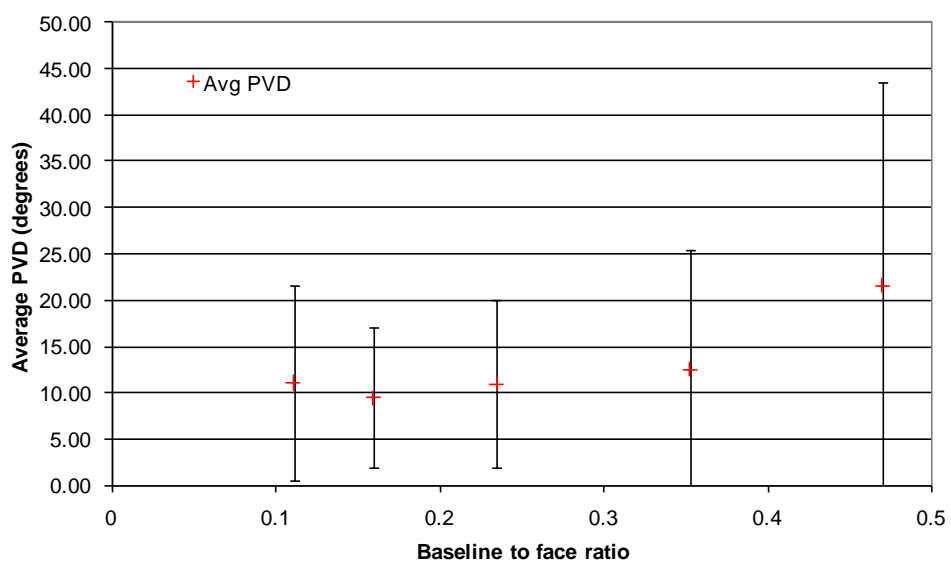


Figure 4-40. Graph showing the average pole vector difference and standard deviation of each photogrammetric setup baseline ratio.

4.6 Baseline Orientation to Face Analysis

Testing the baseline orientation to the face for photogrammetric accuracy against hand-mapping was also conducted at Penlee Quarry, Newlyn, UK (Figure 4-37 and Figure 4-38). The same 50 features that were previously hand-mapped were used as the basis for the analysis. The effect of baseline orientation was tested by moving the photogrammetric baseline obliquely to the face in 15° intervals (Figure 4-41 and Table 4-16).

Table 4-16. Locations of photogrammetry camera and control point setups at Porthgwarra, Cornwall, UK, indicating camera separation, baseline orientation to face and lens used.

GB National Grid (m)			Camera / Control Point	Orientation to Face (°)	Lens
Eastings	Northings	Elevation			
146748	27881	3.5	Control Point		20 mm
146746.3	27873.02	3.373	Camera 1	90	
146747.6	27872.2	3.377	Camera 2		
146746.5	27872.62	3.478	Camera 3	75	
146747.9	27872.43	3.478	Camera 4		
146748.3	27872.29	3.442	Camera 5	60	
146749.7	27872.38	3.439	Camera 6		
146749.9	27872.4	3.444	Camera 7	45	
146751.1	27873.01	3.356	Camera 8		
146751.5	27873.16	3.393	Camera 9	30	
146752.7	27873.86	3.316	Camera 10		
146752.7	27873.89	3.324	Camera 11	15	
146753.8	27874.7	3.275	Camera 12		

The distance from the face was kept at 8.5 m and using a baseline ratio of $\frac{1}{6}$, the cameras were separated by 1.41 m. Photogrammetric images were created for each set up location which were then mapped to identify the same 50 hand-mapped discontinuity features (appendix DVD). Similarly to the baseline ratio method, some of the 3D images were unable to map all the fractures identified by hand-mapping as they existed outside the view of the images. Pole vector differences were calculated for each mapped feature and overall averages were taken for each setup angle as shown in Figure 4-42.

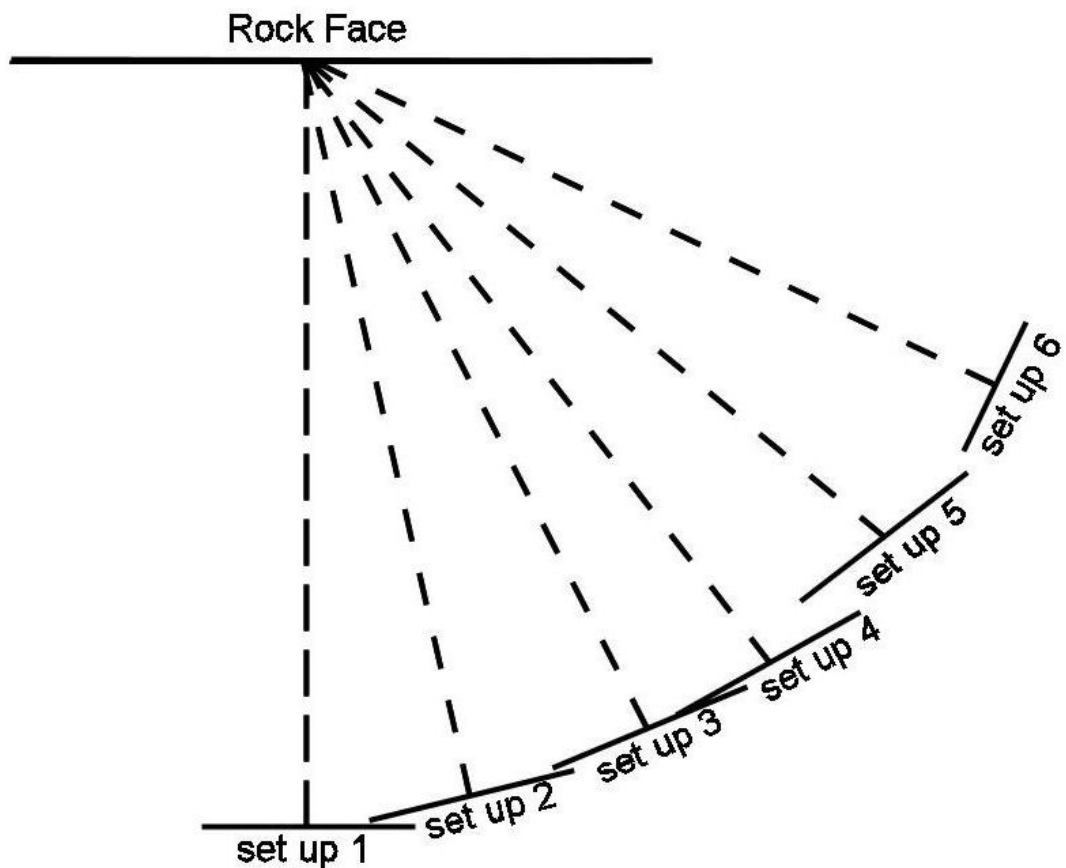


Figure 4-41. Schematic diagram showing the set up method used to test baseline to face angle variations.

The graph indicates that the optimum position for a photogrammetric setup, as expected, is perpendicular to the face. The pole vector difference and the standard deviation increase progressively as the cameras are moved more obliquely to the rock face. It would be expected that as the camera set-up becomes more oblique to the face the view becomes influenced by perspective. This distorts the three dimensional image created, thus producing poor orientation data. It shows that accuracy and precision are more sensitive to baseline to face angle than baseline to face ratio. The error from hand-mapping quickly increases to $\sim 14^\circ$ with just a 15° reduction of angle to the face, where above that, it reaches unacceptable medium PVDs of $20^\circ/25^\circ$ for comprehensive rock mass mapping. However, under certain circumstances, the larger errors may be acceptable for broad rock mass characterisation purposes, where accessibility dictates oblique setups (e.g. poor access to cliff or slope).

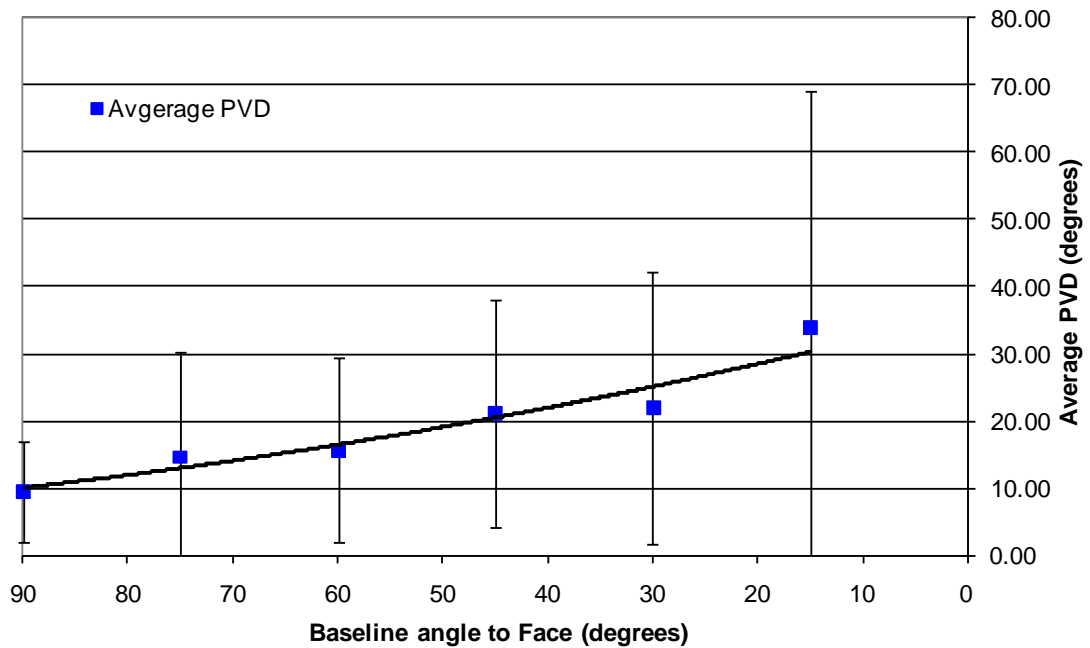


Figure 4-42. Graph showing the average pole vector difference and standard deviation of each photogrammetric setup with varying baseline to face angle (linear best fit line applied).

4.7 Distance to Face Analysis

Testing the ability of the remote data capture systems to capture 3D images for geotechnical applications at large equipment setup distances from the face was completed at two locations: laser scanning was tested at Blackpool Pit - Imerys using the HDS3000, and photogrammetry at Delabole Quarry (appendix DVD). These locations allowed for sufficient maximum distances from the rock face without obstruction or access problems. To test minimum distances, photogrammetry and laser scanning have been used underground at the Camborne School of Mines' Test Mine. The average widths of most of the drives within the mine are 3 m, forcing equipment setups to be relatively close to the study face.

4.7.1 Imerys – Blackpool Pit

Blackpool pit is a working china clay quarry (as of 2006) run by Imerys Minerals Ltd (Figure 4-43). China clay is quarried from the heavily weathered St Austell granite, where only large scale structures remain. Some areas of the pit are less weathered than others exhibiting discontinuity features that can be mapped, although many are inaccessible for hand-mapping.

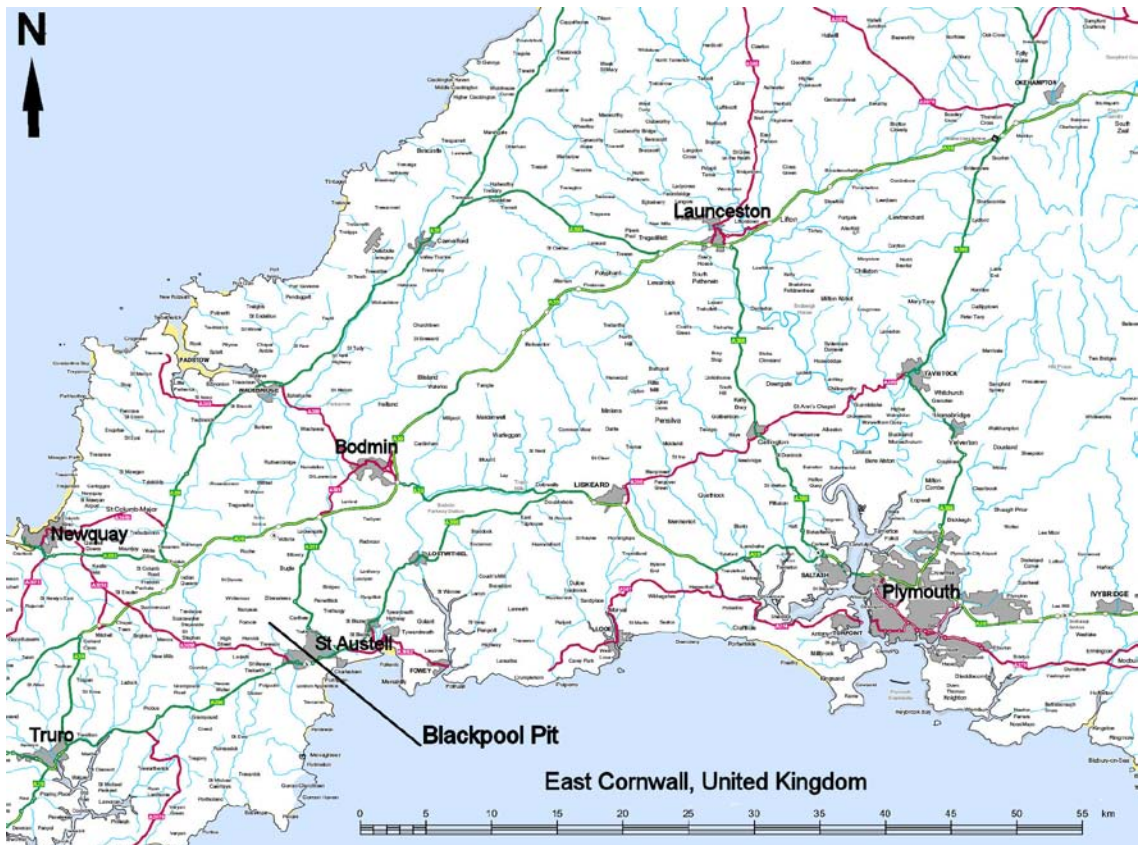


Figure 4-43. Map of East Cornwall, UK, showing location of Blackpool Pit - Imerys. © Crown Copyright/database right 2009. An Ordnance Survey/EDINA supplied service.

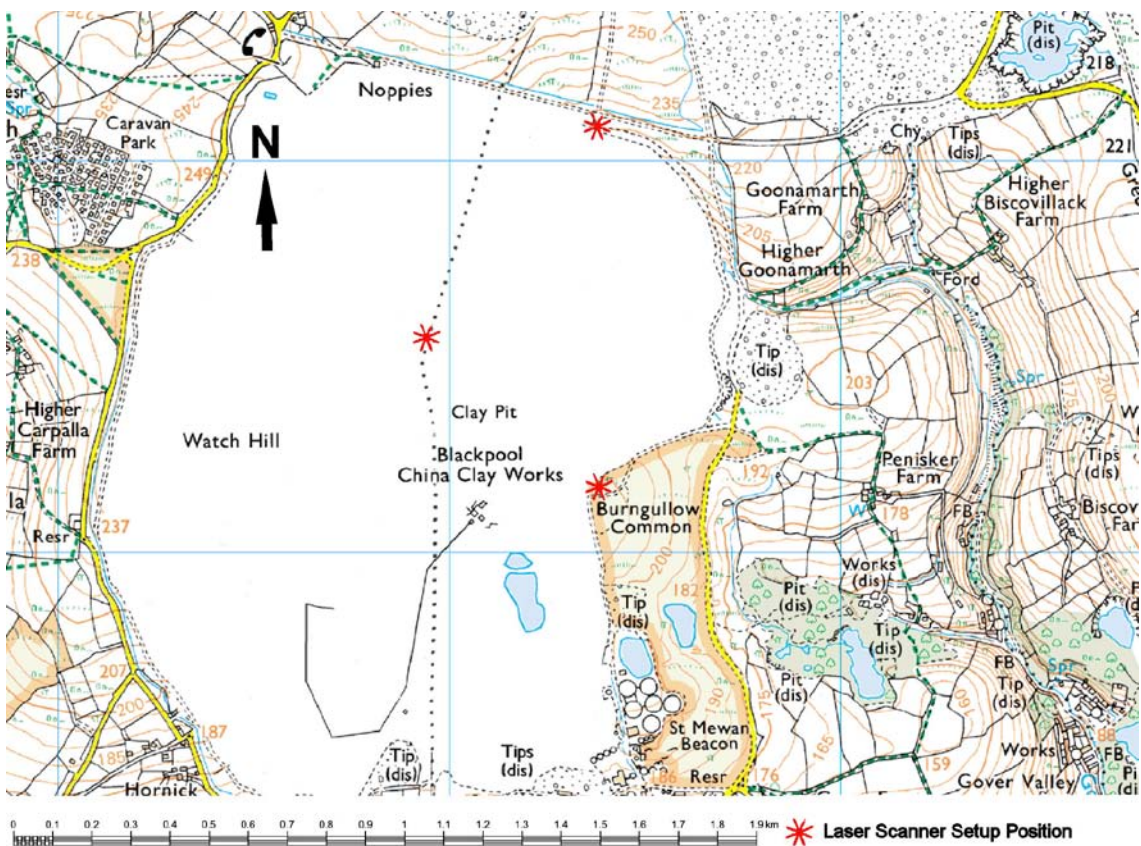


Figure 4-44. Map showing locations of laser scanner setup positions at Blackpool Pit. © Crown Copyright/database right 2009. An Ordnance Survey/EDINA supplied service.

Table 4-17. Locations of laser scanner setup positions at Blackpool Pit - Imerys, Cornwall, UK, also indicating the scan density used.

GB National Grid (m)			Laser Scanner Type	Model	Density
Eastings	Northings	Elevation			
198375	54161	176	Leica HDS3000	Laser 1	50 mm at 100 m distance
197919	54501	184		Laser 2	
198390	55087	157		Laser 3	

Three laser scans were conducted (A. Wetherelt, Camborne School of Mines) within the pit over a four hour time period using the HDS3000, each of which were at a maximum of 200 m from the pit face (Figure 4-44 and Table 4-17). The laser scanner was able to receive the return signal from the transmitted laser beam from the maximum distance. This was to be expected as the material has a high reflectance due to its light colour. The density was set to 50 mm at 100 m distance; however the true density was less as the distance ranged up to 200 m. The spot size of the laser also increased relative to the distance to the face (24 mm at 200 m), causing ‘noise’ within the resulting point cloud. The completed point clouds were filtered for excessive noise and meshed to form 3D models of Blackpool Pit (Figure 4-45).

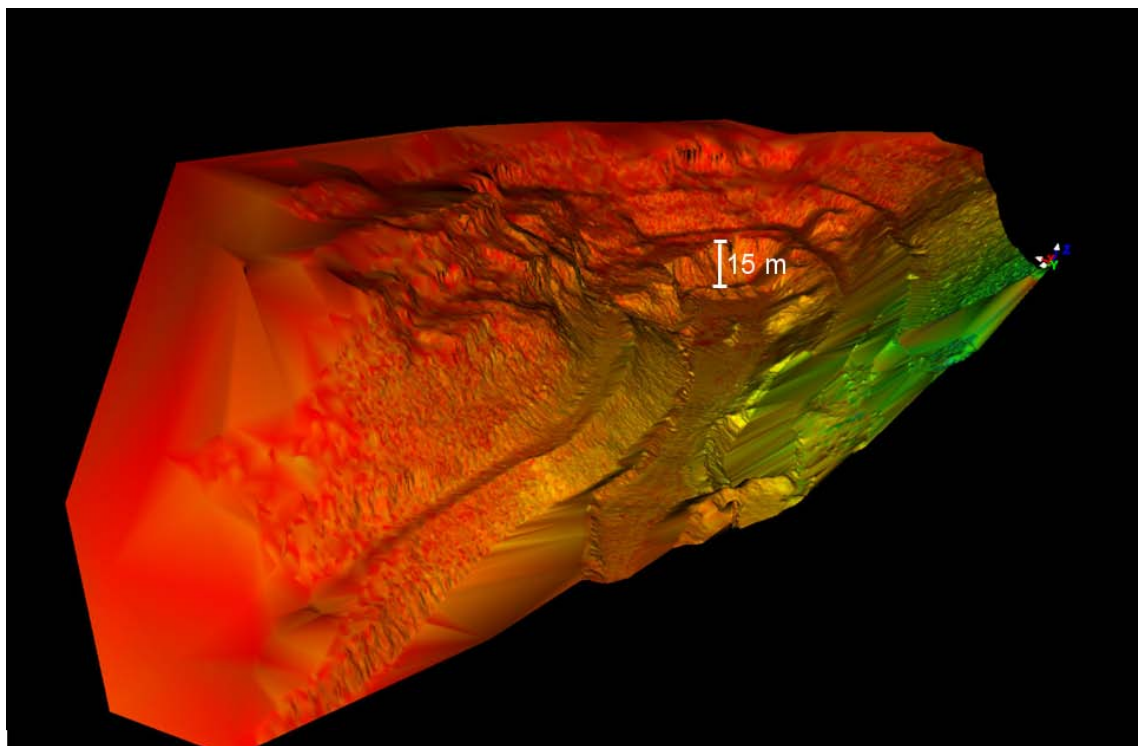


Figure 4-45. 3D model of one point cloud of Blackpool Pit, Imerys, St Austell, Cornwall, UK looking west. Each bench is ~15 m high. The reflectance intensity is represented as a green colour indicating a good reflectance, ranging to red for poor reflectance.

Although the laser scanner was able to collect positional point data from a large distance from the study object, the maximum density and increased laser spot size of the scanned points were unsuitable for extensive geotechnical mapping. Only the largest structures (10 m²) were visualised indicating that laser scanning has a distance

limit (linked primarily to density) for practical collection of data to be used for geotechnical mapping. The laser scan could be conducted at a higher density, but the large spot size would still be problematic and it would mean that an excessive period of time would be spent in the field.

4.7.2 Delabole Quarry

The quarry is run by Delabole Slate Company Ltd (Figure 4-46) and currently extracts grey/ green late Devonian slates from the eastern side of the quarry by drill and blast bulk excavation followed by local extraction using diamond wire saws (Selwood *et al.*, 1998). The quarry dimensions are 400 m wide, 550 m long and 150 m deep. The western side of the quarry experienced a major slope failure in 1967 and has been subject of many geotechnical analyses: Boyd *et al.* (1973), Brown *et al.* (1977), Clover (1978), Coggan & Pine (1996), Costa *et al.* (1999), Stead *et al.* (2006) and Coggan *et al.* (2007). The orientation of the failure face has been split into four sections, corresponding to faults hand-mapped by Clover (1978) using traditional surveying and hand-mapping. The other lower, shallower sections are thought to be controlled by intersections of several other discontinuities (Coggan & Pine, 1996).

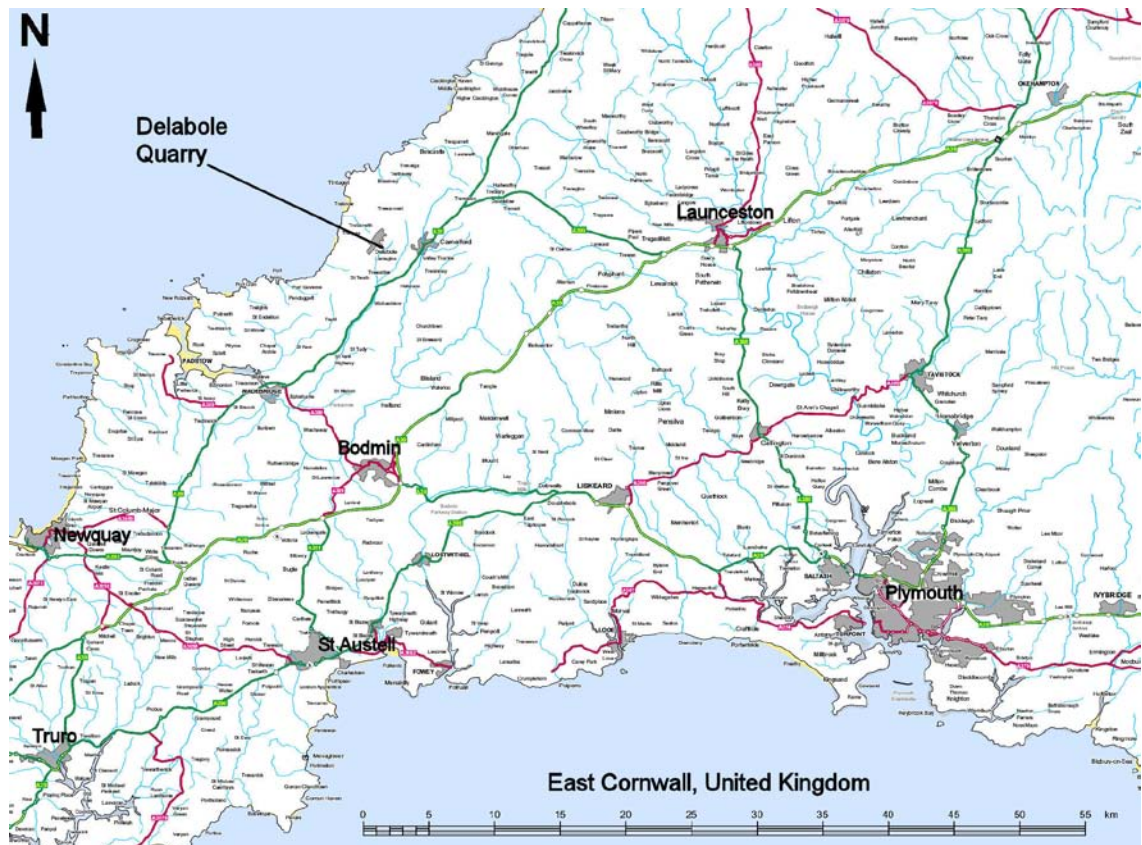


Figure 4-46. Map of East Cornwall, UK, showing location of Delabole Quarry. © Crown Copyright/database right 2009. An Ordnance Survey/EDINA supplied service.

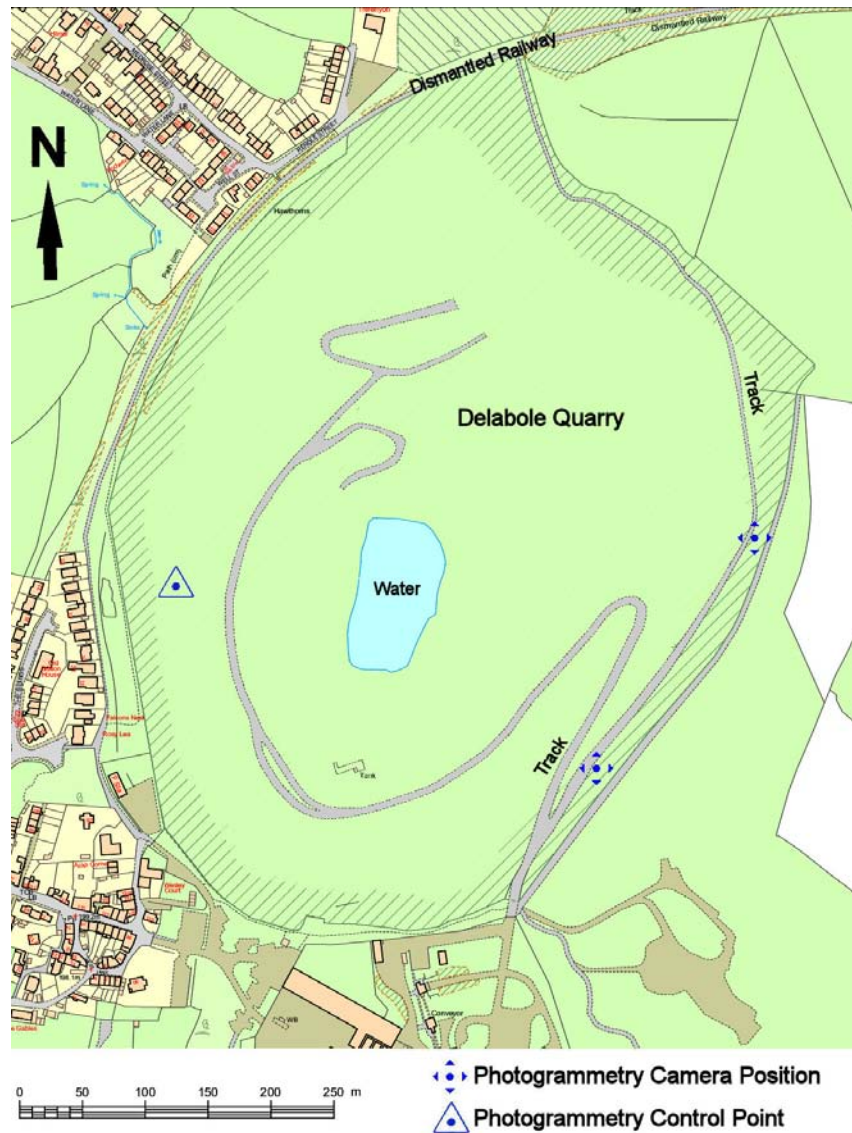


Figure 4-47. Map showing locations of photogrammetry camera and control point setup positions at Delabole Quarry. © Crown Copyright/database right 2009. An Ordnance Survey/EDINA supplied service.

Table 4-18. Locations of photogrammetry camera and control point setups at Delabole Quarry, Cornwall, UK, also indicating lens used.

GB National Grid (m)			Camera / Control Point	Model	Lens
Eastings	Northings	Elevation			
207656.3	83786.6	197.105	Camera 1	Model 1	50 mm
207787	83971.05	199.023	Camera 2		
207325.3	83934.08	161.815	Control Point		

A photogrammetric model was created of the western side of Delabole quarry to capture the site of the 1967 failure plane and associated features (Figure 4-47 and Table 4-18). The two cameras used for the photogrammetric setup were restricted to platforms opposite the failure face used for monitoring the slope, resulting in an unfavourable baseline to face ratio of 0.89, as well as a large distance to the study face. A 50 mm lens was used to capture the two images. A reflector station situated

on the failure face (used for face monitoring) was utilised as the photogrammetric control point. Although the baseline to face ratio was outside the recommended ratio of $\frac{1}{6}$, a good 3D image was produced with 92% matched pixels and no major distortion, displayed in Figure 4-48. The failure plane between 140 m – 190 m AOD was measured to be an average orientation of $71^\circ/092$ with an area of 1132 m^2 . A comparison of the slope profiles is shown in Figure 4-49 and a general photograph of the slope is shown in Figure 4-50.



Figure 4-48. 3D image showing the 1967 failure plane (highlighted red), Delabole Quarry, Cornwall, UK. It is considered that there has been little change in the slope profile since there has been no significant failure subsequently in this regularly monitored face. The camera positions had restricted views of the lower half of the pit slope, so only the upper part, which includes the failure surface, was modelled.

The angles of the corresponding sections seem to be steeper in the photogrammetric cross section. Clover (1978) suggests that the failure face is dipping at $63^\circ/100^\circ$, where the photogrammetric image estimates an average face angle of $71^\circ/092$, resulting in a low pole vector difference of 8.57° . A possible reason for the discrepancy between the slope dip measurements is that the photogrammetric measurement was taken across the entire failure surface where, due to limitation of hand-mapping only spot measurements of the face could be taken previously. The profiles through the 1967 failure surface differ. Even though the photogrammetric setup positions were not ideal, and it is possible that the 3D image may not be highly accurate, the profile

produced will be a better representation of the actual failure surface than the 1978 profile as that profile is an indicative schematic.

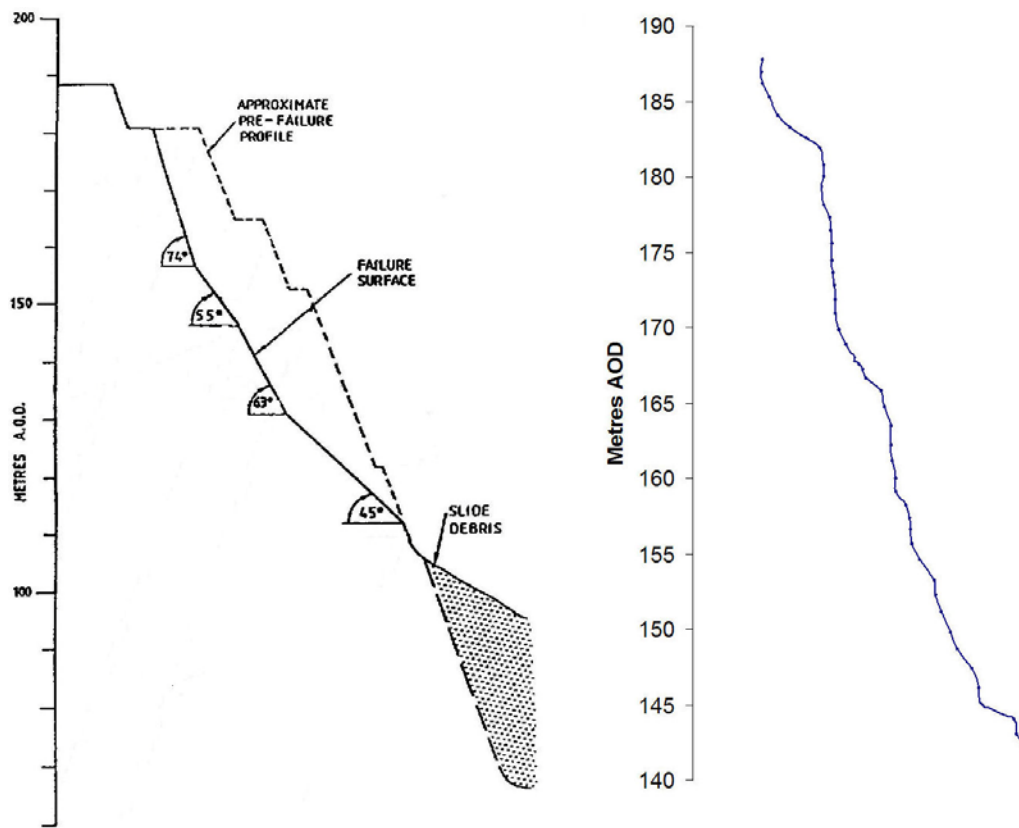


Figure 4-49. Comparison between the cross section of the 3D photogrammetric failure face (140 m and 190 m AOD) and the estimated original quarry profile (50 m – 200 m AOD), after Clover (1978).

The restricted camera setup positions resulting in a large distance to the study face was a reasonable compromise to capture a 3D image of the 1967 failure face. A result close to the traditionally measured dip angle was obtained. It shows that results are good enough for broad profiling and identification of large fractures. Smaller discontinuities existing within the rock mass could not be captured as the relatively low density of the pixels of the photographs could not resolve them at that scale. This is a result of the distance from the face, but it is also linked to the density of the points making up the mesh of the 3D image. Smaller features could be mapped if using a lens with a higher focal length but then only a smaller area could be mapped for each 3D image created.



Figure 4-50. Photograph of the 1967 failure face at Delabole Quarry viewed NNW, with the town of Delabole in the background. The slope is ~100 m high from the haul road.

4.7.3 *Camborne School of Mines' Test Mine*

The minimum distance that the remote mapping techniques can be used is a less critical assessment of their limitations than their maximum range. If close proximity to the face is possible so that contact can be made then hand-mapping may be preferred. However, there are some instances involving personnel safety where very close range remote mapping techniques are beneficial. Most open pit sites do not allow access to a face for safety reasons even though it is physically possible. It is considered that laser scanning systems will be less affected by very close range positioning as the scanning can take places from a single location. Conversely the berm width between some benches can be so small that it can start to affect the choice of photogrammetric camera setup locations, so that baseline to face ratios and angle must be carefully considered.

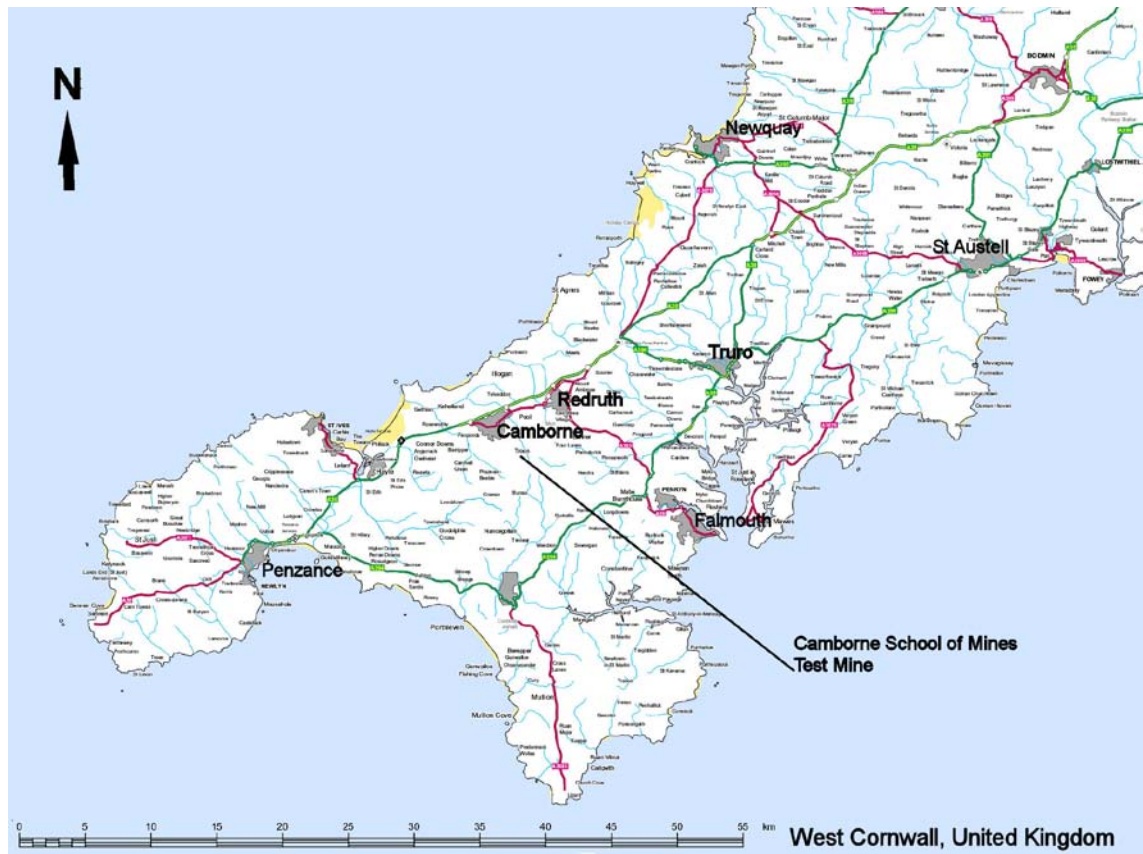


Figure 4-51. Map of West Cornwall, UK, showing location of Camborne School of Mines - Test Mine. © Crown Copyright/database right 2009. An Ordnance Survey/EDINA supplied service.

Very close range remote mapping was tested at the Camborne School of Mines' Test Mine (Figure 4-51) as the potential access restrictions for open pits are also shared by underground operations. Laser scanning was undertaken within a drive 3 m wide to assess how access affects the ease of setup and point cloud creation. Three dimensional point clouds were created showing the blocky nature of the granitic rocks within the Camborne School of Mines' Test Mine as depicted in Figure 4-52. The Leica user manual states that the scanner can be used down to 1 m from the study object to maintain optimum accuracy. It was found that the minimum distance to the face should be kept to 1.5 m for laser scanning a sub-vertical face for geotechnical mapping as the footprint (the area under the laser scanner that it cannot see) is projected onto the scanned face at closer distances.

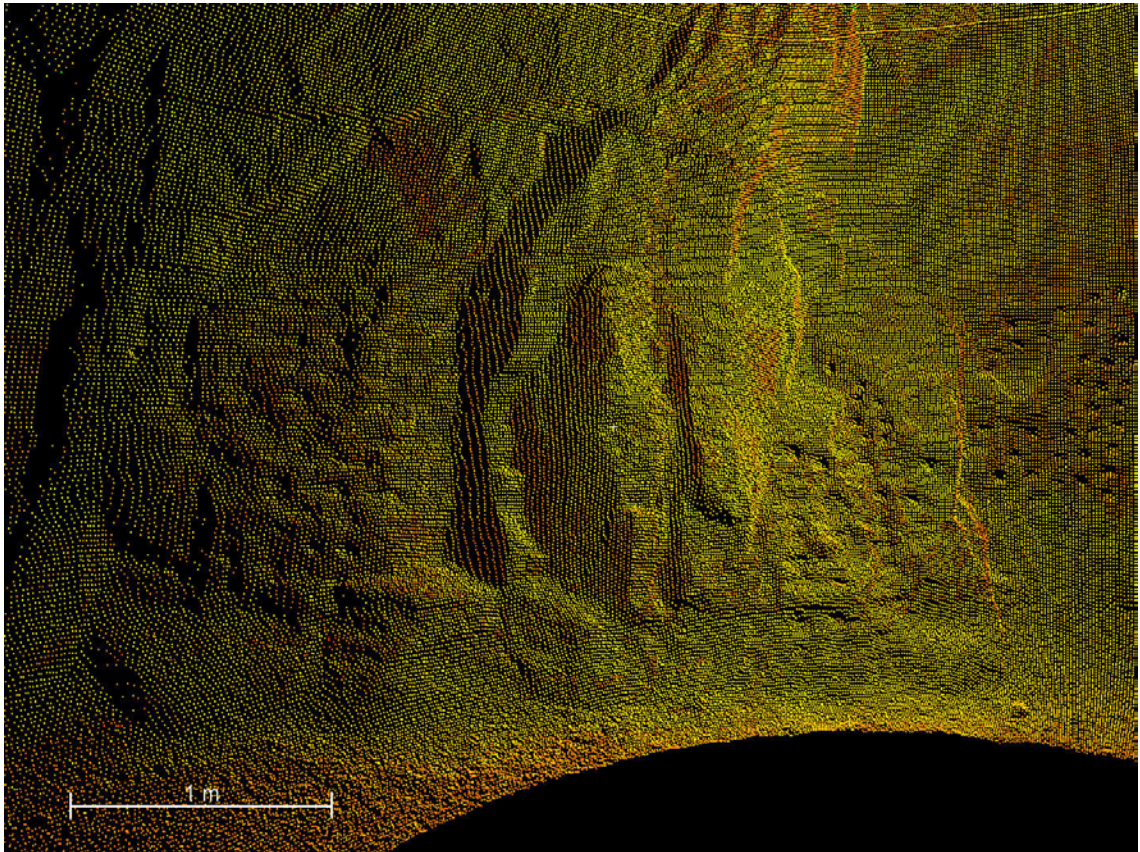


Figure 4-52 . Point cloud of side wall within CSM Test Mine (2.5 m high). The footprint of scanner comes to the base of the rock face when ~1.5 m away from the face.

Multiple photogrammetric models were also made within the drives of the CSM Test Mine (Figure 4-53). The photographs were taken using a 20 mm lens to view the largest area possible from the close camera setup proximity to the face. As the maximum width of the drives was 3 m and to allow for sufficient space so that the cameras can be operated, the cameras were regularly only 2.5 m from the rock face. To maintain a baseline to face ratio of $\frac{1}{6}$ the cameras were only ~0.4 m apart and the width that could be captured by each 3D model had a maximum extent of ~3.5 m. Even though photogrammetric models were produced successfully and without major distortion at this very close range, the amount of setups that were required to map an area to collect sufficient data for geotechnical analysis was excessive.

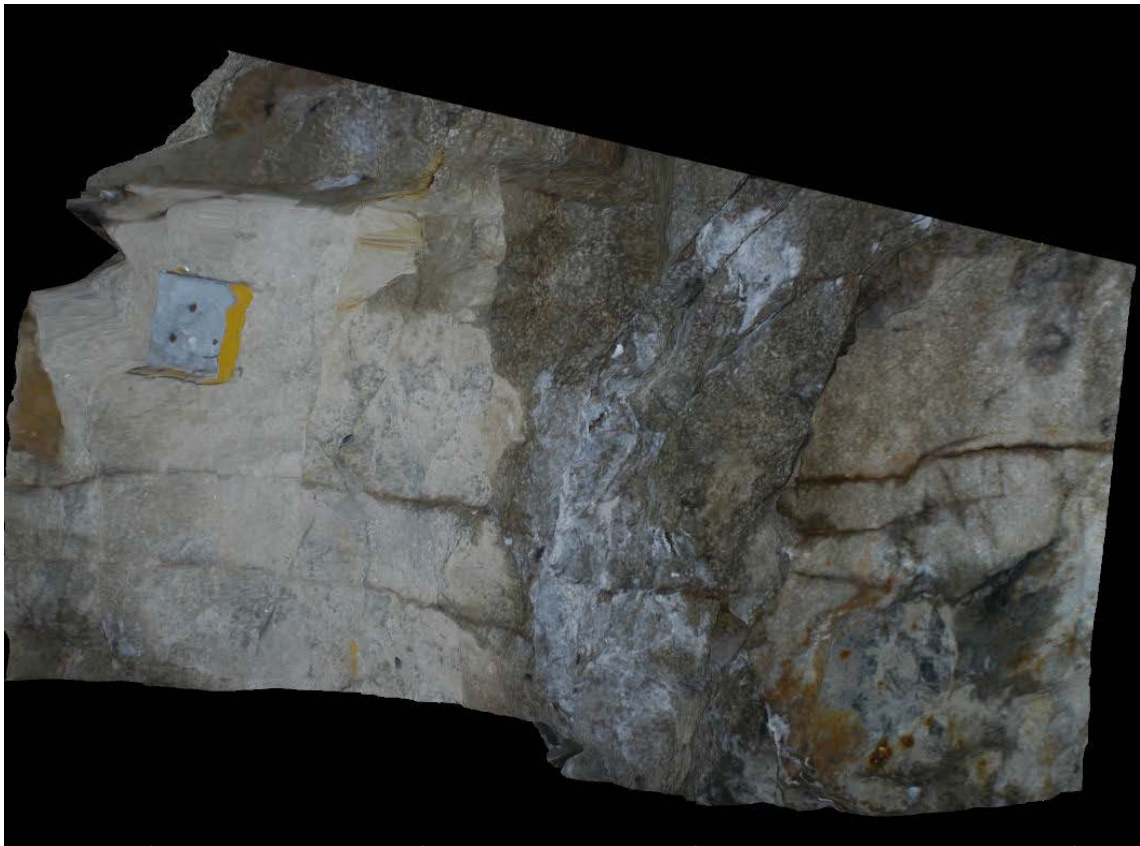


Figure 4-53. An example of the multiple 3D images created of side walls and drives within CSM Test Mine. (2.5 m in height, and 3.5 m wide).

4.8 Equipment and Software Cost Analysis

Obtaining specific cost details of laser scanning and photogrammetric equipment along with associated software packages is difficult, as many variations in product packages exist and prices change with time. The following prices are true for 2007. A price for equipment and software can be compared, although the cost of training and employment of personnel varies depending on experience and location. The price of the Leica HDS3000/ HDS4500 and laser scanning software ranges from \$60,000-\$100,000, with a commercial SplitFX licence costing an additional \$12,995. The hardware needed for photogrammetry is less expensive, it includes: a digital SLR camera, lenses, tripod and geared head, costing around \$3000 combined. The Sirovision photogrammetric software package costs \$18,000 for a single commercial licence.

Most large engineering projects, e.g. quarry and mining operations, have budgets large enough so that prices in these ranges are not problematic. Although, these prices can be restrictive in some situations, where smaller companies require remote data capture, the employment of consultants utilising the equipment can reduce the cost.

There are options to rent the hardware, as well as discounts for research applications that do not need full commercial licences.

4.9 Camera Lens Analysis

The choice of camera lens is closely related to distance-to-face limits, allowing for flexibility of setup positions within the field. Previous sections demonstrate how the 50 mm lens was used for capturing images at distances between 10 m and 400 m. The 20 mm lens has a shorter focal length than so it is able provide a larger view of the study face. When access problems restricted the distance that the camera setups could be from the face the lens that captured the most appropriate area of the face was used. The 20 mm lens was used primarily for very close range photogrammetry (<5 m) when images of the small scale rock fabric were required, or when access was severely restricted, e.g. underground.

Using one zoom lens would provide the answer to carrying multiple lenses in the field, unfortunately the tracking motion in a zoom lens means the lens distortion is always different during lens adjustment. Distortion correction in the 3D image setup process for the subsequent 3D image generation will be inaccurate. There are other software packages that can compensate for this, but as yet they are not incorporated into the Sirovision software suite used during this project.

4.10 Access Analysis

Access is an important factor when choosing the setup position for the remote data capture systems. Variable access problems were encountered during this project in addition to those that affect camera baseline to face angle/ratio covered in Sections 4.5 and 4.6. They range from inability to view the face due to heavy vegetation to restrictions of setup positions due to heavy machinery movement. Each access complication met during the project will be described along with the outcomes and solutions.

4.10.1 *Vegetation / Obstructions*

Working quarries have very little vegetation problems as the faces are usually clean and fresh, although when remote mapping is undertaken at coastal locations or within abandoned areas it becomes a problem. Faces are often obscured by bushes and plants which affect the photogrammetric model creation and/ or the return signal to

laser scanning equipment. Hand-mapping is less affected by vegetation as features can often be accessed behind undergrowth.

Laser scanning a face that is vegetated causes problems in two ways. The first is that the laser beams are obscured from the view of the face. This results in the plants being visualised rather than the study face itself, where only a few of the laser beams emitted from the scanner reach the face and are reflected back. The second problem arises when vegetation, such as moss, is growing on the face as it acts to absorb the laser beams, resulting in a poor/ no return signal, and missing point cloud data.

Vegetation blocking the view whilst a photogrammetric model is being captured can cause defects in the resulting 3D image. However, in most cases, whilst pixel matching is being processed, the algorithms 'flatten/ smooth' the image of the vegetation and other stationary obstructions to the underlying rock face (Figure 4-54). Some distortion occurs, but not enough to affect the overall accuracy of the measured feature. On visual inspection, if the feature is too adversely affected by distortion it would not be mapped.

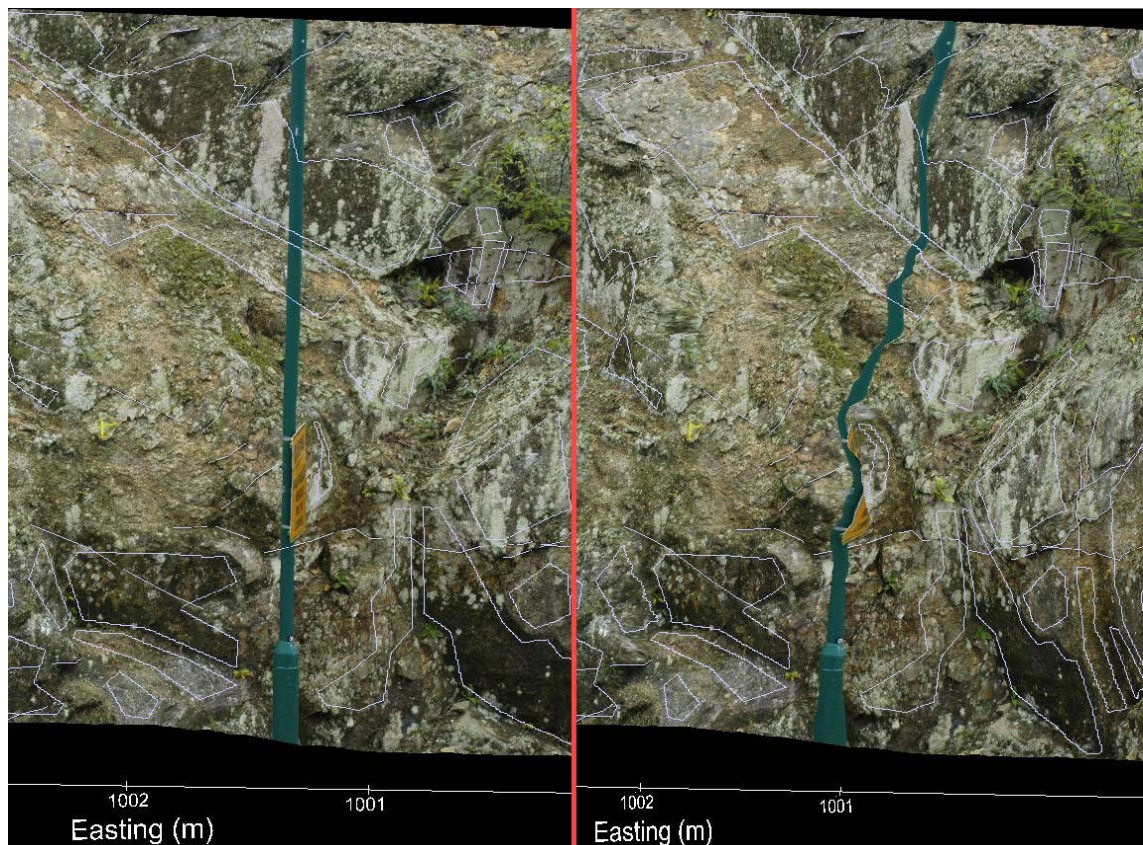


Figure 4-54. Two images showing how the image of the obstruction (lamp post) is smoothed to the rock face. Some distortion has occurred between the yellow sign and the rock face, but it is minimal and does not affect the rest of the 3D model.

Other obstructions, such as moving vehicles or people cause problems when using remote data capture systems. Moving objects affect laser scanning more prevalently, as these objects can move in front of the scanner while the points are being measured. This problem results in 'ghost points' within the point cloud as illustrated in Figure 4-55. Photogrammetry is less affected by moving obstructions as photographs can be taken when these are not within view/ in motion.

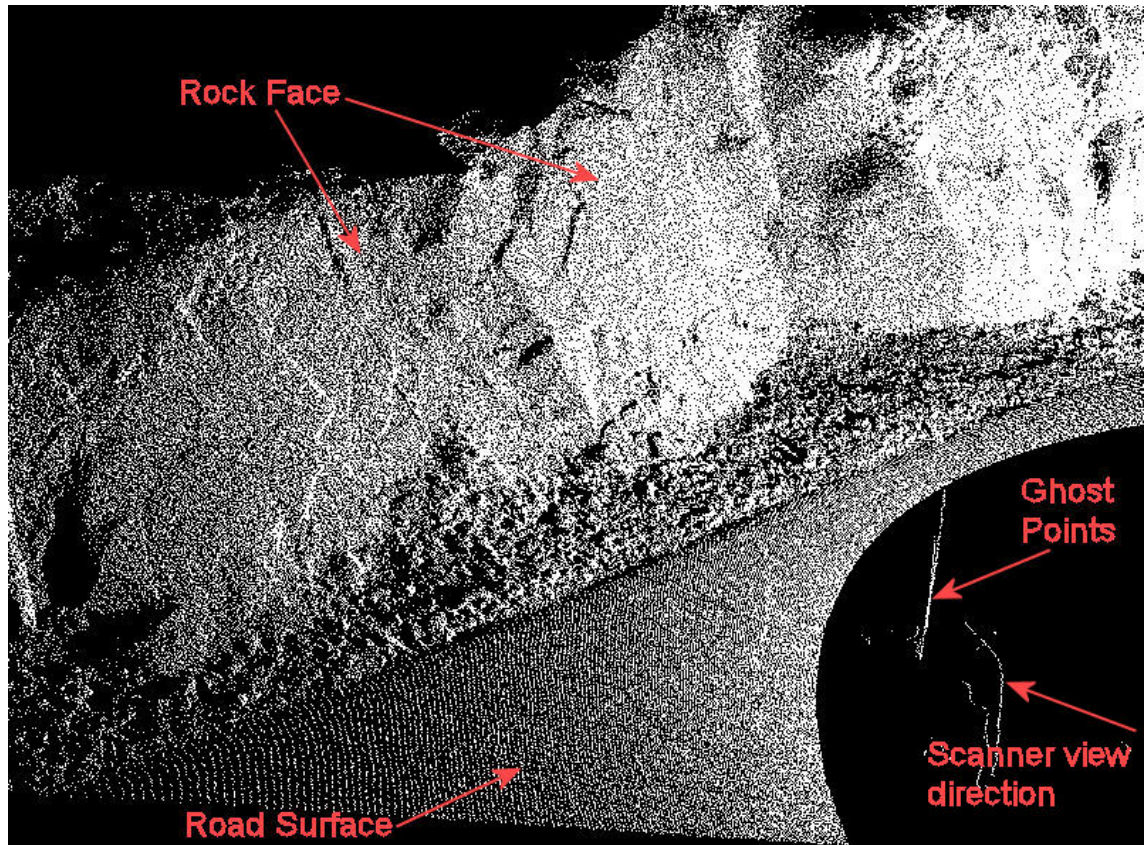


Figure 4-55. Point cloud image showing ghost points created by vehicles passing in front of laser scanner. The rock face is ~3 m high.

Point clouds, once visualised on a computer, can be cleaned for 'ghost points', where each erroneous point is manually deleted from the cloud. This is a tedious and time intensive task but will enable obscured point clouds to be meshed and subsequently mapped.

4.10.2 Water Reflection

Water can be present on or near a rock face as a function of ground water or surface run off which can produce highly reflective surface. If the reflectance is high enough it can cause problems for remote data capture systems. Glare from reflectance of the sun within a photograph used for photogrammetry will distort the final 3D image. High reflectance is usually a benefit for laser scanning systems as a strong laser return signal makes for an easier distance measurement, although in some cases it can

cause erroneous points with a cloud. Figure 4-56 below, is an image taken from a point cloud scanned at CSM Test Mine, where points have been formed from reflectance of the laser beam from the scanner on a puddle, effectively mirroring the roof of the drive. These reflected points can be removed similarly to the 'ghost points' in Section 4.10.1.

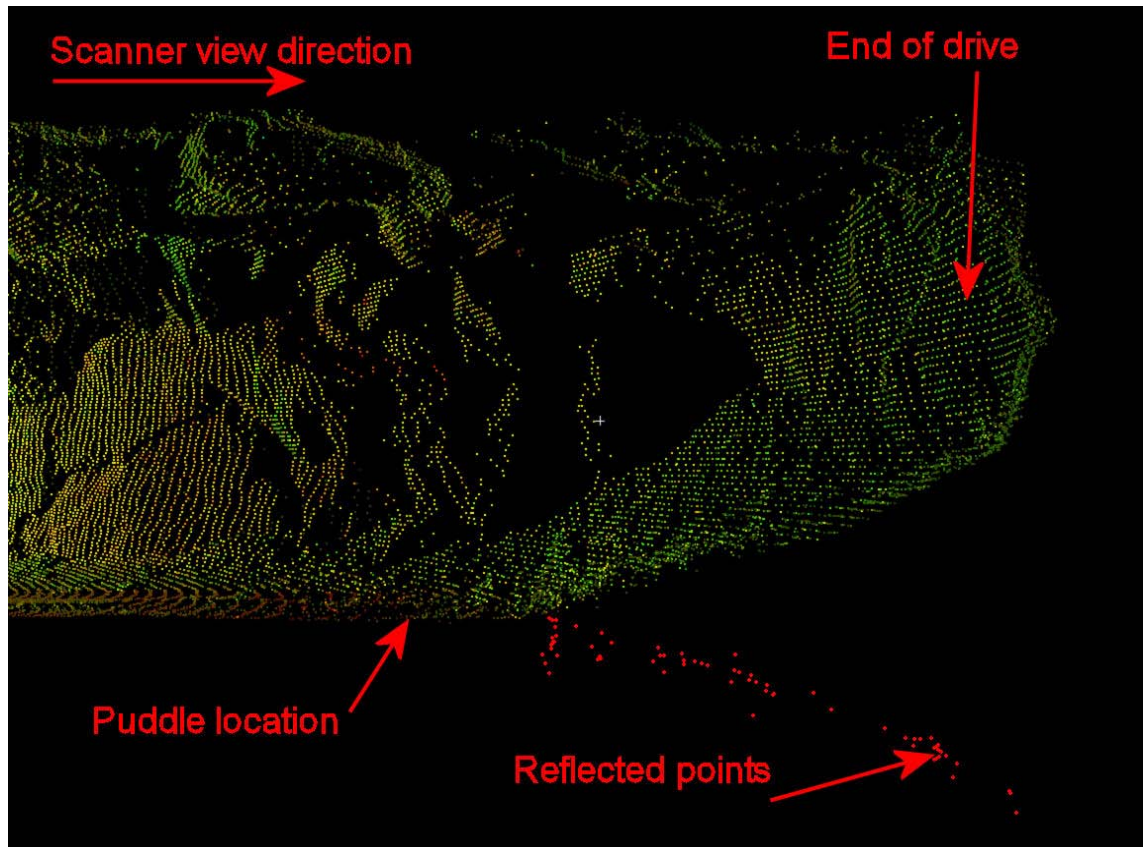


Figure 4-56. Points within laser scanned cloud formed due to reflectance from puddle in the floor at CSM Test Mine (2.5 m tall drive, viewed east) (highlighted red).

4.10.3 Rock Mesh

Rock mesh is commonly used to stabilise slopes, it is effective in preventing blocks falling out of the face moving away from the foot of the face (Ciarla, 1986, cited by Wyllie & Mah, 2004). If rock mesh is present it becomes very difficult to hand-map a rock face. Rock mesh can also affect the remote data capture systems ability to model the rock face as it acts in a similar manner to other obstacles. The remote data capture systems were tested on their ability to deal with rock mesh as it is used so often in stabilising slopes.

Laser scanning is able to visualise a rock meshed face, but to manually remove the points representing the mesh takes an excessively long time to complete. Photogrammetrically captured rock meshed faces have resulted in good 3D models with little/ no distortion (Figure 4-57). Photogrammetric images were taken at an

excavation near Dielette, northern France (Latitude: 49°32'20.67"N, Longitude: 1°52'56.47"W) (appendix DVD). The face is composed of a moderately fractured, fairly blocky, highly metamorphosed limestone hornfels.

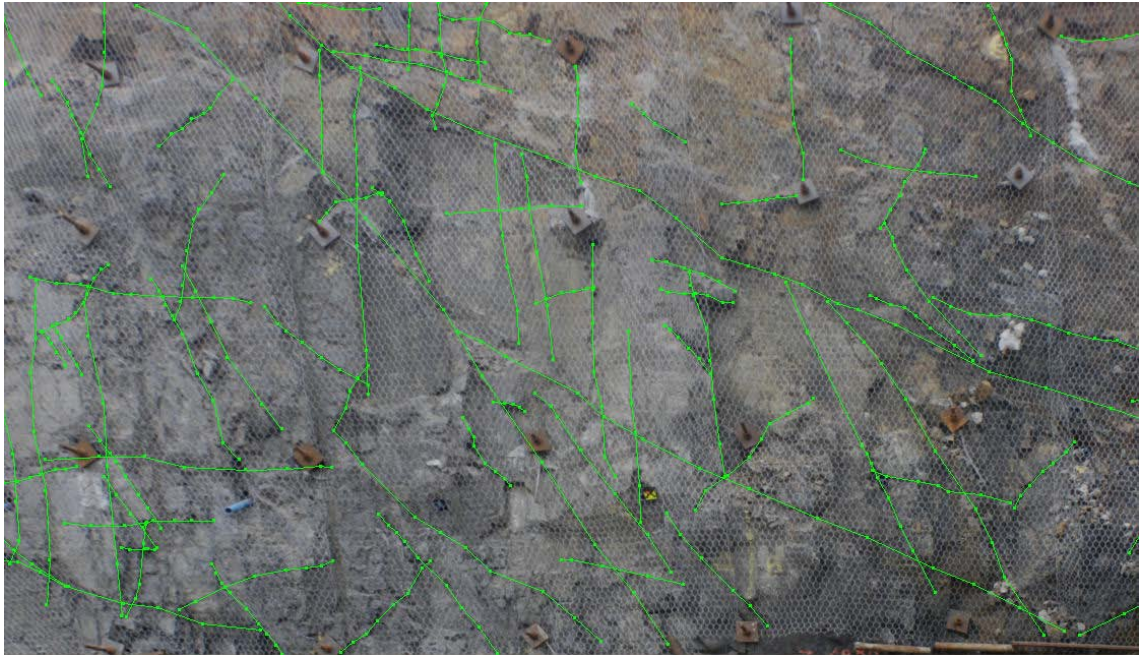


Figure 4-57. Rock meshed face at excavation near Dielette, northern France (only discontinuity traces shown). The rock mesh has been bolted and closely follows to the rock face. Discontinuity orientations and discontinuity trace lengths from 68 features were successfully extracted from the ~3 m high, east - west striking model.

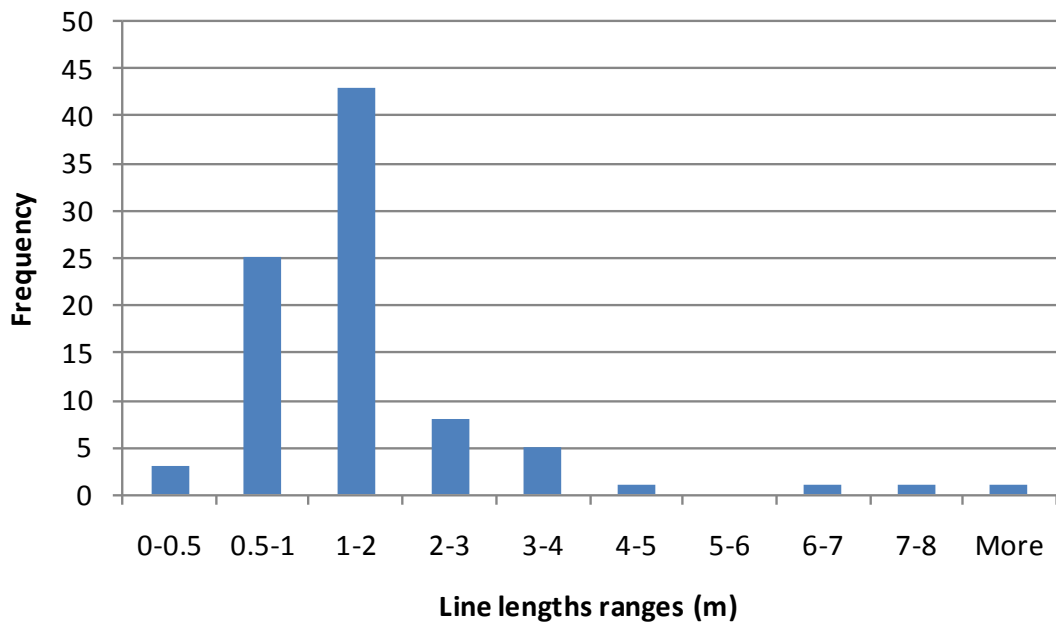


Figure 4-58. Frequency graph showing line lengths collected from rock meshed face. The majority of the 1m - 2 m discontinuities are sub vertical, while the longest are orientated at 35°.

The discontinuity trace length data (Figure 4-58) was subsequently used to aid in the geotechnical stability assessment of a proposed 8 m wide shaft. The high frequency of

1-2 m long discontinuity traces indicated that the majority of blocks formed would not be so large as to interfere with the shaft as it is being excavated. The longest discontinuities (>6 m) were at an unfavourable orientation but their spacing, calculated from the meshed photogrammetric image, reduced the likelihood of unstable blocks being formed.

The mesh was regularly bolted to the rock so that it was reasonably close, conforming to the morphology of the face. It is considered that if the mesh was not fastened and situated further from the face then the model creation may have become distorted. This would occur as the rock mesh would act as an obstruction to the view of the face similarly to the yellow sign on the lamppost in Figure 4-54.

4.10.4 *Blinding*

Access problems, causing a change in the positioning of remote data capture equipment setups, such as avoiding dangerous areas/ machinery, can change the parameters that were decided upon during planning. When conducting remote data capture at coastal locations, the access to the cliff face can be restricted by the terrain of the foreshore and/ or the changing tides. Timing visits to coincide with low tides can enable sufficient distance from the studied face to capture good remote data within a practicable time period. In some cases the tides do not allow for this and multiple small scale models must be made close to the face to cover the full study area. Close proximity to the face can require a more oblique view when scanning/ capturing the images. This may cause blinding where the rock features themselves block the view of the rest of the face. An oblique orientation to the rock face (in both horizontal and vertical directions) would generally result in some features becoming blinded from the view of the remote mapping system. The direction of sight to the studied rock face may vary, but as long as it falls within thresholds, accuracy problems should not arise.

The same test site used in Sections 0 and 4.6, Penlee Quarry (Figure 4-37 and Figure 4-38), was used to test the effect that access has on photogrammetric blinding (appendix DVD). A total of 285 discontinuity features were mapped from a photogrammetric image 90° to the rock face with a baseline to face ratio of $\frac{1}{6}$. If a feature could be mapped as a plane (when viewed in 3D) it was done so. Following this method the features mapped were represented as 196 planes and 89 discontinuity traces. The same features were mapped as each photogrammetric setup was moved increasingly obliquely to the face at 15° intervals (Table 4-16 and Figure 4-41). Some

features in the subsequent 3D models were unable to be mapped as planes, so were mapped as discontinuity traces, and vice versa.

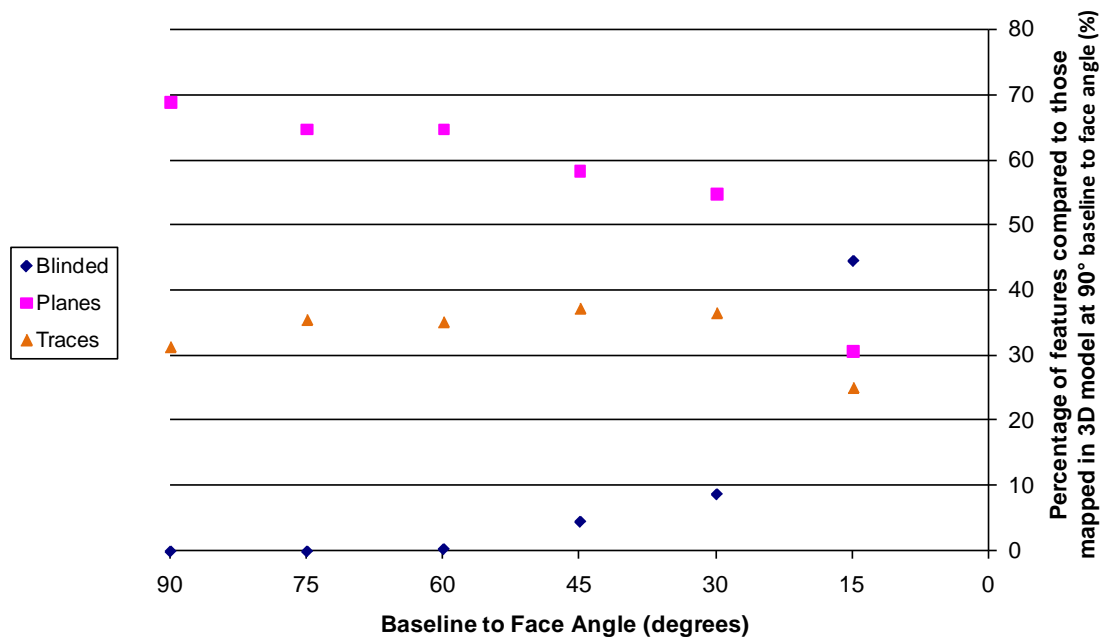


Figure 4-59. Graph showing the percentage of features compared to those mapped in the 3D model at 90° baseline to face angle for models with decreasing baseline to face angles. At 90° - 60° to the face no discontinuity features were missed/blinded, although the number of planes that had to be mapped as discontinuity traces increased to 35%. At a 30° angle to the rock face, the number of blinded features increases to 8% at the expense of the planes (decreasing from 65% to 55%, with a 2% increase in discontinuity traces). At a 15° angle from the study face, 46% of features are blinded, where planes and discontinuity traces combined only make up 54%.

As the models became more oblique to the face, more discontinuity features were unable to be seen and recorded as ‘blinded’ features (Figure 4-59). Only 5% of data has become lost beyond an angle of 45° to the face, but at this angle the inaccuracy in fracture orientation is already twice as much as the best achievable (See Figure 4-42, Section 4.6). A baseline setup angle of less than 30° to the study face increases the problem of blinding significantly.

The test of the effects of blinding on laser scanning was conducted on the weathered granite face at the Tremough Campus road cutting, Penryn, Cornwall, UK (Figure 5-2, Figure 5-3 and appendix DVD). Description of the site is covered in Section 5.2. This was tested by comparing the amount and orientation accuracy of features that were captured by 3 combined scans with the amount captured by using only one scan (Table 4-19). Firstly, five photogrammetric models were made covering a 40 m long, 8 m high rock face, from which 283 discontinuity planes were mapped. Secondly a single laser scan was conducted using the HDS45000 phase shift laser scanner covering the same

area with a 6 mm scan density, from which 242 features of the photogrammetric 283 features were identified.

Table 4-19. Locations of laser scanner setup positions, and photogrammetry camera and control point setups for testing laser scanning blinding, indicating model, lens and scan density used.

GB National Grid (m)			Camera / Control Point/ Laser Scanner Type	Model	Lens / Density
Eastings	Northings	Elevation			
176886	34937.5	96	Camera 1	Model 1	20 mm
176884.1	34938.49	95.792	Camera 2		
176880.4	34926.08	96.706	Control Point A		
176886	34937.5	96	Camera 3	Model 2	20 mm
176889.2	34938.06	97.697	Camera 4		
176888	34926.34	96.284	Control Point B		
176891.6	34936.26	98.63	Camera 5	Model 3	20 mm
176895	34936.25	98.63	Camera 6		
176893.6	34921.26	96.284	Control Point C		
176895	34936.25	98.63	Camera 7	Model 4	20 mm
176898.2	34936.82	98.45	Camera 8		
176897	34925.09	97.037	Control Point D		
176898.2	34936.82	98.45	Camera 9	Model 5	20 mm
176902	34936.81	98.44	Camera 10		
176900.3	34921.29	96.039	Control Point E		

GB National Grid (m)			Laser Scanner Type	Model	Density
Eastings	Northings	Elevation			
176875	34934	96	Leica HDS3000	Model 1	6 mm at 10 m distance
176905.5	34937.5	95.5		Model 2	6 mm at 10 m distance
176888	34938	95.8		Model 3	6 mm at 10 m distance
176888	34938	95.8	Leica HDS4500	Model 4	6 mm at 10 m distance

The phase shift scanner was used in preference to the time-of-flight scanner for scanning from one position, to take advantage of its increased speed, and so avoid ghosting created by any passing traffic. The Leica HDS4500 was used to complete the first scan as it has a much quicker scan time than the HDS3500. The scan of the face had to be completed quickly to reduce traffic congestion. The traffic had to be stopped so that the production of ghost points when vehicles move in front of the scanner would be minimised. The two types of laser scanner have differing positional accuracies of the points they collect, as described in Section 0.0.0. By scanning the face at the same density when using both types of laser scanner, whilst at the same close proximity (<10 m) to the face, negated any positional accuracy differences between them. The geological setting of the Tremough Campus road cutting is covered in more depth in

Section 5.2. Hand-mapping of the rock face yielded orientation measurements for only 153 features. An average pole vector difference of laser scanning from hand-mapping came to 18.83°.

Three combined laser scans using the same 6 mm density as the phase shift laser scanner were conducted of the same rock face using the time-of-flight Leica HDS3000. From the combined point cloud 280 features were identified. Recalculating the laser scanning pole vector difference from hand-mapping gave 11.96°. The results are summarised in Table 4-20.

Table 4-20. Results of blinding effects on laser scanning. The single laser scan only captured 86% of the features mapped using photogrammetry, had a pole vector difference of ~18.83° from hand-mapping and a standard deviation of 16.18°. The three combined laser scans were able to capture 13% more features than the single scan whilst obtaining a 11.96° pole vector difference from hand-mapping. The standard deviation was reduced by 40% to 9.6°.

	No. of Planar Features	Laser Scanning Pole Vector Difference from Hand Mapping	Standard Deviation
Photogrammetry	283	-	-
One Laser Scan Setup	242 (86%)	18.83°	16.18°
Three Laser Scan Setups	280 (99%)	11.96°	9.6°

The accuracy of the captured orientation measurements from one single laser scan would be expected to be lower than from three scans as there would be a lower point density representing the discontinuity planes. The orientation of the features being scanned is also a consideration, the more oblique the plane to the scanner the less points will be present representing it when it is mapped. Scanning from multiple locations from differing angles ensures that each feature is covered by a sufficient amount of points. A larger volume of points captured from a discontinuity allows for more mesh triangles and therefore a more accurate and precise calculation of orientation by SplitFX.

4.11 Atmospheric Conditions

Working temperature ranges are given by most manufacturers of laser scanning and photography equipment. For example the operational ranges for the Leica HDS3000 and the Nikon D100 DSLR camera are both, 0°C – 40°C (Leica, 2005; Nikon, 2005) and are a similar range for most other laser scanners and cameras. The extreme temperatures at the end of each of the ranges were not encountered during the project and would not usually be encountered. Operational manuals state that sudden changes in temperature must also be avoided, as this can cause condensation within the equipment damaging internal components (Leica, 2005; Nikon, 2005).

At varying temperatures remote data capture equipment will fluctuate in the measurements they take. At differing ambient temperatures, laser scanners may experience variations, particularly in their distance measurements (Boehler *et al.*, 2003). This also affects photography, as light refraction and lens distortion, due to temperature and pressure variations, affects the measurements made (Yastiki, 2002). This effect would be more pronounced when capturing data over large distances, but for the short ranges used during this project the variation of temperature was disregarded.

Both laser scanners and cameras have some protection from water, dust and sand due to the tough outer shell applied to the casings. This allows them to operate in adverse conditions, but the presence of water, dust or sand in the environment in which they are working can affect the data captured. The Nikon D100 camera can work in humid conditions of up to 85%, and the Leica HDS3000 can work up to 95%, although if the moisture condenses on the camera lens the data they capture will be distorted. Photogrammetric models were captured during wet periods, although the camera itself was protected from water and the photographs were taken when it had stopped raining. Laser scanning was not undertaken during any precipitation, as water on the windows/mirrors and droplets in the air diffract the laser beams resulting in poor point cloud creation. Problems from dust and sand in the air were encountered when testing the remote data capture equipment at Camborne School of Mines' Test Mine, Troon, Cornwall. Dust in the air was highlighted by the camera flash when the images were taken, and the point clouds produced multiple ghost points when the laser picked up the suspended dust particles (Figure 4-60).

The remote data capture techniques differ in their illumination requirements, as laser scanning is an active system, while photography is passive. Photographs rely on a separate light source restricting their use to conditions where lighting is sufficient, unless artificial lighting can be implemented using a flash or lamps. Very strong sunlight can cause a problem for the creation of photogrammetric images as it produces dark shadows on the study face. These areas can cause poor 3D model creation when the computer algorithms come to match the pixels from the two photographs with one another. Photogrammetry is best undertaken during an overcast day as the light is sufficient and shadows are reduced (CSIRO, 2005). Another possible lighting problem encountered during photogrammetric image capture occurs when there is a time lapse between taking the two stereo photographs. If lighting conditions change between the photographs, e.g. the sun becomes brighter or has

moved significantly in the sky, then the two images captured may look very different, causing poor pixel matching.

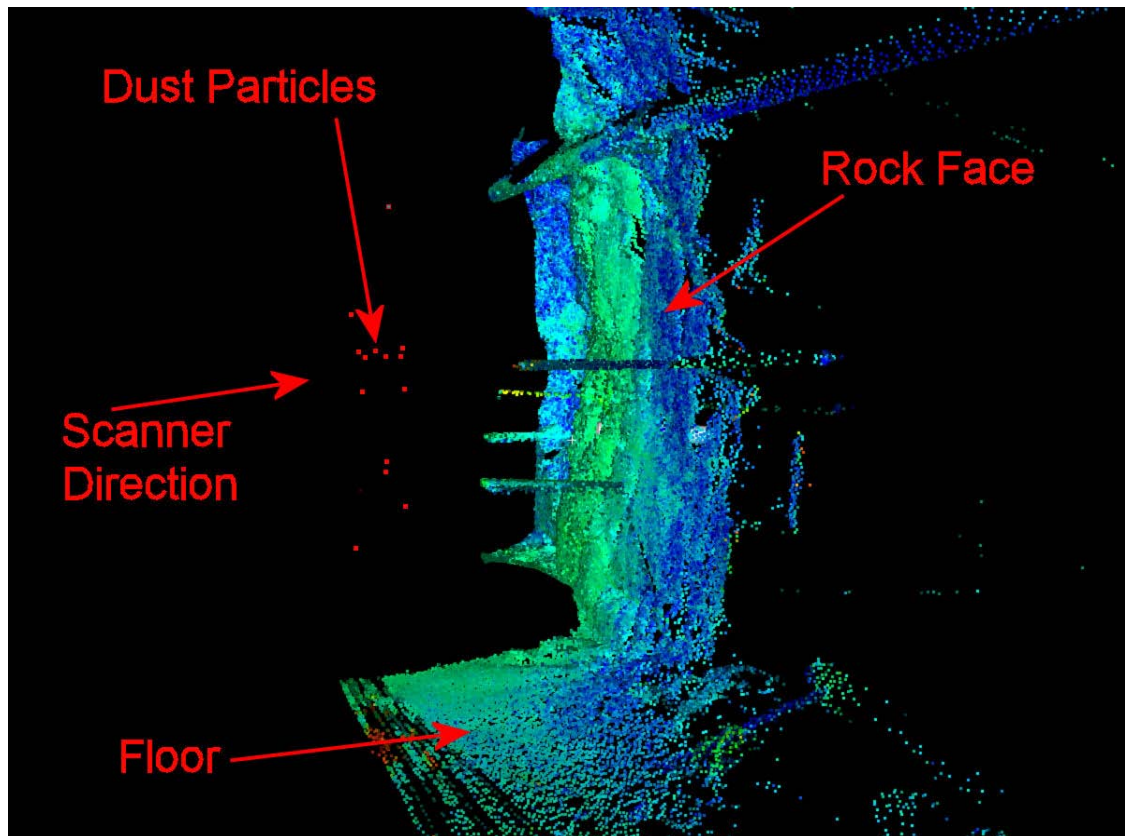


Figure 4-60. Evidence of dust particles picked up during laser scan at CSM Test Mine (highlighted red, 3 m high face).

Laser scanners can be used in areas with no light source (Leica, 2005), although problems can occur when lighting is too bright. If the radiation of the sun, or other illumination source, is stronger than the emitted laser, it can distort the accuracy of the point cloud measurements, possibly preventing any measurements at all (Boehler *et al.*, 2003).

4.12 Field Speed / Time

Ascertaining the time it takes for the remote data capture systems to map a rock face was tested at the Tremough Campus Road cutting, Penryn, Cornwall, UK. The end-uses/ applications of the resultant data vary. For this reason the data output and analysis sections of the work-flow were not considered, as they require varying times for particular end-uses. The most obvious speed/ time comparison is made between remote data capture as a whole against traditional mapping.

One of the most obvious advantages that remote sensing has over hand-mapping is the increased speed and amount of data that can be collected. To quantify this, each

mapping technique was split into individual processes, and the approximate time taken to complete them was recorded. In order to normalise the comparison, the number of features that were evaluated by each technique was restricted to 100. Figure 4-61 shows time comparisons for field mapping for photogrammetry, laser scanning and traditional mapping, covering each of the process work-flow sections.

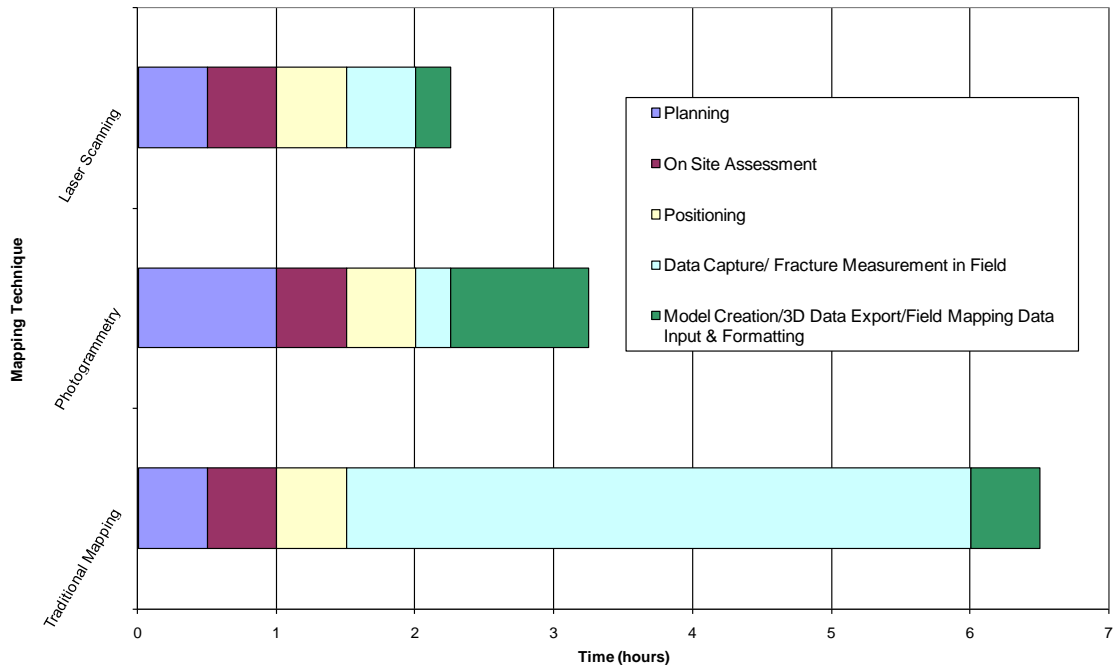


Figure 4-61. Field times comparison between photogrammetry, laser scanning and traditional mapping (100 fractures). Similar time is taken between the three mapping techniques for the preliminary stages, where the data capture/fracture measurement stage of remote mapping is ~8 times quicker than traditional mapping.

Photogrammetry requires more time during planning than laser scanning or traditional mapping as more factors must be considered that are specific to the technique, e.g. baseline ratio and orientation to face. Each technique takes a similar time to complete assessment once on the site, as all but one parameter are generic. The choice of camera lens, particularly during this project, is usually restricted to those that are available. The choice of surveying equipment obviously affects the time that positioning takes during fieldwork. It also depends on the number of subsequent equipment set-up positions. The time to position the equipment was kept constant between the mapping techniques as they share the same positioning systems. The biggest time saving of remote mapping techniques, when compared to hand-mapping, is during the data capture/ fracture measurement stage. As the remote mapping techniques are able to collect data from inaccessible areas, hand-mapping must cover a larger area to achieve the same number of discontinuity feature measurements. Photogrammetry requires slightly less time than laser scanning to collect the raw data as it is as quick as taking two photographs, where the user must wait for scanning

processes to complete. Laser scanning gains time over photogrammetry however, as it does not require as much processing to produce a three dimensional model/ image.

4.13 Development of Positional Techniques

Different positioning techniques were tested in the field and used (where applicable) to position both photogrammetric and laser scanning setups. Their use with relative coordinates and full georeferencing, as well as time taken per setup, were recorded and averaged. Accuracies, environmental robustness and weights, were identified from the operational manuals for each and assessed during the course of the study. The security of the equipment is primarily related to the cost. Table 4-21 shows the comparison of each technique against different parameters.

Table 4-21. Comparison of each positioning technique from experience during study (Additional data sourced: Leica, 2005; CG Surveying Ltd, 2007; RICS, 2007).

Survey type Parameter	Compass/Tape Measure	GPS (Magellan300)	DGPS (Leica GPS1200)	Total Station (Leica TPS1200)
Relative Coordinates	Yes	No	No	Yes
Full Georeferencing	No	Yes	Yes	Yes
Use with Laser Scanning	No	Yes	Yes	Yes
Use with photogrammetry	Yes	Yes	Yes	Yes
Accuracy	1-2 cm	<3m	3mm + 0.5ppm	3 mm + 2ppm
Elevation Accuracy	1-2cm (distance dependant)	<6m	6mm + 0.5ppm	3 mm + 2ppm
Time in field/speed per setup	20 minutes	2 minutes	10 minutes	15 minutes
Environmental robustness	Used anywhere	Working temperature -10°C to +60°C Water Resistant	Working temperature -40°C to +65°C Humidity Up to 100% Waterproof to temporary submersion into water (1m max) Dust-tight	Working temperature range -20°C to +50°C, Humidity: 95%, non-condensing, Dust tight, Protected against water jets
Portability/weight	high / <1kg	high / <200g	bulky/4.15kg for each unit (2 minimum)	bulky / ~5.5kg
Time taken for positional data processing	5 minutes	5 minutes	10 minutes	2 minutes
Cost	<£50	±£250	£17,500 (Dec 2007)	£3000 - £10,000 (Dec 2007)
Security of equipment	Kept on person	Easily kept on person	Needs constant supervision	Needs constant supervision

4.13.1 Compass Clinometer / Tape Measure

This technique was adopted because of the relative low cost of the equipment and the ease of use. It is an environmentally robust, low tech method of surveying and has a high portability allowing a single remote mapping operator. Only relative coordinates can be obtained using this technique, and it takes the longest time in the field. Over larger distances (>20 m) the tape measure can become slack, thus losing accuracy. After trials it was concluded that the time taken to collect the positional data using this method is excessive and should only be used for short camera baselines of less than 20 m. A laser range finder was tested as a replacement of the tape measure and was found to be beneficial as it allowed for remote distance measurements (to control points on the rock face) and decreased the time needed to take those measurements, but it increased the cost of the equipment to greater than £100.

4.13.2 Global Positioning Systems / Differential Global Positioning Systems

The original GPS system does not yield positioning data accurate enough for good 3D image/ point cloud creation (<6 m), even though it is the quickest positioning system. It was not used for the accurate positioning of the remote data capture equipment, but it was used to get GB National Grid positions of the setup areas to within 6 m (if performing a resection using the total station was not possible). These were used to re-orientate the relatively captured coordinates to georeferenced ones, albeit only to sub 6 m accuracy.

Differential GPS however, is more accurate than standard GPS measurements (~6 mm), but it takes time to train to use it efficiently and it is problematic to find the 'control point' for photogrammetric setups. The DGPS receiver must be at the slope face to record the control point; however in many situations access to the face is restricted. Secondly, even if the receiver is moved to an accessible face, it was found during tests that it often loses the satellite signal, rendering it unable to position itself. A laser distometer was tested for finding the control point position on the face after DGPS positioning of camera setups, but calculating the position was time consuming, and it increased the equipment load. Thus, DGPS was not used for photogrammetric positioning. The weight and portability of the DGPS base and rover units is a disadvantage, as more than one person would be needed to carry the equipment. However, the DGPS system suits the positioning of laser scanning equipment, as only the positioning of one point is required. This is completed relatively quickly once the laser scanning system is orientated and has completed its scan of the studied slope.

4.13.3 *Total Station*

The Leica TPS1200 total station can be used to relatively position a photogrammetric setup, and fully georeference both photogrammetry and laser scanning, providing there are previously surveyed points within view of the machine. Its high accuracy suits both data capture systems and it is able to measure coordinates using its reflectorless laser up to distances of 500 m (Leica, 2005). The maximum distance tested during this project for positioning a photogrammetric control point was ~150 m. The battery is inbuilt into the machine, weighing ~5.5 kg in total within a carry box.

The total station was used to collect relative and full georeferenced positional data for the photogrammetric camera setups and the laser scanner. The use of relative coordinates was more common as remote data capture was primarily undertaken in locations where surveyed coordinate points were not available. These were converted to full georeferenced locations (to within 6 m) using a handheld GPS device. The total station was used for full georeferencing for photogrammetric models created at CSM Test Mine, and for laser scanning at Blackpool Pit, Imerys Minerals Ltd.

4.14 Development of Remote Data Capture /Data Compilation

4.14.1 *Photogrammetry*

During repeated photogrammetric fieldwork it was found that certain modifications needed to be made to the equipment in order to better suit the task. The first changes were made to the digital camera setup parameters. The sensitivity was kept at automatic, but the aperture was changed from a fixed F8 to automatic. This allowed the camera to select the best settings for each digital photograph. Cameras can take photographs natively as TIF files (required for Siro3D), but as they are an uncompressed form of data, they take up a lot of space on a camera memory card. A 1 Gigabit memory card can hold approximately 56 high quality TIF files. It was found that this capacity suited the requirements of this project, but for larger projects, capturing the photographs as RAW files which are smaller in size and converting them to TIF files once out of the field would be more beneficial. It was found that a RAW file could be converted to a TIF file in around 1 minute, but if a large number of photographs needed converting, it could add significant time to a project. Due to the relatively small number of photographs taken during each field excursion (<50) the photographs were taken as TIFs, speeding up processing time. The white balance settings were not altered from the Siro3D suggestions (CSIRO, 2005).

As a non-surveying tripod was originally used for taking the digital photographs it was difficult to position the camera over surveyed points. For this reason the tripod was substituted for a standard surveying tripod. The surveying tripods are bulkier and less easy to carry than the camera tripod, but they allow the fitting of a tribrach which is used to position over a surveyed position. As a surveying tripod was to be used, the geared head, used to move the digital camera, could not be attached due to incompatible fittings so they had to be modified (Figure 4-62).

The camera and lenses, along with other smaller equipment needed to fit easily into a small backpack bag. The tripod can be carried in a free hand. This allows for quick and easy packing into a car, and manoeuvrability over rough terrain when transport is unavailable. The overall portability of the photogrammetric equipment alone allows for mapping to be conducted using only one person, although if the preferred positioning equipment of the total station is also used then a second person may be required.



Figure 4-62. Geared camera head fitted with tribrach attachment (highlighted in red). The screw fitting for the geared head was modified so that it may be interchanged between normal photographic tripods and surveying tribrachs.

The most significant change to the photogrammetric field and post-processing methodology was made to the photogrammetric model creation. The software was moved from the office based desktop computer to a laptop. Subsequently, once all the photographs were captured, the camera was connected to the field laptop, the images were downloaded and then catalogued. Three dimensional image creation is now undertaken in the field to ascertain whether or not the process was successful. It was found that if resultant 3D images were seen to have significant poorly matched areas within the 3D image, the process was repeated and the task setup was changed to remove problems areas. Geotechnical mapping using the Sirovision software can be conducted in the field, but due to computer processing power, some laptops struggle to visualise the captured images in 3D. Therefore, geotechnical mapping was conducted using a more powerful desktop computer.

Automatic plane and discontinuity trace recognition was tested upon a number of 3D images. Due to the high resolution camera used, the time it takes for an average computer to recognise planes automatically can exceed 25 minutes. The planes that were found seemed to reflect the overall orientation of the studied face rather than the orientations of the discontinuity sets. The discontinuity traces that were produced automatically did not identify continuous features, resulting in many very short traces. The research into the algorithms used for automatic delineation of features is ongoing (Section 2.5).

4.14.2 Laser Scanning

Little change was made to the field methodology for either the Leica HDS3000 or HDS4500. The portability of the laser scanning system suffered in respect to the carry box that the Leica scanner used. A ~20 kg box (1 m x 0.5 m x 0.5 m approx) with four wheels is used to house and transport the laser scanner. Other laser scanning systems have differing carrying options, although the weight and the sensitivity of the hardware requires bulky protective casing. Both scanners weigh a similar amount, the HDS3000 at 16 kg (Leica, 2005). The scanner requires a separate battery for power, and a tripod. For these reasons two persons are required to transport the laser scanner and associated equipment for geotechnical mapping, especially if crossing rough terrain. As laser scanning only requires a compass to position itself to capture point clouds relative to north, extra positional equipment, such as a total station, is not always required.

As SplitFX cannot currently calculate spacing from the 3D point cloud data, a method was tested using the 'measure distance' tool contained within the program. The perpendicular separation between planar features, identified within SplitFX, can be selected and calculated using this tool from the processed point cloud data. This would be repeated for each feature within the identified set and the average set spacing would be calculated. This method was too time consuming so was not carried forward for analysis.

4.14.3 *Set Analysis*

Each remote data capture system has its own stereographic program, each of which was used to visualise and analyse orientation data in the early stages of the project. It was found that the data produced from each of these programs was not easily comparable, due to differing file formats and methods of use. The programs were therefore used in conjunction with DIPS (Rocscience, 2006), which is a stand-alone stereographic analysis program. Exporting the geotechnical data from Sirovision and SplitFX was completed as tab delimited text files, these were imported into a spreadsheet program and copied into DIPS. This allowed for a normalised platform from which analysis was conducted.

4.15 Summary

4.15.1 *Pole Vector Difference*

A new methodology for the assessment of orientation accuracy between the mapping techniques was developed. The method compares orientation data by converting the two parameters: dip and dip direction, into singular vectors. This methodology can be used to determine accuracies between individual orientation measurements as well as averaged orientation data, e.g. from set analysis. This analysis can only be undertaken upon singular measurements, or averaged measurements; it does not include analysis of data spread/ clustering. The maximum pole vector difference possible is 90°, this occurs when the measured discontinuities are orthogonal to one another.

The hand-mapping comparison at Penlee Quarry, Cornwall, UK, which yielded an average individual feature pole vector difference of 13.75°, does show that there is a difference in accuracy between hand-mapping measurements. The standard deviation of 17.38° shows that there is variation in reliability as well. These values would probably vary depending on the person (human bias) mapping the discontinuities and the rock type being mapped. Herda (1999) showed that the strike of shallow dipping

rock fractures (0° - 47°) varies widely, especially when they are rough, even though the dip may be measured accurately. The majority of the discontinuities hand-mapped for comparison at Penlee Quarry, although reasonably smooth, were less than 70° , which may have given rise to the 13.75° pole vector difference and 17.38° standard deviation.

Descriptions of values for pole vector differences were developed using the results from the hand-mapping comparison at Penlee Quarry. An acceptable, 'low' error between hand-mapping and remote data capture systems should be below 15° , where an error between laser scanning and photogrammetry should only result due to noise and should be less than 10° . A 'medium' PVD value is calculated to be up to 32° where a greater value is deemed to be 'high'.

4.15.2 Scale

Photogrammetry is shown to have the ability collect large and small scale features from differing rock face sizes. In the chalk geology tested, laser scanning was unable to collect orientation data from the smallest scale features as they are primarily represented as discontinuity traces. However, it is considered that a high density scan would resolve small scan planar features. Photogrammetry requires multiple field setups and the use of varying lenses to capture a range of scales, where laser scanning requires a high density of points to capture the smallest features. These requirements need a longer time in the field to complete, as well as increased time in post-processing the data.

4.15.3 Impact of Lithology/GSI

Photogrammetry is shown to collect data from a large range of lithologies, exhibiting varying fracture intensities. For the highly fractured rock types, photogrammetry must be at a reasonably close proximity to the study face, within 50 m with the use of the 50 mm standard lens. The highly fractured rocks at Gwithian had to be mapped using discontinuity traces to attain orientation data. Laser scanning is shown to collect data from blocky lithologies whose features are represented as planes. The exercise undertaken at Portreath highlights the fact that laser scanning struggles to obtain geotechnical orientation data from closely spaced, highly fractured rock masses. However, the digital elevation model data can be used for volume calculations. Remote data capture systems are not currently suited to map rock masses with low GSI ratings.

4.15.4 *Set-up Variations Affecting Data Capture*

For photogrammetry the optimal camera baseline to face ratio was calculated using the fitted curve to the average pole vector difference data in Section 0. The ratio was found to be 0.202, ($\sim 1/5$) of the baseline distance to the studied face. If the pole vector difference had to be within a tolerance level of less than 10° , then the baseline ratio should be between 0.240 ($1/4.166$) and 0.160 ($1/6.22$). These ratios are not quite concurrent with the ratios suggested by the Sirovision user manual of $1/6$ to $1/8$.

As expected, a baseline angle to face angle of 90° results in the highest orientation accuracy when compared with traditional mapping. The increasing average pole vector difference, as the baseline moves more obliquely to the face, shows that it should be kept between 45° and 90° for highly detailed geotechnical measurements. However, if this is not possible, it is still reasonable to conduct remote data capture to collect general rock mass characteristics.

These setup limitations were established at one location for a complexly fractured rock mass. It is considered that if the rock type were different then slightly altered ratios/angles for the setup limitations would occur, but they would not be substantially changed from the values found during this study as the major principals governing photogrammetry are the same.

The maximum distance that the Leica HDS3000 laser scanner can collect three dimensional data was shown to be above the published range of 100 m. Although, the maximum distance that laser scanning can collect data for the use in geotechnical analysis is dependent on many factors and less dependent on laser distance. The primary factor is the data density that the scanner can capture at that maximum distance. Secondly, the scale and lithology of the rock will affect the ability of the laser scanner to capture data sufficiently for geotechnical mapping. These tests suggest that there is a ratio between the spacing between the pixels within the photogrammetric image and the size of the feature that can be mapped. A sufficient number of three dimensional points must be captured from a discontinuity feature before it can be measured geotechnically. The maximum distance that scanners can be used to collect data also depends greatly on the hardware used. Laser scanners are in development that will be able to collect data from greater distances than the hardware tested during this study.

The relative positioning method using a compass clinometer and tape measure was found to produce good photogrammetric 3D models with little or no distortion, and due to the low cost, this method was carried forward as a positioning technique. Using the total station is more complicated than the previous technique and it is also heavier for transportation. However, due to its relative ease of portability when compared to the DGPS systems and high accuracy, it was the preferred method for positioning remote data capture systems during this project. It was combined with the use of a standard GPS system to obtain full georeferenced locations.

Modifications to the equipment and processing methods for both photogrammetry and laser scanning allowed for more robust and rapid remote data capture. Photogrammetry is the more portable of the two remote mapping systems, requiring only one person to complete field mapping. However, the photogrammetric system used in this project always requires positioning equipment, e.g. total station. This adds bulk to the equipment load, unless only a compass clinometer and tape measure is used to capture relative positional coordinates, but this results in a reduction in the accuracy of the positional data.

4.15.5 Distance

Using remote data capture to visualise the Delabole Quarry 1967 failure face shows that photogrammetry can produce data comparable to traditional methods at large camera to face distances. Tests of minimum data capture distances conducted at the CSM Test Mine were successful. However, only small areas were able to be mapped at each setup position as the equipment had to be positioned close to the face due to the small width of the underground drives.

The maximum distance that photogrammetry can capture geotechnical data from is highly dependent on the focal length of the camera lens used. During this project, photogrammetry has been restricted to the type of lens that is available, 20 mm and 50 mm. Zoom lenses can increase the distance that a rock face can be mapped from, although, similarly to laser scanning, the scale of the fractures held within the rock are a limiting factor. When the project commenced the ability to use zoom lenses with the tested photogrammetric software was not available. So to reduce the amount of lenses to be carried with the rest of the field equipment a decision was made to use only two lenses: a Nikon 50 mm 1:1.4d, and a Nikon 20 mm 1:2.8d. The choice of the 50 mm lens was made with advice from George Poropat as it provided the greatest versatility when capturing images at close to medium range distances (Poropat, 2005).

4.15.6 *Costs*

The cost of the laser scanning hardware causes the technique to be more expensive than photogrammetry, even though the geotechnical analysis software programs are of similar cost. However, some projects have budgets large enough so that price is not a deciding factor when choosing a suitable mapping system.

4.15.7 *Access*

Both remote data capture techniques suffer from access problems. Obstructions can be overcome by smoothing during photogrammetric 3D image creation or by deletion of erroneous sections from a point cloud. Oblique views of the study face reduce the accuracy and the number of features that can be made. Photogrammetric setups must be as close to perpendicular as possible to the study face to ensure a maximum volume of orientation data. Also conducting multiple laser scans of a face will enable the visualisation of all of the discontinuity features. It has also been shown that the overall accuracy of orientation data taken from three laser scans, opposed to just one, results in increased accuracy.

4.15.8 *Environmental and Timing Considerations*

Photogrammetric and laser scanning equipment can withstand adverse atmospheric conditions, although this can affect the data that is captured. Laser scanning should not be used in conditions where moisture can come into contact with the window of the scanner. Cameras can be protected from precipitation until a photograph must be taken, although similar lighting conditions between the first and second photo must be maintained. Conditions in which there are large temperature variations must also be avoided so to not damage equipment due to condensation.

Fieldwork processes are rapid when using remote data capture techniques. They take half the time than traditional hand-mapping to map 100 features. There is little difference between laser scanning and photogrammetry field times. Photogrammetry takes slightly longer due to the processing required to produce a 3D model.

4.15.9 *Image Processing*

Photogrammetric 3D images with excessive distortion are identified by visual examination after the image creation process has completed. The sections that cause the distortion can be removed at the 3D image task setup stage by reducing the image size and/or shape. The resultant 3D images will not be affected by those areas and

are suitable for geotechnical analysis. Manual delineation of planes and discontinuity traces is preferred to the automatic methods (for both Sirojoint and SplitFX). This allows for the manual selection of comparable features with similar feature geometries (area/ length) ensuring a more direct comparison between the mapping techniques, covered in Chapter 5.

It was found that calculating spacing within SplitFX was possible using the 'measure distance' tool, although it was considered to be too time consuming and was not carried forward into the data analysis assessment in Chapter 5. As SplitFX cannot calculate discontinuity trace length from laser scan point clouds it is not compared between the remote data capture techniques. Trace lengths collected by traditional mapping using digital photographs (analogous to the SplitFX method of trace length measurement) can be compared to discontinuity trace lengths captured from photogrammetric 3D images. This will be conducted in the next chapter. DIPS (Rocscience, 2006) is preferred to the stereographic programs contained within the software of the remote data capture systems because of its relative ease of use and, as it is the industry standard, compatible with many other applications. DIPS is used as the stereographic analysis program for this thesis.

5 DATA OUTPUT / ANALYSIS PROCESSES

5.1 Introduction

Chapter 5 concentrates on the data output by the remote mapping techniques (Figure 5-1). It will make use of the pole vector error calculation technique described in Chapter 4. This chapter compares the parameters that can be measured using remote data capture techniques. This will test the ability for photogrammetry and laser scanning to provide data that is equivalent to data gathered using traditional methods. This chapter aims to show that the data output by remote mapping techniques can be comparable and as accurate as traditionally captured hand-mapping data.

The first section describes the site and field work undertaken at the Tremough Campus road cutting used for the subsequent analysis. The early sections address the geotechnical data analysis. The accuracy of the orientation data is assessed using the pole vector error calculations. The individual orientation accuracy of each mapped plane is assessed before calculating the error between the set data collected by each mapping technique. Analysis of the orientation accuracy of discontinuity traces is then covered, after which the comparison between discontinuity trace lengths are made between photogrammetry and traditional mapping techniques. The roughness measurements made by each remote mapping technique are assessed for correlation with hand-mapped joint roughness coefficient (JRC) values. The effect of roughness on orientation measurement is then undertaken.

The data collected by the remote mapping techniques can be split between geotechnical data, the digital elevation model data, and visual data end-uses. As the remote data capture techniques collect various types of data it is important to understand the potential extra post processing that is required to be able to use this data for multiple end uses. These end uses for the data captured by photogrammetry and laser scanning, and the work required to utilise the remotely captured data, is covered in the final section of this chapter.

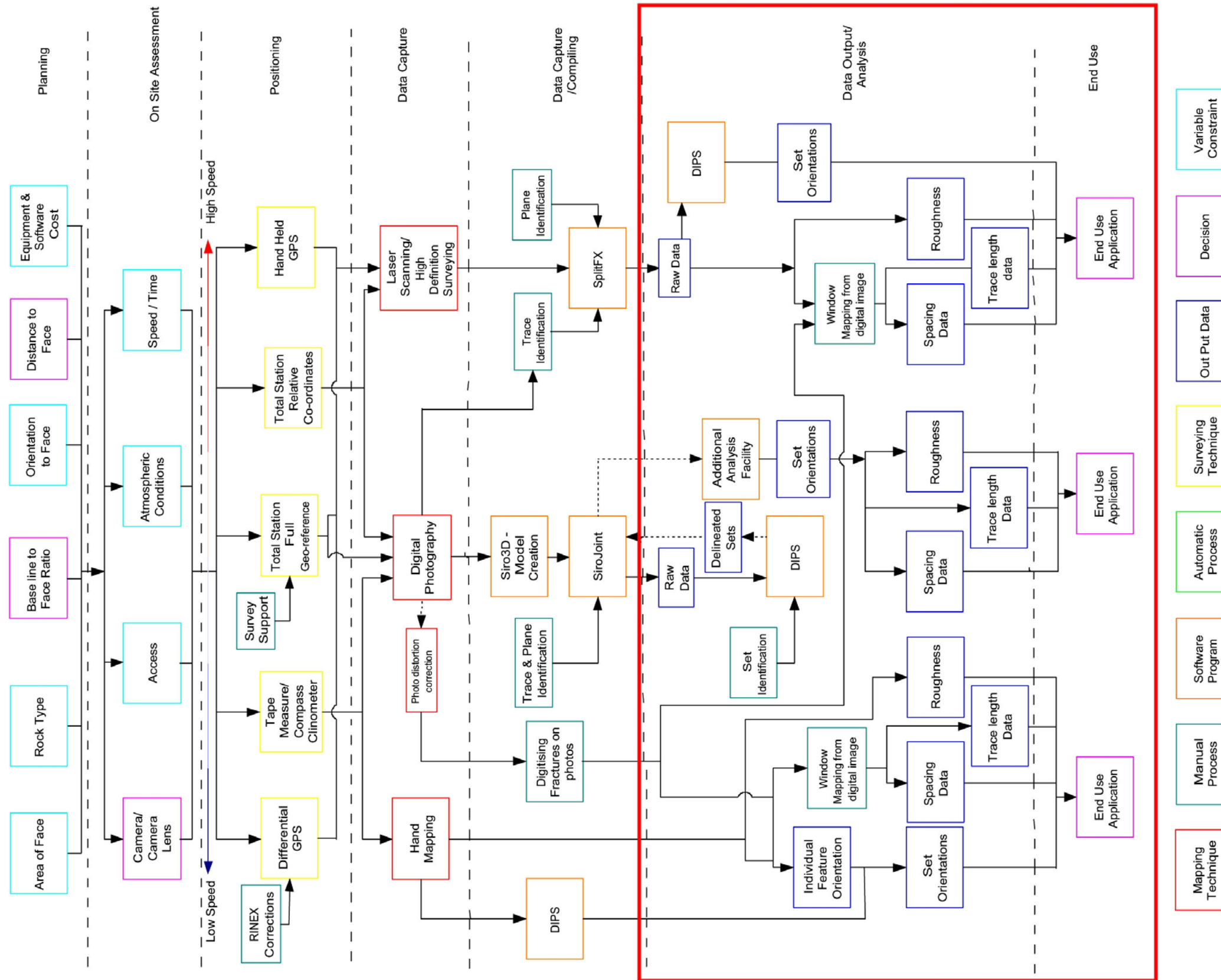


Figure 5-1. Process work-flow diagram - indication of sections covered in Chapter 5 (red box).

5.2 Tremough Campus Road Cutting Overview

5.2.1 Road Cutting Geographical Location and Geology

The road cutting at the entrance to the Tremough Campus, Penryn, Cornwall, UK, shown in Figure 5-2 and Figure 5-3, was selected as a suitable location for accuracy comparison of planar features between the remote mapping techniques over a short target range because of proximity to the University Campus (for repeated visits) and its relatively blocky structure, shown in Figure 5-4. Trace orientations were not assessed, as currently SplitFX (Split Engineering, 2005) necessary for post-processing laser scanning data, is unable to calculate discontinuity trace dip and dip direction from 3D point clouds.

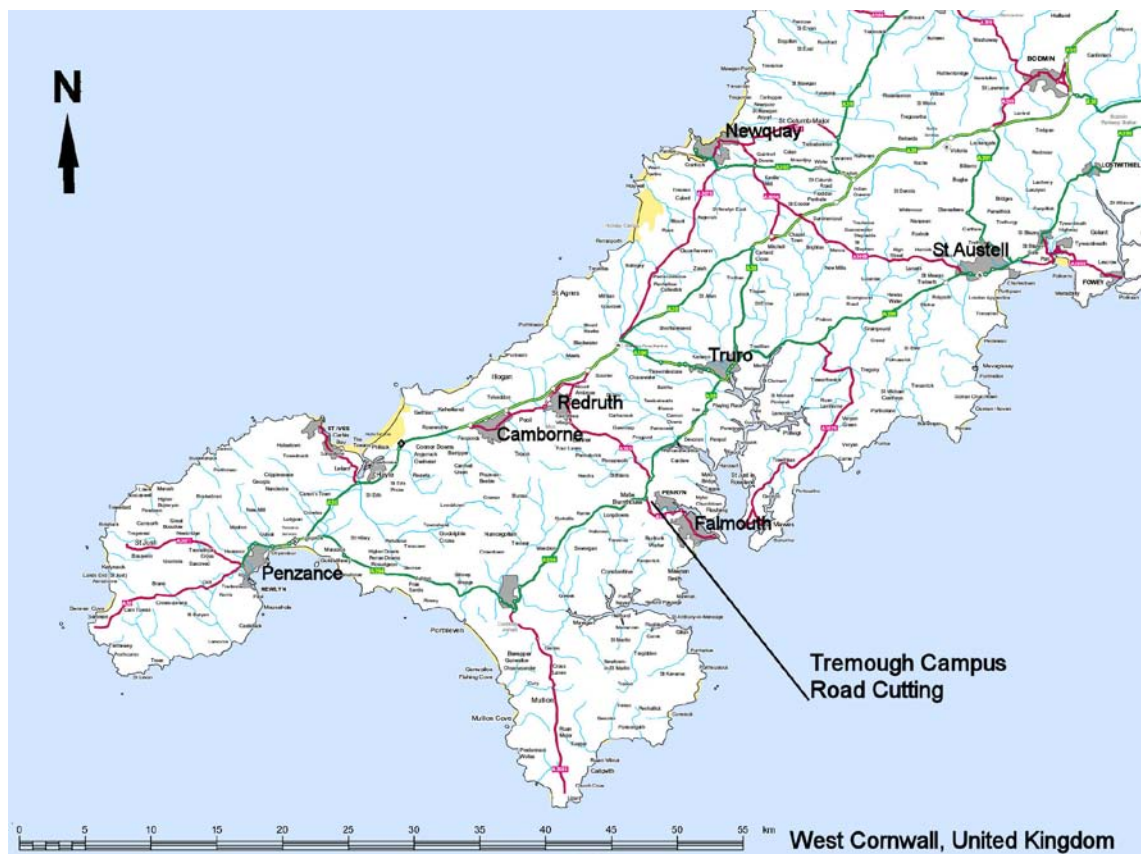


Figure 5-2. Map of West Cornwall, UK, showing location of Tremough Campus road cutting. © Crown Copyright/database right 2009. An Ordnance Survey/EDINA supplied service.

The rock face at the Tremough road cutting was first exposed in 2003 and is composed of coarse grained Carmenellis granite, with two steeply dipping joint sets and two moderately dipping joint sets. One large singular sub horizontal feature dips at approx 20° to the NE. The face dips between 45° - 65° and curves between strikes of WNE – SSE (western side) to ENE – SSW (eastern side). It is moderately weathered and some debris has collected on the gently dipping features.

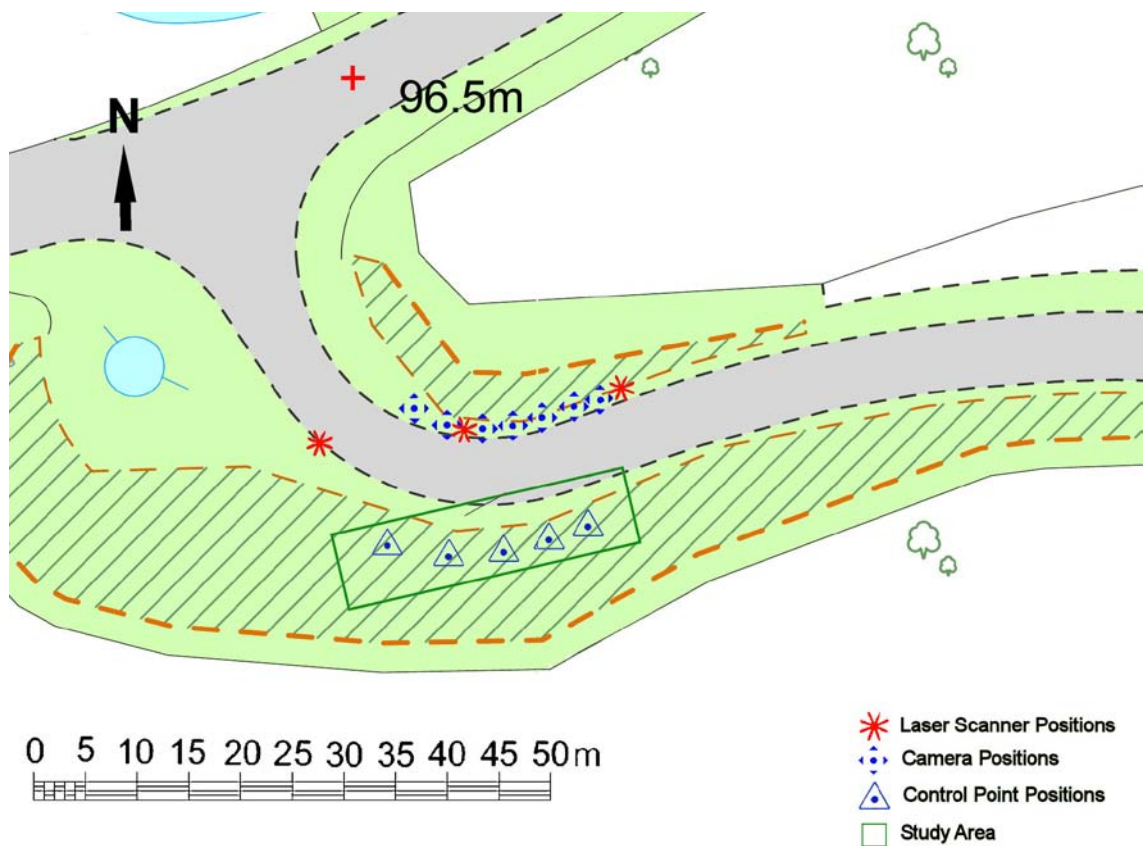


Figure 5-3. Map showing layout of photogrammetric and laser scan setup positions, Tremough, Cornwall, UK. © Crown Copyright/database right 2009. An Ordnance Survey/EDINA supplied service.

The mapped section of the granite rock face is approximately 35 m long and ranges from 5 m to 8 m in height. Few access problems were encountered for either of the two remote sensing techniques, but hand-mapping was restricted to only areas of the face that could be safely reached. Hand-mapping was carried out irrespective of weather, whereas the photogrammetry and laser scanning were performed during ‘dry’ periods. Photogrammetry was the first technique used to map the road cutting, followed by detailed hand-mapping and finally laser scanning. Individual features were specifically identified so as to perform a feature-by-feature comparison for the different techniques used.



Figure 5-4. Image showing blocky nature of the granite rock mass at the Tremough Campus road cutting (3 m wide, 2.5 m high rock face, looking south).

Photogrammetry Field Work

Five photogrammetric models were created of the road cutting, moving from west to east (Table 5-1). Each model slightly overlapped the former and was approximately 8 m wide. The height encompassed all of the exposed features of the rock face (5 m – 6 m). The camera stations were set up approximately 15 m from the rock face.

The cameras were positioned using the Leica TPS1200 Total Station to a relative or local eastings, northings and elevation coordinate system. The first camera location was assigned arbitrary coordinates of 1000 m, 1000 m, 100 m. This location was then geo-referenced using a handheld GPS unit. The photogrammetric control point was then surveyed at the centre of the views of the face from both of the cameras. Subsequently, for each new model setup, the respective camera locations and control points were coordinated relative to the origin.

The digital photographs were then uploaded into the 3D image creation module of the Sirovision software suite, Siro3D (CSIRO, 2005). The images were corrected for a 50 mm lens distortion and orientated using the surveyed positional data. The subsequent 3D models were then imported into geotechnical analysis module of the Sirovision software suite, Sirojoint (CSIRO, 2005), for further analysis and interpretation.

Table 5-1. Locations of photogrammetry camera and control point setups at the Tremough Campus road cutting, Cornwall, UK, indicating model and lens used.

GB National Grid (m)					
Eastings	Northings	Elevation	Camera / Control Point	Model	Lens
176886	34937.5	96	Camera 1	Model 1	20 mm
176884.1	34938.49	95.792	Camera 2		
176880.4	34926.08	96.706	Control Point A		
176886	34937.5	96	Camera 3	Model 2	20 mm
176889.2	34938.06	97.697	Camera 4		
176888	34926.34	96.284	Control Point B		
176891.6	34936.26	98.63	Camera 5	Model 3	20 mm
176895	34936.25	98.63	Camera 6		
176893.6	34921.26	96.284	Control Point C		
176895	34936.25	98.63	Camera 7	Model 4	20 mm
176898.2	34936.82	98.45	Camera 8		
176897	34925.09	97.037	Control Point D		
176898.2	34936.82	98.45	Camera 9	Model 5	20 mm
176902	34936.81	98.44	Camera 10		
176900.3	34921.29	96.039	Control Point E		

Hand-mapping Field Work

In order to assist identification of common features between the hand-mapped data and the remotely captured data, hand-mapping of the rock face was undertaken with the aid of digital photographs, and orthophotos showing the features identified using the photogrammetric software. The face was mapped using a standard compass clinometer using the techniques described in Section 3.6.3. A ladder was employed to aid in reaching some of the less accessible areas.

Laser Scanning Field Work

The same section of the rock face was then scanned from three separate locations using the Leica HDS3000 (Table 5-2). The locations were set up 10 m from the face, each viewing an equal portion of the rock face from differing angles, to eliminate blinding. A manually set point density of 6 mm was chosen for the scan.

The captured data points were then exported by the Leica software into the point cloud geotechnical analysis program, Split FX (Split Engineering, 2005) for subsequent analysis. Manual hand-delineation of features was undertaken for the orientation accuracy analysis. The discontinuities mapped from the point cloud were delineated as the same area and shape as the planes identified by photogrammetry wherever possible.

Table 5-2. Locations of laser scanner setup positions at the Tremough Campus road cutting, Cornwall, UK, indicating the model and scan density used.

GB National Grid (m)			Laser Scanner Type	Model	Density
Eastings	Northings	Elevation			
176875	34934	96	Leica HDS3000	Model 1	6 mm at 10 m distance
176905.5	34937.5	95.5		Model 2	6 mm at 10 m distance
176888	34938	95.8		Model 3	6 mm at 10 m distance

Photogrammetry versus Laser Scanning

A comparison between the resulting photogrammetric 3D mesh and laser scanned point cloud is shown in Figure 5-5. A summary of the number of discontinuities identified by the various techniques is given in Table 5-3 and pole orientations shown in Figure 5-6, Figure 5-7 and Figure 5-8.

Table 5-3. Number of planar features identified using each mapping technique.

Hand Mapping	Photogrammetry	Laser Scanning
153	283	280

Overall there is reasonable correlation between the measured and extracted orientations. It was expected that hand-mapping would identify the least number of features in view of the restricted area of the face that could be safely reached. A clear advantage of the remote systems is their ability to capture data for the whole rock face. Using three laser scans, all but three features identified by photogrammetry were recognised by laser scanning.

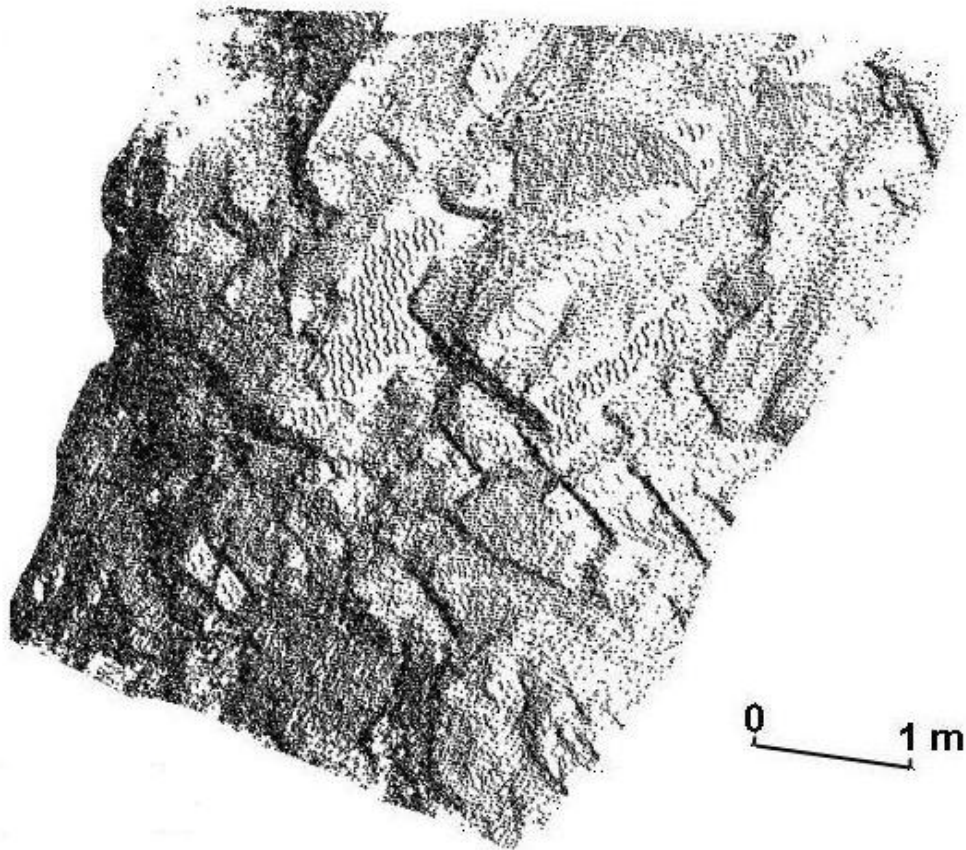
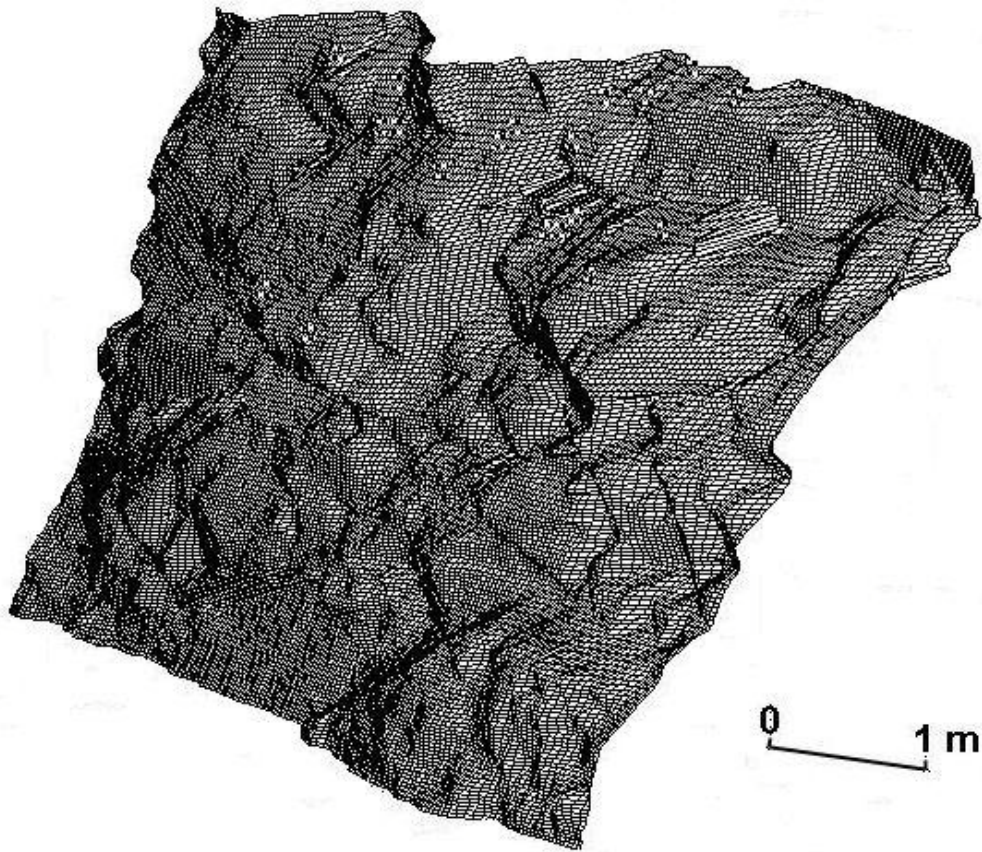


Figure 5-5. Comparison between photogrammetric mesh (top) and point cloud (bottom) taken from Tremough Driveway (view orientated SE).

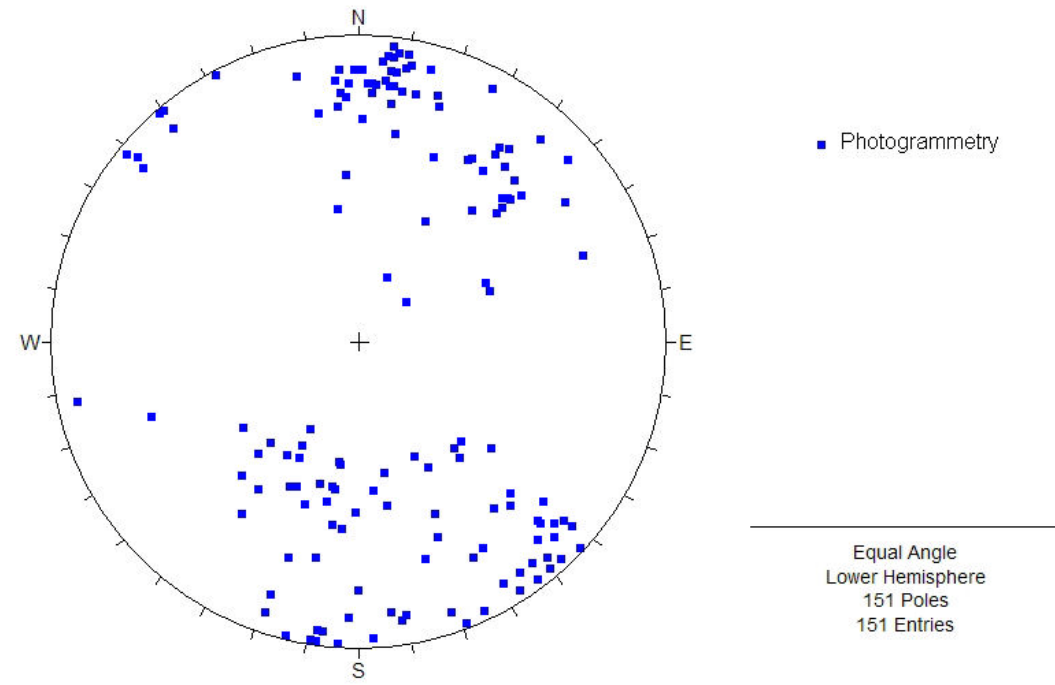


Figure 5-6. Lower hemisphere stereonet showing photogrammetrically captured orientation data.

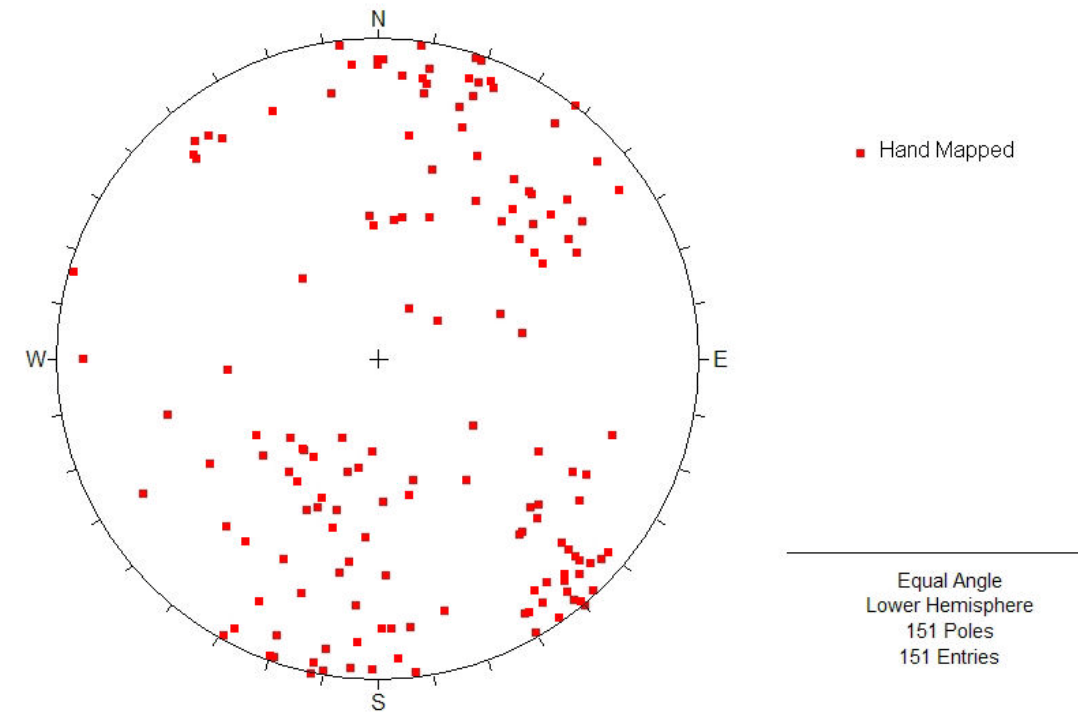


Figure 5-8. Lower hemisphere stereonet showing hand-mapping captured orientation data.

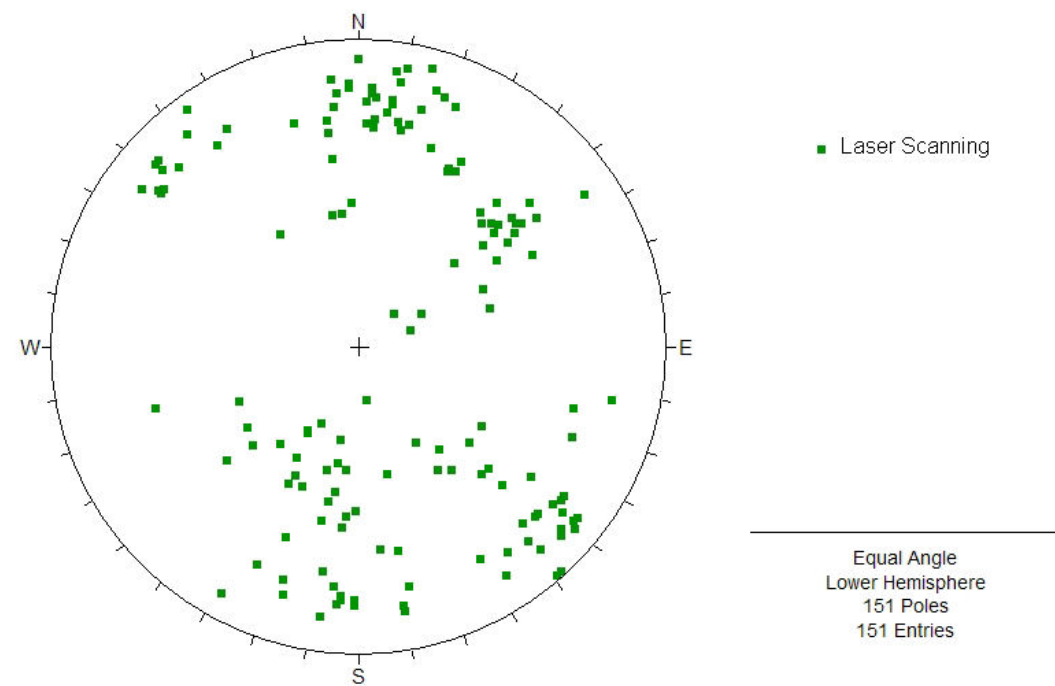


Figure 5-7. Lower hemisphere stereonet showing laser scanning captured orientation data.

5.3 Orientation Comparison

5.3.1 Individual Feature

Comparisons between the dip and dip direction of each feature were undertaken by calculating the pole vector difference, described in Chapter 4. Comparisons were undertaken on 151 features that could be identified and correlated across each of the mapping techniques. The data analysis was then undertaken comparing each mapping technique. Table 5-4 shows the average pole vector difference from hand-mapping taken from each individual feature identified on the rock face.

Table 5-4. A comparative table showing the average pole vector difference and standard deviation between each mapping technique. Data has been split into discontinuities dipping below and above 47°.

	Pole Vector Difference		
	Photogrammetry / Laser scanning	Hand-mapping / Laser scanning	Photogrammetry / Hand-mapping
0.5° - 47° Average	10.11°	13.76°	15.65°
0.5° - 47° S.D.	11.47°	11.98°	15.86°
48° - 90° Average	10.68°	11.74°	11.98°
48° - 90° S.D.	8.66°	9.23°	10.03°
Total Average	10.61°	11.96°	12.39°
Total S.D.	8.91°	9.49°	10.77°

Both photogrammetry and laser scanning have an average pole vector difference from hand-mapping of around 12° for individual features, although the standard deviation is 11° and 10° respectively. Laser scanning and photogrammetry have a smaller pole vector difference between one another of 11°, and a smaller standard deviation of 9°. These values are slightly less than the PDV value of 13.75° produced from comparing two hand-mapping studies at Penlee Quarry (Section 4.2.2). The standard deviations are also lower than the Penlee Quarry data (17.38°). The data split between features dipping above and below 47° showed differing statistics. The average PVD (and standard deviation) between hand-mapping and the remotely mapped data was higher for the shallower dipping features, ~2° for laser scanning, and ~3° for photogrammetry. The average PVD of the shallow dipping features was lower than the steep discontinuities for the compared remote mapping data, with little difference at all (~0.5°).

The pole vector difference of each plane was then plotted against the area of the identified feature, shown in Figure 5-9. Comparison of these values provided an indication of the relative accuracy of each technique at a range of plane sizes.

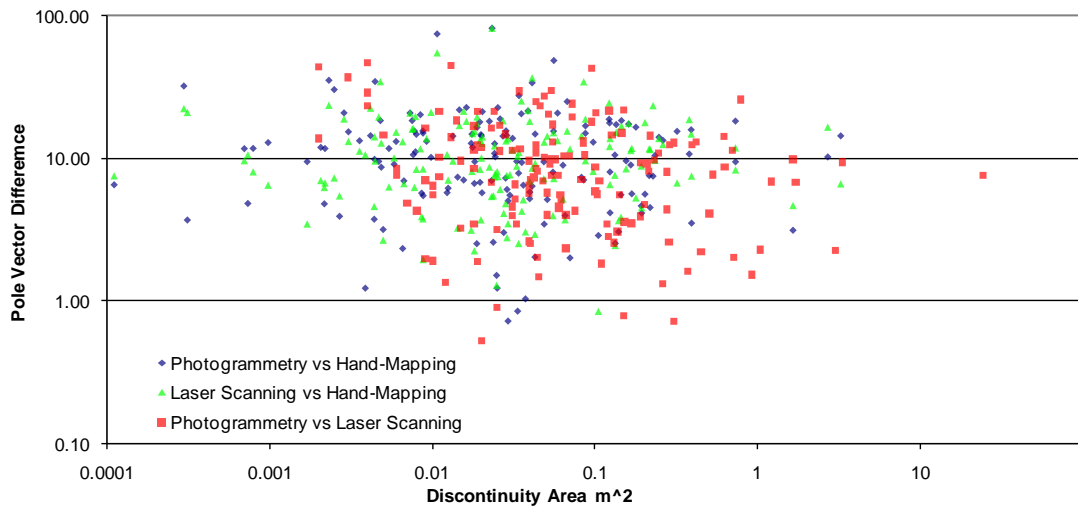


Figure 5-9. Pole vector difference for remotely captured data compared with hand-mapped orientation as a function of area of the identified fracture plane (measured using photogrammetry). Plotted on log-log axes.

A larger discontinuity area allows for a higher amount of positioned 3D points/mesh to be present representing that feature; it was expected that larger discontinuities would produce the lowest pole vector differences when compared between mapping techniques. The majority of mapped features were small (<0.05 m²), but Figure 5-9 shows that the majority of the data points have a pole vector difference below 20°. Increasing the size of the measured discontinuity decreases the likelihood that the PVD moves above 20°, indicating that large plane areas will ensure that the orientation measurements are closer to the measurement of the compared mapping technique. A suggested reason for the few anomalously high (70° - 85°) pole vector differences, indicating that the mapping techniques are measuring the discontinuities to be nearly orthogonal to one another, is that the features were misidentified during mapping because of their small area. The fitted trend-line shows that there is little correlation between pole vector difference and discontinuity area indicating that even a small number of positional points on a discontinuity plane can produce an accurate measurement.

5.3.2 Set Comparison

The comparative orientation data from each mapping technique was also analyzed separately using the stereographic projection program, DIPS (Rocscience, 2006), to identify potential sets for the respective data. Four comparable sets were identified for each data group using both polar and contoured stereographic plots. The pole vector differences between the corresponding sets for each remote technique and the data from hand-mapping were calculated and are displayed in Figure 5-10, Figure 5-11, and

Figure 5-12, summarized in Table 5-5. The same contour interval has been used for each stereographic plot to aid in comparison.

Table 5-5. Set analysis for comparative data collected from Tremough Road Cutting. Each mapping technique is compared with one another. Fisher K and number of poles within each set are included in the set statistics.

Hand Mapping				Photogrammetry				
Dip	Dip Direction	No. of Poles	Fisher K	Dip	Dip Direction	No. of Poles	Fisher K	PVD
88°	320°	28	98.71	86°	319°	28	73.29	2.24°
89°	190°	41	42.63	85°	185°	47	66.89	6.40°
67°	230°	15	88.33	72°	221°	19	67.01	9.80°
45°	026°	17	37.78	52°	021°	21	38.17	7.93°

Hand Mapping				Laser Scanning				
Dip	Dip Direction	No. of Poles	Fisher K	Dip	Dip Direction	No. of Poles	Fisher K	PVD
88°	320°	28	98.71	87°	314°	33	42.84	6.08°
89°	190°	41	42.63	85°	186°	44	29.53	5.65°
67°	230°	15	88.33	63°	231°	16	150.04	4.10°
45°	026°	17	37.78	47°	020°	20	33.16	4.76°

Photogrammetry				Laser Scanning				
Dip	Dip Direction	No. of Poles	Fisher K	Dip	Dip Direction	No. of Poles	Fisher K	PVD
86°	319°	28	73.29	87°	314°	33	42.84	5.09°
85°	185°	47	66.89	85°	186°	44	29.53	1.00°
72°	221°	19	67.01	63°	231°	16	150.04	12.89°
52°	021°	21	38.17	47°	020°	20	33.16	5.06°

The average set pole vector differences from traditional mapping for photogrammetry and laser scanning were 6.6° and 5.1° respectively. The photogrammetric sets average PVD from laser scanning was 6.01°. The maximum remote data capture set pole vector error from the hand-mapped data from the Tremough road cutting was found with set 3 (dipping SW, 67°/230°, hand-mapped data), at 9.80° difference from photogrammetry. The comparison between the remotely captured sets produced the highest and lowest pole vector difference, 1.00°, and 12.89°. Photogrammetry also had the closest match (2.24°) to hand-mapping with the steeply dipping set 1.

The Fisher K values (Fisher, 1953) were calculated for each set using DIPS (Rocscience, 2006). The highest average Fisher K values, indicating a tight data cluster around the mean orientation, were for set three (dipping 63° - 72°). Set one and two, the steeply dipping sets (~88°), had differing Fisher K values. The E – W striking set had lower K values than the NE – SW striking set for each mapping technique. The lowest Fisher K values resulted from the shallowest dipping set, set four. The average Fisher K values across each set for each mapping technique were; hand-mapping, 66.68, laser scanning, 63.89, and photogrammetry, 61.34. The average set pole vector difference was 5.14° from laser scanning and 6.6° from photogrammetry, 5.87° average overall between remotely mapped and hand-mapped data.

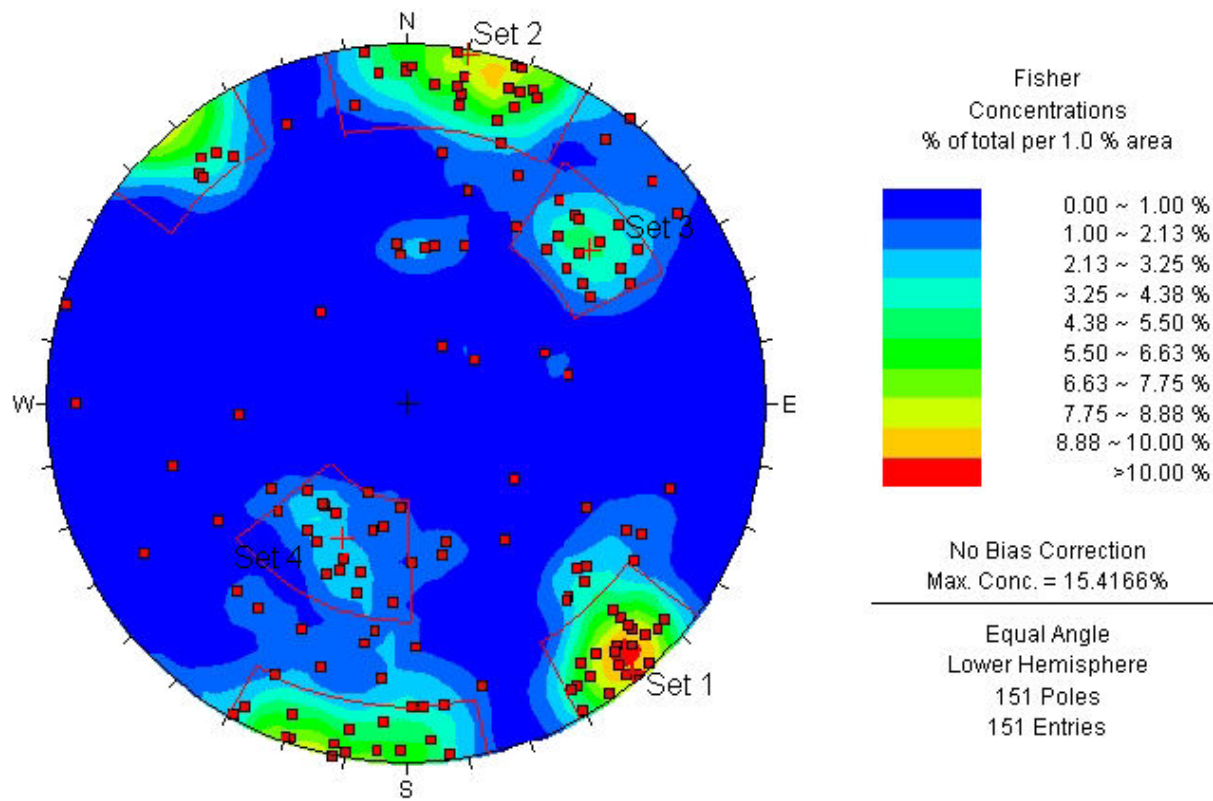


Figure 5-10. Stereonet showing set analysis on hand-mapped data.

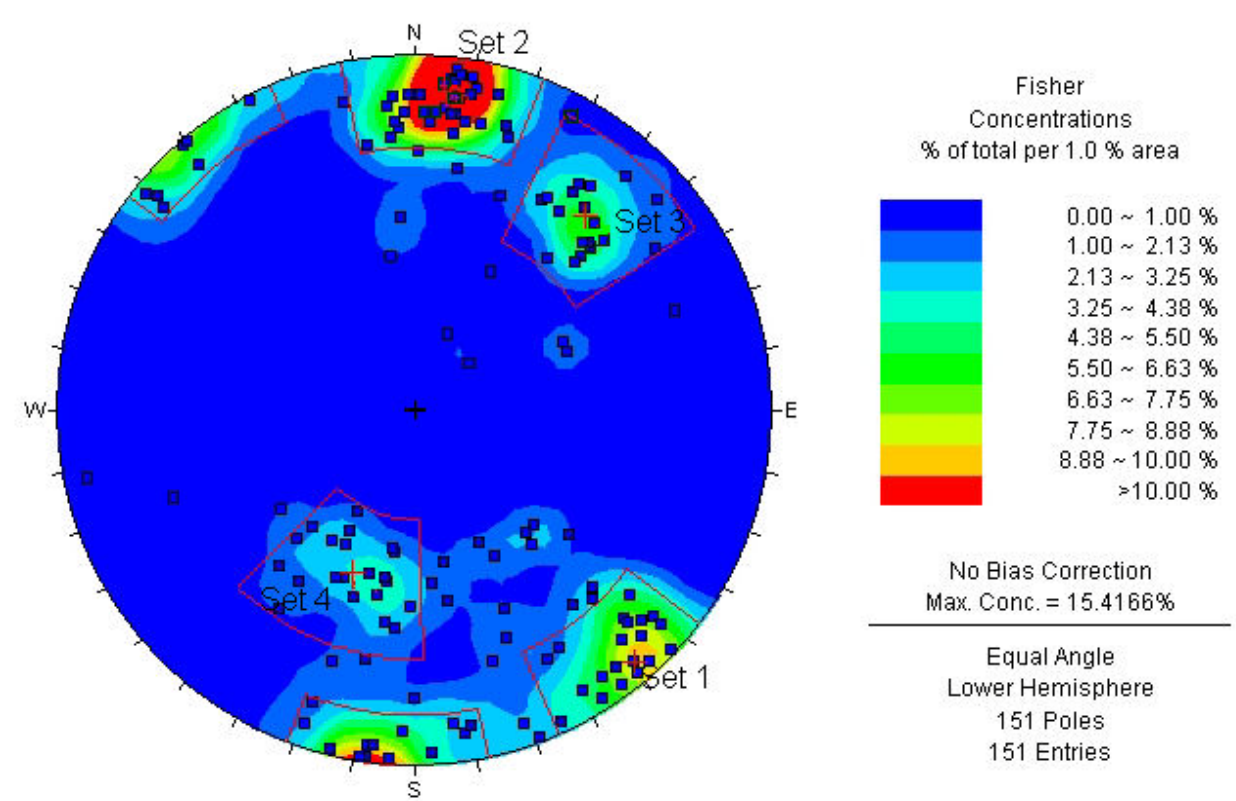


Figure 5-11. Stereonet showing set analysis on photogrammetrically mapped data.

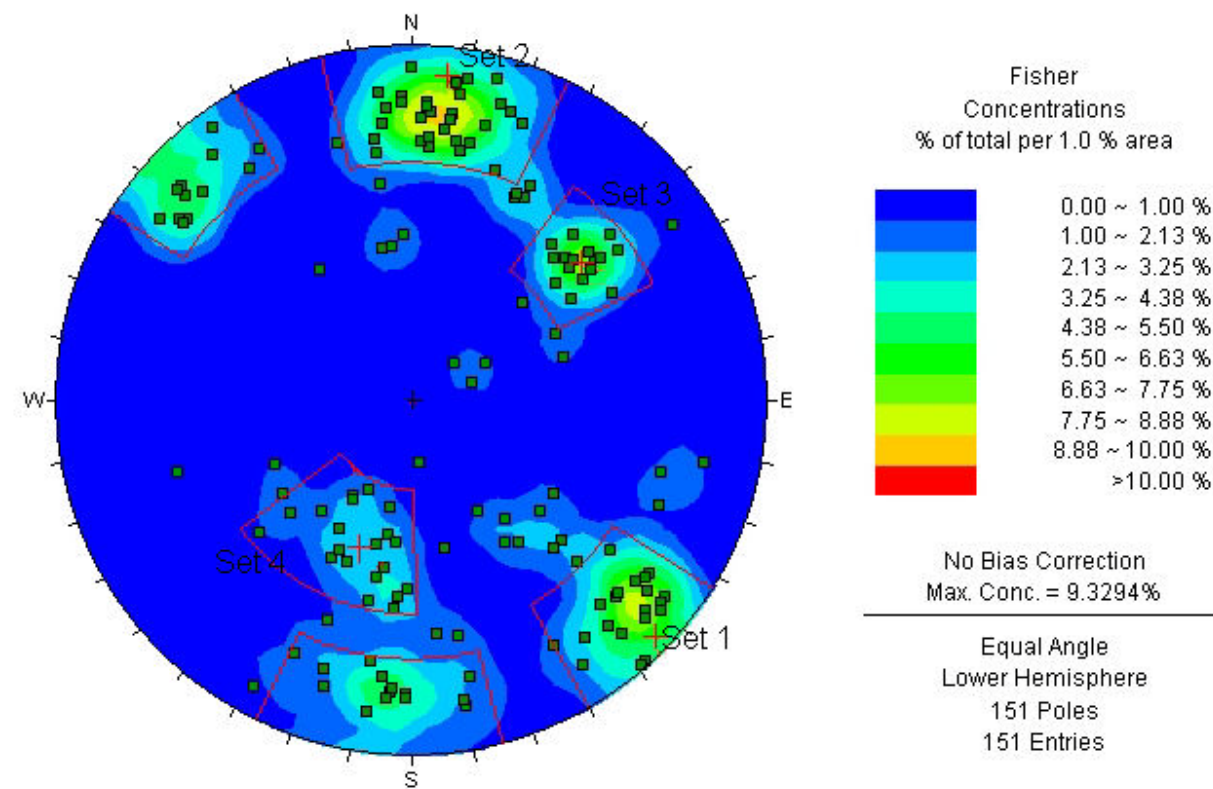


Figure 5-12. Stereonet showing set analysis on laser scanned mapped data.

5.4 Trace Analysis

5.4.1 Trace Orientation Analysis

The Sirovision User Manual (CSIRO, 2005) recommends that care should be taken when using discontinuity traces for capturing orientation, as some ambiguous data could be produced. To test this potential problem, photogrammetric orientation data was taken from a plane, and its corresponding discontinuity trace (Figure 5-13). The mapping was undertaken at the Tremough Campus Road cutting, Penryn, Cornwall, UK as the rock face allowed for the identification of multiple planar features as well as their corresponding discontinuity traces.

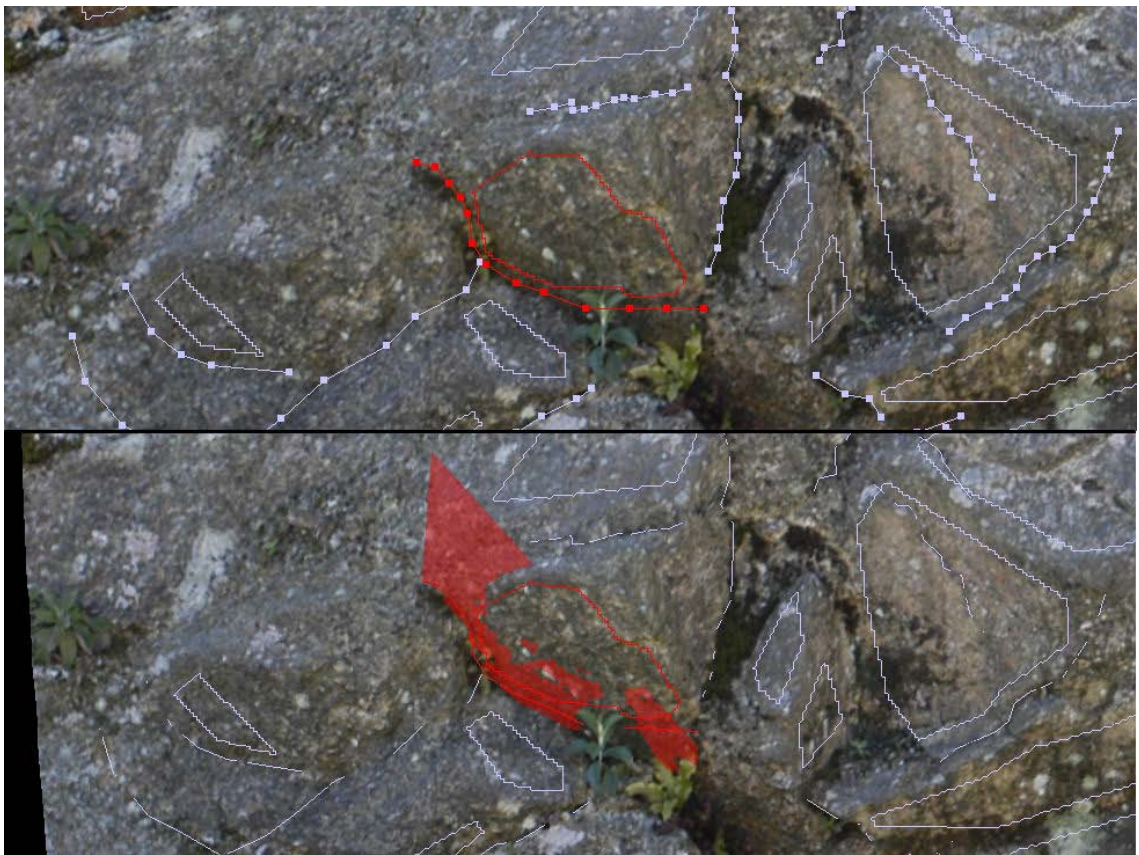


Figure 5-13. Above: 2D orthoimage with discontinuity trace and plane highlighted red. Below: corresponding 3D image showing plane fitted to discontinuity trace.

Multiple plane and discontinuity trace orientations were tested against their hand-mapped equivalents using the pole vector difference calculation (appendix DVD). The results are collated in Table 5-6.

Table 5-6. Plane and discontinuity trace pole vector differences from hand-mapping.

Hand Mapped		Plane Orientation			Trace Orientation			
Dip	Dip Direction	Dip	Dip Direction	PVD from Hand	Dip	Dip Direction	PVD from Hand	
86°	312°	88°	317.3°	5.66°	78.3°	329.1°	18.59°	
85°	228°	76.4°	216.4°	14.31°	24.2°	351.2°	81.71°	
88°	321°	77.9°	332.2°	15.01°	80.3°	113.1°	30.15°	
83°	319°	85.2°	139.3°	11.8°	76°	114.5°	32.13°	
89°	320°	88.5°	323.8°	3.83°	80.9°	125°	18.04°	
60°	230°	59.5°	221.6°	7.27°	54°	247.3°	15.67°	
48°	190°	57.4°	176.5°	14.24°	25.3°	93.4°	55.36°	
21°	212°	23.5°	230.3°	7.33°	17.4°	267.3°	17.85°	
85°	329°	63.4°	335.9°	22.58°	53.6°	65.1°	88.08°	
38°	137°	60.1°	034.2°	74.06°	35.9°	111.6°	15.33°	
90°	320°	88.2°	320.8°	1.97°	51.7°	017.6°	65.13°	
88°	012°	65.2°	227.1°	43.31°	19.3°	299°	82.56°	
80°	145°	89.6°	313.6°	15.39°	80.3°	100.3°	44.01°	
85°	235°	78.6°	236.8°	6.64°	80.7°	239°	5.85°	
85°	317°	88.8°	335.5°	18.86°	87.5°	155.6°	20.04°	
80°	190°	83.5°	187.1°	4.53°	68.3°	195.9°	13.00°	
Average				16.67°	Average			37.72

The standard deviation from the selected planar orientation measurements was 18.3°, where the equivalent traces produced a standard deviation of 28°, just over 150% greater. Additionally the average pole vector difference for planar features is much lower, at 16.67° compared to 37.72° from discontinuity traces, although neither are below the hand-mapping vs. hand-mapping PVD taken from Penlee quarry (13.75°). This indicates that orientations of features taken from discontinuity traces are not as accurate as measurements taken from discontinuities represented as planes. Traces calculate their orientations by calculating a best fit plane through the discontinuity trace, as described in Section 0.0.0. The algorithms used to fit these planes have difficulty with short and straight traces as the number of possible planes increases. Discontinuity features represented as discontinuity traces within the rock mass as the Tremough Road cutting were primarily straight, giving rise to the higher pole vector differences from traditional mapping. This trend was also found at the other localities mapped during this project, so orientations from discontinuity traces were used with care.

5.4.2 Discontinuity Trace Length Analysis

Comparing the discontinuity trace length data taken from photogrammetrically mapped rock faces with the traditional mapping equivalent was undertaken at the Tremough Road cutting, Penryn, Cornwall. The comparison was made between one photogrammetric model and window mapping the same section from a digital photograph (appendix DVD). The digital photograph used was the 'right hand' image

for the photogrammetric model creation so that the same view of the rock face would be mapped. Traces were digitised onto the photograph using image editing software. The digitised discontinuity traces, shown in Figure 5-14, were then scaled and measured using the computer program ImageJ (Rasband, 2007), which is covered in Section 0.0.0. The corresponding area was mapped for discontinuity trace lengths using the Sirojoint photogrammetric software (Figure 5-15). The discontinuity trace lengths were exported as end-to-end lengths.

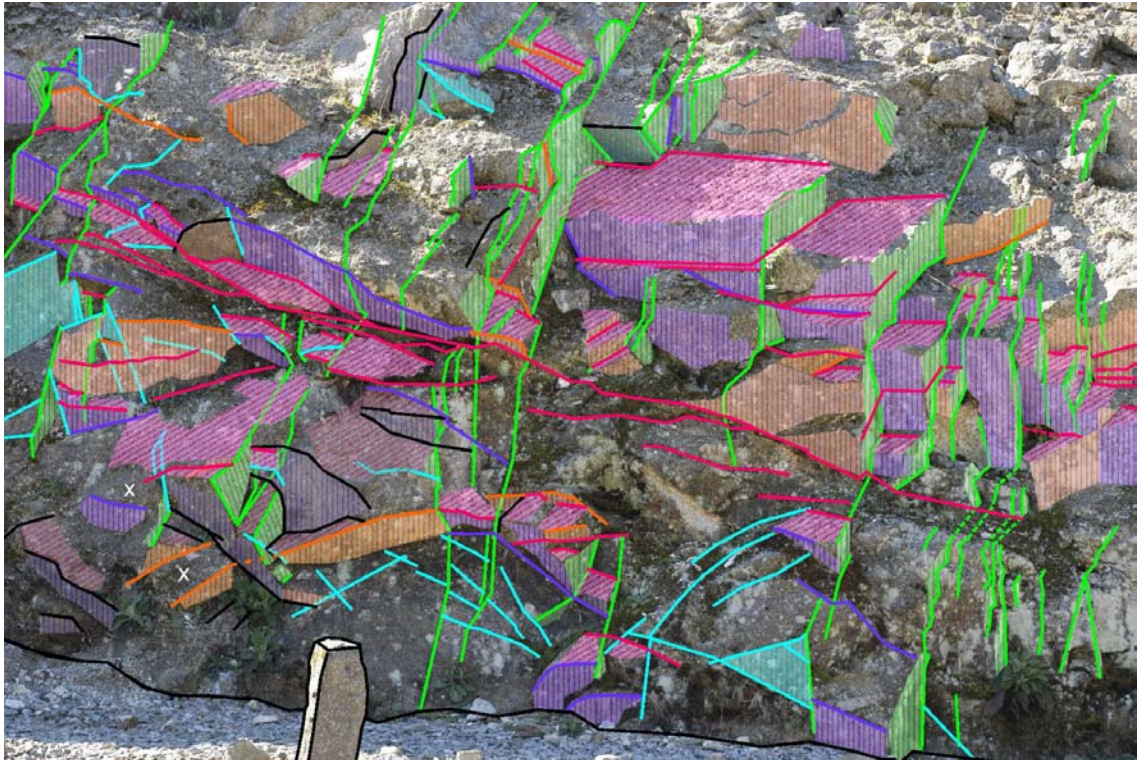


Figure 5-14. Tracelength identification using window mapping from a digital photograph, Tremough Road cutting, Penryn, Cornwall (3 m wide, 2.5 m high rock face, looking south). The discontinuity traces are coloured according to orientation to the rock face. Shaded areas indicate the planes from which the traces are delineated.

The discontinuity trace lengths captured from each technique were compared using their frequency percentage to analyse their distribution across a range of lengths (Table 5-7 and Figure 5-16).



Figure 5-15. Photogrammetric discontinuity trace length identification, Tremough Road cutting, Penryn, Cornwall, UK (~3 m wide, 2.5 m high rock face, looking south).

Table 5-7. Photogrammetric and traditionally mapped discontinuity trace lengths frequency and frequency percentage.

Length Range (m)	Photogrammetry End-to-End Length		Traditionally Mapped ImageJ Length	
	Frequency	Percentage (%)	Frequency	Percentage (%)
0.1	1	0.63	2	1.10
0.2	21	13.13	19	10.44
0.3	41	25.63	29	15.93
0.4	27	16.88	26	14.29
0.5	19	11.88	24	13.19
0.6	9	5.63	18	9.89
0.7	7	4.38	12	6.59
0.8	10	6.25	11	6.04
0.9	3	1.88	9	4.95
1	3	1.88	8	4.40
1.1	4	2.50	4	2.20
1.2	1	0.63	3	1.65
1.3	1	0.63	4	2.20
1.4	2	1.25	1	0.55
1.5	3	1.88	2	1.10
1.6	1	0.63	1	0.55
1.7	2	1.25	1	0.55
1.8	1	0.63	0	0.00
1.9	1	0.63	3	1.65
2	0	0.00	2	1.10
More	3	1.88	3	1.65
Average length	0.54		0.61	

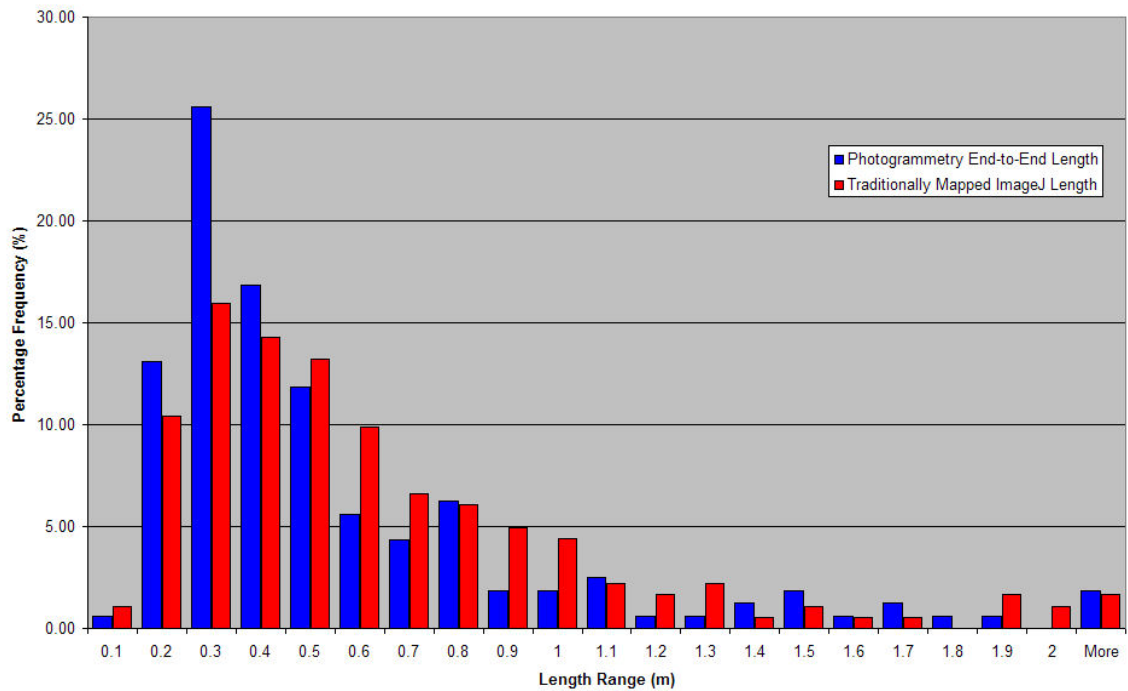


Figure 5-16. Photogrammetric and traditionally mapped discontinuity trace length frequency distribution. Both are positively skewed normal or log normal distributions, although there is some variation in the larger ranges for both photogrammetric and traditional mapping techniques. On average the photogrammetric discontinuity trace lengths were shorter than the traditionally mapped features, 0.54 m and 0.61 m respectively.

A possible reason that the average photogrammetric discontinuity trace lengths are shorter may be due to a step in the 3D image creation process. When the area of 3D image is selected the outer border of the two images is removed as the photographs only overlap by 90% - 95%. For this reason the traditionally mapped image has a slightly larger area covered and the photogrammetric discontinuity trace lengths are, in effect, truncated when near the edge of the 3D image.

5.5 Roughness Analysis

5.5.1 Conversion between Roughness Measurements

Sirovision and Split FX use differing measures of roughness to the conventional terms. Testing the ability for remote data capture systems to describe roughness was conducted on discontinuity planes at the Tremough Campus Road cutting, Penryn, Cornwall, UK as it provides a good range (JRC = 3 – 16). The Sirovision manual has not given a conversion factor between its measurements of roughness and traditional roughness parameters. It is stated that a Sirovision RMS of 0 indicates a perfectly flat surface (CSIRO, 2005), but it does not give an upper boundary. The SplitFX Manual (Split Engineering, 2005) also does not give a conversion factor, but the range of ‘roughness’ outputs are between 0 and 1, 1 being very smooth (Handy, 2007).

Joint roughness coefficients were approximated for a selection of discontinuities situated on the rock face at the Tremough road cutting. The corresponding RMS, variance and roughness values were exported from the photogrammetrically mapped and laser scanned rock face (appendix DVD). The features chosen were all within a similar orientation so to negate variation in photogrammetric and laser scanning accuracy. Table 5-8 gives an example of the readings taken from the rock face (refer to Appendix DVD for full data set).

Table 5-8. Example roughness measurements taken from the Tremough road cutting.

JRC	Laser roughness	Photogrammetry	
		Variance	RMS
14	0.987356	0.33	0.008
8	0.903844	0.09	0.009
12	0.962817	0.35	0.003
12	0.941112	0.08	0.005
8	0.977287	0.16	0.002
8	0.994031	2.04	0.026
3	0.994825	0.02	0.032
5	0.981268	0.19	0.021

Laser roughness, photogrammetric variance and RMS were plotted against the hand-mapped JRC values and assessed for correlation and significance (Figure 5-17, Figure 5-18 and Figure 5-19), which is summarised in Table 5-9.

Table 5-9. Correlation (R) and 95% confidence values of remotely mapped roughness measurements with hand-mapped JRC measurements.

	Laser roughness	Photogrammetry	
		Variance	RMS
N	54	54	54
Critical R (95%)	-0.265	-0.288	0.288
Actual R	-0.163397587	-0.591785777	0.560172158
Confidence	< 95% confident	>95% confident	>95% confident

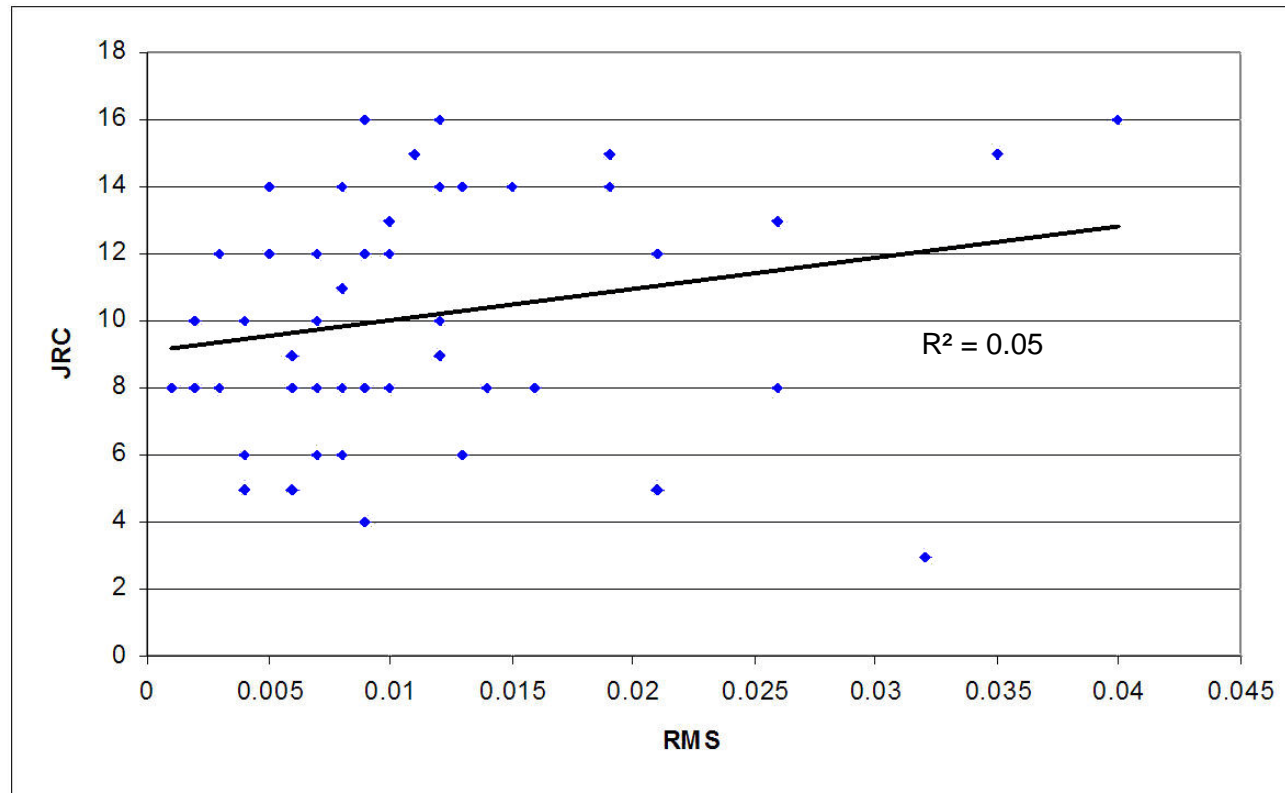


Figure 5-17. Hand-mapped JRC plotted against photogrammetrically mapped RMS showing a weak positive trend.

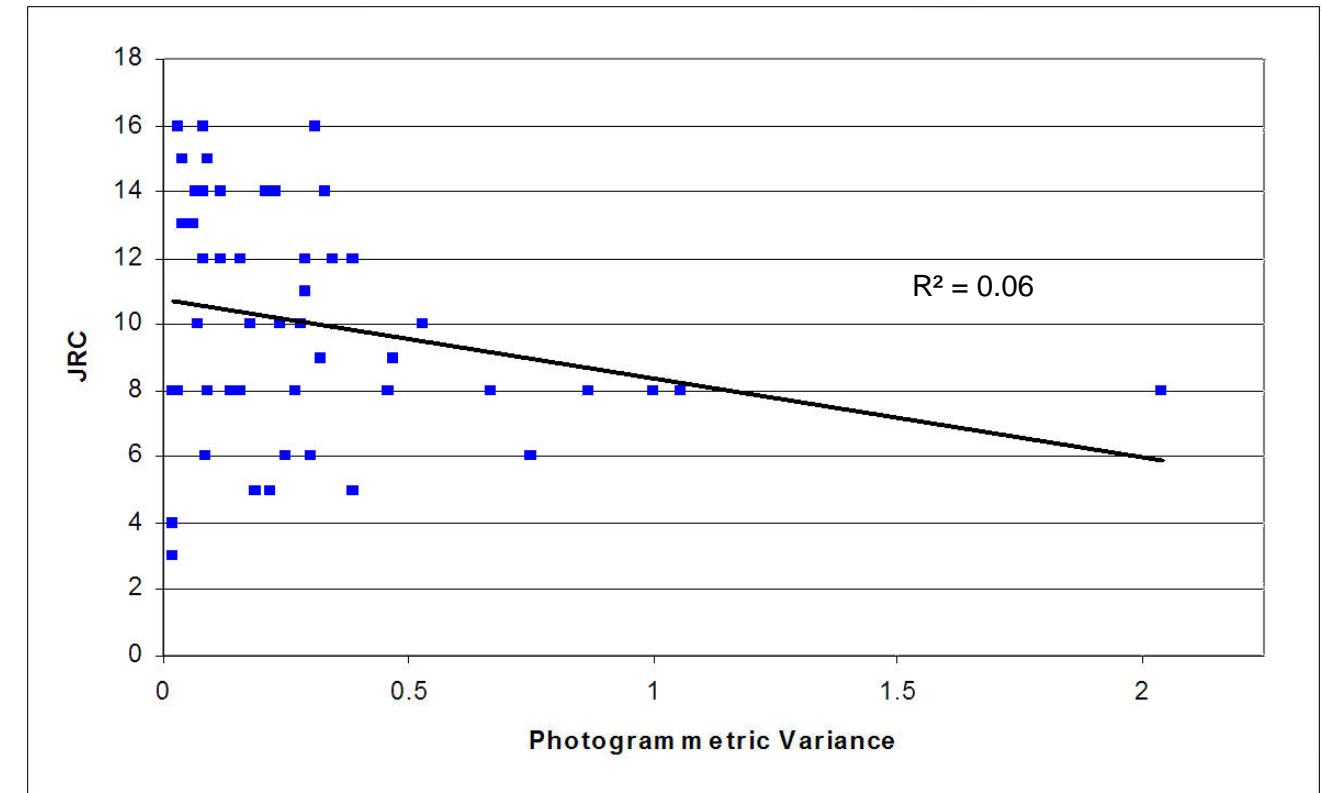


Figure 5-18. Hand-mapped JRC plotted against photogrammetrically mapped variance showing a weak negative trend.

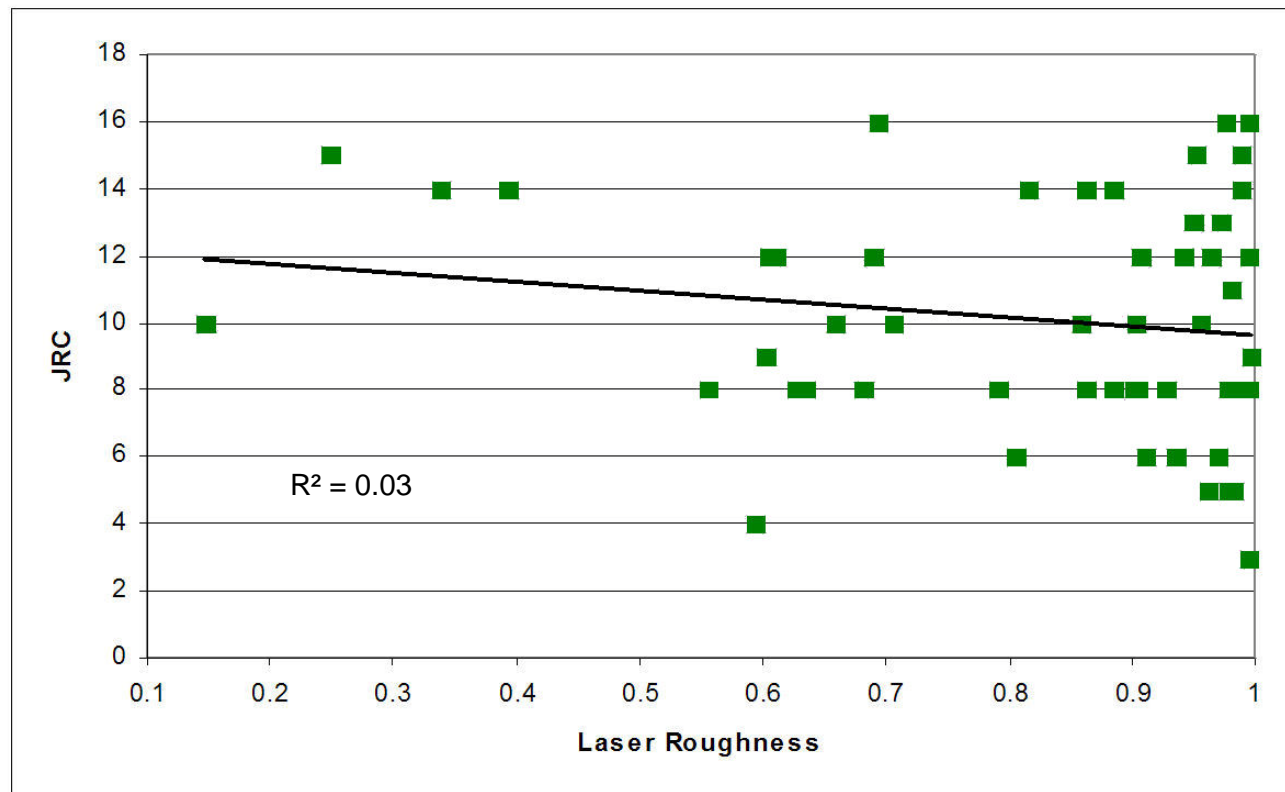


Figure 5-19. Hand-mapped JRC plotted against laser scanned roughness showing a weak negative trend.

All three charts show weak correlations between hand-mapped JRC and remotely mapped measurements of roughness and are statistically insignificant. JRC is a subjective form of roughness measurement and is subject to human bias which may be a reason that the roughness values did not correlate well. Another possible reason that the roughness values did not correlate well was the density of the scan and 3D image, as they were taken to provide models sufficient for orientation measurements. The densities were not high enough to resolve the asperities existing on the surface of the discontinuities.

These remotely mapped roughness values and hand-mapped JRC values were used to form a conversion table between the differing measurements (Table 5-10). This table is not comprehensive as a relatively small amount of data was used to create it, but it forms a useful base to convert remotely mapped measurements into commonly used roughness values.

Table 5-10. Conversion of remotely mapped roughness measurements to JRC values developed from measurements taken from the Tremough Road Cutting.

Laser Roughness	Photogrammetry		JRC
	Variance	RMS	
0.98 - 1.00	>2	0 - 0.001	0 - 2
0.97 - 0.98	1.5 - 2	0.001 - 0.002	2 - 4
0.94 - 0.96	0.5 - 1.5	0.002 - 0.003	4 - 6
0.77 - 0.94	0.05 - 0.5	0.003 - 0.005	6 - 8
0.60 - 0.77	0.016 - 0.05	0.005 - 0.01	8 - 10
0.40 - 0.60	0.005 - 0.016	0.01 - 0.02	10 - 12
0.25 - 0.40	0.0015 - 0.005	0.02 - 0.03	12 - 14
0.10 - 0.25	0.0005 - 0.0015	0.03 - 0.045	14 - 16
0.01 - 0.10	0.00015 - 0.0005	0.045 - 0.05	16 - 18
0.00 - 0.01	0 - 0.00015	>0.05	18 - 20

This table shows that remote data capture methods can be used to calculate roughness, although JRC values between 0 - 2, and 18 – 20, respectively were not measured at the study location. A more complete roughness analysis from closer ranges and higher densities would provide more information to refine the conversion table.

5.5.2 Using Profiles to Characterise Roughness

A method of quantifying roughness from profiles was developed late into the study, so unfortunately has not been fully tested. Poropat (2008) has used the same method to modify a photogrammetric computer program to characterise the roughness of a fracture plane. The process developed during this study is not automated nor incorporated into a computer program so must follow manual steps. It involves the adaptation of the method used by Tse & Cruden (1979), which quantifies roughness

from profiles, and the use of AutoCAD (Autodesk, 2008). The original method uses a profilometer to profile the rough surface. This enables the measurement of the distance (y_i) of the surface from a reference line at specified equal intervals (Δx) over a length of M intervals to calculate a value Z_2 (Tse & Cruden, 1979, cited by Wyllie & Mah, 2004) (Figure 5-20). This coefficient is then used in published equations (Tse & Cruden, 1979, cited by Wyllie & Mah, 2004) to calculate JRC.

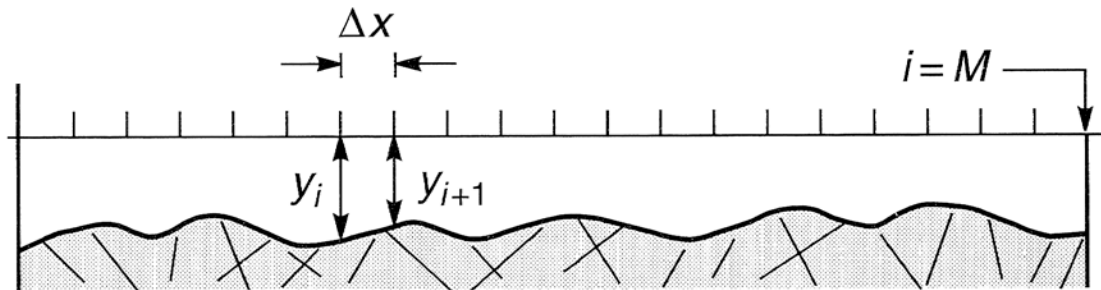


Figure 5-20. Measurement of joint roughness (from Wyllie & Mah, 2004, modified from Tse & Cruden, 1979).

The method developed replaces the use of a profilometer with profiles collected from the photogrammetric and laser scanning 3D images. A 3D section of a discontinuity feature can be cut and exported from the larger 3D model and imported into AutoCAD from the software programs of the remote data capture systems. AutoCAD is used to create multiple 2D profiles from the 3D sections, specifically sections along which any movement is expected. The measurements described in the previous paragraph can be collected and automated so that many can be taken quickly, resulting in a JRC value for the surface. Using AutoCAD the sampling intervals can be varied easily, which would provide a range of JRC values from which an overall average can be calculated.

This method requires that the studied surface has a sufficient number of 3D data points taken so that it is an accurate representation of the real surface. This may require separate scans/photos of the surface, and therefore additional setup locations from close range to ensure a high data density, thus increasing the time in the field. Conversely, using a 3D digital representation to produce 2D profiles rather than using a profilometer increases the speed and the amount of profiles possible for analysis.

This method is also described in Haneberg (2007) where practical use of the technique was used successfully. The new version of Sirovision (CSIRO, February, 2009) has an inbuilt function that allows the Tse & Cruden JRC values and Maerz JRC values (Maerz, *et al.*, 1990) to be calculated from discontinuity planes (Poropat, 2008).

5.5.3 Scale of Roughness Affecting Orientation measurements

A single large fracture plane (JRC=4) was modelled and examined to assess the effect of roughness on the variation of orientation measurement using photogrammetry and laser scanning (appendix DVD). Within both photogrammetry and laser scanning geotechnical analysis programs, virtual boxes, split into 16 equal sections, were superimposed on the study plane as depicted in (Figure 5-21). The orientation of each individual section was recorded. Subsequently the boxes were split into 8 equal sections, then four, and finally the orientations for each entire box were measured. Each individual box will have a slight change in orientation from the average of the largest box. This provides a scatter of orientations around the average, representing the orientation variation due to roughness (Figure 5-22).

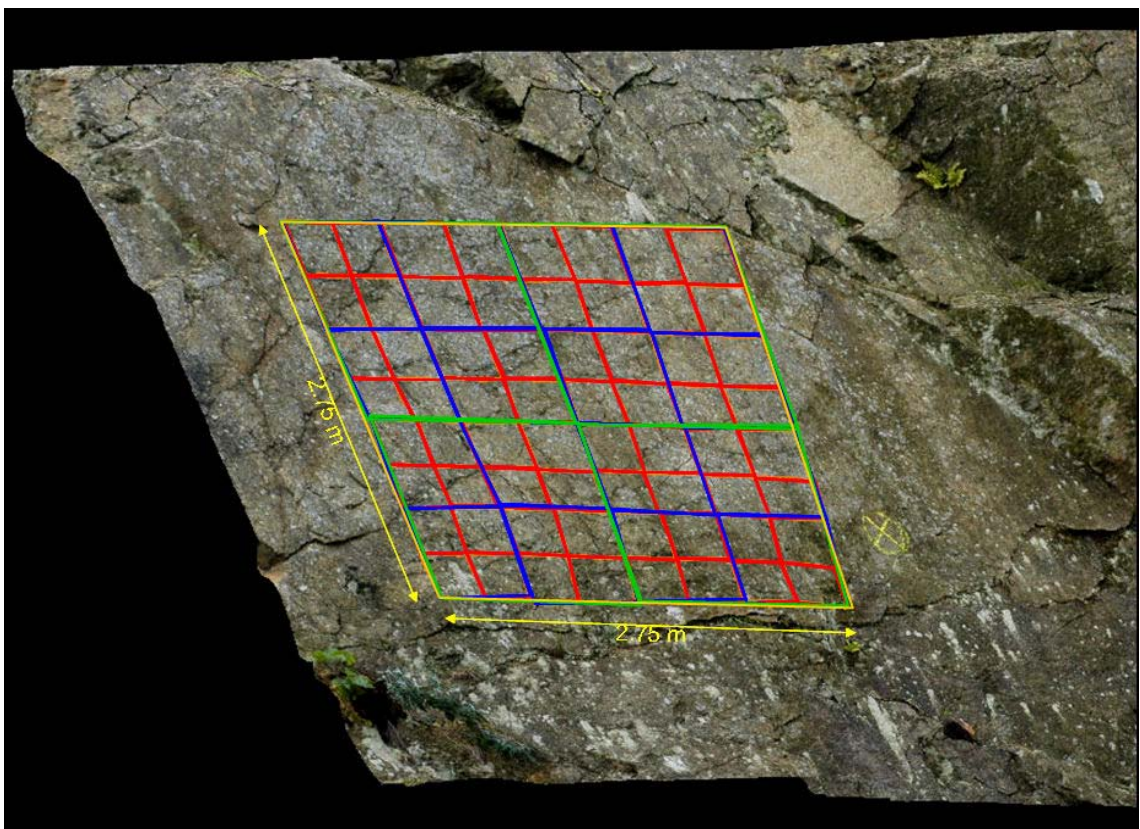


Figure 5-21. Photogrammetric 3D image showing partition of large box (7.6 m^2) into smaller boxes, $4 \times 1.9 \text{ m}^2$, $16 \times 0.475 \text{ m}^2$ and $64 \times 0.119 \text{ m}^2$, Tremough Campus Road cutting, Penryn, Cornwall, UK, looking SSE.

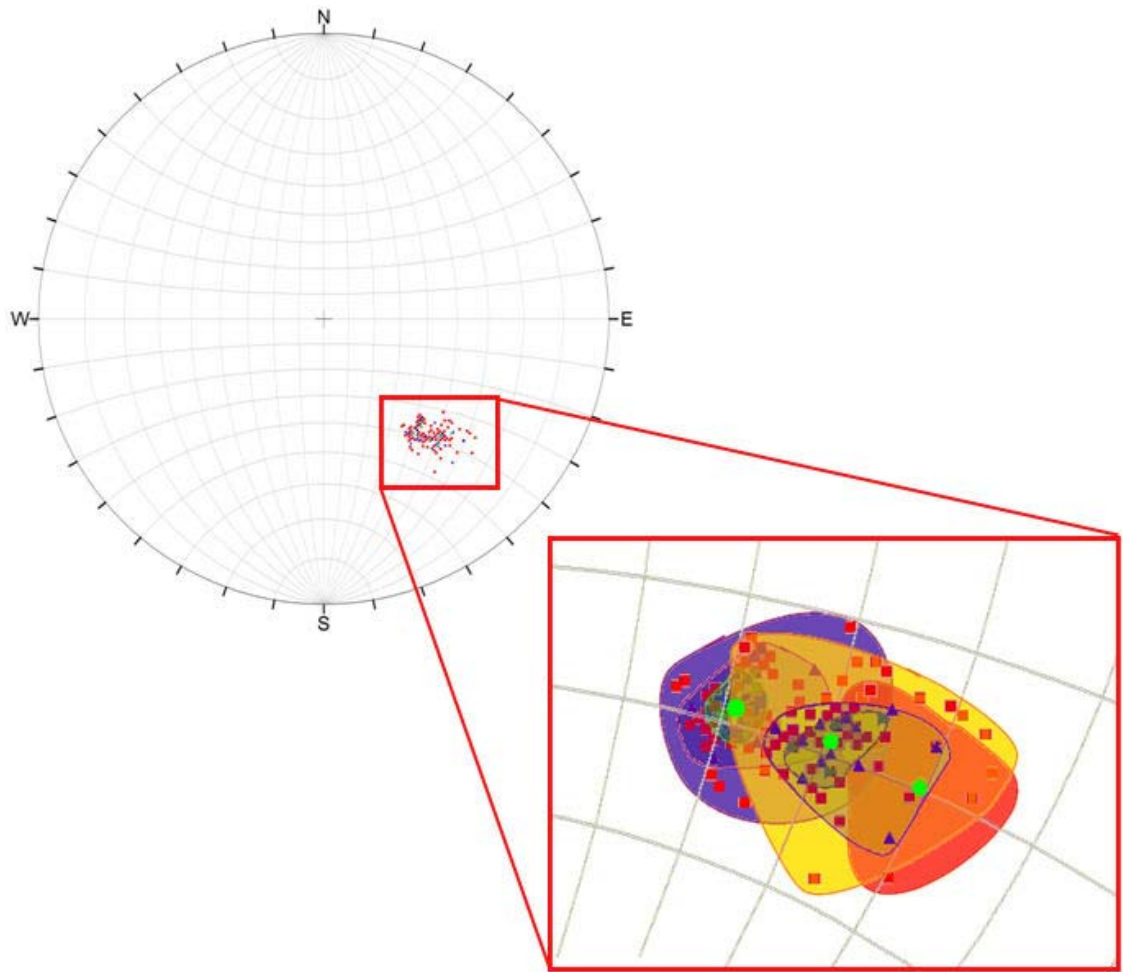


Figure 5-22. Stereonet and zoomed section showing photogrammetric poles (blue), laser scanned poles (yellow) and hand-mapped poles (red) (average shown in green).

The photogrammetric and laser scanned boxes at varying scales had their pole vector difference calculated from the orientation obtained from the total area of the plane (~25 m²) (Figure 5-23 and Figure 5-24).

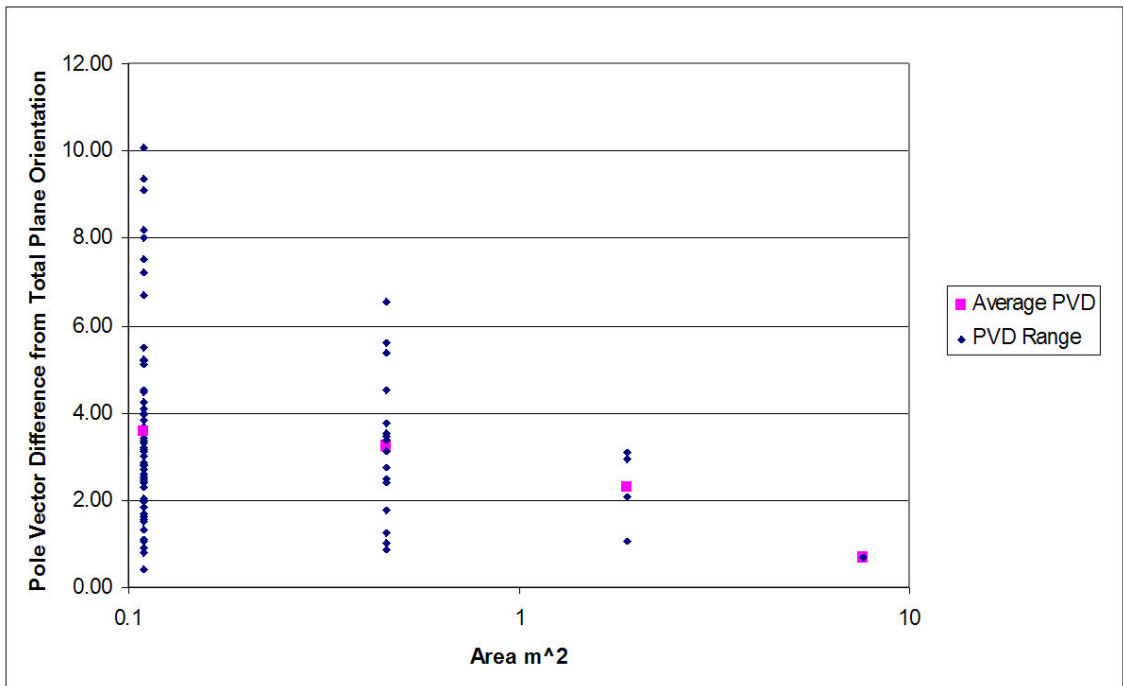


Figure 5-23. Pole vector difference of photogrammetry at varying box areas from average orientation taken from total plane area. It shows that the range of the pole vector differences from the total plane orientation reduces as the size of the plane measured increase.

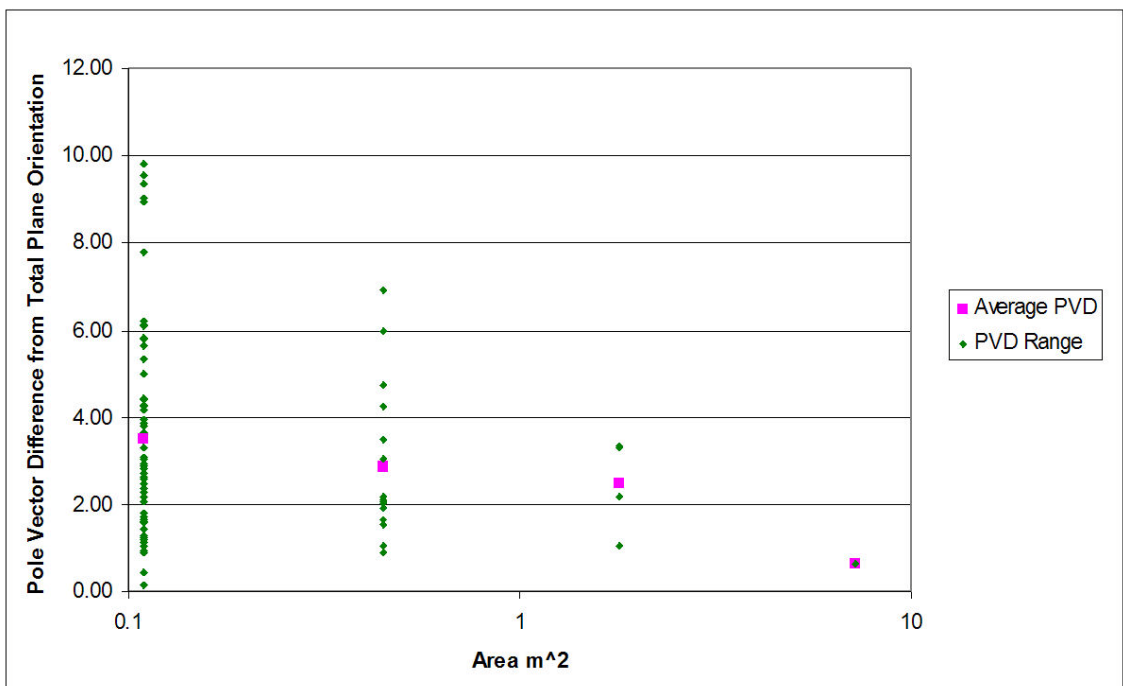


Figure 5-24. Pole vector difference of laser scanning at varying box areas from average orientation taken from total plane area. Mirroring photogrammetry; the graph shows that the range of the pole vector differences from the total plane orientation reduces as the size of the plane measured increase.

A similar range of orientation data about the average is present at each box area for both photogrammetry and laser scanning. These figures show that large scale roughness can cause a change in orientation measurement for laser scanning and photogrammetric geotechnical analysis systems. This has implications for the use of

remotely mapped planes to provide orientation data. If a plane is visible, the whole of its area is taken into account, but it may only represent a small proportion of the total discontinuity and it may not yield the true orientation. However, this effect affects traditional hand-mapping orientation measurements more substantially as usually only one spot measurement is taken of a plane (with several spot measurements taken for larger planes).

The orientation of the study plane was also mapped by hand at three locations within the area of the virtual box to obtain a hand-mapped orientation for comparison (Table 5-11).

Table 5-11. Table showing the pole vector difference between spot hand-mapped data taken from the study plane and the average plane orientation measured from the entire area by photogrammetry and laser scanning.

Hand mapped		Photogrammetry		Pole Vector Difference (°)
Dip (°)	Dip Direction (°)	Dip (°)	Dip Direction (°)	
70	320	53.4	319.3	16.61
70	310	53.4	319.3	18.49
60	312	53.4	319.3	8.98
Average				14.69

Hand mapped		Laser Scanned		Pole Vector Difference (°)
Dip (°)	Dip Direction (°)	Dip (°)	Dip Direction (°)	
70	320	60.6	316.2	10.01
70	310	60.6	316.2	10.95
60	312	60.6	316.2	3.70
Average				8.22

Although one hand-mapped measurement came to within 4° of the laser scanned surface average, the average pole vector differences between spot hand-mapping and the measurement taken from the entire discontinuity surface was ~15° from photogrammetry and ~8° from laser scanning. This highlights the effect described in the previous paragraphs that orientation measurements from a small proportion of a discontinuity may not necessarily reflect the true orientation. Remote data capture systems, by calculating orientation across the whole area of a discontinuity feature, compensate for roughness and orientation variation which could affect spot orientation measurements by traditional hand-mapping.

5.6 Tailoring Data for End-Use Applications

The data collected by photogrammetric and laser scanning systems can be used for several end-uses. The type of data used depends on the application. The geotechnical data collected by the two systems has varying end-uses, such as slope

instability analysis, geotechnical modelling and RMR/Q ratings. The raw digital elevation model data produced from photogrammetric 3D image creation and laser scanning point cloud can also be used without any additional processing. Photogrammetric systems can make use of the visual element of the photographs taken, combining it with spatial 3D data to make geometric measurements.

5.6.1 Geotechnical/Geological Data

The geotechnical data parameters which are captured remotely from the rock face using photogrammetry and/or laser scanning are able to be applied to multiple end-uses. Parameters, such as orientation, roughness, discontinuity trace length, as well as spacing data from virtual scanlines, are carried forward into geotechnical analyses (Figure 5-25). Combining the remote data with data sourced by traditional mapping methods is also possible, as the data is analogous across each mapping technique. Output from the remote data capture work-flow depicted in Figure 5-25 (discontinuity orientation, roughness, etc) may need further processing so that they are compatible with the chosen end-use application, e.g. split into sets, or positioned in 3D space to aid geological mapping.

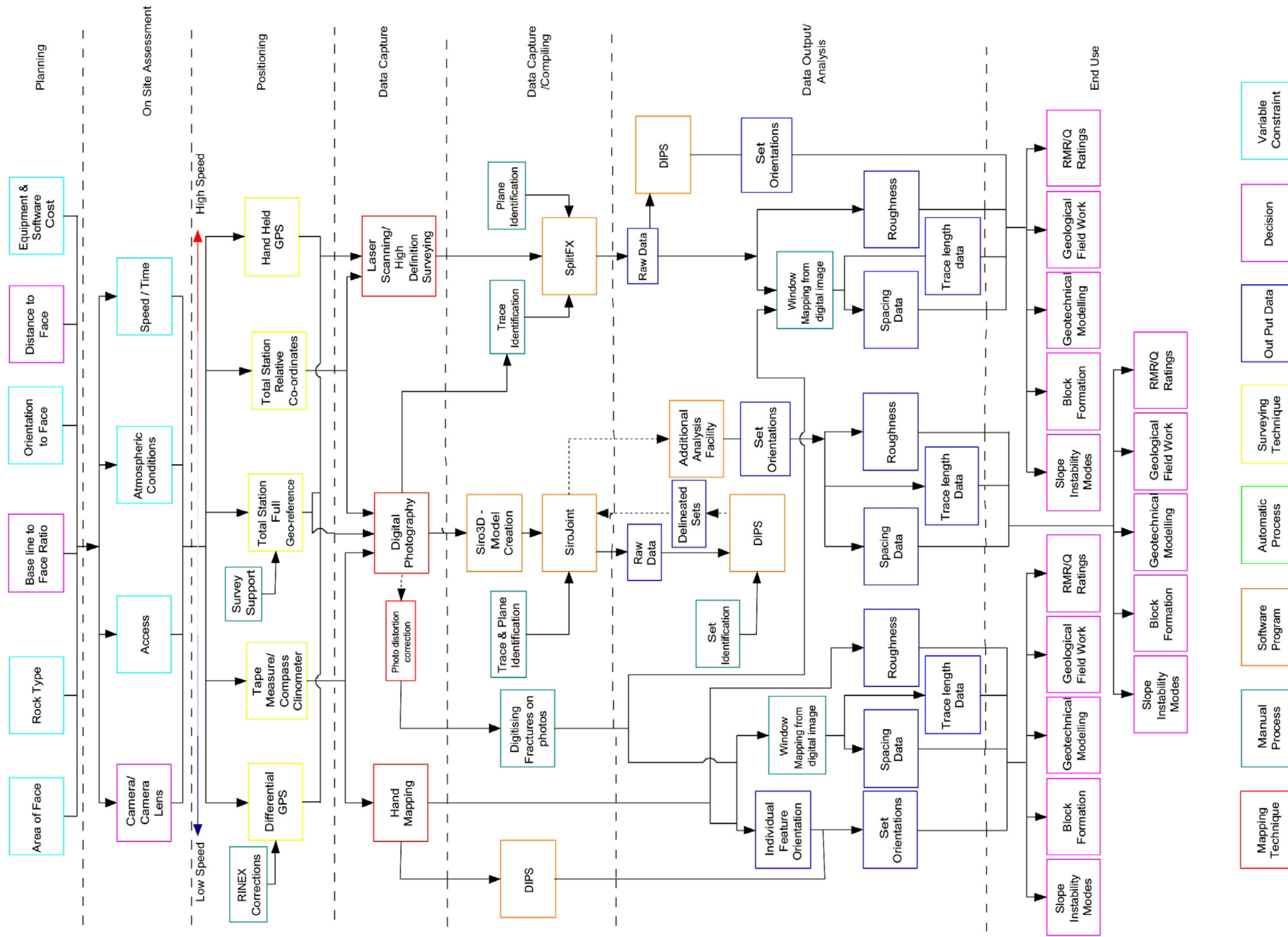


Figure 5-25. Process work-flow diagram for geotechnical end-uses.

Slope Instability Modes

Varying slope failure types, e.g. plane and wedge failures are dependent on the geological structures held within the rock mass and the aspect of the study slope. Kinematic analysis can be used to identify potential instabilities using stereographic projections of geotechnical data. Using the rapid collection and increased volume of geotechnical data captured by remote mapping systems allows for the improved kinematic analysis of potential block failures. Analysis can be applied to many geotechnical situations, e.g. quarry slopes, whose geotechnical analysis alters for each bench due to changes in slope aspect/ angle or variations of discontinuity geometries. Using digital remote data collection, many of possible features that control the strength of coastal slopes can be measured quickly and repeatedly if necessary. The increased amount of data enables better cliff characterisation and stabilization programs to be implemented.

Block Formation – Swedge

Block formation uses the orientation data exported from the remote data capture workflow. Blocks can be analysed by using the intersection of two discrete discontinuities, or by using the statistics of two fracture sets for a probabilistic analysis. Swedge (Rocscience, 2006) is a computer program which is able to complete both types of analyses. A photogrammetric image or laser scan point cloud showing two discontinuities potentially intersecting to form a wedge can be mapped to find the orientation of the individual features. This data can be exported from the respective remote data capture programs, along with the slope geometry (e.g. height, and angle). Importing the orientation data and face geometry into Swedge, combining with the rock strength properties, allows for the calculation of a factor of safety or possibility of failure for the identified wedge. An example is given from Saltdean, Brighton, UK, (Figure 5-26 and Figure 5-27).

Probabilistic analysis using Swedge requires the statistical distribution of the sets identified within the rock face. Exporting the orientation data from the remote data capture programs into DIPS and spreadsheet programs allows for the statistics of each set to be calculated. As photogrammetry and laser scanning capture large amounts of data compared to using traditionally mapped data, the statistical data produced will be more robust.



Figure 5-26. Map showing locations of laser scanner setup position at Saltdean. © Crown Copyright/database right 2009. An Ordnance Survey/EDINA supplied service.

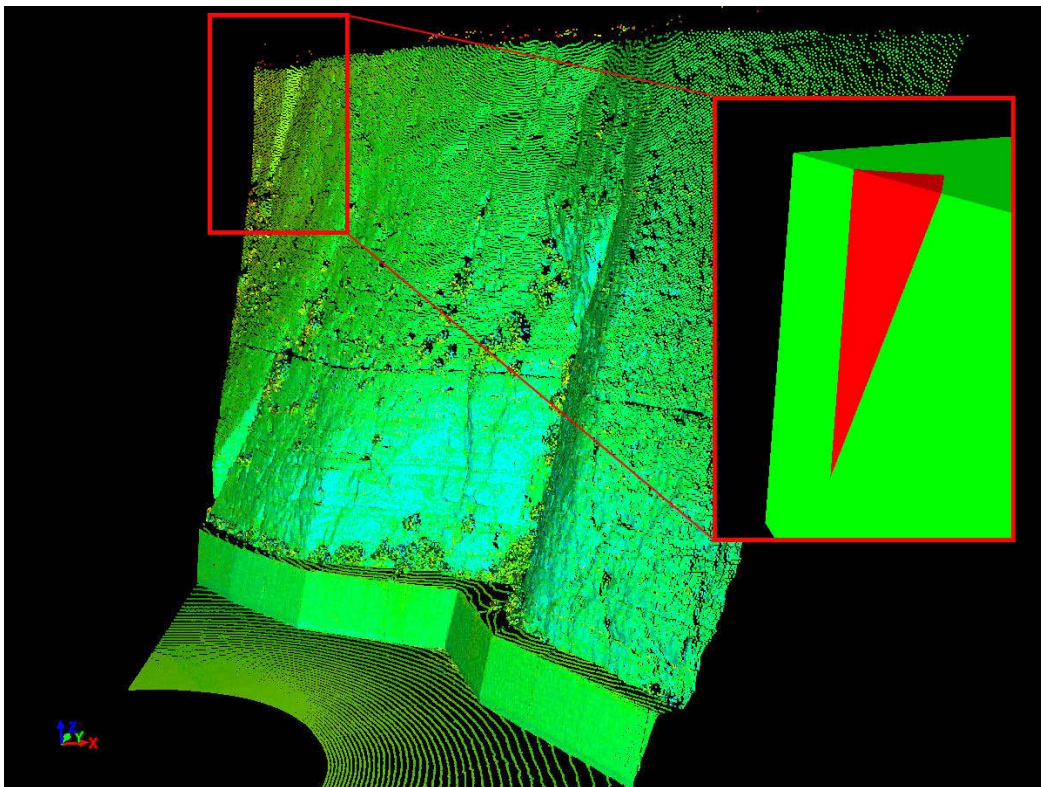


Figure 5-27. Swedge back-analysis on fallen wedge, data collected from laser scanned point cloud at Saltdean, Brighton, UK. The ~18 m high cliff has been scaled for loose blocks and has had a buttress installed to increase stability and to act as a catchment for small rockfall (~1.5 m³).

Virtual Scanline for Block Size Estimation

A method for collecting data similar to a normal scanline across a rock face has been developed during this study. A 'virtual scanline' is placed across the 3D image, the features within a particular set that cross the scanline are exported along with their positional data within 3D space. Using this data, a rough spacing can be calculated for each set. The spacing data collected by the laser scans and photogrammetric images from the close range underground work was used in another project conducted by Saliu (2009). The data has been incorporated into models for calculation of block size for potential dimensional stone production (Figure 5-28).

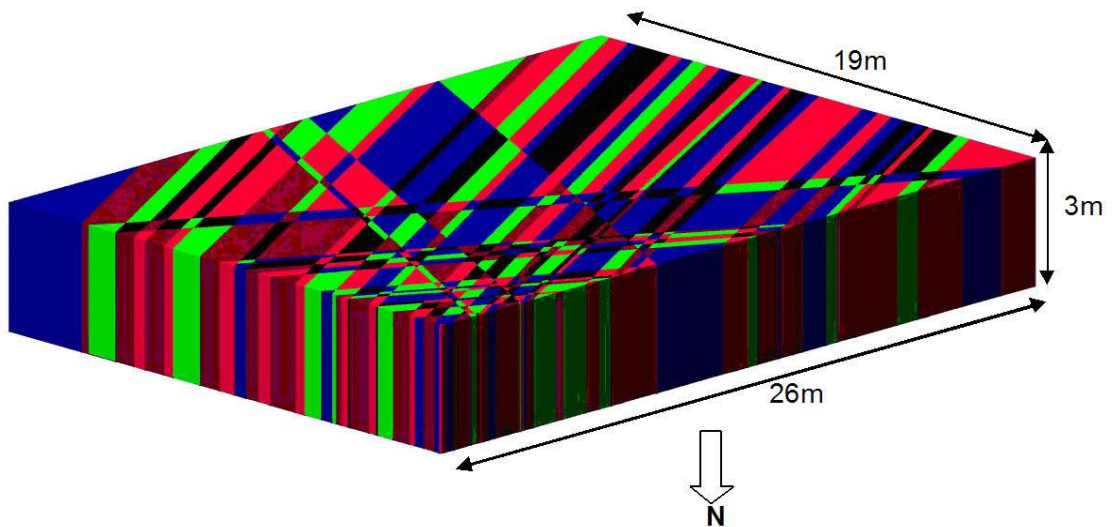


Figure 5-28. AutoCAD (Autodesk, 2008) 3D representation of blocks formed from virtual scanline spacing data (from Saliu, 2009).

Using the methods developed enables geotechnical data to be collected using both methods from setups that are close to the face. Very close range remote data capture does not affect the ability for the systems to collect reliable 3D data, but it can cause logistical problems for positioning and equipment setup. The main difficulty with collecting data in this way is the increased time to cover the required area as many setups are required. Mapping from many models is time consuming and restricts the maximum size of feature that can be mapped if it spans across one or more models. Both systems tested provide ways of combining the numerous models into one large composite model using their software programs, but they are only semi automatic, increasing the model creation and mapping time further.

Geotechnical Modelling

Three dimensional geomechanical modelling of fracture networks is an emerging technique for characterising a rock mass, rather than using empirical estimations of rock mass classification, e.g. RMR, Q. The Sirovision program suite has a module that

is able to visualise each discontinuity feature identified within Sirojoint. Each feature and its spatial position can be superimposed onto a potential 3D rock slope profile. The discontinuity sizes and terminations can be adjusted to suit the scale of the slope. The program can then be used to extract information about possible block formation and their geometries.

Using the remotely collected fracture properties, FracMan (Dershowitz *et al.*, 1998; Golder Associates, 1998), a stochastic fracture characterisation program, can be applied to model the data and represent it in 3D. For the stochastic model to be statistically sound, large amounts of data are preferred. Using these digital remote techniques this data load can be achieved. Once the model is created it can then be used to test fluid flow through the replicated rock mass, as well as creating simulated rock slopes to show potential discontinuity intersections. The data from the stochastic model has also been combined with a geomechanics simulation program, ELFEN (Rockfield Software, 2007), which uses the fracture data to model and calculate the conditions under which the rock mass would fail (Flynn & Pine, 2007). Data processing must be performed on both hand-mapped data and digital remotely mapped data so that it can be entered into 3D modelling programs, such as FracMan. Although, as most geotechnical analysis software programs are not specifically designed for integration with 3D modelling software, the data produced needs to be processed further so that it can be utilised. The parameters described below are required for FracMan 3D model creation, taken from Pine *et al.* (2006).

- Orientation distribution
- Spatial location distribution
- Ratio of fracture discontinuity trace lengths to studied face area (P21)
- Fracture radius distribution

Remotely collected orientation data is used to find the orientation distribution (discontinuity sets) of the studied rock mass. Orientation distribution is the description of the individual sets and their orientations, along with their Fisher K values, which expresses the data 'scatter'. Both of the remote data capture systems can be used to produce the set identification and Fisher K values, after planes and discontinuity traces have been delineated and imported in to DIPS.

The spatial location distribution describes the relationship between positions of the fracture planes. The different distributions include 'Enhanced Baecher', 'Levy Lee' and

'Nearest Neighbour'. Set spacing influences the types of distribution selected for model creation.

Scanlines are taken during field mapping of the outcrop to record set spacing, and they are also digitised onto photographs of the rock face, in differing orientations, to minimise orientation bias. The apparent spacings of individual sets are documented, and actual spacing is estimated using the corrections developed by Terzaghi (1965) described in Section 0.0.0. Little processing of the photogrammetrically collected data is required as spacing for each set is calculated quickly by Sirojoint after discontinuity delineation.

Discontinuity trace length vs. studied face area ratio, a parameter called P_{21} in the FracMan software, is traditionally calculated from photograph data, but photogrammetric 3D models can also be used to calculate this value. Discontinuity trace lengths are measured from photographs or exported from Sirojoint. After the fractures are established into sets, their individual trace lengths would be added to give the total. The total area of the mapped face is measured from scaled photographs, or alternatively, exported by Sirojoint. The total discontinuity trace length from one set and the total mapped area would be used to calculate the P_{21} of that particular set.

The fracture radius distribution is calculated through circular window mapping, to remove any orientation bias that may occur when using rectangular windows. This is traditionally completed from standard digital photographs taken of the rock face. After processing the orientation data collected from the rock face, sets can be delineated and the fractures on the photograph can be colour coded. A circle is then superimposed onto the photograph after which the discontinuity traces must be counted using specific criteria:

- Those that finish within the circle
- Those that one end terminates on the circle edge
- Those that both ends terminate outside the circle.

Using these counts and the radius of the circle, the fracture radius distribution can be then be estimated using methodologies developed by Zhang & Einstein (1998); Zhang & Einstein (2000); La Pointe (2002); and Zhang *et al.* (2000). Their techniques have been imported into Excel spreadsheets that run the calculations automatically once the circular window discontinuity trace count is input. They output the calculated mean

fracture radius of each set for three probability distributions: lognormal, negative exponential and gamma.

The radial distribution of the data is more complicated to acquire using Sirovision or SplitFX geotechnical analysis programs, as they do not yet possess the facilities to automatically complete virtual circular window mapping. Currently a virtual circular window is manually placed over the mapped photogrammetric orthoimage of the studied face using an image editing program. As a demonstration of the current methodology needed to complete circular window mapping an example mapping exercise and results are shown in Figure 5-29, Table 5-12 and Table 5-13. The current process of the fracture radius distribution calculation is performed similarly to hand-mapping, taking a similar time to complete.



Figure 5-29. Example circular window mapping from orthoimage of Carnsew Quarry (lower circles 6 m diameter, upper circles 10 m diameter). Using an orthoimage removes the perspective bias of using normal photographs. The circles were scaled using ImageJ (Rasband, 2007) and superimposed onto the orthoimage showing the discontinuity traces coloured according to orientation.

Table 5-12. By using the superimposed circles on the orthoimage, the discontinuity trace count for circular window mapping can be completed and split according to each set.

Circle Diameter 6m	Set 1	Set 2	Set 3
Finish within circle	3	3	15
One end terminates on the circle edge	11	5	14
Both end terminate on the circle edge	5	2	0
Circle Diameter 10m			
Finish within circle	2	7	10
One end terminates on the circle edge	14	5	10
Both end terminate on the circle edge	3	2	3

Table 5-13. Using the methodologies developed by Zhang & Einstein (1998); Zhang & Einstein (2000); La Pointe (2002); and Zhang *et al.* (2000) the mean fracture radius and standard deviation for each set and probabilistic distribution type can be calculated.

SET 1		
Distribution	Mean Fracture Radius (m)	Standard Deviation
LogNormal	6.35	1.91
Negative Exponential	3.46	3.46
Gamma	6.30	1.99
SET 2		
Distribution	Mean Fracture Radius (m)	Standard Deviation
LogNormal	10.46	6.27
Negative Exponential	7.11	7.11
Gamma	9.11	6.82
SET 3		
Distribution	Mean Fracture Radius (m)	Standard Deviation
LogNormal	18.59	1.97
Negative Exponential	9.40	9.40
Gamma	18.59	1.98

The digital nature of the photogrammetric remote mapping technique and the use of the scaled and lens distortion rectified orthoimages should allow for automatic and more accurate circular window mapping than the current methods.

Geological Mapping / Fieldwork

Remote data capture systems can also be used to assist with geological mapping in conjunction with other digital data capture techniques. Jones *et al.* (2007) demonstrated that photogrammetry, laser scanning and other data capture methods, such as seismic reflection, can be used to create geological models at multiple scales.

They made use of fully immersive 3D geospatial graphical user interfaces to view the captured data. Waggott *et al.* (2005) used laser scanning to geologically map rock sections which can then be used to aid in the characterisation of potential petroleum reservoirs. Waggott *et al.* (2005) also indicate that a fourth, temporal dimension, can be incorporated into the 3D data captured by remote mapping techniques, where it is problematic to do so using traditional 2D media. McCaffrey *et al.* (2003); McCaffrey *et al.* (2005) have established methods and work-flows for geological mapping using digital techniques. The use of digital data capture is suggested to enhance field mapping, whilst using the 3D spatial data to georeference the captured geological data to incorporate it to a larger geological model.

Sirojoint has the ability to add text descriptions to identified features which can be used to aid geological mapping, e.g. to assist recognition of deformation episodes or discontinuity features related to a specific stress environment. Due to the digital nature of the captured geological data, as well as it being georeferenced, it can be dynamically integrated into existing geological models. The data can be quickly transmitted digitally to other researchers, aiding in the interoperability of a project/study across large distances, which is becoming increasingly more common.

5.6.2 RMR, Q System and GSI Ratings

The three most widely used rock mass classifications are; Rock Mass Rating (Bieniawski, 1989), Rock Tunnelling Quality Index, Q (Barton *et al.*, 1974) and the Geological Strength Index, GSI (Marinos & Hoek, 2000). Each method incorporates geological, geometric and design/ engineering parameters in arriving at a quantitative value for their rock mass quality (Hoek, 2007). The RMR and Q system both use a weighting for certain parameters that make up a rock mass. RMR uses intact material strength, RQD, discontinuity spacing, discontinuity condition and ground water to describe the rock mass. The Q system uses an equation consisting of: RQD, joint set number, joint roughness, joint alteration, joint water, and stress reduction factors. Remote data capture systems can be used to assist in estimating these parameters, although most still require contact with the rock mass. Laser scanning and photogrammetry can find the number of joint sets held within the rock mass, as well as help estimate discontinuity conditions for an RMR rating, analogous to the joint roughness and joint alteration numbers for a Q rating (Table 5-14).

Table 5-14. Assessing the ability of photogrammetry and laser scanning to calculate parameters from RMR, Q system and GSI rating systems.

RMR parameters	Ability for remote mapping technique to calculate value
Intact Rock Strength	Inferred from rock type
RQD	Calculated from virtual scan line if 3D image is of metre scale
Spacing	Output from Sirojoint (photogrammetry), or virtual scanline
Discontinuity Condition	Roughness output from planar discontinuities. Persistence can be calculated from trace lengths or inferred from plane
Groundwater	Assessed visually
Effect of Discontinuity strike and dip orientation	Calculated from orientation data collected remotely

Q System parameters	Ability for remote mapping technique to calculate value
RQD	Calculated from virtual scan line if 3D image is of metre scale
Joint Set Number	Calculated from orientation data collected remotely
Joint Roughness	Output from planar discontinuities
Joint Alteration	Cannot be calculated remotely
Joint Water	Assessed visually
Stress Reduction Factor	Assessed visually

GSI parameters	Ability for remote mapping technique to calculate value
Rock Structure	Assessed visually
Surface Conditions	Roughness output from planar discontinuities. Alteration cannot be calculated remotely

5.6.3 Digital Elevation Model Data

The use of the digital elevation model data capture from photogrammetry and/ or laser scanning needs little processing, as essentially it is the raw data output by the remote data capture techniques (Figure 5-30). These end-uses do not follow the same paths along the work-flow process, bypassing the need for geotechnical processing. Measurements can be taken from the 3D morphology data, such as slope height, angle and area. Specialist computer programs are still required for the analysis. For example, Siro3D (CSIRO, 2005) can be used to output data needed, as well as the laser scanning software Cyclone (Leica, 2005) bundled with the HDS3000.

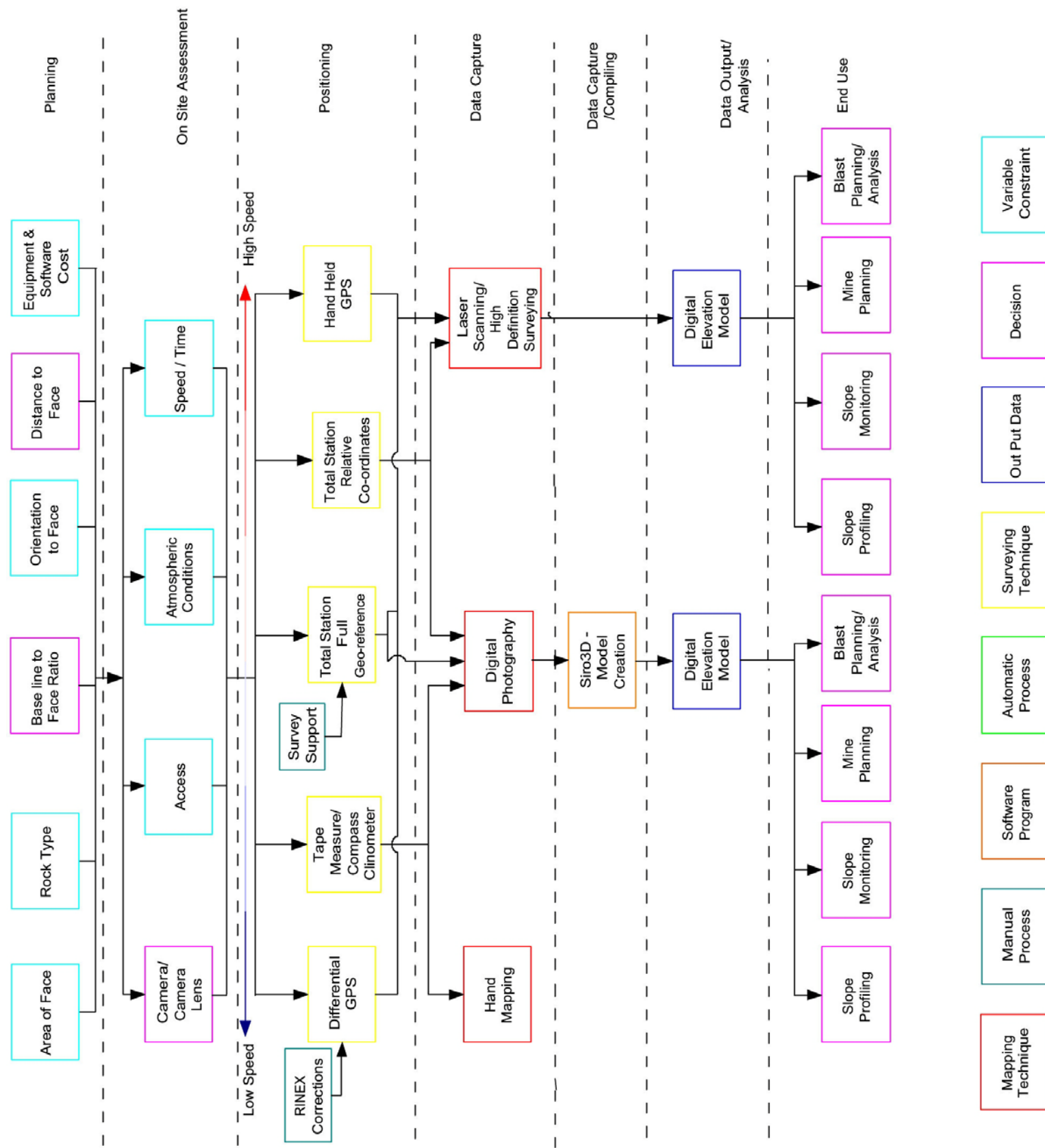


Figure 5-30. Process work-flow diagram for end-uses using digital elevation model data.

Slope Profiling

Slope profiling uses 2D cross sections taken through the captured rock face data. The 2D data consists of a vertical height measurement and a corresponding horizontal measurement. These cross sections can be used to simulate rockfall scenarios where highly accurate slope geometries are critical (Stevens, 1998; Budetta, 2004, cited by Rosser, *et al.*, 2007). An example of the use of remote data capture for slope profiling comes from Saltdean, Brighton, UK (location map: Figure 5-26). Two dimensional profiling of the chalk cliffs has been conducted on laser captured point cloud data (Figure 5-31). The profile could have also come from the photogrammetric models of the same face.

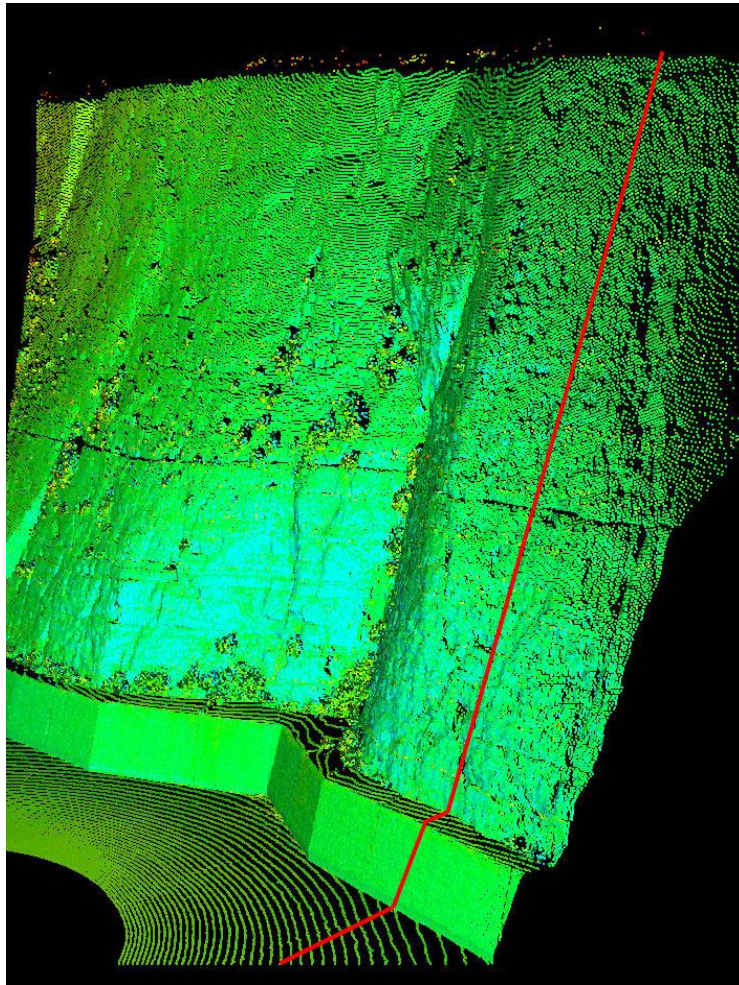


Figure 5-31. Point cloud image showing 2D profile section highlighted in red, Saltdean, Brighton, UK. The ~18 m high cliff has been scaled for loose blocks and has had a buttress installed to increase stability and to act as a catchment for small rockfall.

This 2D data was then exported into RocFall (Rocscience, 2007). RocFall, as its name suggests, aids in the assessment of slopes at risk of rock falls. The program is able to reproduce multiple scenarios of rock fall, including the path, bounce height, energy and velocity of the potentially falling objects as shown in (Figure 5-32).

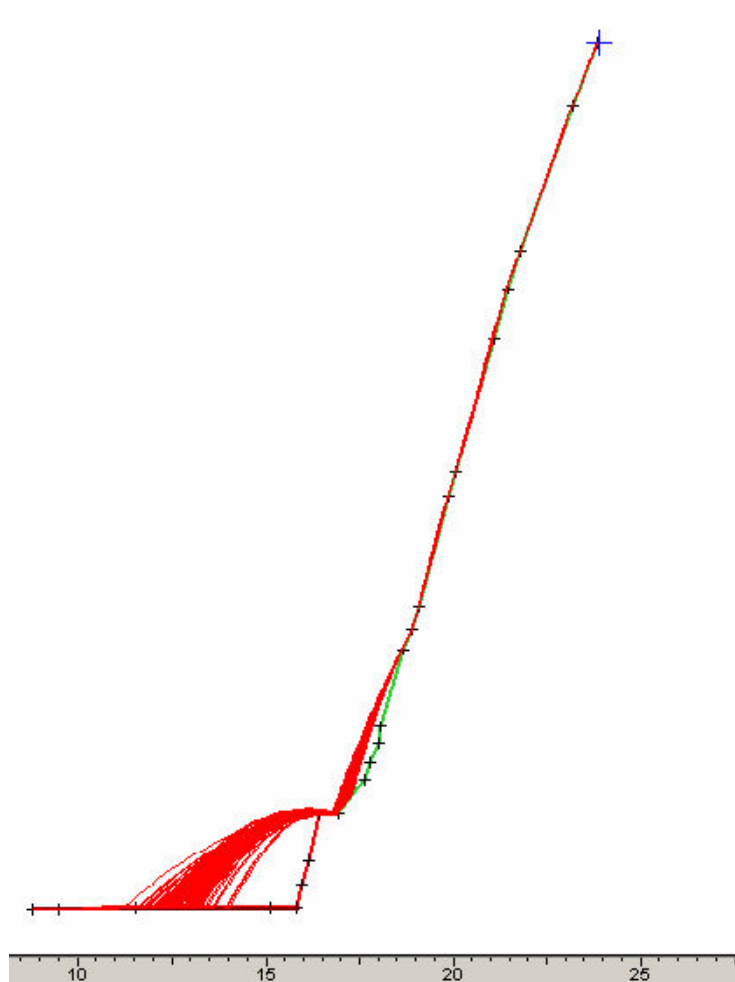


Figure 5-32. Simulated RocFall scenario showing rock fall paths from the cliff profile taken of Saltdean, Brighton, UK. The profile was constructed from a reduced number of points from the laser scanned point cloud as too many were imported for the RocFall program to compute without problems.

The simulation shows that the buttress installed to provide increased stability to the overall slope could act as a platform for rock fall to bounce from onto the coastal path at the base of the cliff. The advantage of using remotely captured 3D models for slope profile creation is that many profiles can be created very quickly and across a large area.

Slope Monitoring

Slope monitoring can incorporate the use of comparative 3D data taken over a period of time to assess changes in the slope morphology. Laser scans or photogrammetric models of the rock face can be overlaid upon one another to highlight changes, e.g. whether or not a previously identified potentially unstable block had moved, and if so, at what volume and how far. Comparison of 3D data is also able to pick up more subtle changes in slope morphology, such as creep or smaller failures, although the point density/ camera resolution must be high enough to visualise these small

structures. The identification of any movement on a slope is very important as usually acceleration in creep is experienced before a larger catastrophic failure (Petley, *et al.*, 2002; Kilburn & Petley, 2003). It is preferable if the scans/ photos are taken from the same position every time so to preserve the same conditions that would affect model creation/ point cloud capture. Barber & Mills (2007) used laser scanners positioned on the top of GPS located vehicles which are driven along the coast capturing point cloud data. This equipment setup would allow for repeated runs to be conducted monthly, monitoring the coastal environment. Rosser, *et al.* (2007) used laser scanning to monitor a cliff face over 15 months where patterns of rock fall and volumes were calculated. The SiteMonitor system has been developed by 3D Laser Mapping (3D Laser Mapping, 2007) which uses a laser scanner at a fixed position to continuously scan a rock face. It can identify deformation of 30 mm at 6000 m and 5 mm at 1000 m with an automatic warning if a large movement is detected.

Mine Planning

The data captured by photogrammetry and laser scanning can also be incorporated into mine planning software to aid numerous applications. Mapping the structure of mines and quarries can be undertaken quickly using low resolution laser scanning, thus delineating buildings, drives, benches, and plant machinery. Multiple laser scans can be registered together to form one large point cloud of the entire site. Modelling software can then fit shapes and surfaces to these point clouds scans, quickly building up a virtual representation of the mine/ quarry site. Figure 5-33 is an image taken from modelling software which has attached surfaces to a point cloud from a silver mine in Mexico scanned by James Jobling-Purser (Camborne School of Mines). The scanning was undertaken over a two day site visit using a laser scanner mounted to a two track remote controlled platform. The task had taken a surveyor two months to map using conventional surveying techniques. Maps and plans can then be drawn from these models, which can be continually updated by subsequent scans.

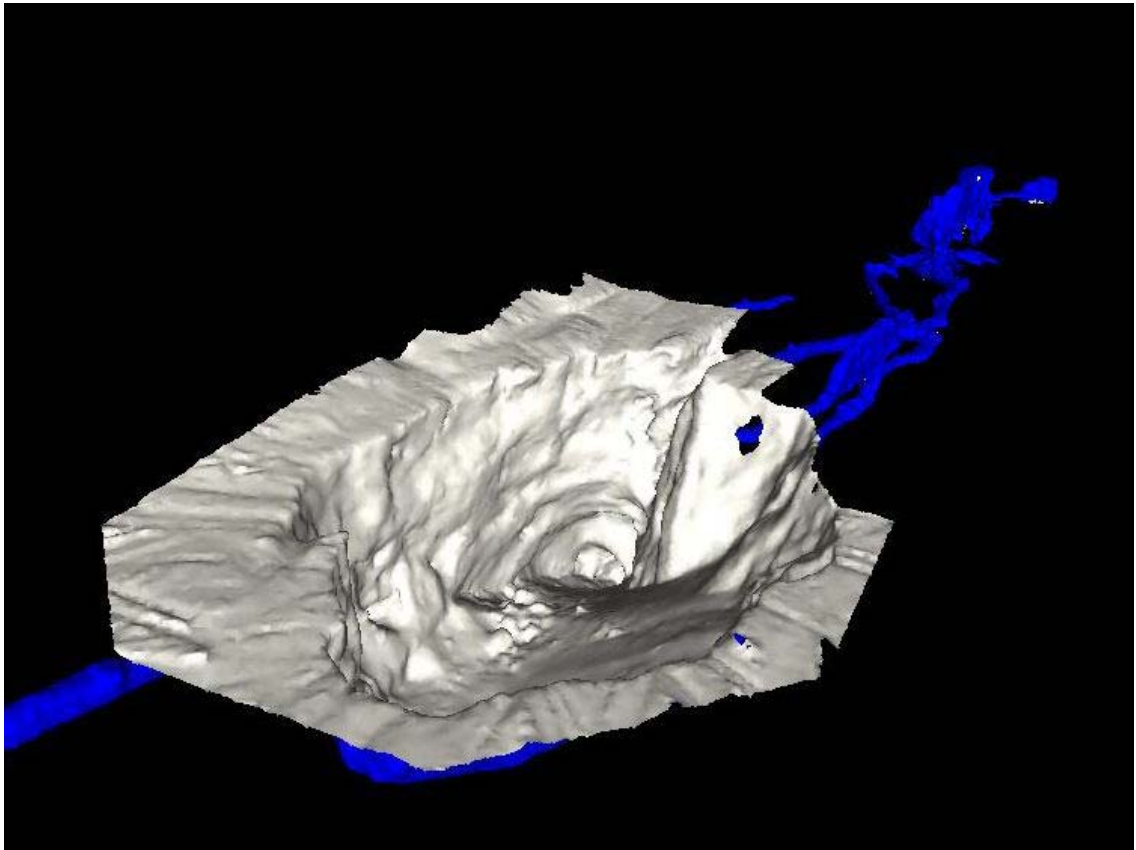


Figure 5-33. 3D mine map from laser scanned point cloud showing drives and collapsed stope (30 m wide approx). The grey indicates the interior surface of the mine, where the blue indicates the exterior.

Using similar techniques for monitoring rock slopes, calculating volumes of extracted material can be completed using photogrammetry and/ or laser scanning. This technique has been employed by china clay quarries at St Austell, Cornwall, UK.

Blasting

Photogrammetry and laser scanning can also be used to aid with blasting design and accuracy analysis. Siro3D (CSIRO, 2005) has a blasting assessment module within its program, allowing for the calculation of the minimum distance between a proposed blast hole and the rock face. It combines this with a post-blast volume calculation module, which uses 'before and after' 3D images of the blast area. The Quarryman Pro system, developed by MDL Laser Systems (2007), uses a laser scanner to complete slope profiling combined with the blast holes positions to calculate blast hole burdens as well as stockpile volumes.

Laser scanning point clouds have been used to quantify the tunnel hole burdens and fragmentation of blasts conducted at CSM Test Mine (Wetherelt & Williams, 2006). Laser scans were conducted on drilled cuts, whose holes had dowelling placed within them. The dowelling was then modelled as cylinders which were then extended into

the rock representing the direction of drilling for each hole. Using these models, inter hole burdens were calculated, assessed for misalignment and the potential effects they have on fragmentation and blast vibration.

5.6.4 *Visual Data*

The Siro3D module of the photogrammetric program Sirovision is able to use the 3D image created by the photogrammetric process to identify colour variation across the studied area (Figure 5-34). A colour range is input and an area is calculated, which can then be visualised on the image. Other programs have the same facility and can be used upon normal digital photographs.

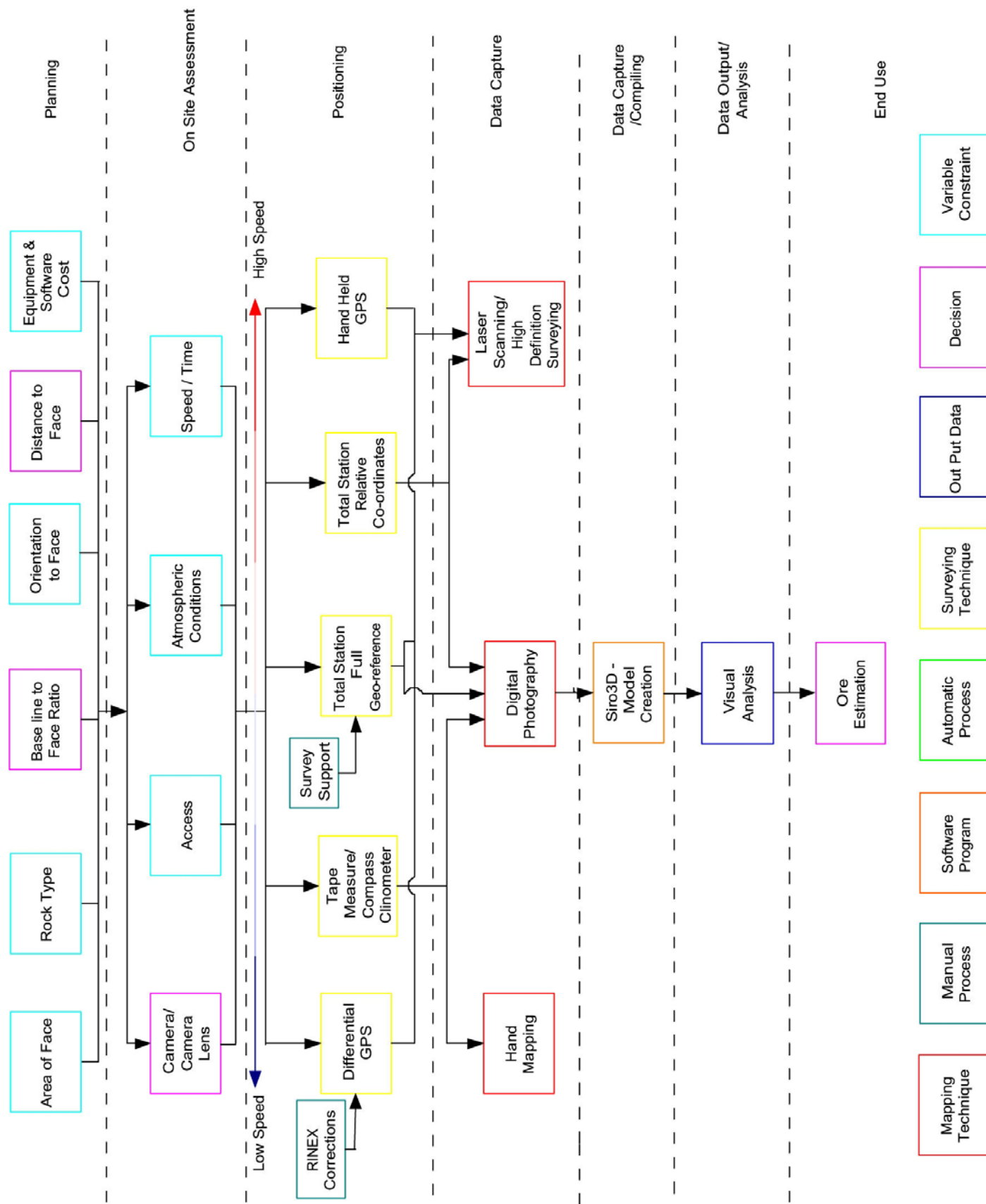


Figure 5-34. Process work-flow diagram for end-uses using visual data.

Ore Estimation

Remote data capture systems are useful in ore identification, and possible grade demarcation, where colour is a key classification feature. Figure 5-35 shows orthoimages of Imerys Blackpool Pit, where kaolin is extracted primarily for the paper industry. Lighter coloured material usually indicates areas where the feldspar within the granite has kaolinised to clay.

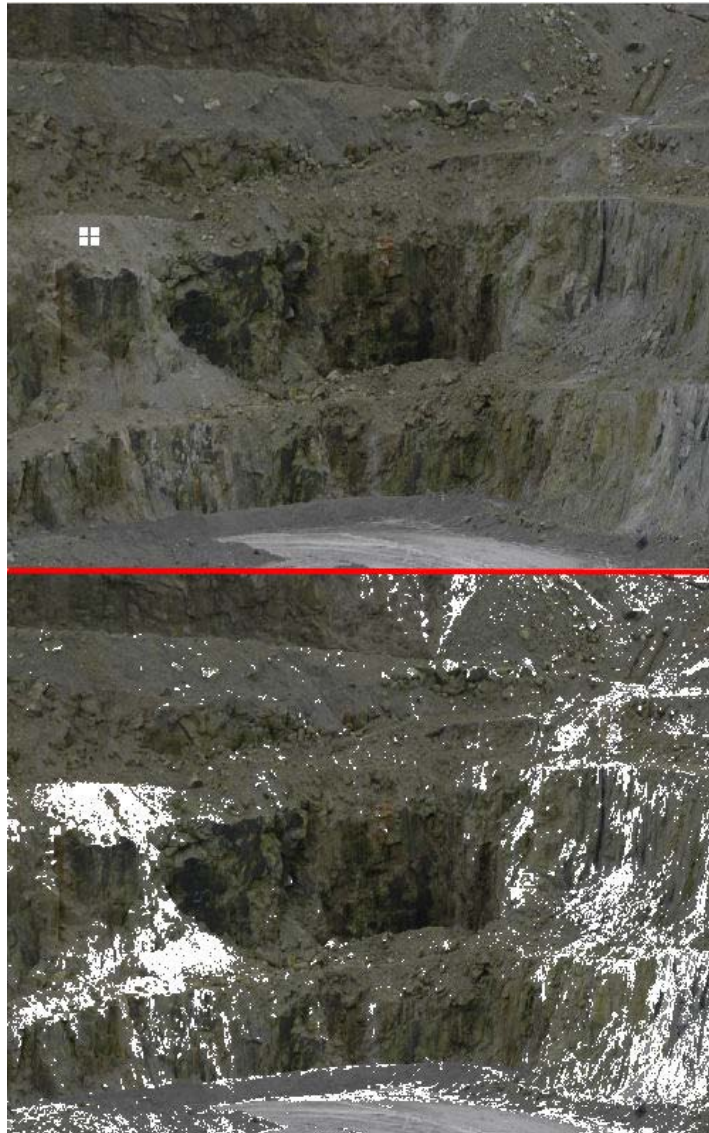


Figure 5-35. Images showing colour recognition. The top image shows the four points from which the colour range is chosen. The bottom image shows the areas of the face that match the colour from selected range.

The whiter coloured material is more valuable than that which has been stained by iron oxide, so selective extraction would be advantageous. The colour recognition module can aid in extraction planning and estimation of grade. The top image shows the area from which the colour range was selected. The areas which match the colour range

are highlighted in the lower image. From a total area of 14,633.3 m², the colour range matches 1449.4 m², 9.9% of the original.

Colour recognition is not restricted to photogrammetry as any photograph can be used, but as photogrammetric images are corrected for distortion and scale, measurements can be taken from them.

6 DISCUSSION

6.1 Introduction

The penultimate chapter of the thesis will include a discussion of the main outcomes of the study, split into fieldwork and mapping, and data output/ analysis processes. Comments are made on the limitations of the field techniques and potential problems faced when data analysis is undertaken. Although the study is based on particular hardware and software the results should remain constant between varying manufacturers as they have been shown to have the same intrinsic accuracies (Butler *et al.*, 1998; Huising & Pereira, 1998; Boehler *et al.*, 2003; Kersten *et al.*, 2004; Fraser *et al.*, 2005; and Heikkinen, 2005). Recommendations for further work and expected advancements in software and hardware are covered in the final section. A final figure is presented showing the work-flow system, should all the proposed software and hardware updates become implemented.

6.1.1 *Field and Mapping Processes*

Both remote mapping techniques are shown to collect orientation data comparable to traditional hand-mapping from varying lithologies and fracture intensities, at a range of distances. However, both techniques struggled to collect orientation data from highly fractured rock masses. This establishes that remote data capture systems can be used for collection of orientation data, but they are more suited to blocky rock masses. This assessment was also made by Struzzenegger, *et al.* (2007b), it was suggested that the GSI of the rock mass can be used to ascertain the suitability of the use of remote data capture systems. An assessment must be made of whether or not the rock mass stability is influenced by the orientation of either: individual large scale features, or by rock mass strength affected by closely spaced small scale features, or a combination of the two (Wyllie & Mah, 2004). For this reason the scale at which the mapping techniques collect geotechnical data is very important; limitations on the density of laser scans and camera lenses prevent multiple scales from being assessed from just one model. Increasing the scan density by repeating multiple close range setups or increasing the focal length would allow for smaller scale features to be visualised, but this would be impractical due to increased time required in the field and increased computing time because of larger data file sizes. Problems with large data file sizes and the inability of current computers to visualise them were experienced by Rosser, *et al.* (2007). As technology advances the problems surrounding 3D model densities will abate, but currently care must be taken when assessing the use of

remote data capture for certain fracture intensities of rock masses. This problem may be overcome by careful selection of representative mapping areas at differing scales, as is also necessary with traditional mapping techniques.

The baseline to face ratio used for photogrammetry that produced the most accurate orientation and precise data was found to be a little lower than the recommended ratio suggested by the Sirovision manual, 0.25 – 0.166 as opposed to 0.166 – 0.125 (CSIRO, 2005). This may be due to the geomorphology of the study face and close proximity of the photogrammetric setups to the face, ~10 m. The study face had numerous small features that were sub-perpendicular to the overall face orientation, so a larger baseline to face ratio allowed for a larger proportion of those features to be seen by at least one photograph of the stereopair (therefore more 3D data points upon the plane will be captured). This has implications on the considerations made to the setup for photogrammetry. It is considered that if the distance to the face is increased (~50 m) then the ratio may tend closer to the Sirovision recommendation, as these smaller perpendicular features will be masked by the larger features shaping the general orientation of the face.

Problems arising from restricted access affect both systems. Obstructions are hard to remediate against, although blinding problems can be overcome by using multiple perpendicular photogrammetric setup positions to the study face and/or multiple laser scans with differing viewing angles. Struzzenegger, *et al.* (2007b) suggest that blinding problems experienced by remote data capture can be serious for rock mass characterisation as features can be missed or inaccurately measured. The study at Penlee Quarry and the Tremough Campus road cutting quantified the problem of blinding/obstruction. Photogrammetric blinding was simulated by rotating the setup positions away from the original perpendicular orientation from the study face. It was found that blinding did not affect the ability to collect discontinuity data until the setups were orientated less than 60° to the rock face. However, this result was achieved from a study conducted upon one rock type with a specific fracture intensity and fracture orientations. If this was repeated for differing locations then the setup orientation at which blinding begins to affect data capture may vary.

Nearly every study undertaken upon remote data capture systems has stated that remote data capture is quicker and more efficient than traditional mapping, but this time advantage is rarely quantified. By completing a quantitative assessment of the time required for each mapping task/step it was found that similar time is taken between the

three mapping techniques for the preliminary stages. However, the data capture/fracture measurement stage of remote mapping is ~8 times quicker than traditional mapping. The data processing from the remote data capture techniques is quicker than for traditional techniques due to the digital nature of the recorded data. These results indicate that the use of remote data capture is beneficial for large scale time sensitive mapping applications, e.g. mining and tunnelling. An exception would be when only a few features are required to be mapped. In the time it takes to setup and complete a scan/photogrammetric model, hand-mapping can be completed on a small area; if that is all that is required then remote data capture may not be suitable. As technology advances, the speed of remote data capture will increase; currently Sirovision is implementing a system (CSIRO StereoCamera) where a user can take the required photographs and survey data using specially built hardware (although only for very close range, 2 m – 10 m, underground applications).

In most major operations where remote data capture will be implemented survey personnel are used to position the equipment setups prior to photogrammetric and laser scanning data capture. By testing the suitability of differing positioning techniques during this study, it has been found that photogrammetry and laser scanning can be used autonomously, without the need for a surveying team. The data capture can be undertaken by one person; however it is always advised to have at least two people for health and safety considerations. Having two persons makes transporting the equipment easier, however over the period of this study, alterations to data capture field techniques have allowed for the reduction in equipment loads. Robust and practical guidelines have been developed for efficient set-up and operation of the two differing techniques, including hardware and any associated software. Laser scanning is the least portable of the two remote mapping systems, as it requires at least two people to conduct fieldwork due to the weight and fragility of the hardware. Only two pieces of laser scanning hardware were tested, both from the same manufacturer (Leica), other lighter, more robust laser scanners are available which would increase the portability. The survey systems required also add load, but if less accurate positioning can be used without a compromise to the data collected then lightweight options can be chosen (handheld GPS and compass clinometer). As technology develops and new hardware is released, the size and weight of the advanced hardware will reduce further to more manageable levels. By developing a fitting that allowed one tripod to be used with both the surveying equipment and the photography equipment photogrammetry also became a more portable remote data capture system. The tasks and environment in which the systems are to be used must

also be taken into consideration; if the mapping sites are accessible by car then portability is not a big issue. However, it is found that in most situations the access is problematic and the user must carry the equipment on foot. It is then important that a suitable remote data capture technique is chosen.

By combining the surveying and remote data capture systems into equipment manageable by one/ two people a requirement has been made that the person undertaking the field work must be sufficiently proficient in both surveying and remote data capture. The use of the basic survey techniques is taught as a generic tool in most earth science degree courses, however advanced surveying equipment requires extra, and sometimes expensive, time consuming training. This would be in addition to the remote data capture technique training required. It is also rare to have expertise in both laser scanning and photogrammetry. These factors will also dictate the field methodology employed to effectively capture data remotely.

6.1.2 Data Output / Analysis Processes

Orientation Data Accuracy Analysis

The accuracy of laser scanned and photogrammetrically captured orientation data compared to traditionally hand-mapped data was conducted at the Tremough Campus road cutting using pole vector differences. The average pole vector difference between remotely mapped and hand-mapped data taken at the study area was found to be $\sim 12^\circ$, lower than the hand-mapped comparison at Penlee Quarry (PVD of 13.75°). The standard deviations were also lower. This could be due to the blocky rock mass at Tremough. The PVD between photogrammetry and laser scanning was 10.61° , this is close to the value suggested in Section 4.2.3 and should only be due to the noise of the 3D images/point clouds. The averages and standard deviations of discontinuity data dipping below 47° are higher than the data dipping above 47° , apart from the comparison of average PDV between the two remote mapping techniques. The steeper dipping features have a higher PDV average, but lower standard deviation. This suggests that the difficulty in mapping shallow dipping structures by hand, as described by Herda (1999), does not affect the remote mapping techniques. This effect may also be a result of the roughness of the discontinuity planes effecting the orientation measurement, remote mapping techniques, by acquiring measurements across the entire discontinuity, smooth out the effects of roughness. The lower standard deviation indicates that the remote mapping techniques are more precise for the steeper dipping features. The ability for remote mapping techniques to be more

precise when capturing steeper dipping features, shown by the lower standard deviations, is directly linked to the viewing plane of the equipment setups. The results in Section 4.6 indicate that remote data capture equipment setups perpendicular to the study face provide orientation data with greater accuracy. This principal also relates to the individual discontinuity features; the steeper features are more likely to be perpendicular to the photogrammetric and laser scanning equipment than the shallow dipping features, hence the higher precision (lower standard deviation).

Smaller planes measured had a high likelihood to produce a higher error in orientation when compared between each mapping technique. This is likely to be due to the low point density or spatial resolution of the 3D triangular mesh of the smaller features. The other possibility is that the discontinuity feature was misidentified (due to its small size) and compared with the wrong remotely captured orientation measurement. Although smaller features have a tendency to produce higher errors from hand-mapping, the majority of the captured data has a pole vector difference of less than 15° between one another, comparable to the hand-mapping vs. hand-mapping PVD of 13.75°. Orientation variability of larger surfaces may be the result of real variation over the fracture surface or variations in the mesh topography due to roughness.

The shallowest dipping set (~45°) was expected to produce the highest pole vector difference due to the difficulties in obtaining accurate orientation measurements discussed in the last few paragraphs. This was not the case; no single set produced the highest PVD across all three comparisons. A possible reason for this is that the grossly anomalous poles (producing the high PVD values for individual discontinuity analysis) would have not been selected during the set analysis. A reason for variation between the pole vector differences between each set captured by photogrammetry and hand-mapping would be their average orientation to the camera setup. Set 3 is oblique to the photogrammetric cameras resulting in fewer data points for those features and therefore poorer accuracy. The laser scanned sets do not show this variation according to set orientation as the three laser setup positions were taken at differing angles to the face. The highest average Fisher K values were for set three (150.04 for laser scanning). This set was not the steepest (63° - 72°), but was it directly perpendicular to the third laser scanner setup position. There was a significant difference in the Fisher K values between the steepest dipping orientation sets; set two was much lower for each mapping technique. This is due to set one striking perpendicular to the remote data capture equipment setup, producing the higher Fisher K, where the other was viewed from a more oblique angle. Although it did not produce

the lowest accuracy (highest PVD), the lowest average Fisher K values resulted from set four, which was the shallowest dipping set. From the individual orientation analysis (and the work done by Herda, 1999) this result was expected, but laser scanning had the lowest K value of 33.16 (photogrammetry, 38.17; hand-mapping, 37.78). Hand-mapping would be expected to have the lowest K value as it has been shown to struggle with measurements of shallow dipping discontinuities (Herda, 1999). However, the set was dipping at $\sim 45^\circ$, towards the upper level of the shallow dipping features boundary ($0.5^\circ - 47^\circ$), which may account for the relatively high hand-mapped Fisher K value. Hand-mapping had the highest average Fisher K value across all four sets, 66.86, although not notably higher than photogrammetry (61.34) and laser scanning (63.89). As the difference in Fisher K values was not significant it is considered that set analysis normalises the precision between the mapping techniques.

Set analysis was conducted manually and therefore subject to bias; another person may delineate slightly different discontinuity sets. Additionally, only four sets were picked from each mapping technique to simplify the analysis; delineating more sets would alter the orientations whilst increasing the Fisher K values. The bias resulting due to the manual delineation of sets will occur in any other study; this is inherent to current analysis techniques. The SplitFX and Sirovision programs each have an automatic set delineation module; through testing it has been found that they are currently not suitable, however as the algorithms used advance then these programs may be able to remove human bias from the set analysis process.

From the orientation data presented from the Tremough Campus Road cutting it would appear that the majority of features remotely mapped showed comparable measurements to traditionally mapped data. However, some errors between individual remotely mapped and hand-mapped features were very high, tending towards 90° , indicating that they were orthogonally orientated to one another. This was either due to misidentification of the discontinuities and/or due to the small area of the feature mapped compared to the overall model size. This would suggest that there is a minimum level of detail of a surface that remote mapping can realistically capture. This will obviously depend on the size of the overall area mapped and 3D model density; these should be considered when undertaking the planning and site assessment processes. This is not unlike hand-mapping where decisions are often made in terms of a minimum fracture length or size of fracture to include in rock mass characterisation. This in turn is often related to the scale of the structure and whether or not fractures have an influence on the engineering behaviour of the rock mass. The

PVD and standard deviation of the remote data capture systems from hand-mapping was found to be lower than the hand-mapping vs. hand-mapping values found at Penlee Quarry. This suggests that both the accuracy and precision of the remote data capture systems is greater than hand-mapping. However, this comparison is made across two differing locations and lithologies, and only on one set of comparative data. It is considered that lithologies with blockier, smoother structures would possibly produce lower pole vector differences as it would produce more accurate hand-mapping measurements as opposed to more accurate remote data capture orientations. The hand-mapping vs. hand-mapping study at Penlee Quarry shows that traditional mapping may not necessarily be the most accurate and precise form of mapping. The majority of comparisons between photogrammetry and laser scanning produced lower PVDs and standard deviations than when they were compared individually to the hand-mapped measurements. Previous studies by Herda (1999) have shown that hand-mapping struggles with accurate measurements at low dip angles. It is possible to say that in certain conditions (e.g. measurement of a large or very rough discontinuity) that remote data capture may be more accurate than traditional hand-mapping. However, hand-mapping is still the most practised and standardised form of obtaining measurements for rock mass characterisation.

From data taken from numerous areas during the study it was found that set statistics are easier to compare when the lithology studied has well defined fracture geometries. However, identifying sets using the software programs involves human interaction introducing a possibility for error. Better accuracy between traditional and remote mapping was found between the steeply dipping sets, attributed to their perpendicular orientation to the viewing angle of photogrammetry and laser scanning. This is corroborated by the baseline to face angle analysis, suggesting that even though equipment setups may be perpendicular to the slope, there will always be features unfavourably orientated, resulting in poor measurement accuracies. Data gathered during this study has allowed for the creation of the stereonet shown in Figure 6-1. It is noted that to achieve a high precision for a remote rock mass mapping exercise, exposures of the rock should be viewed from orthogonal angles to negate possible precision problems, much like traditional hand-mapping.

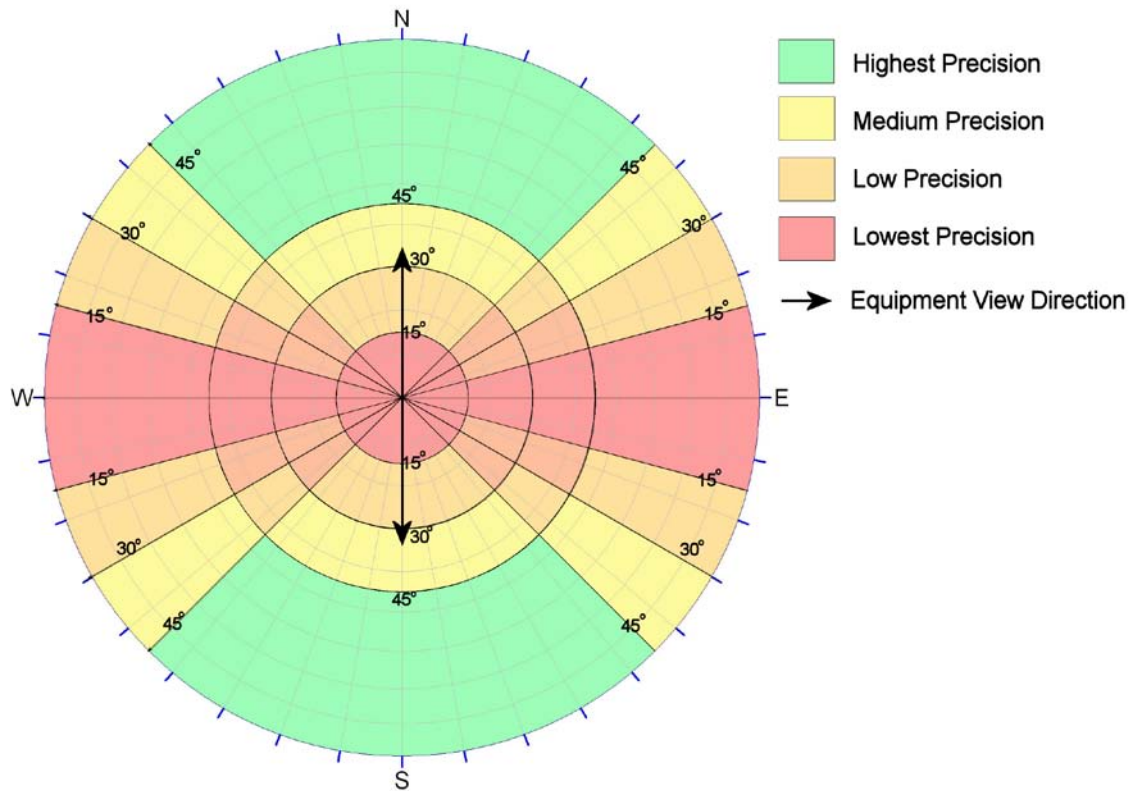


Figure 6-1. Diagram showing stereonet overlay indicating areas of precision for remote data capture systems (viewing along a horizontal plane and from one setup position). The highest precision is achieved for features that are near perpendicular to the viewing angle. As features become more oblique in both the horizontal and vertical planes then the precision decreases.

Testing the accuracy of discontinuity trace orientations captured by photogrammetry using the pole vector difference methods indicate that planar derived orientations are more accurate. Although orientations from planes still have the same possibility as traces to produce a high pole vector difference from hand-mapping, they are more likely to be closer to the hand-mapped measurement. It is considered that the algorithms used to estimate a plane to fit a delineated discontinuity trace from photogrammetric 3D images are not sufficiently accurate, resulting in the large range of discontinuity trace orientation errors seen during analysis. However, this study was conducted using only one software program to calculate trace orientations; the algorithms used vary between the software packages which may produce slightly different results. The morphology of the study face is critical when relying on traces for orientation measurements. If it were very blocky then the traces delineated would have enough spatial data to constrain an accurate plane fit using the software algorithms. The closer a trace is to a straight line (2D) the greater the likelihood that any number of plane orientations could fit to it. It is considered that improvements in algorithms will increase the reliability of orientations calculated from traces, although they will have the same problems concerning traces trending towards straight lines. The tracelength orientation study was undertaken upon a blocky rock mass which should produce the

most accurate trace orientations due to the pronounced morphology. The results were not satisfactory, indicating that the use of traces to characterise rock mass orientations should be treated with care. However, the use of traces during mapping should not be disregarded; they can relay important information on the length of fractures. The discontinuity trace length comparison between photogrammetrically derived traces and traces mapped from photographs that were corrected for distortion shows that they produce similar results. The discontinuity trace lengths that were calculated from photogrammetry were 89% of the length determined from a scaled photograph. A scaled photograph should produce accurate trace lengths as long as the aspect of the photograph is perpendicular to the rock face. A non perpendicular photograph will cause distortion in the length of the features measured, i.e. they will be underestimated if the subject is sloping away from the camera in the horizontal / vertical plane, and vice versa. The tracelength comparison was conducted upon the Tremough Campus driveway which slopes slightly towards the camera. As the tracelengths recorded using photogrammetry were in 3D then they would not have been affected by the perspective. This is a possible reason why the 2D photographic tracelengths were found to be longer, although the photogrammetric lengths may be more accurate. Another possible reason for the slight difference in tracelengths is that due to the photogrammetric model creation, a larger area is seen by the original digital photograph. Some of the photogrammetrically mapped discontinuity traces are truncated around the edge of the 3D image resulting in slightly shorter trace lengths.

Roughness Analysis

It is possible to convert roughness measurements taken using remote data capture systems to conventional roughness units, such as JRC values. Although the analysis suggests that correlation between the remote and traditional measurements may be poor. Noise within the 3D models will have affected the quality of the roughness measurements for the remote data capture systems. The values used for remote roughness measurement were not specifically developed to be used that way, specifically the photogrammetric measurement values of RMS and variance. Producing very close range (sub 2 m) 3D models will negate the problem of noise, but is not particularly practical, as then hand-mapping would become the preferred choice of data capture.

When assessing the effect of roughness on orientation measurements taken by remote data capture, it is indicated that large scale roughness can cause a change in orientation measurement for laser scanning and photogrammetric geotechnical

analysis systems. If only a small section of a larger plane is available for measurement then the true orientation of the plane may be miscalculated by $\pm 9^\circ$, due to large scale roughness/undulation. This scenario will occur often in practice, therefore delineating smaller areas of larger features to obtain an orientation measurement is not recommended. However, when compared with hand-mapping, remote data capture systems are not affected by roughness variations as significantly as spot hand-mapped measurements as they utilise the entire area of a visible plane to calculate orientation.

End-Use Applications

Photogrammetry and laser scanning can be used for multiple end-uses concerned with slope stability and quarrying processes. However, the data used must undergo additional processing, using programs other than those used during the project for certain applications. This will add time to a project, but the time saved during the initial data capture should be taken into account.

The 'virtual scanline' method was developed to obtain rough spacing data from the underground models. It has been used to estimate block size from both close range and larger scale 3D models. However, this method was time consuming for the user and it is noted that data must be captured from multiple rock face orientations so to visualise all aspects of the rock mass. This is also true when using hand-mapping to collect spacing data. Correction for a 'true' spacing can be done automatically using the digital methods of data capture as the orientation of the face and the discontinuity set is delineated during mapping. This method would only be applicable if the underground study face was inaccessible, hand measurement of set spacing would be quicker in some circumstances.

Both laser scanning and photogrammetry can be used for slope profiling and monitoring. The systems provide a method of taking multiple 2D profiles along vast sections of rock slopes/ cliffs, as well as quick 3D comparisons of slopes/ cliffs over time. Using the remote data capture systems for 2D/3D profiling does provide benefits, however there are already systems and methodologies that are currently used to complete these tasks. Slope profiling can be completed using spot measurements from a total station, and where reflector stations are installed then only a theodolite is needed. These methods are not as rapid as photogrammetry or laser scanning but are not as expensive. A compromise is made over the amount of data collected; laser scanning and photogrammetry will collect thousands of data points rapidly, however in some cases of slope profiling only a few data points are required and speed is not

always an issue. When monitoring of a potentially unstable slope is required then laser scanning and/or photogrammetry will become more suitable. The remote data capture systems can visualise a large area or entire slopes and monitor for changes over long time periods, such as coastal erosion. However, real-time monitoring is required for certain applications, such as working quarries and mines. True real-time monitoring is currently undertaken by slope radar systems, such as Slope Stability Radar (Groundprobe, 2008). Photogrammetry requires post-processing to create 3D images so would not fit the requirements for real-time monitoring. A laser scanner can be setup to continually scan a face and record any changes in the morphology of a slope. This will provide real-time data, however a scan of a large face, even when using a phase based laser scanner, would take minutes, a delay which can be critical.

The end-uses for data collected by photogrammetry and laser scanning are broad and the use of remote data capture systems provide many benefits. However, as currently adopted methods of collecting data for these end-uses have developed, they have become more specialised, such as slope profiling and monitoring, which have specialist methods for data capture (mentioned in previous paragraphs, above) and ore estimation, whose data is primarily produced by drilling. The end uses that may benefit greatly from remote data capture systems would be those that traditionally rely on data collected by hand. The geotechnical data collected by remote mapping systems is both suitable and advantageous for most geotechnical applications that require large volumes of data to increase precision. Kinematic analysis and geotechnical modelling programs, such as FracMan (Dershowitz *et al.*, 1998; Golder Associates, 1998), benefit greatly from the increased speed and volume of data capture. The digital nature of the remote systems enables the data to be incorporated more rapidly into geological fieldwork studies. It also increases the safety and negates access problems concerned with geological mapping of quarry slopes and coastal cliffs. Even though these remote data capture systems will benefit these particular end-uses, they are generally undertaken by research groups and smaller scale institutions, which may not be able to afford the equipment, expertise, and possible consultancy fees. Before making the decision for using remote data capture systems an individual case-by-case cost-benefit analysis should be carried out.

6.2 Further Work

Automatic feature identification capability was not analysed in great depth during this project. Preliminary testing found that current systems produced erroneous results, e.g. missing some features of certain orientations. Algorithms used to automatically

identify features are continually being developed and will become more robust. A semi-automatic system is being developed by ITC, Netherlands (Slob, 2007), where a feature is manually selected and a feature automatically 'grows' to fill the plane/discontinuity trace. This would provide quicker feature identification whilst allowing for a knowledgeable user manual intervention and associated interpretation of the rock slope.

Comparison of set spacing analyses were not made during this project as the SplitFX program is not currently able to calculate set spacing. This is not due to a limitation of laser scanned point clouds; Slob *et al.* (2005) have calculated set spacing from laser scanned rock faces. This feature will be incorporated into the SplitFX program in future versions. Once this is completed, spacing and subsequent block size distributions calculations can then be compared between both remote data capture techniques and traditional methods.

New versions of laser scanners are now able to position themselves using back-sights, similarly to theodolites, although to use the new ability, previously surveyed points must be within view of the scanner. If these are unavailable then the laser scanner must be positioned using one of the surveying techniques described in earlier chapters. New hardware versions of laser scanners will also have the ability to scan at larger distances with densities which allow for geotechnical mapping. The introduction of using zoom lenses for photogrammetry and increased laser point cloud range will enable multiple rock mass scales to be captured from single setup positions using multiple models. This will remove the need for numerous setups and increase the speed and efficiency of field mapping.

Developments should also be undertaken to ensure that post-processing is tailored to end-use requirements. Currently the processes involved in achieving output of geotechnical data from the remote mapping systems are convoluted and time consuming. There is no fundamental reason that the remote mapping techniques cannot measure the majority of rock mass characteristics; currently it is the software programs that are the limitation. With the introduction of software updates and feature enhancements the process workflow chart can be simplified and made consistent across the data capture techniques (Figure 6-2).

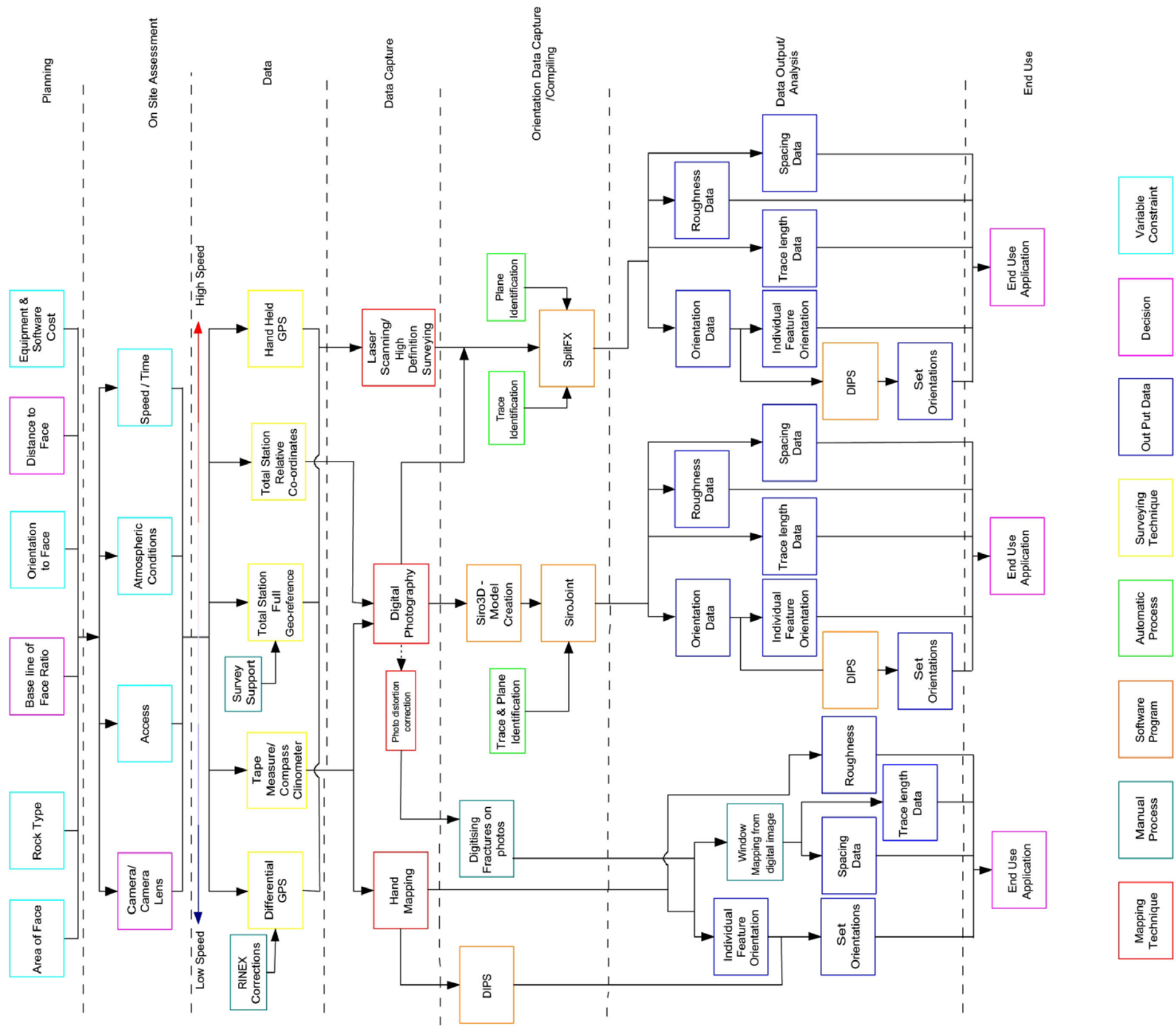


Figure 6-2. Ideal work-flow diagram (with key underneath). The process work-flow is more simplified whilst each mapping technique can assess multiple rock mass characteristics.

7 CONCLUSIONS

7.1 Key Findings

The thesis has developed and evaluated the techniques of digital remote, non-contact, geotechnical data capture using photogrammetry and laser scanning for both natural and manmade rock slopes. During the course of this study, new techniques and methodologies for the use of remote mapping have been developed and compared, and limits identified based on field applications.

Improved field methodologies have been implemented to aid the safe, efficient, and suitable geotechnical characterisation of rock fracture networks. Streamlining of the surveying/ positioning processes has allowed for the reduction of the persons required in the field to one or two people. However, this has required the persons in the field to be proficient at both remote data capture and surveying. Field and post-processing practices have been developed to be sufficiently robust and efficient for the collection of remote data for geotechnical purposes.

The surveying system best suited to photogrammetry for autonomous general use was found to be the total station. The laser scanner only required the use of the compass clinometer to reference the equipment to north. Both surveying systems could be combined with the handheld GPS if near-full geo-referencing was preferred or DGPS if sub centimetre georeferencing is required.

The data capture techniques were compared and demonstrated that remote data capture systems are faster than hand-mapping when collecting and analysing large volumes of geotechnical data. However, in certain applications, i.e. for small scale studies traditional mapping is more time efficient.

Remote mapping techniques must be used within certain field limits to achieve suitable data quality. The most accurate and precise baseline to face ratio for photogrammetry was found to be 0.25 – 0.166, however this was only conducted on one rock type. As the baseline to face angle decreased the accuracy decreased and effects of blinding increased, thus it is recommended that a perpendicular setup to the study face is used when possible. Laser scanning requires a sufficient scan density to visualise discontinuities satisfactorily, this is impacted by the distance that the equipment is to the study face as well as the fracture characteristics of the rock mass studied.

Photogrammetry and laser scanning can be used to characterise rock masses from various lithologies, although they are best suited to blocky rock masses. When using remote mapping techniques considerations must be made about the scales of structures mapped and the geomorphology of the study face. Remote data capture systems cannot efficiently capture certain rock mass characteristics, such as aperture and infill.

An adapted method for quantitatively assessing roughness from a fracture plane (Tse & Cruden, 1979) was proposed, but due to time constraints, has not been tested. It would automate and improve the accuracy by replacing a traditionally used profilometer with profiles produced within AutoCAD. Currently, close range 3D models are required to capture roughness data, which implies access to the study face is not an issue, so traditional methods used to capture roughness data may be more suitable. Long range, high density, 3D images will suffer from noise which will mask the true roughness of the study face. Previous research has indicated that fractal measurements may produce reliable JRC (roughness) values as well as those from profiles, although the results of both are significantly linked to the scale at which the measurement is taken.

When assessing the effect of roughness on orientation measurements taken by remote data capture, it is indicated that large scale roughness can cause a change in orientation measurement for laser scanning and photogrammetric geotechnical analysis systems. If only a small section of a larger plane is available for measurement then the true orientation of the plane may be miscalculated by $\pm 9^\circ$, due to large scale roughness/undulation. However, when assessing the orientation from a 'whole' plane the roughness will not affect the measurement as the average is taken, which is advantageous over hand-mapping which requires multiple spot measurement to achieve an orientation.

A new method of comparing orientation data measurement, pole vector difference (PVD), has been implemented. This eliminates comparative problems between conventional dip/ dip direction orientation measurement by converting them to their constituent vectors. By using a hand-mapping vs. hand-mapping comparative study qualitative descriptions of the pole vector differences were developed. A PVD between hand-mapping and remote data capture systems was deemed to be 'low' if less than 15° , and 'medium' up to 32° , where a greater value is 'high'. A 10° PVD between the

remote data capture systems was thought to be due to noise on the surfaces of the 3D models.

Using the pole vector difference method, the accuracies of the remote data capture systems have been assessed against traditionally mapped data and found have low PVDs between one another ($\sim 12^\circ$ average). The pole vector differences from traditional mapping compared between individual features as well as discontinuity sets are acceptable enough so that the data collected remotely can be used in subsequent geotechnical studies. The results show that the laser scanned and the photogrammetrically-derived orientation data produced results that adequately match the hand-mapped data for both the near-vertical features and the more horizontal features. Photogrammetry and laser scanning have been shown to provide orientation data with similar (and potentially better) accuracy and precision to traditional mapping techniques. A separate comparison between laser scanning and photogrammetry found that the PVD was lower ($\sim 10^\circ$) than when the techniques were compared against hand-mapping. However, orientation data collected from photogrammetric tracelengths should be used with caution as the accuracy and precision is lower than the results achieved using planes. It was also ascertained that discontinuity trace length data from photogrammetry provides $\sim 90\%$ of discontinuity trace lengths mapped from digital photographs.

Currently hand-mapping is the primary form of data capture for mining and quarrying processes; this is due to it being a trusted and understood method of data capture. Remote data capture systems are slowly being incorporated to aid and advance data capture for these industries, using them to visualise excavations and blast zones, whilst also providing rapid collection of detailed geotechnical data which is quickly incorporated in mine planning and geotechnical modelling software, e.g. Datamine software suite (Datamine, 2007) and FracMan (Dershowitz *et al.*, 1998; Golder Associates, 1998). The use of the visual data collected using remote data capture systems, e.g. colour recognition, could be a useful application. To create the images is a step within the photogrammetric 3D model progression, so no extra processing is needed. Similar data can be extracted from normal 2D photographs, but the integration of spatial data allows for additional measurements/data to be taken.

Not all the end-use applications benefit greatly from using remote data capture techniques. For example, RMR and Q ratings, whilst using the remotely captured data to estimate the orientation components, there is a need for close contact with the rock

mass to capture other parameters, such as joint alteration/ condition. Additionally, even though photogrammetry and laser scanning can also be used for slope profiling and monitoring, there are products available that can complete the tasks required more efficiently and cost effectively for certain scenarios (e.g. real-time monitoring). This highlights the importance of selecting the correct form of remote data capture for the particular end-use, or that a combination of the data capture techniques should be adopted.

7.2 Summary

Both photogrammetry and laser scanning case studies have been carried out on both natural coastal cliffs and manmade slopes. They have been shown to provide spatially accurate, detailed 3D representations of the rock mass. The systems allow rapid collection of large quantities of data that can be subsequently analysed to provide realistic representations of the rock mass fracture network. However, these systems are not currently regulated, ISRM guidelines should be introduced to standardise remote data capture fieldwork and post-processing.

Another advantageous aspect of the remote mapping systems is their ability to map inaccessible and potentially dangerous rock faces that would be impossible for conventional hand-mapping. This is inherent to the 'remote' nature of the data capture. It also provides uniformity in the type of data and the method by which it is collected, eliminating many of the biases in data selection and mapping technique adopted by an individual user. The increased data capture, and relatively automated statistical treatment, allowed by these methods can also remove some of the subjectivity involved in the data interpretation. However, there is still a need for manual intervention/ spot checks on data and 3D models by an educated/ trained user who is aware of the advantages and limitations of both the hardware and associated software.

The 3D nature and large amounts of data collected by remote mapping techniques is advantageous to multiple end-uses. The large volumes of data help statistically based programs to produce more robust models, e.g. FracMan. Unfortunately, many applications cannot make efficient use of this mass 3D data. Usually it is reduced and/ or converted into 2D, rather than using the full complement of data collected. Some end-use applications are beginning to actively incorporate the collected data, e.g. Datamine (Datamine, 2007) and are combining the Sirovision program into their software suite. McCaffery (2005) also draws attention to the need to integrate this data into a final interoperable product.

The use of remote mapping techniques has particular advantages where it may be necessary to map at different scales to provide improved characterisation of the rock mass by using different set-up positions or different lenses. Large scale mapping can be undertaken to provide orientation and discontinuity trace length data for major structures which can then be complemented by more detailed traditional mapping on a smaller scale. A combination of photogrammetry and physical contact assessment is beneficial for mapping complex, highly fractured lithologies.

Through testing undertaken during this study it was possible to create a method of quickly assessing the various attributes that the three mapping techniques have. The individual and shared advantages of the mapping techniques are represented in Figure 7-1. When deciding which mapping technique is best suited for a particular application this figure can be referred to.

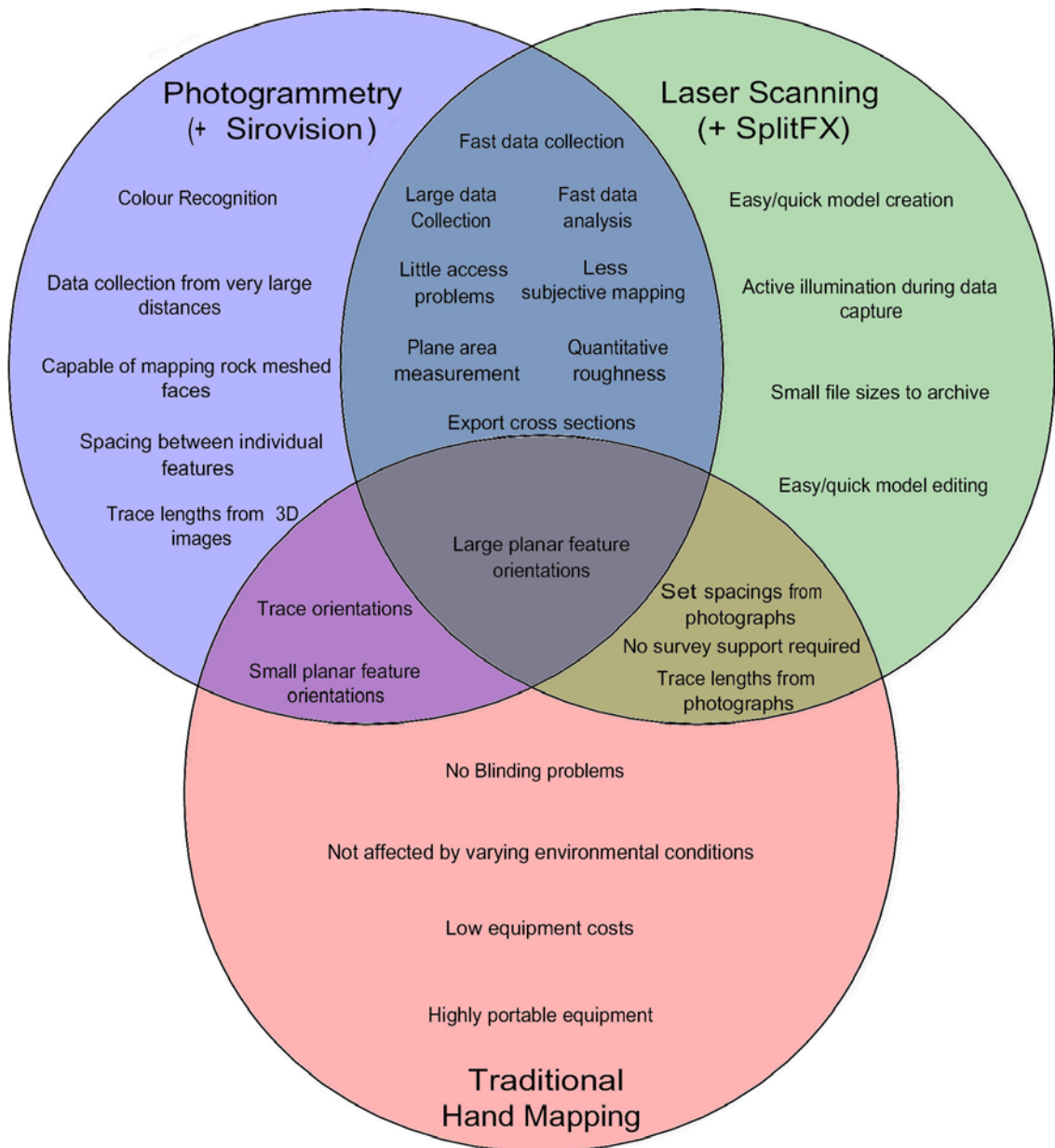


Figure 7-1. Venn diagram showing individual and shared advantages between hand and remote mapping techniques to capture rock mass characteristics.

The continual development and use of remote mapping techniques, whilst supplementing their unique qualities with traditional mapping, have the capability to revolutionise rock mass mapping.

8 REFERENCES

3D LASER MAPPING (2007) SiteMonitor - slope stability monitoring system. www.3Dlasermapping.com.

3G SOFTWARE & MEASUREMENT (2006) ShapeMetriX3D White Paper. http://www.3gsm.at/downloads/SMX_Info_en_v1.16.pdf

ADAMI, A., GUERRA, F. & VERNIER, P. (2007) Laser scanner and architectural accuracy text. In: GEORGOPOULOS, A. (Ed.) *XXI International CIPA Symposium*. Athens, Greece.

ADAMS, J. & CHANDLER, J. (2002) Evaluation of LIDAR and medium scale photogrammetry for detecting soft-cliff coastal change. *The Photogrammetric Record*, 17, 405-418.

ALEXANDER, A. C. & SHAIL, R. K. (1995) Late Variscan structures on the coast between Perranporth and St. Ives, Cornwall. *Proceedings of the Ussher Society*, 8, 398-404.

ATKINSON, K. B. (1996) *Close range photogrammetry and machine vision*. Whittles Publishing, UK.

AUTODESK INC (2008) AutoCAD 2008 (R17.1) - 2D and 3D design and drafting. www.autodesk.co.uk.

BAGDE, M. N., RAINA, A. K., CHAKRABORTY, A. K. & JETHWA, J. L. (2002) Rock mass characterization by fractal dimension. *Engineering Geology*, 63, 141-155.

BAKER, B. R., GESSNER, K., HOLDEN, E. J. & SQUELCH, A. P. (2008) Automatic detection of anisotropic features on rock surfaces. *Geosphere*, April 2008, 4, no 2, 418 – 428.

BARBER, D. & MILLS, J. (2007) Rapid mapping techniques in coastal environment: Monitoring the coastline. RICS and University of Newcastle.

BARNES, J. W. (1990) *Basic geological mapping*, Open University Press New York: Halsted Press.

BARNSLEY, M.F. (1988) *Fractals everywhere*: London, UK, Academic Press.

BARTON, N. R. (1973) Review of a new shear strength criterion for rock joints. *Engineering Geology, Elsevier*, 7, 287-322.

BARTON, N. R., LIEN, R. & LUNDE, J. (1974) Engineering classification of rock masses for the design of tunnel support. *Rock Mechanics*, 6, 183-236.

BELEM, T., HOMAND-ETIENNE, F. & SOULEY, M. (1997) Fractal analysis of shear joint roughness. *International Journal of Rock Mechanics and Mining Sciences*, 34, 130.e1-130.e16.

BEUTLER, G., ROTHACHER, M., SCHAER, S., SPRINGER, T. A., KOUBA, J. & NEILAN, R. E. (1999) The international GPS service (IGS): An interdisciplinary service in support of earth sciences. *Adv. Space Res*, 23(4), 631-635.

BIENIAWSKI, Z. T. (1973) Engineering classification of jointed rock masses. *Transactions of the South African Institute of Civil Engineers*, 335–344.

BIENIAWSKI, Z. T. (1989) *Engineering rock mass classification*, Wiley, Chichester, UK.

BIRCH, J.S. (2006) Using 3DM Analyst Mine Mapping Suite for Rock Face Characterisation. In: TONON, F. & KOTTENSTETTE, J., *Laser and Photogrammetric Methods of Rock Face Characterization*. GoldenRocks 2006, the 41st U.S. Rock Mechanics Symposium, Colorado School of Mines, June 17 - 21, 2006.

BIRD, E. C. F. (2000) *Geomorphology: An introduction*, John Wiley, Chichester, UK.

BOCK, O., KASSER, M., THOM, C. & PELON, J. (1998) Study of a wide-angle laser ranging system for relative positioning of ground-based benchmarks with millimeter accuracy. *Journal of Geodesy*, 72, 442-459.

BOEHLER, W., BORDAS VINCENT, M. & MARBS, A. (2003) Investigating laser scanner accuracy. *XIX CIPA Symposium*. Antalya, Turkey.

BOOTH, B. (1966) Petrogenesis of the Land's End Granites. University of Keele.

BOYD, J. M., HINDS, D. V., MOY, D. & ROGERS, C. (1973) Two simple devices for monitoring movements in rock slopes. *Quarterly Journal of Engineering Geology & Hydrogeology*, 6, 295-302.

BRADY, B. H. C. & BROWN, E. T. (1994) *Rock mechanics for underground mining*, Chapman & Hall, London: 571.

BROWN, E. T., RICHARDS, L. R. & BARR, M. V. (1977) Shear strength characteristics of the Delabole Slates: Proc conference on rock engineering. *International Journal of Rock Mechanics & Mining Science & Geomechanics Abstracts*, 14, 33-51.

BUTLER, J. B., LANE, S. N. & CHANDLER, J. H. (1998) Assessment of DEM quality for characterizing surface roughness using close range digital photogrammetry. *The Photogrammetric Record*, 16, 271-291.

CAMPBELL, J. B. (2002) *Introduction to remote sensing (3rd edition)*, Taylor & Francis, London.

CG SURVEYING LTD (2007) Leica RTK GPS Smart Rover Quote.

CLEVELAND, W.S. (1985) The Elements of Graphing Data, "Graphical Perception,". Wadsworth Inc.

CLOVER, A. W. (1978) Some aspects of the rock excavations on the western face at Delabole slate quarry, Cornwall., *MSc Thesis*, Imperial College, University of London.

COGGAN, J. S. & PINE, R. J. (1996) Application of distinct-element modelling to assess slope stability at Delabole slate quarry, Cornwall, England. *Trans. Inst. Min. Metall. Sect A: Mining Industry*, 105, A22–A30.

COGGAN, J. S., PINE, R. J., STYLES, T. D. & STEAD, D. (2007) Application of hybrid finite/discrete element modelling for back-analysis of rock slope failure mechanisms. *Slope Stability 2007, International Symposium on Rock Slope Stability in Open Pit Mining and Civil Engineering*. Perth, Australia, 267-277

COGGAN, J. S., WETHERELT, A., GWYNN, X. P. & FLYNN, Z. N. (2007) Comparison of hand-mapping with remote data capture systems for effective rock mass characterisation. In: SOUSA, L. R., OLALLA, C. & GROSSMANN, N. F. (Eds.) *11th Congress of the International Society for Rock Mechanics*. Lisbon, Portugal, Taylor & Francis, 201-206.

COSTA, M., COGGAN, J. S. & EYRE, J. M. (1999) Numerical modelling of slope behaviour of Delabole slate quarry (Cornwall, UK). *International Journal of Mining, Reclamation and Environment*, 13, 11 - 18.

CRONE, D. R. (1963) *Elementary photogrammetry*, Arnold, London.

CSIRO (2005) Sirovision 3D imaging mapping system. CSIRO Australia.

CSIRO (2005) User manual for Sirovision structural mapping and analysis system 3.0 ed. Queensland. Australia, CSIRO Exploration and Mining.

CSIRO (2006) User manual for Sirovision structural mapping and analysis system 3.1 ed. Queensland. Australia, CSIRO Exploration and Mining.

DATAMINE (2007) Datamine software suite. www.datamine.co.uk.

DENNIS, J. G. (1967) *International tectonic dictionary*, American Association of Petroleum Geology.

DERRON, M.-H., JABOYEDOFF, M. & BLIKRA, L. H. (2005) Preliminary assessment of landslide and rockfall hazard using a DEM (Oppstadhornet, Norway) *Natural Hazards and Earth System Science*, 5, 285-292, 2005.

DERSHOWITZ, W., LEE, G., GEIER, J. & LAPOINTE, P. R. (1998) *FracMan: Interactive discrete feature data analysis, geometric modelling and exploration simulation*. User documentation. Golder Associates Inc., Seattle, Washington.

DONNADIEU, F., KELFOUN, K., VAN WYK DE VRIES, B., CECCHI, E. & MERLE, O. (2003) Digital photogrammetry as a tool in analogue modelling: Applications to volcano instability. *Journal of Volcanology and Geothermal Research*, 123, 161-180.

DONOVAN, J., HANDY, J., KEMENY, J. & O'BRIEN G. (2005) Automatic acquisition and determination of rock discontinuity properties using three-dimensional laser scanning. Proceedings of Applications of Computers and Operations Research in the Mineral Industry (APCOM 2005), S. Dessureault Editor, Tucson, AZ.

FARDIN, N., FENG, Q. & STEPHANSSON, O. (2004) Application of a new in situ 3D laser scanner to study the scale effect on the rock joint surface roughness. *International Journal of Rock Mechanics & Mining Sciences*, 41, 329-335.

FARO (2005) Faro laser scanner LS brochure. www.faro.com.

FAVEY, E., PATERAKI, M., BALTSAVIAS, E. P., BAUDER, A. & BÖSCH, H. (2001) Digital surface modelling by airborne laser scanning and digital photogrammetry for glacier monitoring. *Photogrammetric Record*, 17(98), 243–273.

FENG, Q., SJOGREN, P., STEPHANSSON, O. & JING, L. (2001) Measuring fracture orientation at exposed rock faces by using a non-reflector total station. *Engineering Geology*, 59, 133-146.

FENG, Q. H. & ROSHOFF, K. (2004) In-situ mapping and documentation of rock faces using a full-coverage 3D laser scanning technique. *International Journal of Rock Mechanics & Mining Sciences*, 41, 139-144.

FISHER, R. (1953) Dispersion on a sphere. *Proc. Royal Society London*, A217, pp. 295-305.

FLYNN, Z. N. & PINE, R. J. (2007) Fracture characterisation determined by numerical modelling analyses. In: SOUSA, L. R., OLALLA, C. & GROSSMANN, N. F. (Eds.) *11th Congress of the International Society for Rock Mechanics*. Lisbon, Portugal, Taylor & Francis, 293-298.

FRASER, C. S., WOODS, A. & BRIZZI, D. (2005) Hyper redundancy for accuracy enhancement in automated close range photogrammetry. *The Photogrammetric Record*, 20, 205-217.

GAICH, A., POTSCH, M. & SCHUBERT, W. (2006) Basics and application of 3D imaging systems with conventional and high-resolution cameras. In: TONON, F. & KOTTENSTETTE, J., Laser and Photogrammetric Methods of Rock Face Characterization. GoldenRocks 2006, the 41st U.S. Rock Mechanics Symposium, Colorado School of Mines, June 17 - 21, 2006.

GAICH, A. (2007) Photogrammetric accuracy. Personal Communication, Lisbon.

GENTER, A., DUPPERRET, A., MARTINEZ, A., MORTIMORE, R. N. & VILA, J. L. (2004) Multiscale fracture analysis along the French chalk coastline for investigating erosion by cliff collapse. In: MORTIMORE, R. N. & DUPPERRET, A. (Eds.) *Coastal chalk cliff instability*. Geological Society, London, Engineering Geology Special Publications.

GOLDER ASSOCIATES (1998) FracMan software suite. Redmond, USA, FracMan Technology Group. www.golder.com.

GOODMAN, R. E. (1989) Deformability of rocks, introduction to rock mechanics (2nd edition), Wiley, New York.

GROUNDPROBE (2008) Slope Stability Radar. South Brisbane Queensland, Australia. www.groundprobe.com

HALL, J. W., MEADOWCROFT, I. C., LEE, E. M. & GELDER, P. H. A. J. M. V. (2002) Stochastic simulation of episodic soft coastal cliff recession. *Coastal Engineering*, 46(3).

HANEBERG, W.C., (2007) Directional roughness profiles from three-dimensional photogrammetric or laser scanner point clouds. In: EBERHARDT, E., STEAD, D., & MORRISON, T., (Eds) Rock Mechanics: Meeting Society's Challenges and Demands. Proceedings of the 1st Canada-US rock mechanics Symposium, Vancouver, Canada, 27 – 31 May 2007.

HANDY, J. (2007) SplitFX roughness analysis email correspondence. Personal Communication, email.

HEIKKINEN, J. (2005) The circular imaging block in close range photogrammetry. *Department of Surveying, Institute of Photogrammetry and Remote Sensing*. Helsinki, Helsinki University of Technology.

HERITAGE, G. L., FULLER, I. C., CHARLTON, M. E., BREWER, P. A. & PASSMORE, D. P. (1998) CDW photogrammetry of low relief fluvial features: Accuracy and implications for reach-scale sediment budgeting. *Earth Surface Processes and Landforms*, 23, 1219-1233.

HOEK, E. (2007) *Practical rock engineering*, Institute of Mining and Metallurgy, London.

HOEK, E. & BRAY, J. W. (1977) *Rock slope engineering*, Institute of Mining and Metallurgy, London.

HUDSON, J. A. & HARRISON, J. P. (1997) *Engineering rock mechanics, an introduction to the principles*, Elsevier, Oxford, UK.

HUISING, E. J. & PEREIRA, L. M. G. (1998) Errors and accuracy estimates of laser data acquired by various laser scanning systems for topographic applications. *ISPRS Journal of Photogrammetry and Remote Sensing*, 53, 245-261.

Health and Safety Commission (1999) Health and safety at quarries. Quarries Regulations 1999, approved code of practice. HSE Books, Sudbury, UK.

ISRM, I.S.F.R.M. (2007) The complete ISRM suggested methods for rock characterization, testing and monitoring: 1974-2006, Oxford, UK, Pergamon.

JABOYEDOFF, M. & BAILLIFARD, F. (2004) Structural analysis using DEM and COLTOP- 3D computer program. 2nd Swiss Geoscience Meeting, Lausanne, 19 – 20 November, 2004.

JABOYEDOFF, M. & COUTURE (2003) Report on the project COLTOP3D for March 2003: stay of Michael Jaboyedoff at GSC – Ottawa. Quanterra administrative document – Activity report – RA01.

JABOYEDOFF, M., METZGER, R., OPPIKOFER, T., COUTURE, R., DERRON, M.H., LOCAT, J. & TURMEL, D. (2007) New insight techniques to analyze rock-slope relief using DEM and 3D-imaging cloud points: COLTOP-3D software. Proceedings of the 1st Canada-US rock mechanics Symposium, Vancouver, Canada, 27 – 31 May 2007.

JONES, R. R., MCCAFFREY, K. J. W., CLEGG, P., WILSON, R. W., HOLLIMAN, N. S., HOLDSWORTH, R. E., IMBER, J. & WAGGOTT, S. (2007) Integration of regional to outcrop digital data 3D visualisation of multiscale geological models. *Computers & Geosciences*, 33.

KEMENY, J. & DONOVAN, J. (2005) Rock mass characterisation using LIDAR and automated point cloud processing. *Ground Engineering*, November, 26-29.

KEMENY, J., HANDY, J., DONOVAN, J. & THIAM, S. (2004) Automatic Discontinuity Characterization of Rock Faces Using 3D Laser Scanners and Digital Imaging. *Gulf Rocks 2004 (ARMA 2004 Rock Mechanics Symposium and the 6th NARMS)*, Houston, TX.

KEMENY, J. & POST, R. (2003) Estimating Three-Dimensional Rock Discontinuity Orientation from Digital Images of Fracture Traces. *Computers & Geosciences* Vol. 29, pp. 65-77.

KEMENY, J., TURNER, K. & NORTON, B. (2006) LIDAR for rock mass characterization: Hardware, software, accuracy and best practices. In: TONON, F. & KOTTENSTETTE, J., *Laser and Photogrammetric Methods of Rock Face Characterization*. GoldenRocks 2006, the 41st U.S. Rock Mechanics Symposium, Colorado School of Mines, June 17 - 21, 2006.

KERSTEN, T., STERNBERG, H., MECHELKE, K. & ACEVEDO PARDO, C. (2004) Terrestrial laser scanning Mensi GS100 GS200 accuracy tests experiences and projects at the Hamburg university of applied sciences. *Panoramic Photogrammetry Workshop*. Stuttgart, Germany, ISPRS WG.

KILBURN, C. R. J. & PETLEY, D. N. (2003). Forecasting giant, catastrophic slope collapse: lessons from Vajont, Northern Italy. *Geomorphology*, 54, 21 – 32.

KOHOUSĚK, I. (2006) Laser scanning for geotechnical engineering. *3rd IAG, 12th FIG Symposium*. Baden, Germany.

KULATILAKE, P., BALASINGAM, P., PARK, J. & MORGAN, R. (2006) Natural rock joint roughness quantification through fractal techniques. *Geotechnical & Geological Engineering*, 24, 1181-1202.

LA POINTE, P. R. (2002) Derivation of parent fracture population statistics from trace length measurements of fractal populations. *International Journal of Mechanics & Mining Sciences*, 39, 381-388.

LATO, M., DIEDERICHS, M.S., HUTCHINSON, D.J., & HARRAP, R. (2008) Optimization of LiDAR scanning and processing for automated structural evaluation of discontinuities in rock masses. *International Journal of Rock Mechanics and Mining Sciences*, 46, 194 – 199.

LAWRENCE, J. (2007) Hand-mapped data from Portobello cliff, Brighton, UK. Personal Communication.

LEBOUTILLIER, N. G. (2003) The tectonics of Variscan magmatism and mineralisation in South West England. *Camborne School of Mines*. Camborne, University of Exeter.

LEICA (2005) *HDS3000 user manual*, Leica Geosystems AG, Germany.

LEICA (2005) *Leica DGPS 1200 user manual*, Leica Geosystems AG, Germany.

LEICA (2005) *Leica TPS 1200 user manual*, Leica Geosystems AG, Germany.

LEICA (2006) *HDS4500 user manual*, Leica Geosystems AG, Germany.

LEICA (2006) Cyclone. Germany, Leica Geosystems.

LICHTI, D. D., & HARVEY, B. R. (2002) The effects of reflecting surface material properties on time-of-flight laser scanner measurements. *Geomatics research Australia*, 74, 1 – 22.

- LIM, M., PETLEY, D. N., ROSSER, N., ALLISON, R. J., LONG, A. J. & PYBUS, D. (2005) Combined digital photogrammetry and time-of-flight laser scanning for monitoring cliff evolution. *The Photogrammetric Record*, 20, 109-129.
- LIM, S. S. & YANG, H. S. (2004) An analysis of plane failure of rock slopes by quantified stereographic projection. *International Journal of Rock Mechanics and Mining Sciences*, 41, 744-749.
- LINTZ, J. & SIMONETT, D. D. (1976) *Remote sensing of the environment*, Addison-Wesley, London.
- MAERZ, N.H., FRANKLIN, J.A. & BENNETT, C.P. (1990) Joint roughness measurement using shadow profilometry. *International Journal of Rock Mechanics and Mining Sciences* 27:55, 329 – 343.
- MARINOS, P. & HOEK, E. (2000) GSI: A geologically friendly tool for rock mass strength estimation. *GeoEng2000 at the international conference on geotechnical and geological engineering*. Melbourne, Australia, Technomic Publishers, Lancaster.
- MCCAFFREY, K. J. W., HOLDSWORTH, R. E., CLEGG, P., JONES, R. R. & WILSON, R. (2003) Using digital mapping and 3D visualization to enhance and modernise undergraduate fieldwork experience. *Planet*, Special Edition, 34-36.
- MCCAFFREY, K. J. W., JONES, R. R., HOLDSWORTH, R. E., WILSON, R. W., CLEGG, P., IMBER, J., HOLLIMAN, N. & TRINKS, I. (2005) Unlocking the spatial dimension: Digital technologies and the future of geoscience fieldwork. *Journal of the Geological Society, London*, 162, 927–938.
- MCCLAY, K. (1992) *The mapping of geological structures*, John Wiley & Sons, Chichester, UK.
- MCGLONE, C. J. (2004) *Manual of photogrammetry (fifth edition)*, Maryland, US, American Society for Photogrammetry and Remote Sensing.
- MDL LASER SYSTEMS (2007) Quarryman Pro. www.mdl.co.uk.

MEREL, A. P. & FARRER, P. J. (1998) The monitoring of soil surface development using analytical photogrammetry. *Photogrammetric Record*, 16(92), 331-345.

METZGER, R., JABOYEDOFF, M. & DERRON, M. H. (2008) Coltop-3D: A software for analyzing landslides using 3D-imaging cloud points. *International Geological Congress (33IGC), Oslo, Norway, 6-14 August, 2008*

MORTIMORE, R. N., LAWRENCE, J., POPE, D., DUPERRER, A. & GENTER, A. (2004) Coastal cliff geohazards in weak rock: The UK chalk cliffs of Sussex. In: MORTIMORE, R. N. & DUPERRER, A. (Eds.) *Coastal chalk cliff stability*. Geological Society, London, Engineering Geology, Special Publications, 3-31.

NIKON (2005) *User manual for Nikon D100 digital camera*, Nikon Corporation, Tokyo, Japan.

OKA, N. (1998) Application of photogrammetry to the field observation of failed slopes. *Engineering Geology*, 50, 85-100.

OLARIU, M. I., FERGUSON, J. F., AIKEN, C. L. V., & XU, X. (2008) Outcrop fracture characterization using terrestrial laser scanners: Deep-water Jackfork sandstone at Big Rock Quarry, Arkansas. *Geosphere*, February 1, 2008, 4, 247 - 259.

ORDNANCE SURVEY (2005) How GPS works. www.ordancesurvey.co.uk.

PARKER, H. (2004) Estimation and production of armour stone at Penlee Quarry. MSc Thesis, Camborne School of Mines, University of Exeter.

PEDRAZZINI, A., JABOYEDOFF, M., FROESE, C. R., LANGENBERG, W., & MORENO, F. (2008) Structure and failure mechanisms analysis of Turtle Mountain. Proceedings of the 4th Canadian Conference on Geohazards: From Causes to Management, Québec City, Québec, May 20 – 24, 2008

PETLEY, D. N., BULMER, M. H. & MURPHY, W (2002) Patterns of movement in rotational and translational landslides. *Geology*, 30, no. 8, 719 – 722.

PINE, R. J., COGGAN, J. S., FLYNN, Z. N. & ELMO, D. (2006) The development of a new numerical modelling approach for naturally fractured rock masses. *Rock Mechanics and Rock Engineering*, 39, 395-419.

POROPAT, G. V. (2001) New methods for mapping the structure of rock masses. *CSIRO Exploration and Mining*. Queensland Centre for Advanced Technologies.

POROPAT, G. V. (2005) Sirovision operation. Personal Communication, email.

POROPAT, G. V. (2006) Remote 3D mapping of rock mass structure. In: TONON, F. & KOTTENSTETTE, J., *Laser and Photogrammetric Methods of Rock Face Characterization*. GoldenRocks 2006, the 41st U.S. Rock Mechanics Symposium, Colorado School of Mines, June 17 - 21, 2006.

POROPAT, G.V. (2008) Remote characterization of surface roughness of rock discontinuities. In: POTVIN, Y., CARTER, J., DYSKIN, A., & JEFFREY, R. (Eds) *Proceedings of the 1st Southern Hemisphere International Rock Mechanics Symposium (SHIRMS-08)*

POROPAT, G., V., ELMOUTTIE, M.K. & WALFORD, D. (2007) Joint set definition using topology based structure mapping. *Proceedings of the 1st Canada-US rock mechanics Symposium, Vancouver, Canada, 27 – 31 May 2007.*

POTERASU, M., MORALES, M. O. & AZPEITIA, J. (2001) A laser system for high accuracy measurement of small apertures in mechanical parts. *Optics and Lasers in Engineering*, 36, 545-550.

PRICE, N. J. & COSGROVE, J. W. (1990) *Analysis of geological structures*, Cambridge University Press, Cambridge.

PRIEST, S. D. (1993) *Discontinuity analysis for rock engineering*, Chapman and Hall, London.

RAHMAN, Z., SLOB, S. & HACK, R. (2006) Deriving roughness characteristics of rock mass discontinuities from terrestrial laser scan data. *Proceedings of the 10th IAEG Congress, Nottingham, United Kingdom, 6-10 September 2006.*

RASBAND, W. (2007) ImageJ 1.38x. National Institutes of Health, USA. www.rsweb.nih.gov/ij/.

RATCLIFFE, S. & MYERS, A. (2006) Laser scanning in the open pit mining environment, a comparison with photogrammetry. I-SiTE 3D Laser Imaging.

REEVES, R. G. (1975) *Manual of remote sensing*, American Society of Photogrammetry, Virginia, US.

ROCKFIELD SOFTWARE (2007) ELFEN 2D/3D numerical modelling package. Rockfield Software Ltd., Swansea.

ROCSCIENCE (2006) Rocscience software. Toronto, Rocscience Inc.

RONCELLA, R. & FORLANI, G. (2005) Extraction of planar patches from point clouds to retrieve dip and dip direction of rock discontinuities. *SPRS WG III/3, III/4, V/3 Workshop "Laser scanning 2005"*. Enschede, the Netherlands.

ROSSER, N. J., PETLEY, D. N., LIM, M., DUNNING, S. A. & ALLISON, R. J. (2005) Terrestrial laser scanning for monitoring the process of hard rock coastal cliff erosion. *Quarterly Journal of Engineering Geology and Hydrogeology*, 38, 363-375.

ROSSER, N. J., DUNNING, S. A., LIM, M., & PETLEY, D. N. (2007). Terrestrial laser scanning for quantitative rockfall hazard assessment. In: HUNGR, O., FELL, R., COUTURE, R. & EBERHARDT, E., *Landslide Risk Management*. Amsterdam: A.T. Balkema.

ROYAL INSTITUTE FOR CHARTERED SURVEYORS (RICS) and SURVEY SYSTEMS (2007). Equipment for surveyors - total station price list. www.surveyors-equipment.com.

SALIU, M.A. (2009) Investigation into factors controlling the potential for dimension stone production of selected granites in South West Nigeria, *PhD Thesis*, Camborne School of Mines, University of Exeter.

SCHENK, T. (1999) Digital photogrammetry, TerraScience, Laurelville, OH, US

SELWOOD, E. B., DURRANCE, E. M. & BRISTOW, C. M. (1998) *The geology of Cornwall and the Isles of Scilly*, Exeter University Press.

SHAIL, R. K. & ALEXANDER, A. C. (1997) Late Carboniferous to Triassic reactivation of Variscan basement in the western English Channel: Evidence from onshore exposures in South Cornwall. *Journal of the Geological Society*, 154, 163 - 168.

SHAIL, R. K. & WILKINSON, J. J. (1994) Late- to post- Variscan extensional tectonics in South Cornwall. *Proceedings of the Ussher Society*, 8, 262-270.

SLAMA, I. (1980) *Manual of photogrammetry (4th edition)*, American Society of Photogrammetry, Virginia, US.

SLOB, S. (2007) Advancements in semi-automatic plane delineation from laser scanned point clouds. Personal Communication, Lisbon.

SLOB, S., HACK, R., FENG, Q. H., ROSHOFF, K. & TURNER, A.K. (2007) Fracture mapping using 3D laser scanner techniques. In: SOUSA, L. R., OLALLA, C. & GROSSMANN, N. F. (Eds.) *11th Congress of the International Society for Rock Mechanics*. Lisbon, Portugal, Taylor & Francis, 201-206.

SLOB, S., HACK, R., VAN KNAPEN, B., TURNER, A.K. & KEMENY, J. (2004) Automated identification and characterization of discontinuity sets in outcropping rock masses using 3D terrestrial laser scan survey techniques. *Proceedings of Eurock 2004 and 53rd Geomechanics Colloquy*, Salzburg, Austria.

SLOB, S., VAN KNAPEN, B., HACK, R., TURNER, K. A. & KEMENY, J. (2005) A method of automated discontinuity analysis of rock slopes with 3D laser scanning. *Transportation research record, Washington, USA*, 1913, 187-208.

SPLIT ENGINEERING (2005) *SplitFX user manual, beta version 1.0*, Split Engineering LLC, Arizona, US. www.spliteng.com.

STEAD, D., EBERHARDT, E. & COGGAN, J. S. (2006) Developments in the characterization of complex rock slope deformation and failure using numerical modelling techniques. *Engineering Geology*, 83, 217-235.

STROUTH, A. & EBERHARDT, E. (2006) The use of LIDAR to overcome rock slope hazard data collection challenges at Afternoon Creek, Washington. In: TONON, F. & KOTTENSTETTE, J., Laser and Photogrammetric Methods of Rock Face Characterization. GoldenRocks 2006, the 41st U.S. Rock Mechanics Symposium, Colorado School of Mines, June 17 - 21, 2006.

STRURZENEGGER, M., STEAD, D., FROESE, C., MOREN, F., JABOYEDOFF, M. (2007a) Ground based and airborne LiDAR for structural mapping of the Frank slide. Proceedings of the 1st Canada-US rock mechanics Symposium, Vancouver, Canada, 27 – 31 May 2007.

STURZENEGGER, M., YAN, M., STEAD, D. & ELMO, D. (2007b) Application and limitations of ground-based laser scanning in rock slope characterization. Proceedings of the 1st Canada-US rock mechanics Symposium, Vancouver, Canada, 27 – 31 May 2007.

TERZAGHI, R. (1965) Sources of errors in joint surveys. *Géotechnique*, 15, 287-304.

TONON, F. & KOTTENSTETTE, J.T. (2006) Summary paper on Morrison field exercise. In: TONON, F. & KOTTENSTETTE, J., Laser and Photogrammetric Methods of Rock Face Characterization. GoldenRocks 2006, the 41st U.S. Rock Mechanics Symposium, Colorado School of Mines, June 17 - 21, 2006.

TRIMBLE (2005) Trimble GPS tutorial. www.trimble.com.

TURNER, K., KEMENY, J., SLOB, S. & HACK, R. (2006) Evaluation and management of unstable rock slopes by 3D laser scanning, Proceedings of the 10th IAEG Congress, Nottingham, United Kingdom, 6-10 September 2006.

TSE, R. & D. M. CRUDEN (1979). Estimating joint roughness coefficients. *Int. J. Rock Mechanics and Mining Science & Geomechanics*. 16: 303-307.

UNAL, M., UNVER, B. & TERCAN, A.E. (2000) Modelling of discontinuity surface roughness by digital photogrammetry and geostatistical methods. *Proc. of 9th Int. Symp. On Mine Planning and Equipment Selection*, Athens, Greece. 391- 396.

VAN DER PLUIJM, B. A. & MARSHAK, S. (2004) *Earth structure, an introduction to geology and tectonics*. W.W. Norton & Company, London.

VOYAT, I., RONCELLA, R., FORLANI, G. & FERRERO, A.M. (2006) Advanced techniques for geostructural surveys in modelling fractured rock masses: application to two Alpine sites. In: TONON, F. & KOTTENSTETTE, J. *Laser and Photogrammetric Methods of Rock Face Characterization*. GoldenRocks 2006, the 41st U.S. Rock Mechanics Symposium, Colorado School of Mines, June 17 - 21, 2006.

WAGGOTT, S., CLEGG, P. & JONES, R. R. (2005) Combining terrestrial laser scanning, RTK GPS and 3D visualisation: Application of optical 3D measurement in geological exploration. *7th Conference on Optical 3-D Measurement Techniques*. Vienna, Austria.

WETHERELT, A. & WILLIAMS, D. C. (2006) Using high definition surveying (HDS) to quantify tunnel hole burdens and fragmentation. *8th International Symposium on Rock Fragmentation by Blasting: FRAGBLAST 8*. Santiago, Chile.

WOLF, P. R. (1983) *Elements of photogrammetry*, Mc-Graw Hill Inc, New York.

WYLLIE, D. C. & MAH, C. W. (2004) *Rock slope engineering, civil and mining (4th edition)*, Sabon Press, London.

YANG, Z. Y. & DI, C. C. (2001) A directional method for directly calculating the fractal parameters of joint surface roughness. *International Journal of Rock Mechanics and Mining Sciences*, 38, 1201-1210.

YASTIKI, N. (2002) The effect of system calibration on direct sensor orientation. Yildiz Technical University, Civil Engineering Faculty, Besiktas, Istanbul, Turkey.

ZHANG, L. & EINSTEIN, H. H. (1998) Estimating the mean trace lengths of rock discontinuities. *Rock Mechanics and Rock Engineering*, 31 (4), 217-235.

ZHANG, L. & EINSTEIN, H. H. (2000) Estimating the intensity of rock discontinuities. *International Journal of Rock Mechanics and Mining Sciences*, 37, 819-837.

ZHANG, L., EINSTEIN, H. H. & DERSHOWITZ, W. S. (2000) Stereological relationship between the trace length and size distribution of elliptical discontinuities. *Géotechnique*, 52(6).